Technische Universität Dresden

Organ-on-a-Disc: A Scalable Platform Technology for the Generation and Cultivation of Microphysiological Tissues

M. Sc.

Stefan Schneider

der Fakultät Elektrotechnik und Informationstechnik der Technischen Universität Dresden

zur Erlangung des akademischen Grades

Doktoringenieur

(Dr.-Ing.)

genehmigte Dissertation

Vorsitzender:	Prof. Dr.-Ing. habil. Gerald Gerlach	Tag der Einreichung: 15.10.2021
Gutachter:	Prof. Dr.-Ing. Andreas Richter	Tag der Verteidigung:13.07.2022
Gutachter:	Prof. Dr. Albert van den Berg	
Gutachter:	Prof. Dr. Peter Loskill	

Acknowledgements

First of all, I would like to thank my supervisors Prof. Dr. Peter Loskill and Prof. Dr.-Ing. Andreas Richter for their guidance, support and advice at each stage of this process, which made this work possible in the first place. Furthermore, I would like to thank Prof. Dr. Ir. Albert van den Berg for agreeing to examine this thesis.

I would like to thank Prof. Dr. Katja Schenke-Layland and Dr. Markus Wolperdinger as former and current institute head of the Fraunhofer Institute for Interfacial Engineering and Biotechnology IGB, as well as the Fraunhofer Gesellschaft for the opportunity to pursue my research at the Fraunhofer IGB in Stuttgart.

I would like to thank Jun. Prof. Dr. Michael Heymann from the Institute of Biomaterials and Biomolecular Systems at the University of Stuttgart and Associate Professor Dr. Andries D. van der Meer from the Applied Stem Cell Technologies institute at the University of Twente for helpful discussions regarding microfabrication, microfluidics and cell biology.

I would like to thank Dr. med. Ulrich E. Ziegler from the Klinik Charlottenhaus in Stuttgart, and Dr. med. Zekeriya Yurttas form the Praxisklinik in Stuttgart for the kind provision of human biopsies, Jun. Prof. Dr. med. Martin Weiss form the Department of Women's Health at the Eberhard Karls University Tübingen for the kind provision of human blood samples and Dr. Thomas Schiestel form the Fraunhofer IGB for the kind provision of hollow fiber membranes.

My special thank goes to all that accompanied and supported me during my time at the Fraunhofer IGB, especially my co-workers Oliver Schneider, Dr. Eduardo J. S. Brás, Julia Rogal, Katharina Schlünder, Cristhian Rojas, Dr.-Ing. Christopher Probst, Tengku Ibrahim Maulana, Dr. Madalena Cipriano, Dr. Silke Keller and my supervised students Florian Erdemann, Thomas Hutschalik, Marvin Bubeck, Huub J. Weener, Victor Zhang and Katrin Bindrum. I would like to thank my co-workers Silvia Kolbus-Hernandez, Kirstin Linke, and Julia Roosz for their assistance in cell isolation and the student assistants Moritz Engelhardt, Anna-Lena Streifling, Stefan Veit, Marina Albaladejo Siguan and Ing Tien Khaw for their active support in the Micro Organo-Lab.

Furthermore, I would like to thank my family that has been continuously supporting me in each possible way.

Finally, I would like to thank my wife Karin for taking care that the light at the end of the tunnel is always shining (and not a train).

Abstract

Organ-on-Chip (OoC) systems culture human tissues in a controllable environment under microfluidic perfusion and enable a precise recapitulation of human physiology. Although recent studies demonstrate the potential of OoCs as alternative to traditional cell assays and animal models in drug development as well as personalized medicine, unmet challenges in device fabrication, parallelization and operation hinder their widespread application. In order to overcome these obstacles, this thesis focuses on the development of the Organ-on-a-Disc technology for the scalable generation and cultivation of microphysiological tissues. Organ-Discs are fabricated using precise, rapid and scalable microfabrication techniques. They enable the pump- and tubing-free perfusion as well as the parallelized generation and culture of tailorable and functional microtissues using rotation-based operations. The Organ-Disc setup is suitable for versatile tissue readouts, treatments and even whole blood perfusion with minimal handling and equipment requirements. Overall, the Organ-Disc creates a scalable and user-friendly platform technology for microphysiological tissue models and paves the way for their transition towards high-throughput systems.

Kurzfassung

In Organ-on-Chip (OoC)-Systemen werden menschliche Gewebe mittels mikrofluidischer Versorgung in einer kontrollierten Umgebung kultiviert und so die Physiologie des Menschen nachgebildet. Obwohl aktuelle Studien zeigen, dass dieser Ansatz Alternativen zu herkömmlichen Zellbasierten Tests und Tiermodellen in der Arzneimittelentwicklung und der personalisierten Medizin bietet, stehen einer breiteren Anwendung Hürden im Bereich der Herstellung, Parallelisierung und Handhabung im Weg. Deshalb ist das Ziel dieser Arbeit die Entwicklung der Organ-on-a-Disc-Technologie, die eine skalierbare Erzeugung und Kultur von mikrophysiologischen Geweben ermöglicht. Für die Herstellung von der Organ-Disc kommen präzise, schnelle und skalierbare Mikrofabrikationsmethoden zum Einsatz. Die Organ-Disc schafft die Basis für die parallelisierte Erzeugung und Kultur von maßgeschneiderten und funktionellen Mikrogeweben, sowie deren Versorgung durch rotationsbasierte Prozesse und ohne zur Hilfenahme von Pumpen oder Schläuchen. Die Organ-Disc eignet sich für unterschiedliche Charakterisierungsmethoden sowie der Gewebestimulation und sogar der Vollblutperfusion mit minimalem Aufwand und Equipment. Insgesamt stellt die Organ-Disc eine skalierbare und benutzerfreundliche Plattformtechnologie für mikrophysiologische Modelle dar und bereitet den Weg für Hochdurchsatzanwendungen.

Table of Contents

Abbreviations

2D	Two-dimensional
3D	Three-dimensional
Ang-2	Angiopoietin 2
ASC	Adipose tissue-derived stem cells
BSA	Bovine serum albumin
CAD	Computer-aided design
CD	Cluster of differentiation
COC	Cyclic olefin copolymer
COP	Cyclic olefin polymer
DC	Direct current
DMEM	Dulbecco’s modified Eagle’s medium
ECM	Extracellular matrix
EV	Extracellular vesicles
FB	Fibroblasts
FBS	Fetal bovine serum
FDA	Fluorescein diacetate
FEP	Fluorinated ethylene–propylene
HUVEC	Human umbilical vein endothelial cells
IL-6	Interleukin 6
IL-8	Interleukin 8
IPA	Isopropanol
iPSC	Induced pluripotent stem cells
LCD	Liquid-crystal display
LoC	Lab-on-a-Chip
LoD	Lab-on-a-Disc
OoC	Organ-on-Chip
OSTE(+)	Off-stoichiometry thiol–ene–epoxy, also-called Ostemer
PBPK	Physiologically based pharmacokinetics
PBS	Phosphate buffered saline without calcium or magnesium
PBS+	Phosphate buffered saline with calcium and magnesium
PC	Polycarbonate
PDMS	Polydimethylsiloxane

PECAM-1	Platelet endothelial cell adhesion molecule 1
PET	Polyethylene terephthalate
PI	Propidium iodide
PMMA	Polymethylmethacrylate
PP	Polypropylene
PS	Polystyrene
PTFE	Polytetrafluoroethylene
R&D	Research and development
rph	Revolutions per hour
rpm	Revolutions per minute
RT	Room temperature
sccm	Standard cubic centimeters per minute
SEBS	Styrene–ethylene/butylene–styrene
SLA	Stereolithography
TEER	Trans-epithelial electrical resistance
TNF-α	Tumor necrosis factor alpha
TPE	Thermoplastic elastomer
USD	United States dollar
UV	Ultraviolet
VECAM-1	Vascular cell adhesion molecule 1
WAT	White-adipose-tissue
WSS	Wall shear stress

Symbols

A	m^2	Area
b	-	Number of steel balls
c	$mol \cdot m^{-3}$	Molar concentration
C	(m, m, m)	Cross-section (coordinates)
∂C	(m, m, m)	Channel walls (coordinates)
CN	-	Cell number
D	m	Capillary/channel diameter
d	m	Diameter (*e.g.* steel ball trajectory)
f	$N \cdot m^{-3}$	Volumetric forces
F	N	Force
g	$m \cdot s^{-2}$ (= 9.81 $m \cdot s^{-2}$)	Gravitational acceleration
H	m	Channel height
h	m	Height (*e.g.* fluid level)
L	m	Channel length
L_0	m	Characteristic channel dimension
m	kg	Mass
n	mol	Amount of substance
N	-	Number of samples
OC	$mol \cdot s^{-1}$	Oxygen consumption
p	Pa	pressure
Q	$m^3 \cdot s^{-1}$	Volumetric flow rate
r	m	Channel radius, radial position
Re	-	Reynolds number
R_{hyd}	$Pa \cdot s \cdot m^{-3}$	Hydraulic resistance
t	s	Time
T	°C	Temperature
T_g	°C	Glass transition temperature
T_m	°C	Melting temperature
u	$m \cdot s^{-1}$	Velocity
U_0	$m \cdot s^{-1}$	Characteristic fluid velocity
U_{Motor}	s^{-1}	Motor speed (angular frequency)
V	m^3	Volume
W	m	Channel width

x, y, z	m	Coordinates
α	m^3	Pump channel compression
η	$Pa \cdot s$	Dynamic viscosity
θ	deg (= π / 180 rad)	Contact angle
λ	m	Wavelength
ρ	$kg \cdot m^{-3}$	Density
σ	$N \cdot m^{-1}$	Surface tension
τ	$dyn \cdot cm^{-2}$ (= 0.1 Pa)	Shear stress
ω	s^{-1}	Angular frequency

1 Introduction

It is widely accepted that the overall pharmaceutical research and development (R&D) efficiency is declining, which results in steadily rising drug development costs. From 1950-2010, the amount of drugs approved by the Food and Drug Administration per development expenses has halved approx. every nine years [1]. Scannel *et al.* named this observation "Eroom's law", which reads "Moore's law" backwards, to emphasize the opposite development progress compared to the microchip industry [1]. In recent years, the estimated total R&D costs per new drug have reached the range of 2.5 billion USD (United States dollar) [2], while the number of approved drugs remained on a relatively stable level for several decades [3].

In order to increase the productivity of the overall drug development process, a more stringent filtering of drug candidates in preclinical phases has been demanded in order to avoid unsuccessful drug candidates from entering the later and more expansive clinical phases [4]. However, an overall 'fail early and fail cheap' approach requires the right tools for decision making during preclinical phases. The low predictive power of current preclinical testing is drastically demonstrated by an overall success rate of a drug candidate entering the clinical phases to obtain a final approval below 12% [2]. Thereby, the reasons for failure in the clinical phases 2 and 3, which hence become visible during human testing, are primarily associated to efficacy and safety concerns [5]. This emphasizes that traditional preclinical models, such as cell assays and animal models, fail frequently to predict the effect of drugs in humans and to sufficiently filter unsafe drug candidates. Overall, this begs the question if there aren't new preclinical tools that could perform better and allow for a more efficient as well as safer drug development process.

Organ-on-Chip (OoC) technology offers a potential solution to this and targets a more precise recapitulation of human physiology as well as a reduction, up to the point of replacement, of ethically problematic animal testing [6]. OoCs are microfluidic systems that allow for the generation and culture of microtissues in a controllable, tissue-specific microenvironment with precisely tunable microfluidic perfusion. A variety of OoC systems have been developed in recent years and led to a continuously growing portfolio of physiologic models of various human tissues or organs [7]. These advances generate a new tool box for preclinical testing with higher predictive value compared to traditional cell culture or animal models, which has been successfully demonstrated in a number of proof-of-concept studies [7, 8]. Estimates from experts in the field of drug research and development predict that OoC can help to reduce development costs by up to 26% [9]. Unsurprisingly, OoC has gained increasing attention not

only from academy but also from industry, which resulted in the emergence of several start-ups commercializing OoC systems in the last decade [10].

Nevertheless, the widespread application of OoC by pharma companies has yet to come [11]. One major drawback of current OoC systems is their low-throughput character compared to conventional cell assays [12]. Though the field of OoC has started the transition towards higher-throughput applications, current efforts rely frequently on comparable concepts hence share the same limitations. Several factors limiting the throughput of current OoC systems can be identified, such as elaborate chip fabrication, low degrees of parallelization as well as manual and time-consuming operation steps [13].

A role model for parallelization and automation in microfluidic research are centrifugal, microfluidic systems or Lab-on-a-Disc (LoD) devices. LoD systems achieve high levels of parallelization and automation by utilizing centrifugal unit operations that rely primarily on rotation of a microfluidic device with a rotationally symmetric channel layout [14]. Different to other high-throughput concepts trying to recreate microfluidic equivalents to electronic integrated circuits [15, 16], LoD technology provides a pump- and tubing-free approach. So far, LoD devices were mainly developed as analytical systems targeting, for instance, biomedical diagnostic applications [14, 17, 18]. Yet, LoD systems have been shown to be able to conduct essential unit operations of OoC approaches, such as cell transport and fluid actuation [19, 20].

In order to pave the way towards high-throughput OoC applications, the focus of this thesis is the development of the so-called Organ-on-a-Disc technology. Organ-Discs combine aspects of centrifugal microfluidics, tissue engineering and OoC in order to create a novel platform technology for OoC systems. They enable the generation and culture of tailorable tissue structures under precisely tunable perfusion by utilizing user-friendly, rotation-based processes.

The Organ-Disc concept allows for 1) the utilization of scalable chip fabrication techniques, 2) pump- and tubing-free perfusion in single-pass as well as closed-loop configuration, 3) the parallelized formation of both three-dimensional (3D) microtissues and perfusable blood vessel-like tissues, 4) the compatibility to multiple characterization techniques demonstrating tissue functionality and even 5) the integrated perfusion of human whole blood. Overall, the Organ-Disc technology builds a versatile and powerful basis for the further progress of OoC research towards higher-throughput applications by transferring OoC models ‘on-disc’.

2 Background

2.1 Fluid Dynamics

The theoretical discourse about fluid dynamics in the following sections, unless otherwise specified, is based on the derivations of Henrik Bruus [21]. It is important to emphasize that the following sections will only focus on Newtonian fluids with a constant, dynamic viscosity η that are incompressible, hence feature a constant density ρ. Thereby, the following theoretical discourse is limited to the fluid dynamics relevant for the fluid actuation utilized in this thesis.

2.1.1 Flow Equations

The conservation of mass in classical mechanics results in the continuity equation. The continuity equation for a fluid describes that the fluid mass in a set region can only vary by mass flux across the boundary of that region. In the case of an incompressible fluid with ρ = constant and a flow velocity field $\vec{u}$, the continuity equation is

$$\nabla \cdot \vec{u} = 0 \,. \tag{2.1}$$

If transferred into Cartesian coordinates (x, y, z) and using the abbreviation $\partial_{\mathrm{i}}\mathrm{X} \equiv \partial\mathrm{X} / \partial\mathrm{i}$, the continuity equation can be written as

$$\partial_{\mathrm{x}} u_{\mathrm{x}} + \partial_{\mathrm{y}} u_{\mathrm{y}} + \partial_{\mathrm{z}} u_{\mathrm{z}} = 0 \,. \tag{2.2}$$

The momentum of a fluid inside a set region can vary by flux of momentum, such as convection, and through forces acting on the fluid. The individual forces can either act on the fluid surface, such as pressure and viscosity forces, or on the fluid volume, such as gravitational, electric or magnetic forces. Both the conservation of fluid mass and the rate of change in momentum in a fluid can be combined to an equation describing the fluid motion, the so-called Navier-Stokes equations. The Navier-Stokes equations in the form of

$$\rho \left[\frac{\partial \vec{u}}{\partial t} + (\vec{u} \cdot \nabla)\vec{u} \right] = -\nabla p + \eta \nabla^2 \vec{u} + \vec{f} \tag{2.3}$$

describe an incompressible, Newtonian fluid with pressure p and external, volumetric forces $\vec{f}$.

The ratio of inertia to viscous forces in a fluid flowing through a channel is described by the dimensionless Reynolds number,

$$Re = \frac{\rho U_0 L_0}{\eta}, \tag{2.4}$$

whereby U_0 reflects a characteristic flow velocity of the fluid and L_0 a characteristic channel dimension. For low *Re*, viscous forces dominate and the fluid flow is laminar (Figure 2.1 a). Laminar fluid flow occurs in parallel layers or streamlines without lateral transport. For high $Re > Re_{crit}$ the transition from laminar to turbulent flow occurs with flow perpendicular to the main flow direction and the formation of eddies (Figure 2.1 b). The reported values of Re_{crit}, for instance, for perfused tubes range usually between 1,000-3,000 and are still focus of current research [22, 23].

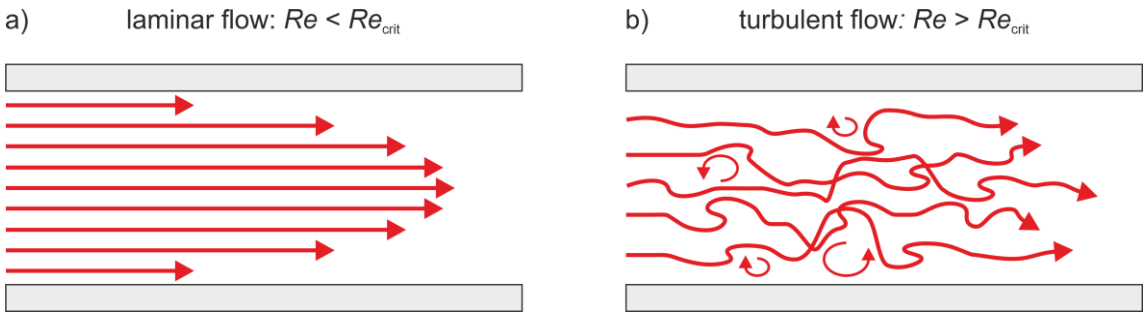

Figure 2.1 Laminar and turbulent flow: a) Fluid flow with low *Re* is laminar with parallel streamlines. b) Fluid flow with high *Re* is turbulent with fluid transport perpendicular to the main flow direction and the formation of eddies.

In microfluidic systems, the characteristic channel dimensions are in the µm to low mm range, which usually results in laminar fluid flow. Poiseuille, also called Hagen-Poiseuille flows, allow for an appropriate description of fluid flow in microfluidic systems. In principle, the theory of Poiseuille flows originates from studies on perfused tubes. However, Poiseuille flows can be further generalized to laminar, steady-state fluid flow through a channel with constant cross-section C and rigid, channel walls ∂C, driven by a constant pressure gradient Δp across the channel length L (Figure 2.2).

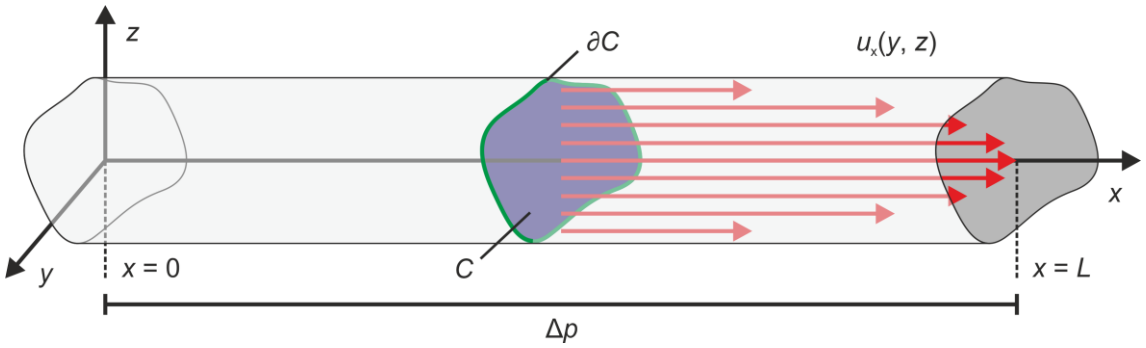

Figure 2.2 Generalized Poiseuille flow: Steady-state fluid flow through a channel with constant cross-section C and rigid, channel walls ∂C driven by a constant pressure gradient Δp present along the channel length L (x-direction). Overall, a translation invariant system in x-direction is generated with a fluid velocity field $u_x(y, z)$. Figure inspired by Ref. [21].

Overall, a translation invariant system along the channel length (x-direction) is present and the velocity field is simplified to

$$\vec{u} = \begin{bmatrix} u_x(y,z) \\ 0 \\ 0 \end{bmatrix}. \tag{2.5}$$

The assumption that the fluid in direct contact to the channel wall moves with the same speed as the wall results in the no-slip boundary condition. Therefore, in a stationary channel the fluid speed at the channel wall is zero with

$$u_x(y,z) = 0, \quad \text{for } (y,z) \in \partial C. \tag{2.6}$$

In the absence of external, body forces, the Navier-Stokes equation is hence simplified to

$$\rho\left[\underbrace{\frac{\partial \vec{u}}{\partial t}}_{=0} + \underbrace{(\vec{u}\cdot\nabla)\vec{u}}_{=0}\right] = -\nabla p + \eta\nabla^2\vec{u} + \underbrace{\vec{f}}_{=0} \tag{2.7}$$

$$0 = \frac{\Delta p}{L} + \eta\left[\partial_y^2 u_x(y,z) + \partial_z^2 u_x(y,z)\right], \quad \text{for } (y,z) \in C\,. \tag{2.8}$$

The solutions for $u_x(y, z)$ depend on the channel cross-section and are well-known for several geometries:

- cylindrical pipes with radius r

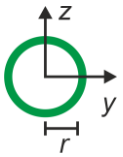

$$u_x(y,z) = \frac{\Delta p}{4\eta L}(r^2 - y^2 - z^2), \quad \text{for } y^2 + z^2 \le r^2 \tag{2.9}$$

- infinite parallel-plate channels with distance H

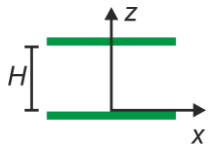

$$u_x(z) = \frac{\Delta p}{2\eta L}(H - z)z\,, \quad \text{for } 0 \le z \le H \tag{2.10}$$

- rectangular channel cross-sections with distance H, width W and $H < W$ (derived by a Fourier series transformation [21])

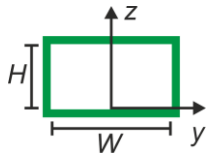

$$u_x(y,z) = \frac{4H^2\Delta p}{\pi^3\eta L}\sum_{n,\text{odd}}^{\infty}\frac{1}{n^3}\left[1 - \frac{\cosh\left(n\pi\frac{y}{H}\right)}{\cosh\left(n\pi\frac{W}{2H}\right)}\right]\sin\left(n\pi\frac{z}{H}\right), \quad \text{for } -\frac{1}{2}W \le y \le \frac{1}{2}W,\ 0 \le z \le H\,. \tag{2.11}$$

2.1.2 Hydraulic Resistance

Once a solution is found for $u_x(y, z)$, the volumetric flow rate Q through the channel with cross-section C can be calculated using

$$Q = \int_C u_x(y,z)\,dy\,dz\,. \tag{2.12}$$

An important aspect of Poiseuille flows is that a constant pressure drop Δp results in a constant volumetric flow rate Q. According to the so-called Hagen-Poiseuille law, in a cylindrical pipe with radius r, a linear relationship between Δp and Q with

$$Q = \frac{\pi r^4}{8\eta L}\Delta p \tag{2.13}$$

exists. Thereby, the hydraulic resistance R_{hyd} can be defined as proportionality factor between Δp and Q with

$$R_{\text{hyd}} = \frac{\Delta p}{Q}, \tag{2.14}$$

which resembles the fluidic equivalent to Ohm's law for the relationship between electrical current through a conductor and the applied electrical potential across the conductor.

The hydraulic resistance can be formulated for several channel geometries:

- cylindrical pipes with radius r

$$R_{\text{hyd,pipe}} = \frac{8}{\pi}\frac{\eta L}{r^4} \tag{2.15}$$

- parallel-plate channels with distance H, width W and $H < W$ (theoretically infinite plates without side walls)

$$R_{\text{hyd,plates}} = 12\frac{\eta L}{H^3 W} \tag{2.16}$$

- rectangular channel cross-sections with distance H, width W and $H < W$

$$R_{\text{hyd,rect.}} = \frac{12}{1 - \frac{192}{\pi^5}\frac{H}{W}\sum_{n,\text{odd}}^{\infty}\frac{1}{n^5}\tanh\left(n\pi\frac{W}{2H}\right)}\frac{\eta L}{H^3 W}, \tag{2.17}$$

which can be further simplified by using

$$R_{\text{hyd,rect.}} \approx \frac{12}{1 - 0.630\frac{H}{W}}\frac{\eta L}{H^3 W}. \tag{2.18}$$

Equation (2.18) provides a suitable approximation for rectangular channels with $H < W$. The deviation is lower than 0.2% for channels with aspect ratios of $H/W \leq 0.5$ [21].

2.1.3 Wall Shear Stress

Many microfluidic systems culture cells directly on inner channel surfaces. These cells are exposed to fluid shear stress, the so-called wall shear stress (WSS). WSS effects on cells are frequently studied, for instance, in parallel-plate flow chambers. These systems are usually assumed to replicate infinite parallel plates without any influence from lateral side walls. The WSS τ_{WSS} is calculated with

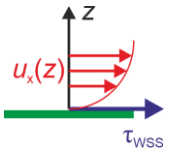

$$\tau_{\text{WSS}} = \eta\frac{\partial u_x(y,z)}{\partial z}, \quad \text{for } z = 0. \tag{2.19}$$

Using the velocity field $u_x(z)$ for parallel-plate flow from equation (2.10) and substituting the pressure gradient using equation (2.14) in combination with (2.16),

$$\tau_{\mathrm{WSS,plate}} = \frac{6\eta Q}{H^2 W}\,. \tag{2.20}$$

Besides parallel-plate flow, equation (2.20) provides a good estimate for the WSS in rectangular channels with side walls and low aspect ratios *H/W*. In principle, the WSS in rectangular channels varies along the channel width *W* in lateral direction (*y*-direction), as studied in detail in Ref. [24].

2.1.4 Centrifugal Microfluidics

Centrifugal microfluidics relies primarily on rotation to actuate and manipulate fluid flows. In general, three distinct forces are present in a centrifugal platform spinning at an angular frequency $\vec{\omega}$ and act on a point-like body with mass *m* at a radial position $\vec{r}$ [14]. These forces are (*cf.* Figure 2.3 a):

- the centrifugal force $\vec{F}_c$ acting in radial outward direction:

$$\vec{F}_c = -m\vec{\omega} \times (\vec{\omega} \times \vec{r}) \tag{2.21}$$

- the Coriolis force $\vec{F}_{Co}$ acting perpendicular to the rotation axis and the velocity of a moving object:

$$\vec{F}_{Co} = -2m\vec{\omega} \times \vec{u} \tag{2.22}$$

- and the Euler force $\vec{F}_{Eu}$ acting perpendicular to $\vec{F}_c$ (zero for constant spinning speed):

$$\vec{F}_{Eu} = -m\frac{d}{dt}\vec{\omega} \times \vec{r}\,. \tag{2.23}$$

These forces can be manipulated by the rotation velocity and acceleration as well as the channel design. For instance, centrifugal forces can be used for fluid or particle transport, whereas Coriolis and Euler forces allow for flow switching or mixing in centrifugal systems [14, 25].

For the calculation of fluid flow due to centrifugation, the scalar pressure difference over a liquid column can be used [14]. The centrifugal pressure gradient is

$$\Delta p_c = \frac{1}{2}\rho \cdot \omega^2 (r_2^2 - r_1^2)\,, \tag{2.24}$$

whereas r_1 and r_2 are the radial inner and outer edge of the liquid respectively (Figure 2.3 a). Additional scalar pressure gradients that can be present are hydrostatic pressure gradients

$$\Delta p_h = \rho \cdot g \cdot h \tag{2.25}$$

due to standard gravity on earth g and a difference in height h of liquid columns in connected reservoirs (Figure 2.3 b), or pressure gradients due to capillary forces (Figure 2.3 c). The latter can, *e.g.*, lead to pinning of a liquid at a diverging channel section. Considering a circular capillary with diameter D, the capillary pressure gradient is

$$\Delta p_{cap} = -\frac{4\sigma \cdot \cos\theta}{D}, \tag{2.26}$$

which is built up by a pinned droplet with contact angle θ from a liquid with surface tension σ [26]. Capillary pinning at a diverging channel section can be used for capillary burst valves counteracting, for instance, centrifugal pressure gradients. These valves retain fluid until a critical centrifugal pressure (or corresponding angular frequency) is reached that exceeds the maximum capillary pressure Δp_v of the valve and the liquid can spread beyond the diverging section [27]. The exact value for Δp_v depends on multiple aspects including channel fabrication methods and is usually hard to predict [28].

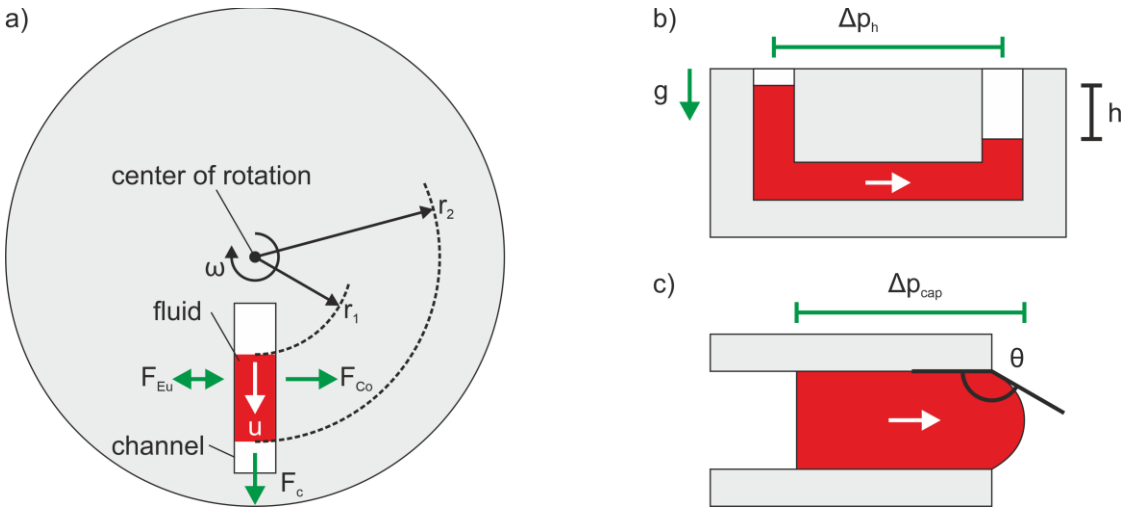

Figure 2.3 Forces and pressure gradients in centrifugal microfluidics: a) Forces acting on a fluid during rotation at an angular frequency ω. The centrifugal force F_c acts in radial direction outwards. The Coriolis force F_{Co} acts perpendicular to ω and the velocity u of the fluid. The Euler force F_{Eu} acts perpendicular to F_c. Figure inspired by Ref. [14]. b) Hydrostatic pressure gradient Δp_h due to (earth) gravitational acceleration g and height difference h of liquid in connected reservoirs. c) Capillary pressure difference Δp_{cap} due to pinning of liquid at a diverging channel section.

2.2 Microfluidic Chip Fabrication

In the field of microfluidic cell culture and OoC, the general fabrication process of microfluidic devices includes three main steps: 1) the selection of a suitable chip material, 2) the precise structuring of the channels into the material and, finally, 3) the tight connection of the individual layers to seal the chip and its channels.

2.2.1 Chip Materials

Over the last decades, polymers became the material of choice for microfluidic cell culture devices and displaced almost entirely silicon or glass as chip material [29]. The characteristics of polymers depend on their chemical structure, which leads to three main polymer groups [30, 31]:

- Thermoplastics are based on linear or branched polymer chains. They are usually amorphous (glass-like) or semi-crystalline with both crystalline and amorphous phases. Amorphous polymers or amorphous phases in semi-crystalline polymers change from a glassy to a soft, rubbery state above the glass transition temperature T_g and become steadily less viscous with increasing temperature. Crystalline phases melt above their melting temperature T_m, which is generally higher than T_g of the amorphous phases [31].
- Elastomers feature a low degree of cross-linking between polymer chains and allow for reversible deformation without permanent flow. The polymer network of elastomers can extend if stress is applied but returns into its original shape once stress is released again. Common types of elastomers feature a T_g below 0 °C hence are flexible at room temperature (RT) but are incapable of melting.
- Thermosets feature a highly crosslinked polymer chain network. This structure limits polymer chain extension to a minimal amount and results in a rigid and highly stable material. Thermosets are as well incapable of melting and solely degrade at high temperatures.

The most frequently applied material for microfluidic chips is the elastomer polydimethylsiloxane (PDMS) as it allows for a simple chip fabrication process (*cf.* sections 2.2.2 and 2.2.3). After curing, PDMS features a low stiffness with an elastic modulus of 1-3 MPa that simplifies subsequent fabrication steps, such as demolding or bonding of chip layers, but also enables the integration of flexible components into microfluidic systems [32]. Moreover, PDMS is popular in the field of microfluidics because of its high optical clarity

(transparent for wavelengths of 240-1100 nm) enabling optical readouts in microchannels [33]. PDMS has also a high permeability to several gases, such as oxygen and carbon dioxide [34, 35], as well as to water vapor [36]. Further important aspects of PDMS are its tendency to absorb small, hydrophobic compounds [37] and the leaching of uncrosslinked oligomers from PDMS [38].

Compared to elastomers, thermoplastic materials are rigid and usually feature a Young's modulus of approx. 2-3 GPa [39]. Polymethylmethacrylate (PMMA), polycarbonate (PC) or cyclic olefin copolymer (COC) are examples for popular thermoplastic materials in the field of microfluidics. These polymers usually feature a T_g of 70-155 °C, low water absorption, good chemical resistance and high optical transmittance [39, 40]. Further, important aspect of thermoplastics are their compatibility to mass production techniques, such as injection molding, and their lower material price compared to PDMS [41].

Thermosets are also used for microfluidic chips, however, to a much lower extend than PDMS or thermoplastics and mainly for chips requiring rather extreme pressure, solvent or temperature tolerances [42, 43]. Some examples are photocurable epoxy or polyimide [44], thermoset polyester [45], adhesives for optical applications [46] and off-stoichiometry thiol–ene–epoxy (OSTE(+), also called Ostemer) [47, 48].

An interesting material group that does not directly fall into one of these mentioned categories are thermoplastic elastomers (TPE) that combine characteristics of both elastomers and thermoplastics. Styrene block copolymers are an important subtype of TPE and ideally suited for biomedical applications as they achieve elasticity without the need for chemical crosslinkers [49]. Styrene–ethylene/butylene–styrene (SEBS) is a styrene block copolymer that has been used frequently for microfluidic chip fabrication [50–52]. SEBS consists of a soft, rubbery phase (ethylene/butylene segments) between hard phases (polystyrene blocks) and features two glass transition temperatures [53]. SEBS becomes elastic above the T_g of the soft segments (approx. -65 °C), comparable to the elasticity of PDMS, and starts to flow above the T_g of the polystyrene phase (approx. 90 °C) [51], which allows for shaping using the same techniques as for thermoplastics.

2.2.2 Microstructuring

The general, polymer-based microstructuring process starts with the design of the microfluidic system (Figure 2.4). Whereas replication techniques, such as casting or embossing, require an intermediate master structure featuring the negative of the final, desired channel layout, subtractive and additive methods allow for the direct transfer of the design into the chip material.

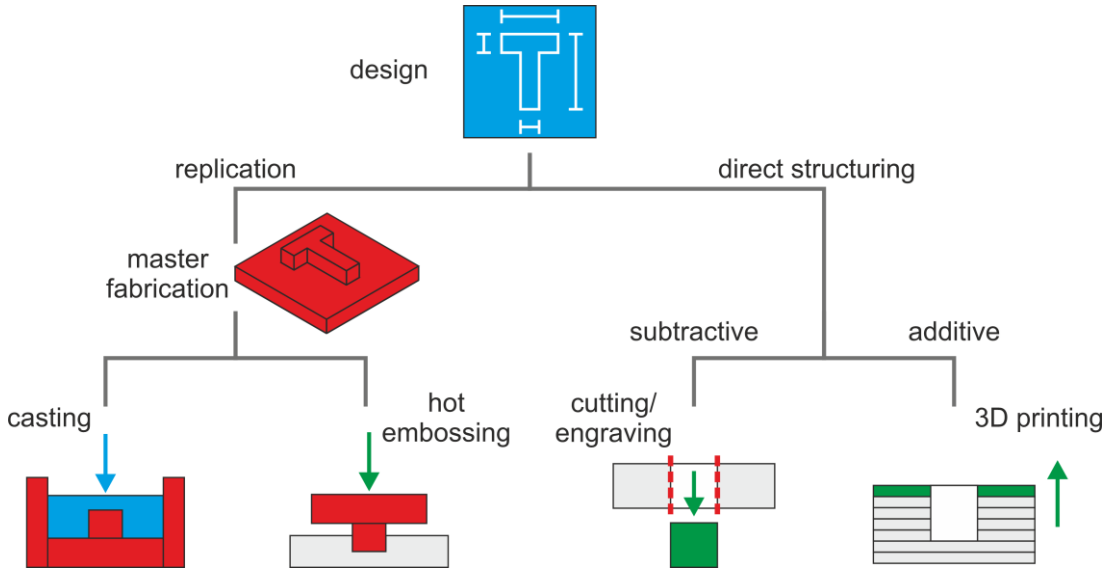

Figure 2.4 Polymer-based microstructuring: Replication techniques, such as casting or hot embossing, require an intermediate master fabrication step. Subtractive or additive manufacturing, such as cutting/engraving or 3D printing, allow for a direct transfer of the designed structures into the chip material.

Casting, also called replica molding, is the standard structuring technique for elastomers, such as PDMS [54], but also for multiple thermoset materials [45, 46, 48]. It involves preparing of a prepolymer mixture, pouring it onto the master and curing of the prepolymer. After demolding, the microfluidic module features the negative structure profile of the initial master. In the case of PDMS replica molding, the master is most commonly fabricated by ultraviolet (UV) lithography using SU-8 photoresist. The fabrication of SU-8 microstructures is well-established and discussed in detail in Ref. [55].

In contrast to elastomers and thermosets, thermoplastics become soft and start to flow at high temperatures. This allows for shaping of a thermoplastic material by replication techniques, such as hot embossing. Thereby, the thermoplastic material is heated above its T_g and a master is pushed into the soft polymer, which generates a negative microstructure profile in the material [56]. After cooling, the polymer solidifies again and can be demolded from the master. Alternative replication techniques are injection molding, which involves pressing of a polymer

melt into a microstructured cavity [57], or thermoforming, which is achieved by 3D stretching of a thermoplastic film against a master [58]. Replication, for instance, by hot embossing [59] or injection molding [60], is as well possible for TPE materials as they melt and behave as thermoplastics at high temperatures. A general requirement of these replication techniques is, however, the availability of rigid and temperature stable masters due to the relatively high process temperatures and pressures. Those replication masters are commonly fabricated using epoxy resin [61–63], metal [64] or silicon [65].

Subtractive or additive manufacturing provide a different structuring strategy and do not require an intermediate master. Subtractive manufacturing generates channels directly in the chip material by cutting or engraving. Frequently applied methods are micromilling [66], xurography with a cutting plotter [67] or laser structuring [68–70]. In contrast to the mechanical removal of material by milling or plotting, laser cutting relies on thermal and/or photochemical processes depending, for instance, on the laser source and the structured polymer [71].

Additive manufacturing or 3D printing is a relatively new technique for microfluidic chip fabrication. For instance, stereolithography (SLA) printing has gained attention in recent years and is based on layer-by-layer printing of a photocurable resin by localized light exposure [72]. Besides SLA, alternative printing techniques, such as multi jet modeling or fused deposition modeling, are being explored in the field of microfluidics [73].

2.2.3 Bonding

To assemble microfluidic platforms featuring enclosed channels and chambers, the individual microstructured layers have to be bonded together. PDMS devices are typically bonded via surface oxidation utilizing an oxygen plasma and bringing these surfaces into conformal contact to each other [54]. After an oxygen plasma treatment of a crosslinked PDMS surface, the amount of oxygen atoms is increased and the amount of carbon atoms is decreased [74]. It is further widely accepted that oxygen plasma results in the formation of silanol groups (-Si-OH) on the PDMS surface [75]. It is expected that the underlying bonding mechanism relies on a condensation reaction between silanol groups to covalent siloxane (-Si-O-Si-) bonds [54]. Plasma-activated PDMS can form stable bonds to another plasma-activated PDMS or glass surface [76, 77], or chemically modified thermoplastic substrates [78, 79].

Different to the well-established and relatively simple to perform PDMS bonding, the fusion of thermoplastic materials is usually more challenging. This has resulted in a wide spectrum of

bonding techniques for thermoplastic systems [40, 80]. Especially thermal fusion bonding and solvent bonding are popular in the field of microfluidics and provide a good compromise between the required equipment, the overall process time and scalability as well as the freedom in chip design and feature sizes [80]. Thermal fusion bonding relies on the interdiffusion of polymer chains across a contact interface of two thermoplastic substrates under the influence of pressure for intimate contact and heat for increasing the polymer chain mobility [81]. For sufficient mobility of the polymer chains, the work pieces have to be heated close or above their T_g, which bears the risk of channel distortion or collapse due to the accompanied softening of the polymer [40]. Solvent bonding or solvent welding similarly relies on the interdiffusion of polymer chains between two substrates but uses a suitable solvent for solvation of polymer chains [82, 40]. This results in the increase of chain mobility and leaves a permanent connection after interdiffusion and subsequent evaporation of the solvent [82]. However, solvent bonding can also result in channel distortion or collapse if the materials are over exposed to the solvent [40].

In comparison to the bonding of thermoplastic systems, TPE, such as SEBS, facilitates the connection of individual layers due to their self-adhesive properties. They enable a reversible bond between multiple SEBS layers or to other thermoplastic substrates and glass just by conformal contact at RT or a further improved, irreversible bonding when combined with a simple heating step [52, 83, 84].

3 State of the Art

3.1 Cell Culture Systems

Cell culture systems can be roughly categorized into static and dynamic cell culture systems whereas both configurations allow for the culture of two-dimensional (2D) and 3D cell structures. According to Berthier *et al.*, static cell culture techniques in 2D can be traced back to the beginning of the 20th century, when Ross G. Harrison observed nerve fiber outgrowth from a frog embryo on a glass surface [32, 85]. Further important landmarks in the history of cell culture techniques are the development of aseptic culture techniques, the generation of immortalized cell lines, cryopreservation, and achievements in stem cell research [32]. Over the last decades cell culture became a tool for both basic research in biology but also for biotechnology applications, such as cell-based high throughput screening in drug discovery [12], or mass production of vaccines [86] and antibodies [87].

In 2D cell culture systems, cells form monolayers on flat surfaces, whereas 3D cell culture systems incorporate cells growing *e.g.* on scaffolds or densely packed in a spheroid [88]. In recent years, advances in the field of 3D cell culture techniques have pointed out that 2D systems lack important aspects of *in vivo* tissues, such as cell-to-cell and cell-to-extracellular matrix (ECM) interaction [89].

Both 2D and 3D systems are usually kept under static conditions and rely on periodic media exchanges for the supply of nutrients and the removal of waste products and metabolites. The relatively simple procedures in static cell culture workflows have resulted in automated cell culture equipment that allow for high-throughput cell expansion and maintenance [90, 91]. However, the lack of continuous fluid flow and convective transport in static cell culture results in poorly controlled, time dependent gradients between the supernatant and the cells and overall concentrations hence an uncontrolled microenvironment [92, 93].

Therefore, novel cell culture technologies have been developed that add convective fluid flow for improved mass transport or targeted cell simulation, for instance, due to fluid forces. An example of perfused 2D culture systems are parallel-plate flow chambers that achieve defined fluid flow over a cell monolayer, which has enabled studies focusing on the effect of shear stress on endothelial cells [94]. An important tool for dynamic, 3D cell culture are bioreactors and their use in tissue engineering during cell expansion and maturation of 3D tissues for later diagnostic *in vitro* applications or implantation in humans [95]. Bioreactor designs are diverse

and range from flasks with elements for media agitation to continuously perfused columns and hollow fibers over to miniaturized, microfluidic bioreactors [96, 97].

Thereby, microfluidic systems have gained interest as capable tools for cell culture applications with unique advantages compared to their macroscopic counterpart, among them precisely controllable, laminar fluid flows, generation of concentration gradients, more physiologic cell-to-media ratios as well as high potential for scale-up [92, 93].

3.2 3D Tissue Generation in Microfluidic Systems

It is generally accepted that standard 2D cell culture on hard glass or polymer surfaces lacks physiologic relevance and that 3D tissues represent better models of *in vivo* tissues and organs [89]. Several techniques have been established to generate more physiological 3D tissues and integrate them into a microfluidic system for improved control over the microenvironment of the tissue (Figure 3.1).

3D tissues are frequently formed via injection of cell-laden hydrogels (mixtures of cells in hydrogels) into a microfluidic channel or cavity, followed by the gelation of the hydrogel (Figure 3.1 a). This technique allows for the self-assembly of cells into a 3D construct with structural support of the hydrogel scaffold. Cell-laden hydrogels are used, for instance, for the generation of cardiac tissue [98], white-adipose-tissue (WAT) [99], as well as liver and tumor tissues on-chip [100].

Bioprinting is another technique for the generation of 3D tissues from cell-laden hydrogels [101]. 3D printing a cell-laden hydrogel allows for a precise deposition and for the generation of a predefined scaffold geometry with embedded cells (Figure 3.1 b). Whereas many bioprinting applications aim at the fabrication of tissue or organ replacements for transplantation, some combinations of bioprinting and microfluidic systems have been presented as well [102]. The integration of bioprinted cell structures into microfluidic systems is achieved by either direct printing into channels or cavities [103], placing cell-seeded scaffolds into a microfluidic setup [104], or printing both the 3D cell construct and the surrounding chip parts [105].

An alternative scaffold-free tissue generation in the micrometer range is achieved by filtration of a cell suspension using a microchannel with porous channel wall [106–108]. The cell suspension is pumped in the channel, the cells retained by the porous barrier and the excess

media removed out of the filter structure (Figure 3.1 c). This has been applied, for instance, in systems emulating heart [106], or liver structures [107].

3D tissues can also be generated off-chip, for instance, using cell culture plates with low attachment surfaces preventing cell adhesion, thereby enabling the transformation of single cells into dense spheroids (Figure 3.1 d). These pre-formed cell aggregates can be transferred into microfluidic systems for subsequent perfused culture [109, 110]. This approach allows for the integration of off-chip generated organoids [111], as well as, the arrangement of multiple spheroids on-chip by using microfluidic trapping structures [112].

Alternatively, spheroid formation and perfusion can be achieved in a single, microfluidic device, so-called hanging drop systems (Figure 3.1 e). In hanging drop systems, the spheroid can be formed directly at the liquid air interface of a stationary fluid drop that is stabilized by capillary forces [113].

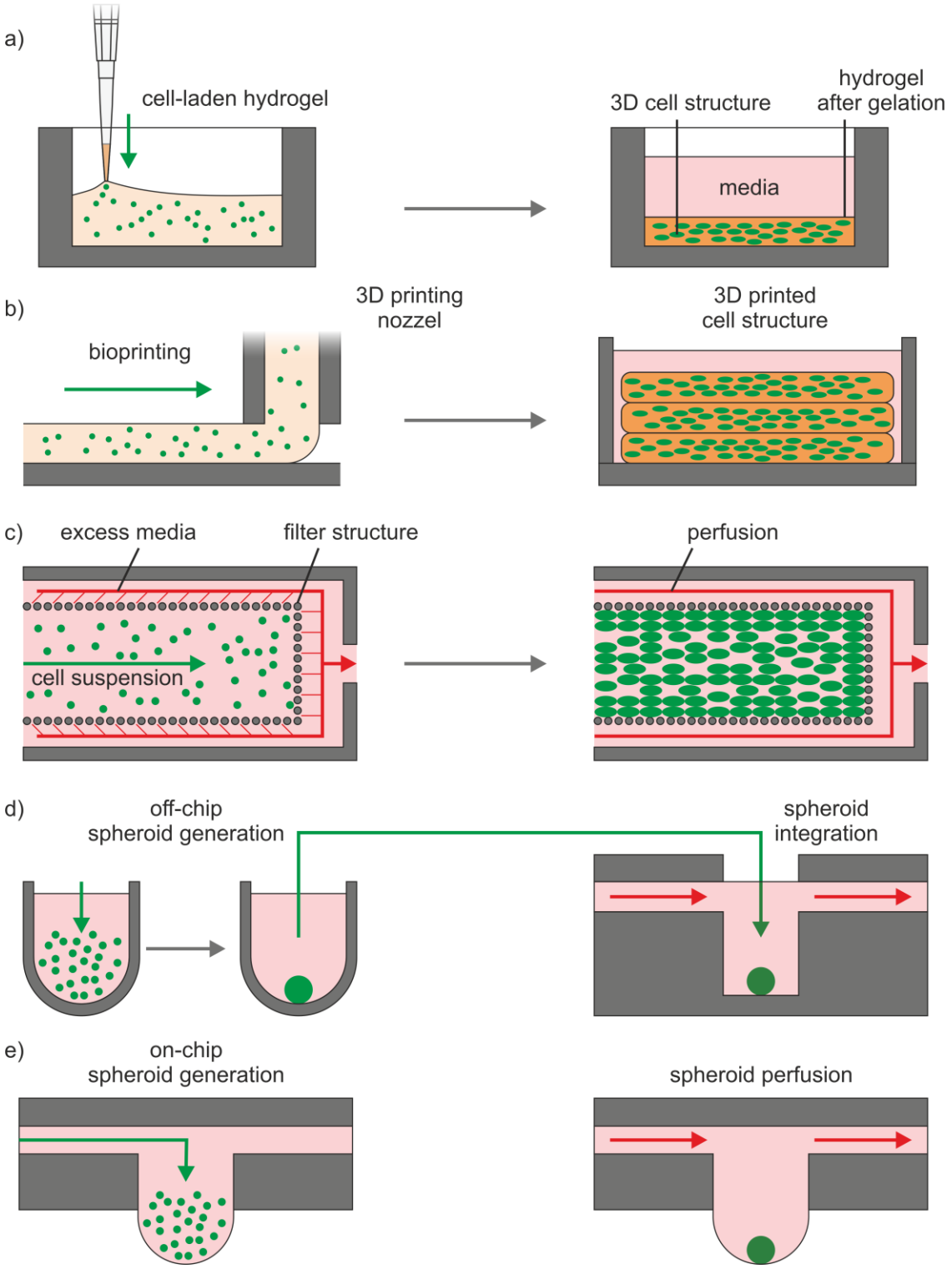

Figure 3.1 3D tissue generation in microfluidic systems: a-b) Hydrogel-based 3D tissue generation by a) mixing cells with a hydrogel and injecting the cell-laden hydrogel into a chip or by b) bioprinting a cell-laden hydrogel into a pre-defined print geometry. c) Filtration-based cell loading for 3D structure formation by cell retention in front of pores and removal of the excess media. d) Off-chip spheroid generation and integration into a chip for perfusion. e) On-chip spheroid generation and perfusion in hanging-drop system.

3.3 Organ-on-Chip

OoC systems culture human cells arranged into tissue or organ replicates under microfluidic perfusion and, thereby, aim at a more precise recapitulation of human physiology compared to traditional cell assays and animal models. A definition trying to cover all relevant aspects of an OoC device is as follows:

An OoC system is "*a fit-for-purpose microfluidic device, containing living engineered organ substructures in a controlled microenvironment, that recapitulates one or more aspects of the organ's dynamics, functionality and (patho) physiological response* in vivo *under real-time monitoring* [emphasis in original]", as defined in Ref. [114, p. 651].

On the one hand, the definition highlights that the scope of OoC technology goes beyond the efficient culture of cells in a miniaturized or microfluidic system. On the other hand, it makes clear that OoC systems are not aiming at building real organs but try to replicate specific functions of an organ or tissue. Thereby, the degree of complexity is depending on the specific application or research question that an OoC system is designed for (Figure 3.2).

The microfluidic chip allows for the control over the environment in which the tissue is embedded. The microfluidic channels in OoC systems, often in combination with porous membranes, aim at a recapitulation of a blood vessel including a vasculature-like perfusion of the tissue [115, 116]. Similarly, a popular barrier model uses a chip layout with two microfluidic channels sandwiching a porous membrane and 2D cell layers on both sides of the membrane [117, 118]. Cells and tissues in an OoC device can be stimulated in a targeted manner. Different substances or even cells can be transported through the chip [119]. Furthermore, OoC systems have the potential to exert controlled mechanical forces on a tissue [118, 120, 121]. Besides real-time monitoring by microscopy and off-chip analysis of the perfused media, OoC systems can be equipped with on-chip sensors for specific *in situ* readouts such as dissolved oxygen in the media [122].

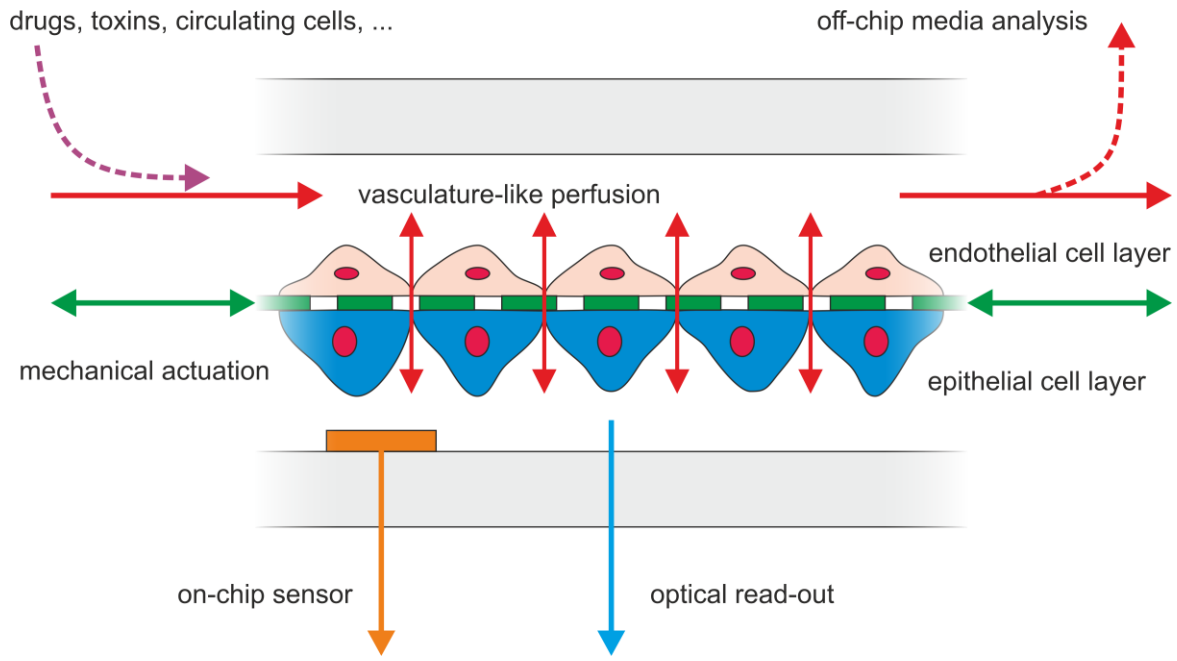

Figure 3.2 Elements of a fit-for-purpose OoC system: Different levels of complexity can be implemented on an OoC system, such as, the integration of a vasculature-like perfusion, the exertion of mechanical forces or the perfusion of substances for the targeted stimulation of cells and tissues. In addition to the optical readout of cells and tissues, the perfused media can be analyzed off-chip or with on-chip sensors.

In general, OoCs combine achievements in microfluidic, cell-based research, cell biology and tissue engineering [7]. Thereby, the term organ-on-chip is usually attributed to the pioneer work of Donald E. Ingber and co-workers due to the famous lung-on-chip system from Huh *et al.* that demonstrated organ-level functions in a stretchable microfluidic device [118]. However, this systems shares similarities to an earlier microfluidic airway system from Huh *et al.* without mechanical actuation [123]. This demonstrates that the basis for OoC research origins from even earlier work. According to Zhang *et al.*, it can be traced back to the early 1990s [7], with an *in vitro* system for the patterned growth of rat heart cells marking one of the earliest milestones [124].

Other important devices paving the way of OoC were developed by Michael L. Shuler and co-workers that achieved the connection of lung and liver cells by fabricating a microfluidic network with culture chambers in a silicon-based cell culture analogue [125, 126]. For instance, Viravaidya *et al.* demonstrated that their system is capable of replicating a physiologically based pharmacokinetics (PBPK) model showing the impact of toxin metabolites produced from liver cells in one of the chip compartments on lung cells embedded in another, connected chamber [125].

A disruptive biologic discovery impacting OoC is the reprogramming of adult cells from mice or human into induced pluripotent stem cells (iPSC) [127, 128]. It has been shown that it is possible to generate iPSC from humans, for instance with different genetic diseases [129]. In combination with the recent development of differentiation protocols of iPSC into various single cell types or multi-cell type organoids, a basis is created for complex, patient-specific and disease-specific cell and tissue models [130, 131]. This technology has also found its way into OoC research and resulted, for instance, in OoC systems integrating cardiomyocytes [106], or retinal organoids [111] both derived from human iPSC. An alternative way for the personalization of OoC systems is the integration of adult cells directly from patient-derived biopsies. Recent examples are the integration of white adipocytes from skin biopsies in a WAT chip [99], or lung epithelial cells from lung biopsies [132].

Overall, the combination of a precisely controllable microfluidic environment, readout technology and patient-specific cells demonstrates the potential of OoCs as microphysiological tissue models for the discovery and development of new drug candidates or even for personalized medicine [8, 133].

Even though OoC is still an emerging technology, the overall interest in OoC has led to multiple commercialized systems [10]. So far, already a few OoCs have been used as supporting tools by the pharmaceutical industry in the development process of new drugs [6]. However, it is also worth mentioning that up to now no submission for drug approval is known that included data from OoC systems [11], which shows that there are still several hurdles in the way of OoC research.

3.4 Scale-up of Organ-on-Chip Systems

A general concern regarding the future progress of OoC is the transition from individual modules with only one or a few tissues per chip to parallelized and automated systems for higher-throughput applications. Though current OoC systems are still far away from high-throughput systems, first milestones towards OoC scale-up have been presented in recent years [13]. Thereby, important key aspects that determine the scalability of OoCs are suitable industry-compatible fabrication techniques, parallelization in order to increase the number of tissues per chip and automation approaches for perfusion and readouts.

3.4.1 Scalable Fabrication Technologies

The emergence of PDMS fabrication technologies in the late 1990s has immensely influenced the field of microfluidic research [54, 33, 134]. Compared to traditional glass or silicon-based approaches, PDMS replica molding and plasma-activated bonding are simpler, faster and require less sophisticated equipment. Therefore, it is not surprising that most OoC devices in academia and even a few commercial system use PDMS components [7, 10, 117].

Highly optimized PDMS fabrication protocols have been developed, for instance, using multiple 3D printed molds placed in a rig for parallelized molding of channel modules [135]. However, several manual handling steps, such as PDMS degassing and pouring, demolding, chip trimming as well as alignment of multiple chip layers during bonding, remain in the overall fabrication process. Furthermore, the throughput of PDMS fabrication is especially limited by the curing times required for crosslinking PDMS and take usually several hours for each chip component. Reduced curing times are achievable by increased curing temperature but go hand in hand with higher shrinkage of the PDMS mold after crosslinking [136]. This is especially a limitation for large PDMS modules [137]. This indicates that the fabrication of OoC devices in PDMS with larger footprints, for instance well plate size, is difficult if correct channel alignment between multiple fluidic layers is required.

Furthermore, there is growing awareness that PDMS can interfere with microfluidic cell culture and especially OoC systems [32, 138]. Observations such as small molecule or drug absorption into the bulk of PDMS [37, 139], leaching of uncrosslinked PDMS components into the cell culture media [38, 140] and osmolality shifts due to high evaporation [141] raise the question if PDMS is reliable enough for OoC applications (Figure 3.3).

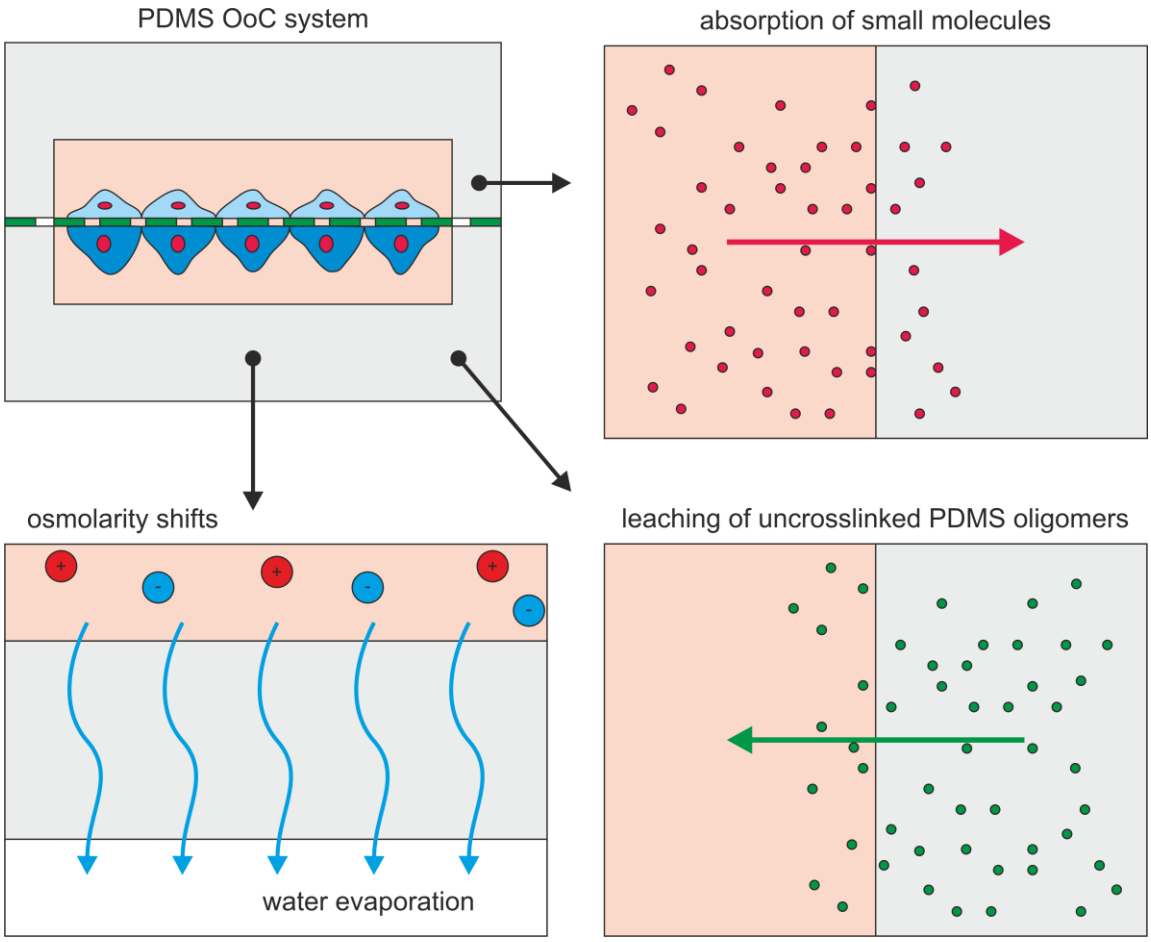

Figure 3.3 Known challenges of PDMS-use for OoC systems: Absorption of small, hydrophobic molecules into the bulk of PDMS channel walls, leaching of uncrosslinked PDMS oligomers into the cell culture media and high water transmission rates that can lead to changes in osmotic concentrations.

Due to the challenges related to PDMS as chip material and to its limited fabrication scalability, alternative materials are being explored in microfluidic research [138]. Promising substitutes are thermoplastics that enable microfluidic systems featuring less absorption and water transmission than PDMS-based devices and are based on cheaper raw materials with comparable transparency [41]. Thermoplastic device fabrication ranges from in-house, rapid prototyping techniques [62, 142] to industry-scale production using micro-injection molding [39, 57]. However, the latter requires expansive machinery that is unusual for labs focusing on OoC development. In recent years, external contract manufacturing became an affordable option for medium scale fabrication. For instance, so-called rapid injection molding became a feasible method for higher-throughput fabrication of thermoplastic systems with batches in the range of 500-10,000 chips without the need for in-house machinery [143].

A limitation of rigid thermoplastic systems is that some OoC models require mechanical actuation [144–146], the integration of thin, porous membranes [111, 99, 147], or even a

combination of both [118, 120, 121]. For all of these aspects, PDMS remains the most prominent chip material. However, there are several, alternative strategies to achieve flexible chip components or to integrate membranes into PDMS-free systems.

If flexible chip elements are essential for the respective OoC device, TPE is a promising alternative to PDMS. Thermoplastic fabrication approaches are transferable to TPE and allow for thermal bonding between flexible TPE layers and thermoplastics [148]. Furthermore, it has been shown that the complete transfer of monolithic PDMS systems into TPE is feasible and achieved by using industry-scale techniques, such as injection molding [60].

An advantage of PDMS-based fabrication approaches is that the integration of membranes is well established. PDMS allows for membrane integration by joining PDMS chip parts and PDMS membranes using plasma activation [135] or using different amounts of curing agent in the respective chip parts [149]. Similarly, membranes from other materials are frequently simply sandwiched between clamped or plasma-bonded PDMS chip parts [150–152], or surface functionalized for covalent connections to PDMS [78, 79].

The integration of membranes into PDMS-free systems poses more challenges but is also possible. Promising techniques and substitutes for PDMS have been recently reviewed in detail in a collaborative study (*cf.* Table 3.1) [80]. The use of clamping setups [153, 154], adhesives [155] and surface functionalization [156, 157] are rather manual but in-expansive approaches ideally suited for prototypes. Sophisticated fabrication techniques for the direct patterning of pores into chips by ion-track etching or phase separation have been presented but might either not be feasible with the standard lab equipment of OoC developers [158], or result in undesirable, opaque chips [159]. Therefore, scalable integration techniques for thermoplastic systems that are promising for higher-throughput OoC fabrication are thermal fusion bonding [160, 161], ultrasonic welding [162], laser welding [163] and solvent bonding [164–166]. Besides thermoplastics, Ostemer/OSTE(+) [47, 48], or TPE [60, 167] are further PDMS substitutes that have been successfully used for membrane integration.

Table 3.1 PDMS-free membrane integration. Classification: "+" (good), "+/−" (medium), "−" (poor). Reproduced from Ref. [80] with permission from the Royal Society of Chemistry.

Integration	Equipment requirements	Process time	Scalability	Freedom in design and structure size	Remarks
Clamping	+	+	+/−	−	Usually requires gaskets.
Adhesives	+/−	+/−	+/−	+/−	Potential cytotoxicity of adhesives; Precautions against channel clogging required.
Thermal fusion bonding	+/−	+/−	+	+	Risk of membrane deformation during process.
Ultrasonic welding	−	+	+	−	Usually requires energy directors surrounding channel structures.
Laser welding	−	+	+/−	−	Requires absorbing, not transparent material or specialized coating.
Solvent bonding	+/−	+/−	+/−	+/−	Complete removal of toxic solvents is crucial; Precautions against excessive solvent exposure required.
Surface chemistry	+/−	−	−	+	Complete removal of toxic solvents and unbound reagents required.
TPE-based bonding	+/−	+	+/−	+	Usually requires hot embossing for structuring; Flexible TPE with low structural support.
OSTE(+)-based bonding	+/−	+	+/−	+	Relative high material costs; Reduced transparency < 420 nm.
Porous chip material	−	+/−	−	+/−	Ion-track generation: access to irradiation apparatus (*e.g.* particle accelerators) required; Phase separation: opaque materials.

3.4.2 Parallelization Approaches

Most OoC systems are still individual units that integrate one or only a few tissues per system but in recent years more and more parallelized OoC platforms evolved and increased the number of microtissues per chip. Thereby, microwell plates act as model for most parallelized OoC systems. Microwell plates feature a standardized arrangement of open wells in a rectangular matrix with equal distance according to the number of wells per plate. Well plates are the common platform for parallelized experimentation in biomedical research and drug discovery and compatible to automated workflows, for instance, high-throughput screening applications with cell assays [12].

Therefore, a frequent approach to parallelize OoC devices is to arrange multiple, identical systems on a single platform with a well plate conform arrangement. For instance, Phan *et al.* placed twelve identical systems on a 96-well plate format and used some of the wells as ports for the individual microchannels [168]. In order to fit to the standardized well layout, parallelization required the adaption of the initial system, which was earlier presented for the generation of vascularized microtumors [169]. Thereby, Phan *et al.* used a single PDMS mold featuring the multiple, individual systems and bonded it to a bottom-less well plate [168]. Another possibility is to insert individual OoC devices into an adapter or cartridge featuring the outer dimensions of a standardized well plate [110]. This approach is attractive for integrating OoC prototypes that are frequently based on microscope slides into a parallelized workflow without changing the overall chip design. Using this approach, Lohasz *et al.* integrated four chips with microscope slide dimensions in a well plate adapter that enabled the use of liquid handling robots for loading 80 pre-formed spheroids into the individual ports, which were located on standard well positions [110].

An even higher amount of individual OoC systems on a single plate was presented previously [170]. Thereby, 96 two channel systems and 40 three channel systems were arranged on a well plate footprint and enabled later studies, for instance, on barrier integrity in intestinal tubes [171], or on endothelial cell sprouting [172]. The underlying concept of these systems relies on so-called phaseguides [173]. Phaseguides line neighboring channels and allow for meniscus pinning of a fluid, such as a cell-laden hydrogel, during injection. After gelation, channels next to the hydrogel can be perfused without the need for a separating, porous structure.

Alternatively, a parallelized version of common two-channel setups with a sandwiched membrane have also been presented recently [174, 175]. This platform distributes in total 96 systems with two perfused channels each homogeneously on the footprint of a 384-well plate.

Thereby, the central region of the individual OoC systems form a standard 96-well plate matrix, which enabled the use of a rapid imaging system for high content screening [176].

It is a common approach to 'outsource' complexity and integrate further, functional components to well plate sized OoC systems through an additional well plate lid or base. For instance, Tan *et al.* developed a well plate lid for their system that integrates multiple micropumps for perfusion [174, 175]. In a later version an additional electric sensing setup for trans-epithelial electrical resistance (TEER) measurements was integrated by using the perfusion cannulas from the perfusion lid as electric contacts [176]. Similarly, but lacking components for perfusion, a lid for TEER measurements has been introduced to phaseguide-based, parallelized OoC systems [177].

Following the alternative approach of a well plate base, Domansky *et al.* developed a pumping manifold into the base of a parallelized liver system allowing for perfusion in the individual wells [178]. In this version, up to twelve scaffolds seeded with cells can be cultured in parallel. Besides increasing the number of independent replicates, updated versions of this system aimed at the perfusion and connection of multiple, different organs in a single device [179, 180]. Thereby, the individual organ models are formed by seeding porous scaffolds in-chip with cells or prepared off-chip in transwell inserts before being transferred into the platform [179, 180]. Another multi-OoC system uses a comparable perfusion platform underneath the well plate system but allows for a customizable arrangement of up to twelve open, plug-in wells that hold the individual transwell inserts or cell-seed scaffolds [181].

Hanging drop technology provides another possibility to arrange and perfuse multiple spheroids in a homogenous matrix arrangement. Thereby, up to 192 spheroids have been generated on chip by flushing cell suspension into each row of the drop array [113]. At the same time, each line of the drop matrix can be individually perfused by a pump in perpendicular direction to cell loading.

In principle, systems have been developed that generate drastically higher amounts of microtissues per chip, such as a previously presented system generating 500 cell-laden hydrogel compartments [182]. However, this device lacks the possibility to independently address the individual hydrogel compartments and to create different conditions on the chip.

For this purpose, monolithic valves, often called Quake-valves referring to the work by Stephen R. Quake and co-workers [183], provide a powerful tool for on-chip fluid manipulation. These valves have been integrated into highly-multiplexed, microfluidic bioreactors, which usually

lack the flexibility in tissue generation required for OoC but demonstrate successful parallelization and automation approaches in principle adaptable to OoC. Thereby, an important achievement of these systems is the possibility to program a fluidic path on the chip and independently perfuse the individual culture compartments on the device. For instance, Gómez-Sjöberg *et al.* integrated in total 96 independent addressable culture chambers in a single device [184]. More recently, parallelized bioreactors have been presented with 1,500 independent culture compartments [185]. However, another limitation of those systems are the numerous tubing connections and pressure controllers that are required for actuating the individual valves. Similarly to the outsourcing of complexity in well plate OoCs, Vollertsen *et al.* developed a base for their system that enables a modular bioreactor configuration [186]. Thereby, up to three modules with each featuring a bioreactor with 64 culture chambers can be plugged into the base module. All pressurized control channels for valve actuation are connected to the base and guided to the individual modules with built-in connectors. Though, the overall number of connected tubing is still high, solely lines that are required for actual transport of media or cell suspension are connected to the individual bioreactors.

3.4.3 Integrated Fluid Actuation

Defined fluid flow is one of the key components in OoC systems that allows to control the microenvironment of the cultured tissues and organs and is required for emulating the *in vivo* blood flow. Several technologies have been developed for fluid actuation in microfluidic channels and have found adaption in microfluidic cell culture and OoC systems [187].

OoC systems can be categorized depending on the respective fluid circuit on the chip. Open-loop, also called single-pass, systems pump fluid only a single time through the chip, while closed-loop systems recirculate the effluent back to the inlet of the chip (Figure 3.4 a). Open- and closed-loop setups allow for different applications. For instance, open-loop systems allow for steady input concentrations and one-way, consecutive organ communication, whereas closed-loop systems enable the study of time-dependent effects and bidirectional multi-organ effects [188].

Off-the-shelf solutions are available for both open-loop and closed-loop perfusion. Syringe pumps create a precisely controllable volumetric flow rate by moving the plunger of a syringe with a set speed (Figure 3.4 b). Those pumps are frequently used for unidirectional fluid flow and have been applied in numerous OoC systems [111, 118, 189]. Commercially available pumps for closed-loop perfusion are, for instance, peristaltic pumps and pressure pumps (Figure

3.4 c, d). Common peristaltic pumps displace fluid in a flexible tubing and can be connected into a closed circuit with in-line connected chip and reservoir for unidirectional circulation [190]. Pressure pumps usually create a single-pass fluid flow from a pressurized reservoir through a microfluidic channel. However, setups for unidirectional, closed-loop perfusion are available as well. Those setups use multiple, periodically actuated valves for switching air pressure levels and fluid flow between two reservoirs that periodically switch between feeding or collecting media to or from the perfused chip [119, 191].

Though external pumps provide a straightforward solution for fluid actuation, they are usually expansive, bulky and require tubing connections to the channels. Overall, this increases the complexity of an OoC system and its operation hence interferes with automation approaches. Especially the tubing is problematic as it requires time consuming preparation, increases the overall systems' dead volume and bears the risk of leakage and molecule ad- and absorption [192–194].

Integrated fluid actuation in microfluidic systems provides an alternative to external pumps and allows for a tubing-free perfusion, for instance, by frequently applied hydrostatic or gravity-driven pumping. Gravity-driven pumping is based on a difference in fluid level between in- and outlet reservoirs. A prolonged hydrostatic fluid flow can be achieved by fluidic resistors [195], however, a constant flow rate due to the declining level difference requires adaptions to gravity-driven pumping. This has been achieved, for instance, using horizontally tilted reservoirs [196]. For closed-loop perfusion, several OoC systems are mounted on rocker setups for periodic tilting, which results in a bidirectional circulation [110, 171]. However, the physiologic emulation of *in vivo* blood flow requires unidirectional circulation. Especially endothelial cells are sensitive to bidirectional flow patterns, which can trigger inflammatory reactions [197]. Thereto, adaptions to gravity-driven pumping are required that prevent backflow during reverse tilting (Figure 3.4 e). A possible adaption is, for instance, including a bypass between the reservoirs that guides the effluent back into the inlet reservoir together with capillary valves that limit backflow in the perfused channel during reverse tilting [198]. However, this technique leads to inevitable, periodic flow interruptions. Though flow without interruption using a rocker has been presented, it only achieved unidirectional perfusion in a short-cut channel between two bidirectional perfused channels [199]. Alternatively, unidirectional and closed-loop flow is as well achievable by refilling feed reservoirs with effluent (Figure 3.4 f). This has been recently presented in a parallelized, OoC in well plate format [174, 175]. However, the presented setup requires a complex multi-layer lid featuring a pneumatic actuated micropump for each channel on the plate.

Another approach for integrated fluid actuation are peristaltic pumps that are directly integrated into the chip. Identically to their macroscopic counterparts, these miniaturized, integrated pumps are ideally suited for unidirectional, closed-loop perfusion. Identical to external peristaltic pumps, the underlying fluid transport relies on fluid displacement by mechanical actuation, for instance, an elastic, dense membrane (Figure 3.4 g). Pneumatic actuation of integrated, peristaltic pumps is a frequently applied method, for instance, for perfusion of a multi-well system [200], or a parallelized liver-on-chip [178].

A general limitation of pneumatic actuated pumps is that they are not (pneumatic-)tubing-free. Common concepts of pneumatic diaphragm micropumps require three externally controlled gas pressure lines to the chip for each individually addressable pump [201]. For instance, a recently presented platform connecting up to ten organs in a multi-OoC uses in total 36 pneumatic lines switching between two pressure levels [179].

Several alternatives to pneumatic actuation for integrated peristaltic pumps have been presented. For instance, moveable braille pins from a tactile display [202], deflectable piezoelectric discs [203], electromagnetic actuators [181], or integrated permanent magnets that are actuated with magnets outside the chip [204]. Besides, periodic actuation of multiple, in-line connected valves, peristaltic pumping is achievable by compressing flexible channels with an object and moving it along the channel (Figure 3.4 h). This approach has been presented in external, micropumps using dragged steel balls on top of a flexible PDMS channel, which were actuated with moving, permanent magnets [205, 206].

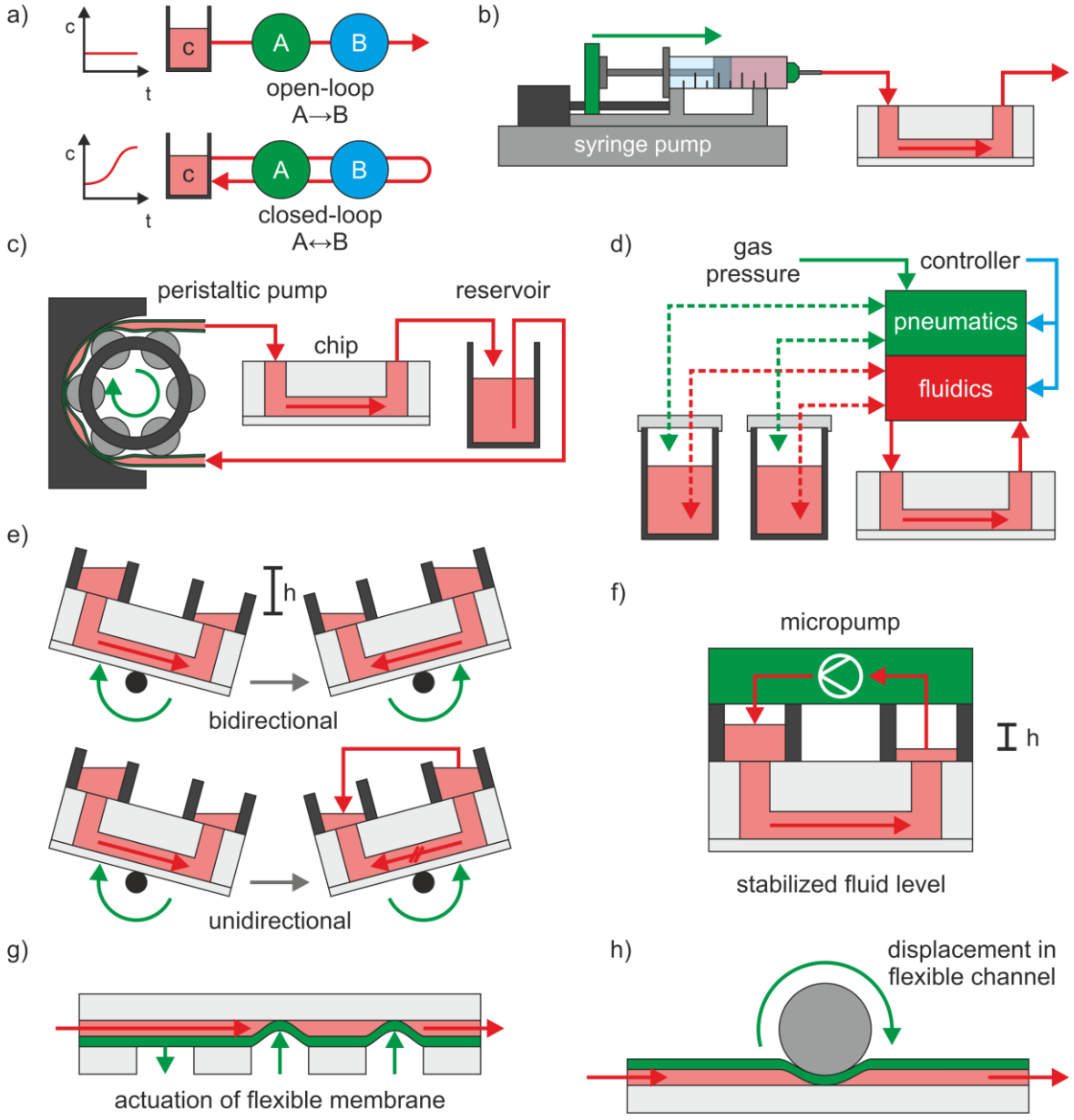

Figure 3.4 Fluid actuation in OoC systems: a) Open-loop configuration for steady input condition and one-way communication. Closed-loop configuration for time dependent effects and bidirectional organ communication. b) Open-loop perfusion with external syringe pump. c) External, peristaltic pump system with in-line connected chip and reservoir. d) Pressure pump setup with external, controlled pneumatic and fluidic valves for fluid circulation. e) Hydrostatic perfusion through periodic tilting of a chip. Unidirectional, circulatory flow requires measures against backflow in the microchannel during back tilting. f) Stabilized, hydrostatic perfusion by pumping the effluent continuously back into the inlet reservoir. g-h) Integrated, peristaltic pumps allow for circulatory perfusion by g) periodic actuation of a flexible, dense membrane or h) dragging an object on top of a flexible channel for fluid displacement.

3.5 Centrifugal Microfluidics

Different to conventional Lab-on-a-Chip (LoC), centrifugal LoD systems enable the actuation of various steps of analysis workflows primarily by centrifugation and capillary forces.

Centrifugal microfluidic systems evolved over the last decades mainly as a sample-to-answer tool in diagnostic settings [17]. As reviewed in Ref. [17], early centrifugal analyzers were already developed in the 1960s to 1970s [207, 208], whereas the overall field of LoD expanded rapidly after Marc J. Madou and Gregory J. Kellogg introduced their centrifugal platform for miniaturized, diagnostic tools aiming at point-of-care applications and field use [209].

Centrifugal microfluidic platforms unite two important aspects: 1) centrifugal systems do not require external pumps or tubing as they rely primarily on centrifugation and 2) several systems can be operated simultaneously on a single device by arranging them symmetrically around the rotation axis. Thereby, centrifugal microfluidics provides a promising alternative to conventional, microfluidics for automatable high-throughput applications.

So far, numerous unit operations have been implemented on microfluidic discs, such as liquid transport, valving, flow switching, aliquoting, mixing, separations and optical detections [14]. LoD research focuses primarily on biomedical diagnostic applications [14, 17, 18]. Recent examples are:

- isolation of extracellular vesicles (EV) [210], platelets [211], or circulating tumor cells from biological samples [212].
- detection of respiratory tract infection pathogens [213], or mosquito-borne diseases both by on-disc reverse transcriptase polymerase chain reaction [214]
- incubation, lysis and analysis of bacteria focusing on antibiotic susceptibility tests [215]

In principle, microfluidic discs are capable of processes that are also important for an OoC system, such as pumping of media and cell transport by centrifugal forces. For instance, centrifugal, single-cell trapping has been presented using discs [216, 217] and combined more recently with optical tweezers for cell manipulation [218], as well as with label-free, optical readout approaches [219].

Besides single-cell trapping, centrifugal cell loading into microwells at the periphery of a disc has been used to generate single and multi-cell type spheroids under continuous hyper-gravity ($\geq 26 \times g$) but without perfusion during self-assembly of the cells into spheroids [220]. Therefore, this technique provides primarily an alternative to static cell culture techniques for

spheroid formation, such as centrifugation of well plates with pyramid-shaped microwells [221], however demonstrates as well the feasibility of on-disc tissue generation.

Besides cell centrifugation, centrifugal systems are as well suited for versatile fluid transport by so-called centrifugal pumping that solely requires rotation of the disc [27, 209]. First attempts in the direction of perfused cell culture using centrifugal pumping have been presented. Focusing on the implementation of cell-based assays on disc, centrifugal pumping has been used for media and assay reagent transport in and out of chambers with adherent 2D cell layers [222]. Other disc systems achieved media agitation, similar to shake flask culture, in a chamber for *Pichia pastoris* (yeast) culture [223], or periodic media exchanges for the culture or *Caenorhabditis elegans* (worms) [224]. Though these systems present important operations required for cell assays or microfluidic cell culture systems, they are lacking important aspects of OoC, such as physiologic tissues with continuous, vasculature-like perfusion.

Finally, recent studies demonstrate the overall compatibility of centrifugal unit operations and OoC research. For instance, breast cancer-derived EV were isolated using a centrifugal disc and then injected into a conventional liver-on-chip system in order to study the roll of EV during breast cancer metastasis [225]. Alternatively, placing an OoC device into a centrifuge tube and using a lab centrifuge for centrifugal cell loading allowed for dense cell packing in a heart-on-chip that was afterwards perfused with conventional syringe pumps during culture [147].

4 Objectives

The focus of this thesis is the development of a novel platform technology that provides a foundation for higher-throughput OoC applications. Thereby, the primary goal was to build the basis for a parallelizable and automatable generation of microtissues with precisely tailorable shape and cellular composition as well as their culture under controllable microfluidic flow. Building on the achievements of centrifugal microfluidics, this platform technology should adapt and implement rotation-based processes for the individual unit operations in order to reduce manual handling and equipment requirements.

To realize this the following sub goals featuring distinct requirements needed to be achieved:

The platform should feature a compact footprint and allow for industry-compatible fabrication processes. This includes the application of materials that eliminate the limitations of PDMS and enable a rapid but also precise microfabrication. The individual processes for structuring and bonding should be compatible with a wide range of materials and pave the way for a scalable, higher-throughput fabrication.

The tissue generation in this platform should allow for the construction of microtissues with a precisely tailorable structure and physiologic function. The platform should demonstrate compatibility with processes for different cell and tissue types. At the same time, the tissue generation should be parallelizable, cell-efficient and require minimal, manual handling steps.

The microfluidic perfusion during cell culture should be achieved without external pumping equipment and avoid obstructive tubing connections. The integrated fluid actuation in this platform should stand out through low technical requirements in terms of chip material, fabrication and operation hardware as well as precisely controllable flow conditions.

The platform requires compatibility to different readout technologies that allow for the assessment of cell and tissue viability and functionality. This includes the possibility for visual inspection by high-resolution microscopy and the continuous access to the perfused media. The latter should be amenable for analysis of the perfused media as well as treatment of tissues during culture.

5 Materials and Methods

5.1 Organ-Disc Fabrication

5.1.1 Materials

Organ-Discs were fabricated using commercial PMMA, PC and COC foils as well as track-etched polyethylene terephthalate (PET) membranes (Table 5.1). Custom TPE foils were used for the fabrication of flexible Organ-Disc layers, which were extruded from commercial SEBS pellets into approx. 750 µm thick films by an external service provider (Fraunhofer Institute for Process Engineering and Packaging IVV).

Table 5.1 Materials used for Organ-Disc fabrication and the applied structuring method for the individual materials.

Material	Product, Manufacturer	Structuring
175 µm PMMA	PLEXIGLAS Resist Clear 99524 GT, Röhm	Laser cutting, plotting
75 µm PMMA	PLEXIGLAS Film 0F072, Röhm	Plotting
15 µm PET	track-etched membrane, 3 µm pores, 030444, SABEU	Plotting
2 mm PMMA	Oroglas cast acrylic glass, Trinseo (former: Arkema)	Laser cutting
750 µm SEBS	Mediprene OF400M, HEXPOL TPE AB	Hot embossing
500 µm PC	Makrofol DE 1-1, Covestro	Hot embossing
175 µm PC	Makrofol DE 1-1, Covestro	Plotting
240 µm COC	EUROPLEX Film 0F305, Röhm	Plotting
80 µm COC	EUROPLEX Film 0F305, Röhm	Plotting

5.1.2 2D Structuring

Channels in thermoplastic Organ-Disc layers were generated by 2D structuring techniques as described in Ref. [226] and Ref. [227]. Briefly, in Organ-Discs, used for centrifugal cell loading and perfusion, PMMA layers as well as PET membranes were structured using a CO_2 laser cutter (VLS2.30, Universal Laser Systems). Solely the media channels in 75 µm PMMA as well as 175 µm PMMA for Organ-Discs with a peristaltic pump were structured using a knife plotter (Graphtec CE6000–40 Plus, Graphtec).

In the case of COC and PC foils, all channel structures were generated by plotting. In both structuring processes, cuts through the whole material thickness were performed. Afterwards, cutouts were peeled out and the surfaces cleaned with cleanroom tissues soaked with isopropanol (IPA) and compressed nitrogen before bonding the individual Organ-Disc layers.

5.1.3 Hot Embossing

The hot embossing stamp fabrication as well as hot embossing of TPE was used for the fabrication of peristaltic pump modules and TPE-hybrid fabrication, as described in detail in Ref. [227] and Ref. [228] respectively.

Stamp Fabrication

The overall epoxy stamp fabrication was adapted from previous studies [83, 229] and is based on three, successive steps: i) generation of SU-8 structures, ii) replica molding of SU-8 with PDMS and iii) replica molding of PDMS with epoxy resin.

This procedure is here exemplary described for the fabrication of TPE pump modules [227]. In the first step, photoresist (SU-8 2075, Kayaku Advanced Materials) was spin coated with 1500 revolutions per minute (rpm) final speed on a silicon wafer (150 mm, Siegert Wafer) and soft baked (7 min at 65 °C, 30 min at 95 °C). Microchannel layouts were designed (CorelCAD 2018, Corel Corporation), printed on transparent films by an external service provider (KOPP-desktopmedia) and used for UV light exposure of the SU-8 (275 mJ/cm^2, ABM Series 60 Exposure Systems, ABM, Inc.). After post-exposure baking (5 min at 65 °C, 12 min at 95 °C), SU-8 was developed (16 min, SU-8 developer, Kayaku Advanced Materials) and washed with IPA. After the following hard bake (30 min at 160 °C), wafers were coated overnight with trichloro(1H,1H,2H,2H-perfluorooctyl)silane (Sigma-Aldrich) in a desiccator at reduced pressure.

In the second step, intermediate PDMS molds were generated by replica molding of the SU-8 structures with freshly mixed PDMS (Sylgard 184, Dow Corning) in a 10 : 1 base : curing agent mass ratio. In order to achieve molds with a homogenous thickness and without meniscus, an O-ring (138 × 2 mm FPM 75, Dichtelemente arcus) was mounted around the photoresist structures on the wafer and both clamped between PMMA plates. PDMS was degassed and injected by under pressure into the generated cavity above the microstructures with syringes (50 mL, BD Plastipak, BD) connected to ports in the upper PMMA plate. After curing overnight at 60 °C (Universal Oven UN110, Memmert), PDMS was demolded, cleaned with IPA and compressed nitrogen.

For the third step of epoxy replica molding, a molding tool was developed and CNC-manufactured in aluminum by an external service provider (CNCTeile24). Intermediate PDMS molds were inserted into the tool and replica molded with a two-component (100 : 16 parts A : B mass ratio) epoxy resin (EpoxAcast 670 HT, Smooth-On). For reduced viscosity of the resin, part A was supplemented with 10% (w/w) epoxy thinner (Epic Epoxy Thinner, Smooth-on). Prior injection, the resin was degassed for 3 min in a desiccator and inserted for 10 min in an ultrasound bath (JP-031S, RS PRO). For the first 24 h for partial curing of the epoxy inside the tool, a vacuum pump was connected to the tool's base plate (LABOPORT N 86 KN.18, KNF), which generated a vacuum underneath the PDMS for air bubble removal. The epoxy-filled syringes remained attached to the tool after resin injection and during the first 24 h of RT curing. This is intended to counteract the small (0.2% according to the manufacturer) shrinkage of the epoxy resin during curing.

Subsequently, the pump and syringes were disconnected and the tool placed for 24 h at 60 °C for complete epoxy curing. At this point, the epoxy was demolded from the tool and tempered (2 h at 80°C, 3 h at 150 °C, Universal Oven UN30, Memmert) and then slowly cooled-down to RT.

Hot embossing stamps with semicircular channel structures were fabricated by 3D printing of a temperature stable resin (High Temp Resin, Formlabs) using a SLA printer (Form 3, Formlabs). After printing, stamps were washed (Form Wash, Formlabs), dried at RT for 30 min and cured for 60 min at 60 °C as well as UV light exposure (Form Cure, Formlabs).

TPE Hot Embossing

For TPE structuring, hot embossing stamps were placed on the extruded TPE films, which were previously laminated on 250 µm polytetrafluoroethylene (PTFE) carrier foil (High-tech-flon films and fabrics) and supported by a 150 mm silicon wafer. The stamps were hot embossed into TPE using a manual hot press (LabManual 300, Fontijne Presses) at 140 °C for 10 min with 0.4 MPa in the case of peristaltic pump channels and 0.8 MPa for channels with semicircular cross-section. Before opening the hot press, the plates were water cooled in 4-5 min below 40 °C. TPE layers were demolded applying a few drops of IPA and cut to size. Through holes in the TPE were punched (World Precision Instruments) or drilled (RoNa Werkzeuge).

PC/TPE-hybrid embossing was identical to standard TPE structuring but with the difference that TPE was laminated on to 500 µm PC instead to PTFE carrier foils and embossed at 130 °C with 0.8 MPa. During embossing, PC layers were placed on mirror polished, stainless steel plates (TGA GmbH), which were previously coated with a release agent (Weicon).

5.1.4 Bonding

Solvent Vapor Bonding

Solvent vapor bonding was adapted from the original protocol in Ref. [230] and used for stepwise bonding of Organ-Discs consisting of PMMA layers and a PET membrane, as described in detail in Ref. [226]. Briefly, PMMA was exposed for 4 min to evaporating chloroform (pure, stabilized with ethanol, neoLab) at RT, whereas PET surfaces remained untreated. For this step, the PMMA layers were attached to the lid of a glass Petri dish (Anumbra, $120 \times 20 mm^2$, neoLab) using small magnets and the bottom dish filled with chloroform. After 4 min of exposure to the chloroform vapor, PMMA layers developed an adhesive surface and were then laminated on another, untreated PMMA layer using an alignment jig based on two 8 mm PMMA plates with aluminum pins. Silicone layers (2 mm, Elastomer plate VMQ 50 Shore A, Angst+Pfister) were added on both sides of the jig for a homogenous pressure distribution during subsequent bonding in an automated hydraulic press (LabEcon 150, Fontijne Presses). PMMA-PMMA and PMMA-PET membrane bonds were pressed for 10 min with 50 kN (approx. 6.4 MPa) and 25 kN (approx. 10.4 MPa) respectively at RT. Then, Organ-Discs were placed overnight in a vacuum oven (60 °C, 20 mbar, Model VD 23, Binder) for solvent removal.

Thermal Fusion Bonding

Thermal fusion bonding was used for the fabrication of the disc-shaped module in Organ-Discs with a peristaltic pump, as described in detail in Ref. [227]. A thermal fusion bonding tool for parallelized bonding of up to seven Organ-Discs was developed and manufactured in aluminum by an external service provider (MAAS Vorrichtungsbau). The aluminum base plate was equipped with pins (DIN 427 M5 screws, Reidl) for the alignment of individual disc layers. Inside the tool, the individual thermoplastic layers were sandwiched between two polished, stainless steel plates (0.8 mm, TGA GmbH), as well as two silicone layers (1 mm, Elastomer plate VMQ 50 Shore A, Angst+Pfister) facing the bottom and top aluminum plate of the tool.

For temperature measurements, four thermocouples (type K, class 1, KA01-3, TM Electronics) were attached to different spots inside the tool and read out in 1 s intervals with a data logger (RS-1384, RS Components). Thermal fusion bonding was conducted in a pre-heated, automated hot press (LabEcon 150, Fontijne Presses). After reaching a stable plate temperature, the tool was inserted and the hot press closed at the lowest possible pressure (approx. 0.18 MPa per disc). After reaching a stable temperature inside the tool, the pressure was increased to the respective bonding pressure. After the respective bonding time, the press was opened and the tool removed from the press and cooled down to RT overnight before removing the bonded discs.

TPE Bonding

For peristaltic pump integration into Organ-Disc, both TPE layers of the pump module were bonded after each other on top of PMMA-based discs, as described in Ref. [227]. Briefly, the TPE surface was activated for 1 min with a pressure < 2 mbar, 3.3 standard cubic centimeters per minute (sccm) O_2-flow and a power of 50 W inside a plasma generator (Zepto, Diener), laminated on top of the respective substrate and temporarily covered with a release liner film (3M Scotchpak 1022 Release Liner, 3M). For thermal fusion bonding, disc and TPE were placed between stainless steel plates, a weight (2-5 kg or 6-15 kPa) was added on top and all components placed in an oven (Universal Oven UN30, Memmert) for 1 h at 95 °C.

PC/TPE-hybrid layers were bonded by a similar protocol to various substrates by overnight incubation at 60 °C in an oven (Universal Oven UN30, Memmert) but without additional pressure, as described in more detail in Ref. [228]. The substrates were extruded, unprocessed TPE films, commercial COC and PC foils (*cf.* Table 5.1) as well as polystyrene (PS) cell culture dish surfaces (CELLSTAR, Greiner Bio-One).

5.1.5 Characterization Methods

The following characterization methods were used for the individual Organ-Discs from different material combinations including Organ-Discs used for centrifugal cell loading and perfusion [226], or peristaltic pumping [227], as well as for the characterization of PC/TPE-hybrid modules [228].

Structure Sizes

Structure sizes were measured from bright field microscopy images of channel top views and channel cross-sections that were obtained by cutting through the channels with scalpels or scissors. Images were acquired with a stereomicroscope (SteREO Discovery.V8, Carl Zeiss MicroImaging) and structure sizes measured with Fiji (Image J version 1.53c) [231].

Bonding Strength

The bonding strength of different material combinations was analyzed by connecting channels to an in-house nitrogen pressure line. For this, luer connectors (BDMFTLL-9, Nordson MEDICAL) were glued to channel inlets, whereas channel outlets were sealed in order to generate a dead-end channel. In both cases, epoxy glue (UHU PLUS ENDFEST, UHU) was applied and cured at RT for at least 24 h. The pressure was stepwise increased approx. every 10 s until either the bonding failed or the maximum pressure of the respective pressure setup was reached. Bonds in thermoplastic Organ-Discs and TPE pump layers were tested up to the highest possible pressure of 3.5 bar of the applied gas pressure controller (DR 022-00-3, Landefeld Druckluft und Hydraulik).

Bonds between PC/TPE-hybrid layers and respective substrates were tested in collaboration with Eduardo J. S. Brás [228]. In this case, all material combinations were stress tested immediately after bonding and after seven days submerged in phosphate buffered saline (PBS) (Dulbecco's phosphate buffered saline w/o calcium w/o magnesium, Biowest) at 37 °C inside an incubator (Heraeus BBD 6220, Thermo Scientific). For subsequent tests of the bonding strength, nitrogen gas pressures were increased up to 7.5 bar (maximum output pressure of the in-house nitrogen line).

During the bond strength test, the Organ-Disc and PC/TPE-hybrid devices were placed in a water bath for the observation of potential gas leaks. Nitrogen pressures were increased in 0.2-0.5 bar steps and holding the pressure for at least 10 s before going to the next, higher pressure.

Pressures were increased until gas leaked out of the channels, layers visibly bended or the maximum gas pressure was reached without failure.

Optical Properties

The optical properties of PC/TPE-hybrid layers, the base materials of the hybrid layers – unprocessed 750 µm TPE film and the 500 µm PC foil – as well as 1 mm PDMS and Ostemer layers (Ostemer 322 Crystal Clear, Ostemers) were analyzed in collaboration with Eduardo J. S. Brás, as described in Ref. [228]. Briefly, light absorption of the individual layers at wavelengths of 300-600 nm was analyzed using a plate reader (Infinite M200 Pro, Tecan). Thereto, the individual layers were placed in a 6-well plate (CELLSTAR, Greiner Bio-One) and the individual absorbance values were corrected for the absorbance of an empty well of the used 6-well plate and then converted into transmittance values.

5.2 Organ-Disc Spinner

The centrifugal loading and centrifugal perfusion setup were developed in collaboration with Oliver Schneider (Fraunhofer Institute for Interfacial Engineering and Biotechnology IGB, Stuttgart, Germany) [226].

5.2.1 Centrifugal Loading Setup

The centrifugal loading spinner was used for the initial filling of Organ-Discs with liquid, cell loading by centrifugal forces and initialization of the centrifugal perfusion. The cubicle case of the spinner was built from PMMA plates (5mm, Oroglas cast acrylic glass, Trinseo, former: Arkema) that were laser cut (VLS2.30, Universal Laser Systems) and connected with adhesive (45570, UHU). A brushless, direct current (DC) motor (QBL4208–41-04–006, TRINAMIC Motion Control) inside the spinner was controlled by a speed controller (367661, maxon motor) and a microcontroller (ATmega328P Board, Eckstein). A liquid-crystal display (LCD; I2C 16 × 2 LCD Display Module, Eckstein) and a rotary encoder (KY-040, reichelt elektronik) were connected to the spinner case and provided a user interface together with the microcontroller for setting rotation parameters.

5.2.2 Centrifugal Perfusion Setup

The basis of the centrifugal perfusion setup was a PMMA base plate equipped with a stepper motor (SY42STH38–1684A, Pololu Corporation) that was attached to the shelf of an incubator (Heraeus BBD 6220, Thermo Scientific). The stepper motor was controlled by a motor driver (2128, Pololu Corporation). The centrifugal perfusion spinner featured an identical user interface of display, rotary encoder and microcontroller, however, connected by a thin cable to the electric motor.

5.2.3 Peristaltic Pumping Setup

The peristaltic pumping setup was used for integrated, closed-loop perfusion in Organ-Discs [227]. It featured the same electronic components as the centrifugal perfusion spinner, however, Organ-Discs were mounted on an elevated platform connected to the spinner's base plate. Thereby, Organ-Discs were standing still and positioned above a magnet holder connected to the motor shaft and spinning below the disc. In total eight magnets (S-10-05-N52N, maximum adhesion 32.4 N, remanence 1.42-1.47 T, Webcraft) were inserted into the holder. Each magnet dragged a steel ball above the disc (diameter 5 mm, stainless steel 1.4034, HSI-Solutions). A thrust ball bearing (S51204, CQ GmbH) assured that the steel balls were rolling on a defined circular path above the Organ-Disc's pump channels. Another magnet holder (8× S-05-05-N, maximum adhesion 9.22 N, remanence 1.32-1.37 T, Webcraft) was added on top of the thrust ball bearing for a sufficient compression of the steel balls into the pump channels.

5.3 Organ-Disc Perfusion

The Organ-Disc perfusion was achieved by either centrifugal perfusion [226], or peristaltic perfusion [227].

5.3.1 Centrifugal Perfusion

Organ-Disc reservoirs for centrifugal perfusion consisted of a 2 mm bottom plate, 8 mm middle segment, and 2 mm lid on top of each other. All layers were fabricated from PMMA plates (all Oroglas cast acrylic glass, Trinseo, former: Arkema) that were laser cut (VLS2.30, Universal Laser Systems) and connected with adhesive (45570, UHU). For complete curing of the adhesive, reservoirs were left overnight at RT.

For centrifugal perfusion, the reservoirs were cleaned with IPA and left under a laminar flow cabinet for drying. Then, the reservoirs were connected to Organ-Discs by either biocompatible, double-sided adhesive tape (ARcare 90106, Adhesives Research) or by clamping a 2 mm thick layer of cured PDMS between reservoir and disc. Before mounting the Organ-Disc to the centrifugal perfusion spinner for continuous rotation, the inner reservoir compartment was filled with media and the media channels of the Organ-Disc were flushed for 30 s at 500–1000 rpm using the centrifugal loading setup.

Centrifugal pumping experiments for flow rate measurements were conducted in Organ-Disc versions only containing media channels and de-ionized water instead of cell culture media, however, using the identical procedure and conditions as used for centrifugal perfusion for 3D tissue generation. Effluents were pumped at 0-200 rpm under culture conditions, collected over 1 h and weighed using a fine balance (40SM-200A, Precisa Gravimetrics). The flow rates were approximated using OriginPro (Version 2019b, OriginLab Corporation).

5.3.2 Peristaltic Perfusion

The reservoirs for closed-loop peristaltic perfusion were fabricated in polypropylene (PP) by an external service provider (CNCTeile24) and autoclaved before connection to Organ-Discs with adhesive tape (ARcare 90106, Adhesives Research). The reservoir compartments were filled with the respective media and sealed with a gas permeable tape (Z380059, Sigma-Aldrich). Organ-Discs were fixed on the PMMA platform of the peristaltic perfusion setup and then equipped with steel balls, the thrust ball bearing and the upper magnet holder.

The flow rate was measured at RT by using a linear perfusion configuration. Two syringes with a volumetric scale (1 mL, Omnifix-F, B. Braun Melsungen) were connected to in- and outlet instead of the reservoir. The syringes were attached to the Organ-Disc using custom connecters consisting of a 2 mm PMMA plate, a Luer adapter (BDMFTLL-9, Nordson MEDICAL) and double-sided adhesive tape (ARcare 90106, Adhesives Research).

Before each measurement, equal amounts of de-ionized water, colored with a few drops of watercolor (Ecoline Liquid Watercolour, Royal Talens), were filled in both syringes. After ramping the motor up to its final speed in 5 s, fluid levels in both syringes were monitored over time. For each measurement, 6-8 data points, which represent the time for a 0.05 mL volume change in the syringe, were recorded and averaged.

5.4 Preparatory Cell Culture

Three human, primary cell types were used for on-disc culture:

- juvenile fibroblasts (FB) from foreskin
- adipose tissue-derived stem cells (ASC) from adult skin
- human umbilical vein endothelial cells (HUVEC) from pooled donors

Cryopreserved HUVEC were obtained from a commercial supplier (C2519A, Lonza) and used for blood vessel-like tissues [227]. FB and ASC were isolated from patient-derived biopsies by Silvia Kolbus-Hernandez, Kirstin Linke and Julia Roosz (all: Fraunhofer Institute for Interfacial Engineering and Biotechnology IGB, Stuttgart, Germany) according to previously published procedures in Ref. [232, 233] and used for on-disc 3D tissue generation [226].

Foreskin biopsies were provided by Dr. med. Zekeriya Yurttas (Praxisklinik, Stuttgart, Germany) and skin biopsies from Dr. med. Ulrich E. Ziegler (Klinik Charlottenhaus, Stuttgart, Germany) from volunteers under informed consent according to the permission of the "Landesärztekammer Baden-Württemberg" (F-2012–078). All procedures were done according to the Declaration of Helsinki defining the rules for medical research of human subjects.

All cell types were pre-cultured in filter cap cell culture flasks (75 and 175 cm^2, CELLSTAR, Greiner Bio-One). The individual cell culture media were the same for pre-culture and on-disc culture, unless otherwise specified. FB were cultured using Dulbecco's modified Eagle's medium (DMEM; FG0445, Biochrom) containing 10% (v/v) fetal bovine serum (FBS; HyClone FetalClone II, Thermo Scientific) and 1% (v/v) antibiotics (penicillin/streptomycin, 10.000 U/ml, Gibco). The cell culture media for ASC was mesenchymal stem cell medium enhanced, serum-free (PB-C-MH-675–0511-ad, PELOBiotech) containing 1% (v/v) antibiotic-antimycotic (100X, Thermo Fisher Scientific). For co-culture experiments, FB and ASC were both cultured in the same media used for FB mono-cultures. The cell culture media for HUVEC was endothelial cell growth medium (EGM-2 BulletKit, CC-3162, Lonza) supplemented with 1% (v/v) antibiotics (gentamicin 10 ng/mL, Gibco).

Cell suspensions for cell loading into Organ-Discs were generated by washing the confluent cell layers in the culture flasks with PBS and then detached by a 2-3 min incubation step at 37 °C in 0.05% (v/v) trypsin in versene (Trypsin-EDTA Solution 10X, SIGMA Life Science; Versene 1:5000 1X, Gibco). The detached cells were transferred into centrifuge tubes (50 mL CELLSTAR Polypropylene Tube, Greiner Bio-One) and supplemented with 10% (v/v) FBS in

order to inactivate trypsin. The viable cell number of FB and ASC in the cell suspension was determined in a 10 µL sample of the cell suspension by adding 10 µL trypan blue (Trypan blue 4 g/l in aqueous solution, VWR chemicals) for staining dead or damaged cells. The viable cell number was then counted in 10 µL of the mixture using a hemocytometer (C-Chip Neubauer improved DHC-N01, NanoEnTek). FB and ASC were subsequently centrifuged for 5 min at 1000 rpm or 216 × *g* (Multifuge 3S-R, Heraeus). In the case of HUVEC, the procedure was identical with the only difference that cell counting was conducted after centrifugation and adding 1 mL of cell culture media to the cell pellet.

In all cases, the cell concentration for cell loading was subsequently adjusted by adding respective amounts of the individual cell culture media to the cells.

5.5 Organ-Disc Cell Loading

Organ-Disc cell loading was achieved by centrifugal cell loading for 3D tissues [226] or by an endothelial-lining for blood vessel-like tissues [227].

5.5.1 Centrifugal Cell Loading

Before centrifugal cell loading, Organ-Discs were plasma activated (5 min, < 2 mbar, 3.3 sccm O_2, 50 W; Zepto, Diener) for sterilization and improved hydrophilic properties. Then, all channels were filled with PBS and the disc spun for 5 min at 4,000 rpm (743 × *g* at the tissue chambers) for air bubble removal. In the case of single cell type tissues, 5 µL of a cell suspension with 4,000 cells/µL of FB or ASC were injected into the inlet region of each cell channel. For cell loading, the Organ-Disc was spun at 1,000 rpm (46 × *g*). In the case of an insufficient filling of the tissue chamber, this loading procedure was repeated a second time.

For the generation of stratified tissues from ASC and FB, a previously published protocol was used as a guideline for sequential cell loading [220]. For each cell layer, 5 µL cell suspension of fluorescently labeled FB or ASC with 1,000 cells/µL were injected into the inlet region (*cf.* 5.6.1, “Live Cell Labeling” for details about the staining procedure). Compared to single cell type tissues, denser, individual cell layers were generated by spinning the Organ-Disc at 1,500 rpm (104 × *g*) for 5 min. Before adding another cell layer, an initial cell aggregation was achieved during a 2 h incubation step adding media-filled pipette tips to the media channels for media supply.

5.5.2 Endothelial-lining

For sterilization and hydrophilization, Organ-Discs were first sprayed with 70% (v/v) ethanol and then plasma activated (4 min, < 2 mbar, 3.3 sccm O_2, 50 W; Zepto, Diener). Afterwards, each system was flushed with 70% (v/v) ethanol in order to achieve a complete, initial filling and sterilization of inner channel surfaces. Ethanol was removed by flushing the individual systems with PBS.

The inner channel surfaces were coated for improved cell adhesion by filling PBS with 0.1 mg/mL collagen-I (FibriCol, Catalog #5133, Advanced BioMatrix) into each system. The coating solution remained inside the channels during an incubation step of 1 h at 37 °C. Then, the excess coating solution was flushed out with PBS and all channels were filled with cell culture media before cell loading.

HUVEC were injected into the cell channels by connecting pipette tips with 75 µL cell suspension containing 6×10^6 cells/mL to each cell channel outlet. Cells were injected with gentle pressure on the pipette tip from the micropipette or pressing with a thumb on the tip. This process was monitored using a brightfield microscope (Leica DMi1, Leica Microsystems) in order to achieve complete cell channel filling with cell suspension and to stop the injection just before cells enter the TPE module and to avoid cells from entering the pump channels.

Endothelial cells were seeded on the ceiling of the cell channel by flipping the disc upside down for 1 h at 37 °C with a sub-confluent seeding density of approx. 1000 cells/mm^2. Subsequently, endothelial cells were supplied with cell culture media using a gentle, closed-loop perfusion at ten revolutions per hour (rph) for 72 h. Endothelial cells spread onto all inner cell channel surfaces during that period and fresh cell culture media was added to the reservoir before following experiments.

5.6 Organ-Disc Cell Culture

5.6.1 Staining and Imaging

The staining and imaging procedures involving ASC and FB or HUVEC are described in more detail in Ref. [226] and Ref. [227] respectively.

Live Cell Labeling

ASC and FB were fluorescently labeled using different dyes before centrifugal cell loading into the Organ-Disc in order to distinguish between both cell types in the resulting stratified tissues. ASC were labeled in the cell culture flask before the cell detachment. Thereto, adherent ASC were treated with cell labeling solution containing 12.5 µM (CellTracker Green CMFDA Dye, Thermo Fisher Scientific) in FBS-free cell culture media during a 45 min incubation step at 37 °C.

FB were labeled in suspension after the dissociation step by adding another labeling solution (Vybrant DiD Cell-Labeling Solution, Thermo Fisher Scientific) in a 1 : 200 (v/v) ratio to the cell suspension. Cells were labeled during a 20 min incubation step at 37 °C. Subsequently, the cells were washed twice with cell culture media by centrifugation at 1500 rpm or 485 × *g* (Multifuge 3S-R, Heraeus) for 5 min and resuspension in cell culture media.

Stratified cell pellets and tissues were imaged using a fluorescence microscope (BZ-X800, Keyence).

Live/Dead Staining

Live/dead staining after on-disc culture experiments were conducted using fluorescein diacetate (FDA, Sigma-Aldrich) for the labeling of viable cells and propidium iodide (PI, Sigma Aldrich) for the labeling of the nuclei of dead cells. The exact live/dead staining procedure varied with regards to the tissue structure.

The 3D tissues of FB or ASC were first washed by attaching PBS-filled pipette tips to the media channels. Afterwards, the tissues were stained by injecting a labeling solution in the same way with 25 µg/mL FDA and 225 µg/mL PI in PBS into the media channel. The labeling solution was left inside the media channel for 3-5 min at 37 °C and was subsequently washed out by another flushing step with PBS.

Endothelial cells were stained similarly but using PBS+ (Dulbecco's Phosphate Buffered Saline with $MgCl_2$ and $CaCl_2$, Sigma-Aldrich) instead of PBS. For HUVEC, the labeling solution contained 27 µg/mL of FDA and 135 µg/mL of PI.

Images of stained tissues were acquired with a fluorescence microscope (Leica DMi8, Leica Microsystems) at 37 °C. In the case of 3D tissues, z-stack images were acquired and transferred into maximum intensity projections using Fiji (Image J version 1.52p–1.53c) [231].

CD106 Staining

Endothelial cells were stained for cluster of differentiation (CD) 106 in order to visualize the effect of cytokine-induced, inflammatory stimulation. Endothelial-lined cell channels were washed with PBS+ containing 10 mg/mL bovine serum albumin (BSA, Sigma-Aldrich). HUVEC were then stained with CD106 staining solution (130-104-164, CD106 Antibody, anti-human, REAfinity, APC, Miltenyi Biotec, diluted 1 : 10 (v/v) in PBS+ containing 10 mg/mL BSA) for 30 min at 37 °C and washed with PBS+ before imaging. Images of the stained HUVEC were acquired with a fluorescence microscope (Leica DMi8, Leica Microsystems) at 37 °C.

CD41 Staining

Platelets in human whole blood were labeled by a fluorescent antibody staining for CD41 according to a previously published protocol [234]. Thereto, 1% (v/v) CD41 antibody (MHCD4104, CD41 Monoclonal Antibody, PE, Invitrogen) was added to freshly collected whole blood in blood collection tubes (VACUETTE TUBE 9 mL 9NC Coagulation sodium citrate 3.2%, Greiner Bio-One). The supplemented blood was stored at RT for 10 min in the dark for staining and before proceeding with subsequent blood perfusion experiments.

Fixation, Permeabilization and Blocking

After on-disc culture, 3D tissues were fixed by flushing a fixation solution (Roti-Histofix 4%, Carl Roth) into the media channels and a subsequent incubation step for 1 h at RT. Afterwards, the fixation solution was flushed out with PBS and the 3D tissues permeabilized for 30 min by filling the media channels with 0.1% (v/v) Triton X-100 (Sigma-Aldrich) in PBS at RT.

In the case of endothelial-lined channels, the fixation was comparable but using only a 15 min incubation step and adding 30 mg/mL BSA for blocking unspecific binding.

Actin/Nuclei Staining

Filamentous actin were stained with phalloidin (Alexa Fluor 488 phalloidin, Invitrogen) and cell nuclei labeled with 4′,6-Diamidino-2-phenylindole dihydrochloride (DAPI, Sigma-Aldrich) in fixed and permeabilized 3D tissues. The staining solution contained 0.165 µM phalloidin, 1 µg/mL DAPI, 10 mg/mL BSA and 0.1% (v/v) Triton X-100 in PBS. The staining solution was filled into the media channel, left inside the channel for 60 min at RT and flushed out with PBS.

Combined z-stacks and tile scans of the stained tissues were acquired with a confocal Laser-Scanning-Microscope (LSM 710, Carl Zeiss MicroImaging), stitched (ZEN black edition 2.3 SP1, Carl Zeiss Microscopy) and transferred into maximum intensity projections (Fiji, Image J version 1.52p–1.53c) [231].

CD31/Nuclei Staining

After fixation, permeabilization and blocking, HUVEC were stained for CD31 and cell nuclei. Thereto, PBS supplemented with 30 mg/mL BSA and 0.1% (v/v) Triton X-100 was used for the dilution of all antibodies and dyes. In the first step, primary CD31 antibody (M0823, mouse anti-human, Agilent Technologies) was diluted 1 : 50 and injected into the endothelial-lined channels and washed out with PBS after 2 h at RT. Afterwards, the staining solution with 1 : 100 diluted secondary antibody (A-11003, goat anti-mouse, Alexa Fluor 546, Invitrogen) and 1 µg/mL Hoechst (Hoechst 33342, Thermo Scientific) were injected and left inside the cell channels for 1 h at RT and flushed out using PBS.

The stained endothelial cells were imaged with a confocal Laser-Scanning-Microscope (LSM 710, Carl Zeiss MicroImaging). Combined z-stacks and tile scans over the full cell channel were first stitched (ZEN black edition 2.3 SP1, Carl Zeiss Microscopy) and then converted in maximum intensity projections (Fiji, Image J version 1.53c) [231]. Single z-stacks acquired in the center of the cell channel were either converted in maximum intensity projections with Fiji or rendered into 3D views with Fiji's Volume Viewer plugin (Volume Viewer 2.01.2, https://github.com/fiji/Volume_Viewer; Last accessed: 14.10.2021).

5.6.2 Media Analysis

The closed-loop perfused media was monitored during long-term HUVEC culture, as described in detail in Ref. [227]. Briefly, HUVEC were first injected into collagen-I-coated cell channels and left under static conditions for 1 h. Then, the pump was ramped up to 100 rph over 4 h and kept at 100 rph for 24 h. At this point (Day 0), the media was exchanged in order to remove non-adherent cells.

In 24 h intervals (Day 1-7), the motor was stopped briefly, 110 µL of the perfused media were removed for analysis and replaced with fresh cell culture media before the motor was ramped up again to 100 rph within 1 h. The individual samples were frozen and kept at −80 °C until subsequent analysis. A complete media exchange was performed on day 3 and 6 after sampling. Throughout the perfusion experiment, qualitative flow tests were conducted on each day and included the connection of an empty pipette tip to the channel outlet. A raising fluid level in the pipette tip served as indication if fluid transport was present.

The individual media samples were thawed and tested with a bioanalyte analyzer (Vi-CELL MetaFLEX, Beckman Coulter) for potassium (K^+), sodium (Na^+), chloride (Cl^-) and calcium (Ca^{2+}) in samples of a cell-free system ("reference system") or for glucose and lactate in systems with HUVEC. Basal media concentrations of all components were measured as well in four samples of fresh cell culture media.

5.6.3 Endothelial Cell Activation

Inflammatory stimulation with tumor necrosis factor alpha (TNF-α) was analyzed in collaboration with Julia Rogal (Fraunhofer Institute for Interfacial Engineering and Biotechnology IGB, Stuttgart, Germany) and described in more detail in Ref. [227].

Briefly, cell channels were lined with HUVEC during 72 h of gentle perfusion using a pump speed of 10 rph. The cell lining process included a media exchange 48 h after the initial cell injection. This was done in order to assess the baseline cytokine release over the following 24 h by measuring the accumulating cytokines in the media. Thereto, samples of the perfused media were taken before conducting subsequent treatments.

Afterwards, the media in all systems was exchanged completely and replaced with either cell culture media containing 20 ng/mL TNF-α (SRP3177, Sigma-Aldrich) or fresh, standard cell culture media without TNF-α. The respective media was perfused for another 24 h at 10 rph.

Subsequently, the samples of the perfused media were taken in order to measure the accumulated cytokines from treated and untreated HUVEC.

At each sampling time point, the respective media samples were first centrifuged at 3000 rpm or 1942 × *g* for 5 min (Multifuge 3S-R, Heraeus) in order to remove any debris and then frozen and kept at −80 °C until following analysis steps.

Cytokine concentrations were measured by Julia Rogal using a fluorescent bead-based multiplex assay (LEGENDplex Human Angiogenesis Panel 1, 740697, BioLegend). The assay was read out by flow cytometry (Guava easyCyte 8HT, Merck) and analyzed with the LEGENDplex Cloud-Based Data Analysis Software Suite (BioLegend).

Thereby, the concentrations of interleukin 6 (IL-6), interleukin 8 (IL-8) and angiopoietin 2 (Ang-2) were measured in technical duplicates for each condition and time point. Cytokine release experiments included in total eight systems on two Organ-Discs, whereas half of the systems were either treated or not treated.

5.6.4 Whole Blood Perfusion

Blood was collected by Jun. Prof. Dr. med. Martin Weiss (Department of Women's Health, Faculty of Medicine, Eberhard Karls University Tübingen, Tübingen, Germany) from volunteers under informed consent according to the permission of the ethical committee of the Eberhard Karls University Tübingen (Nr. 495/2018-BO02). All procedures were done according to the Declaration of Helsinki.

Whole blood perfusion was conducted as described in more detail in Ref. [227]. After fluorescent labeling of platelets (*cf.* section 5.6.1 "CD41 Staining"), blood was supplemented with ions required for coagulation by adding a re-calcification buffer with a previously published composition [234]. This buffer contained 63.2 mM calcium chloride ($CaCl_2$, Sigma-Aldrich) and 31.6 mM magnesium chloride ($MgCl_2$, Invitrogen) in 1 M 4-(2-hydroxyethyl)-1-piperazineethanesulfonic acid (HEPES, 1 M, Gibco) and was added 1 : 100 (v/v) to the blood sample.

Before blood perfusion experiments, cell channels were lined with endothelial cells for 96 h under gentle, closed-loop perfusion at 10 rph, treated using PBS+ containing 10 mg/mL BSA and finally flushed with PBS+. Blood was perfused linearly through the system by adding a

blood-filled and an empty pipette tip to the reservoir ports. The reservoir compartments were filled with cell culture media for the preparation of the washing step after the blood perfusion.

For blood pumping, the peristaltic pump was ramped up to 800 rph within 1 min and held at this speed for 5 min. Afterwards, both pipette tips in each system were pulled out, which initiated the washing step of the channels with media under closed-loop perfusion for 5 min at 800 rph. After washing, the motor was stopped, the media was aspirated and the channels were flushed manually with PBS+ before the following CD31 and cell nuclei staining (*cf.* section 5.6.1 "CD31/Nuclei Staining"). In this case, the staining procedure included incubation of the primary CD31 antibody at 4 °C overnight and a different secondary antibody (A32723, goat anti-mouse, Alexa Flour 488 Plus, Invitrogen) in order to avoid the overlapping of fluorescent signals related to CD41 and CD31. The fluorescently labeled platelets and the stained HUVEC were imaged using a fluorescence microscope (Leica DMi8, Leica Microsystems).

5.7 Data Presentation and Statistics

Unless stated differently, data is presented as mean or as mean ± standard deviation in text, tables and diagrams, whereas error-bars represent the standard deviation and the number of sample *N* is stated in each case.

OriginPro (Version 2019b-2021, OriginLab Corporation) was used for the approximation of the flow rates of centrifugal pumping and for the linear regression between flow rates and motor speed of the Organ-Disc's peristaltic pump. The Paired Comparison Plot plugin (version 3.6) of OriginPro was applied using Tukey's range test in order to determine if cytokine concentrations were significantly different.

6 Concept and Design

The concepts and designs presented in this chapter, as specified in each case, were published in Ref. [226] and Ref. [227].

6.1 Organ-Disc Technology

The Organ-Disc technology enables the generation and culture of human microtissues using rotation-based processes. In the first step of the Organ-Disc process, tissues are generated by using either centrifugal cell loading into dead-end channels by spinning of the disc or by endothelial cell lining of perfused cell channels (Figure 6.1 a) [226, 227]. Thereby, different tissue structures can be generated. Whereas centrifugal loading achieves 3D tissues with high cell densities, cell-lining results in complete coverage of the inner channel surfaces with endothelial cells recapitulating a blood vessel-like setting.

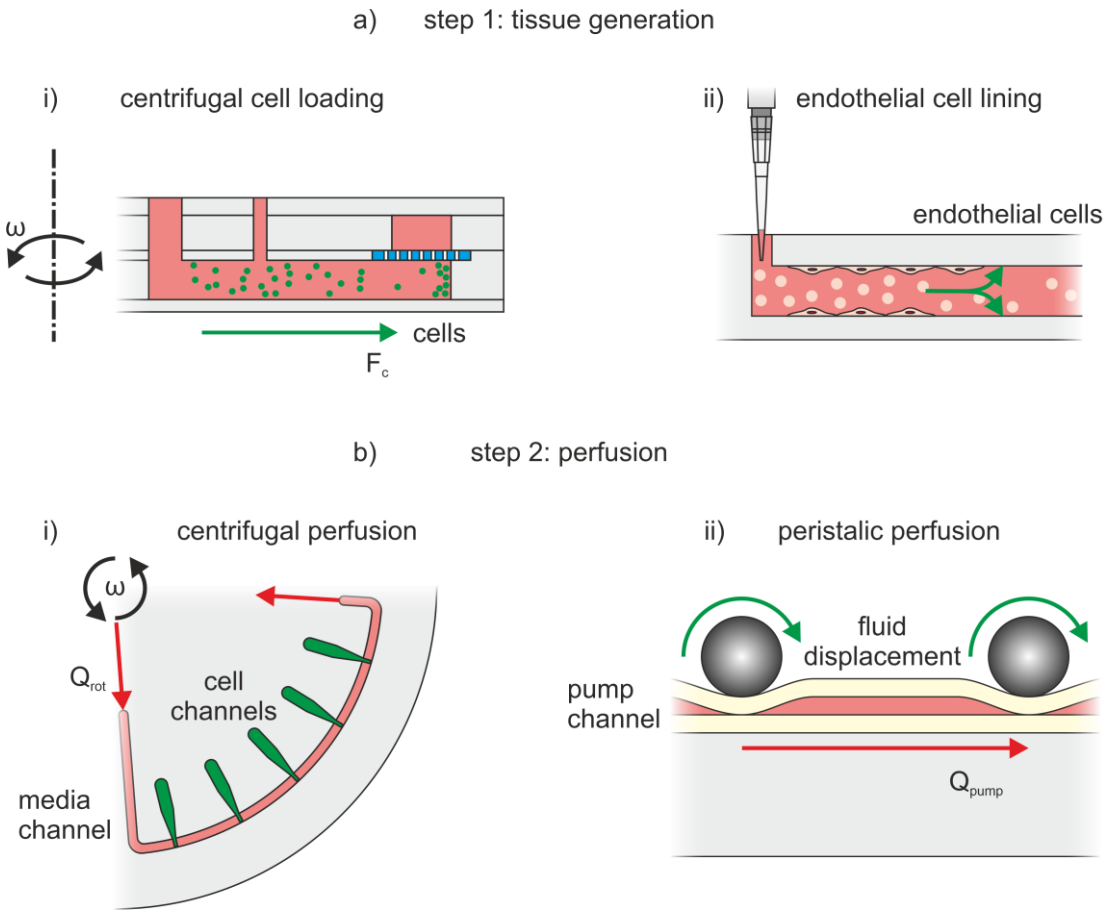

Figure 6.1 Organ-Disc concept: a) Tissue generation is achieved by i) centrifugal cell loading through Organ-Disc rotation for dense 3D tissues or ii) by endothelial cell lining of inner cell channel surfaces for blood vessel-like structures. b) Integrated perfusion in the Organ-Disc generated by i) spinning of the disc for centrifugal pumping or by ii) implementing peristaltic pumping on-disc. a-i), b-i) adapted from Ref. [226] available under the CC BY 4.0 license and a-ii), b-ii) adapted from Ref. [227] with permission from the Royal Society of Chemistry available under the CC BY-NC 3.0 license.

In the second step, continuous supply of cell culture media is achieved by perfusing the microchannels in the Organ-Disc. The media perfusion can be achieved either via centrifugal pumping by disc rotation or via an integrated peristaltic pumping mechanism (Figure 6.1 b) [226, 227]. In both cases, the Organ-Disc concept omits the need for external pumps for fluid transport in the microchannels as well as error-prone tubing connections to the microfluidic system.

6.2 Organ-Disc Design

Organ-Discs have an outer diameter of 10 cm and consist of multiple, thermoplastic layers stacked on top of each other, which form channels on both sides of a porous membrane (Figure 6.2 a) [226]. The footprint of the Organ-Disc recapitulates the size of a 4” wafer in order to maintain compatibility to potential, alternative fabrication approaches in later settings.

Each disc contains four systems, each featuring five cell channels, in order to achieve a parallelized platform with independent systems and to build the basis for future studies on tissue-tissue interactions within each system (Figure 6.2 b). Thereto, the cell channels are in-line connected to a shared media channel for media supply to the individual tissues while a porous membrane separates the cell channels from the media channels.

All cell channels are symmetrically arranged on the Organ-Disc and point radially outwards for cell loading by centrifugal forces into the tissue chambers at the end of each channel. The individual tissue chambers are located at identical radial positions ($r = 41.5$ mm) for equal, centrifugal conditions. The media channel requires different radial positions for in- and outlet in order to achieve a pressure gradient for perfusion due to centrifugation (*cf.* section 8.1). The outlet of the media channel is shifted towards the Organ-Disc center at the radial position of the inner cell channel loading port in order to prevent centrifugal pressure gradients across the membrane barrier during centrifugal loading and perfusion.

The tissue chambers can be tailored to the desired tissue shape. For instance, both rectangular as well as dogbone-shaped chambers, as used in previous systems for the generation of an anisotropic, fiber-like tissue [147, 235], have been used (Figure 6.2 c). The tissue chambers in the Organ-Disc have a footprint of 0.3 mm^2 and 0.5 mm^2 for the rectangular and dogbone chamber respectively and are 175 µm high. The media channels above the tissue chambers are each 75 µm high and 1.4 mm wide. Media channels and tissue chambers are separated by an

approx. 15 µm thick membrane with 3 µm pores (*cf.* appendix, section 13.1 showing the complete 2D channel layout).

The individual cell and media channel heights represent a compromise between multiple aspects. For both tissue and media layer, the channel heights are governed by the individual foil thicknesses, which sets a limit to the freedom of design with regards to the portfolio of commercially available foils.

The thickness of the tissue layer sets the height of cell channels and tissue chambers. The desired thickness of the 3D microtissues, controlled by the tissue chamber height, is below approx. 200 µm, which arises out of the diffusion limitation in 3D spheroids. Spheroids usually feature a necrotic core if their size exceeds 500 µm in diameter due to insufficient mass transport to and from the spheroid center [236]. At the same time, the cell channel requires a sufficient height for reliable cell transport into the tissue chambers by centrifugal loading (*cf.* section 6.3), which makes a too thin tissue layer material unsuitable as otherwise cells could get stuck in the channel.

The 75 µm thin media layer allows for an appropriate hydraulic resistance of the media channel and the achievement of suitable flow rates during centrifugal pumping (*cf.* section 8.1). Thereby, the media channel height is much smaller than the width hence the most effective parameter for adjusting the hydraulic resistance (*cf.* section 2.1.2). In principle, adjusting the channel resistance would be as well possible by changing the width of the channel. This was avoided as the media channel width above tissue chambers is set by the lateral size of the tissue chambers. Furthermore, the fabrication of narrow, lateral channel regions poses challenges to the microstructuring processes for through-hole structures (*cf.* section 7.1.1 “2D Structuring”).

For access to the individual channels, a 2 mm thick port layer and 175 µm thick connector layer are added above the media layer. As bottom of the Organ-Disc, solely a 175 µm thin layer is added underneath the tissue chambers in order to allow for unrestricted, high-resolution microscopy of the microtissues.

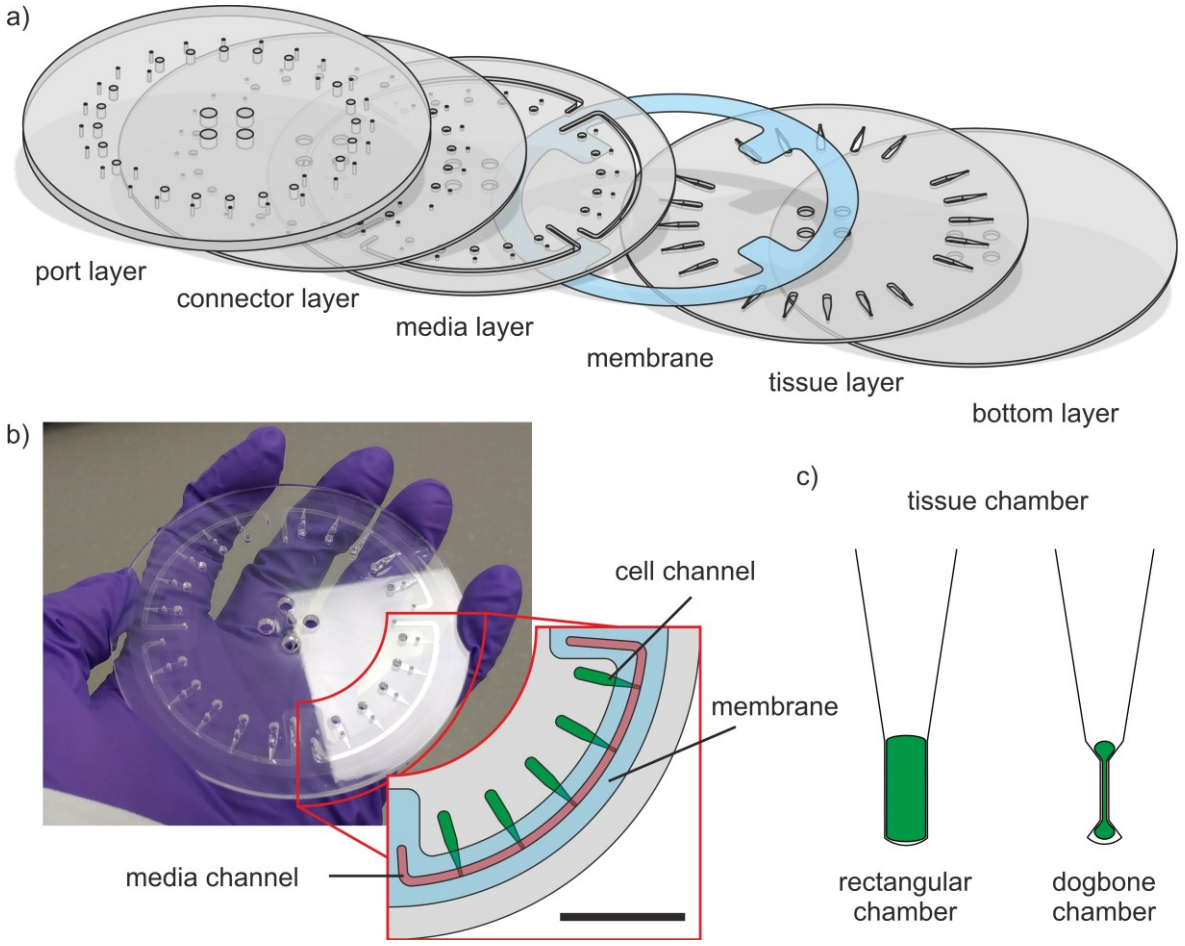

Figure 6.2 Design of the centrifugal Organ-Disc: a) Individual layers of the Organ-Disc. b) Photograph of an Organ-Disc with a schematic close-up view of a single system with five cell channels, a shared media channel and the separating membrane. Scale bar: 20 mm. c) Top view of individual tissue chamber designs for tailored 3D tissues in rectangular or dogbone shape, as used in previous systems for anisotropic, fiber-like tissues [147, 235]. a) adapted from Ref. [226] available under the CC BY 4.0 license.

6.3 Centrifugal Cell Loading

The Organ-Disc allows for the generation of dense cell pellets in the tissue chambers by centrifugal cell loading [226], which is similar to previous systems using centrifugal forces for cell injection [147, 220]. In the first step of centrifugal cell loading, a cell suspension is injected into the cell channels through the loading ports of the Organ-Disc (Figure 6.3 a). In the following step, rotation of the Organ-Disc generates precisely controllable centrifugal forces. Thereby, the cells are transported radially outwards into the tissue chamber at the end of the cell channel (Figure 6.3 b). The cells accumulate in the tissue chamber and form dense cell pellets in the shape of the tissue chamber geometry (Figure 6.3 c).

Centrifugal cell loading provides an alternative to cell loading based on injection of a cell suspension by pressure gradients and retention of the cells in front of a porous barrier, *e.g.* membranes or channel walls with gaps [99, 106, 107]. Eventually, filtration-based cell loading results in cell accumulation in front of the porous barrier and clogging of the pores or gaps. The cell transport into those chambers will be limited at some point due to the increasing hydraulic resistance across the permeable barrier. Increasing pressure gradients are required in order to flush even more cells into the camber and to pump out the excess fluid of the cell suspension through the barrier and out of the chamber. In contrast to that, cell loading by centrifugation is independent of the filling state of the tissue chamber and allows for complete tissue chamber filling with a compact cell packing without high pressure gradients. Furthermore, cell transport happens in all cell channels at the same time as the centrifugal forces act on all cells inside the disc. This allows for parallelized cell loading and pellet formation in all tissue chambers and subsequent maturation into dense 3D tissues.

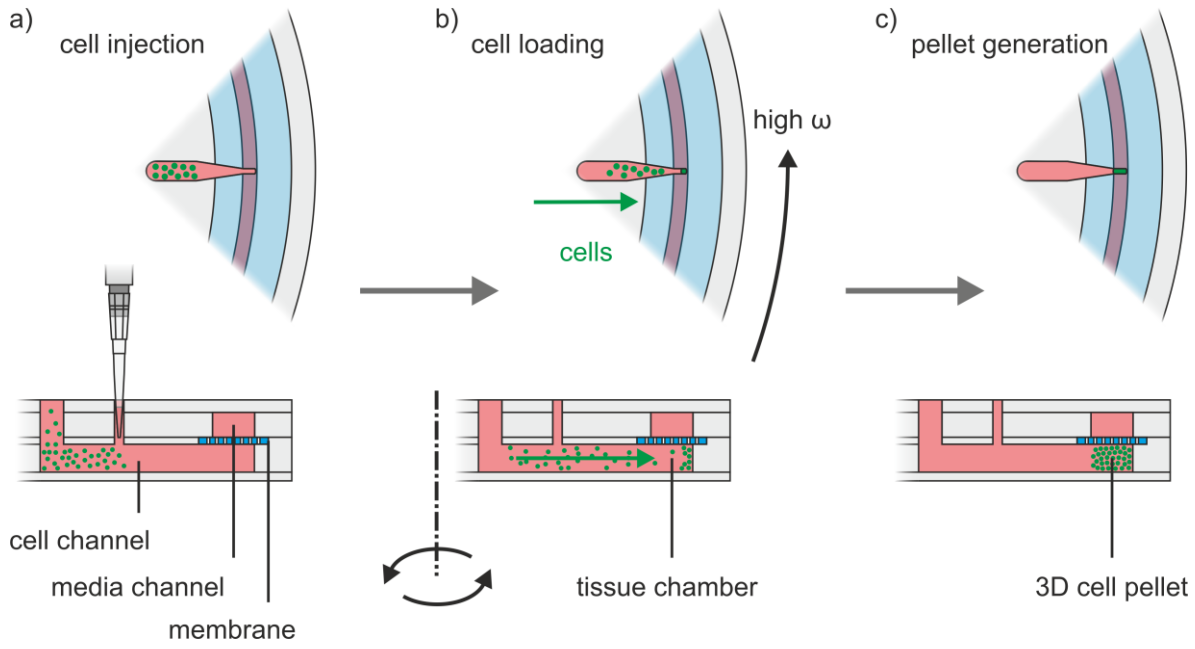

Figure 6.3 Concept of centrifugal cell loading: a) A cell suspension is injected into the cell channels. b) Organ-Disc rotation generates centrifugal forces for cell loading. Cells are transported radially outwards along the cell channel and accumulate in the tissue chamber at the end of the cell channel. c) Thereby, dense 3D cell pellets are generated inside the tissue chamber, which adapt to the shape of the chamber. Figure adapted from Ref. [226] available under the CC BY 4.0 license.

6.4 Endothelial Cell Lining

In addition to dense 3D tissues, the generation of an endothelial lining of perfused microchannels has been implemented in the Organ-Disc [227]. Cell channels are completely filled with an endothelial cell suspension using micropipettes for a homogenous cell distribution along the channel (Figure 6.4 a). After a short incubation, cells adhere on the inner channel surfaces and remaining, uncovered gaps between endothelial cells are closed through advancing cell proliferation (Figure 6.4 b). Thereby, endothelial cells spread and line the entire cell channel and form a blood vessel-like structure. After achieving confluent cell lining, this endothelium can be perfused with cell culture media or even with whole blood (Figure 6.4 c).

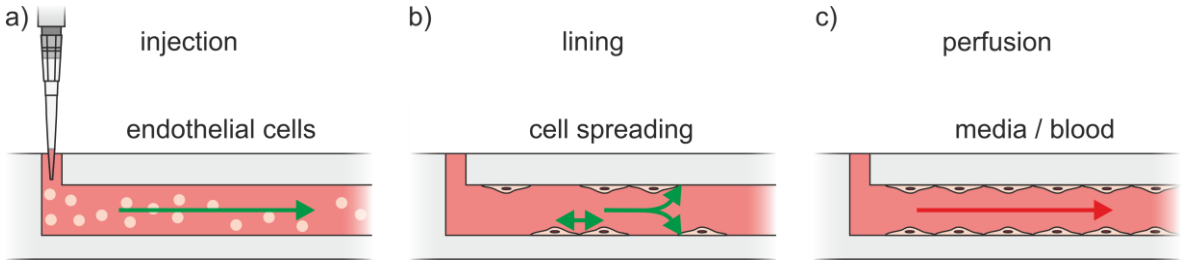

Figure 6.4 Concept of endothelial cell lining: a) Injection of endothelial cells by flushing a cell suspension into a continuous cell channel using a micropipette. b) Lining of inner channel surfaces through cell attachment and proliferation. c) Completely lined channels with endothelial cells form blood vessel-like structure and can be perfused with media or blood.

6.5 Centrifugal Perfusion

Centrifugal perfusion is based on previously reported centrifugal pumping [27, 209], which allows for fluid transport in the Organ-Disc's media channels by slow rotation of the disc [226]. During centrifugal pumping, the perfused media is stored in the Organ-Disc's reservoir, which is added directly on top of the disc (Figure 6.5 a). The Organ-Disc reservoir does not require tubing connections to the disc and allows for fluid storage in a compact format. A central compartment stores fresh media flowing into the individual media channels of each system on the disc. The individual media channels on the Organ-Disc supply multiple microtissues in-line. Thereby, each system's effluent is collected in individual compartments at the periphery of the reservoir.

Fluid transport is achieved through the generation of centrifugal forces by rotation of the Organ-Disc and its reservoir (Figure 6.5 b). Thereby, fluid is pumped radially outwards from the

central reservoir, through the media channel and into the effluent compartment. The generated, convective media flow is confined to the media channel above the tissue chambers (Figure 6.5 c, d). A porous membrane separates the media channel from the microtissues and creates a permeable barrier, which is commonly applied in OoC research for artificial endothelial barriers [80, 99, 111, 147]. As demonstrated in previous studies, this allows for diffusive nutrient transport to the cells and shields the microtissues from excessive shear forces [115, 116].

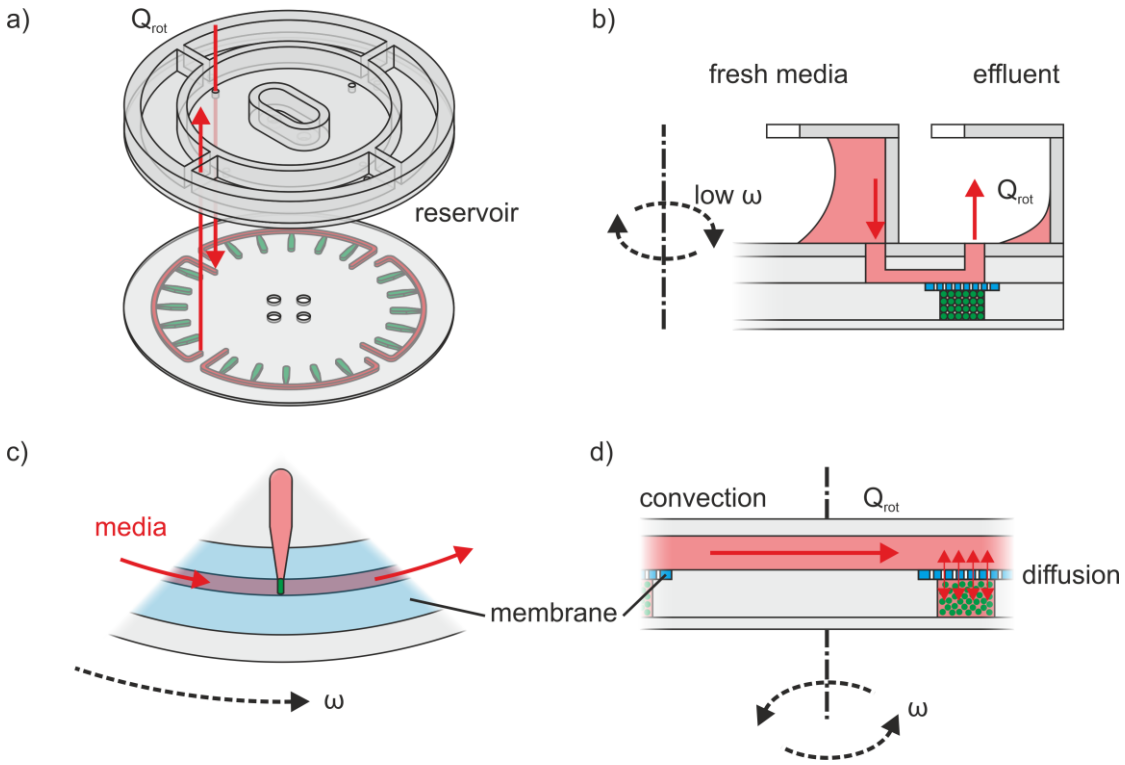

Figure 6.5 Concept of the centrifugal Organ-Disc perfusion: a) During centrifugal perfusion, all fluids are stored in a reservoir with compartments for fresh media and individual effluents (here shown without lid), which is connected directly to the Organ-Disc (exploded view). b) Centrifugal pumping is achieved by slow rotation of the Organ-Disc. Media is pumped form the inner reservoir compartment radially outwards, through the media channel and then collected in the effluent compartment (radial side view). c) Convective media flow is confined to the media channels that are separated by a porous membrane from the tissue chambers (view from below). d) The membrane emulates an endothelial barrier that allows for diffusive transport to the microtissue and shields the cells from shear forces (tangential side view). Figure adapted from Ref. [226] available under the CC BY 4.0 license.

6.6 Peristaltic Perfusion

Besides centrifugal perfusion, integrated peristaltic pumping has been implemented on the Organ-Disc and applied for the perfusion of cell channels lined with endothelial cells [227]. Peristaltic pumping in the Organ-Disc is based on previously presented concepts for fluid displacement in a flexible channel by magnetically dragged steel balls [205, 206]. During peristaltic perfusion, media is stored in a central reservoir on top of the Organ-Disc (Figure 6.6 a). Identically to centrifugal perfusion, the fluid transport between Organ-Disc and reservoir compartments is achieved without interconnecting tubing by direct connection of the reservoir on top of the disc.

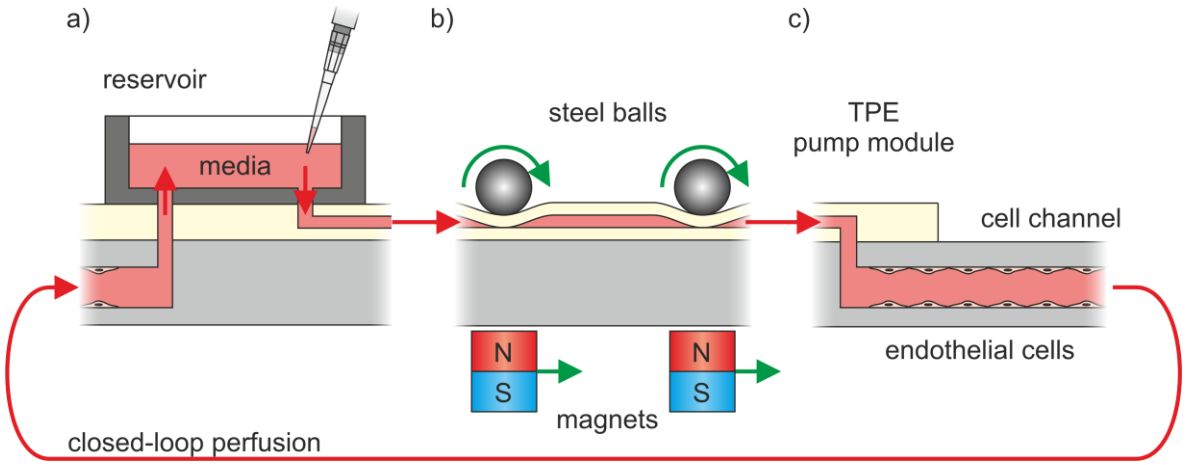

Figure 6.6 Concept of closed-loop perfusion: a) The perfused media is stored in an open reservoir on top of the disc. b) For peristaltic pumping, steel balls are dragged over flexible pump channels by magnets moving underneath the stationary disc. c) Media is transported in closed-loop through cell channels and pumped back in to the reservoir. Figure adapted from Ref. [227] with permission from the Royal Society of Chemistry available under the CC BY-NC 3.0 license.

For peristaltic pumping, steel balls are dragged by moving magnets underneath the stationary disc and roll over flexible pump channels on top of the Organ-Disc (Figure 6.6 b). Thereby, the steel balls compress the flexible channel, displace the media inside the channel and transport it from the reservoir further through the cell channels (Figure 6.6 c). A closed-loop media perfusion is created by pumping the media leaving the cell channel back into the same reservoir compartment.

For the implementation of peristaltic pumping on the Organ-Disc format, a flexible pump module is added on top the disc (Figure 6.7 a). The individual systems are arranged symmetrically on the Organ-Disc footprint and perfused simultaneously by the steel balls rolling on top of the pump module. Thereto, a magnetic holder underneath the disc keeps the

steel balls on a circular track around the central axis of the disc. Each system features a pump channel and cell channel as well as an individual compartment in the reservoir, which is connected to both inlet and outlet of the cell channel. The pump channels inside the flexible pump module are formed by adding two flexible layers – pump and pump support layer – on top of the disc (Figure 6.7 b). The disc module consists of three thermoplastic layers forming continuous cell channels for the formation of a blood vessel-like endothelial cell structure (*cf.* appendix, section 13.1 showing the complete 2D channel layout).

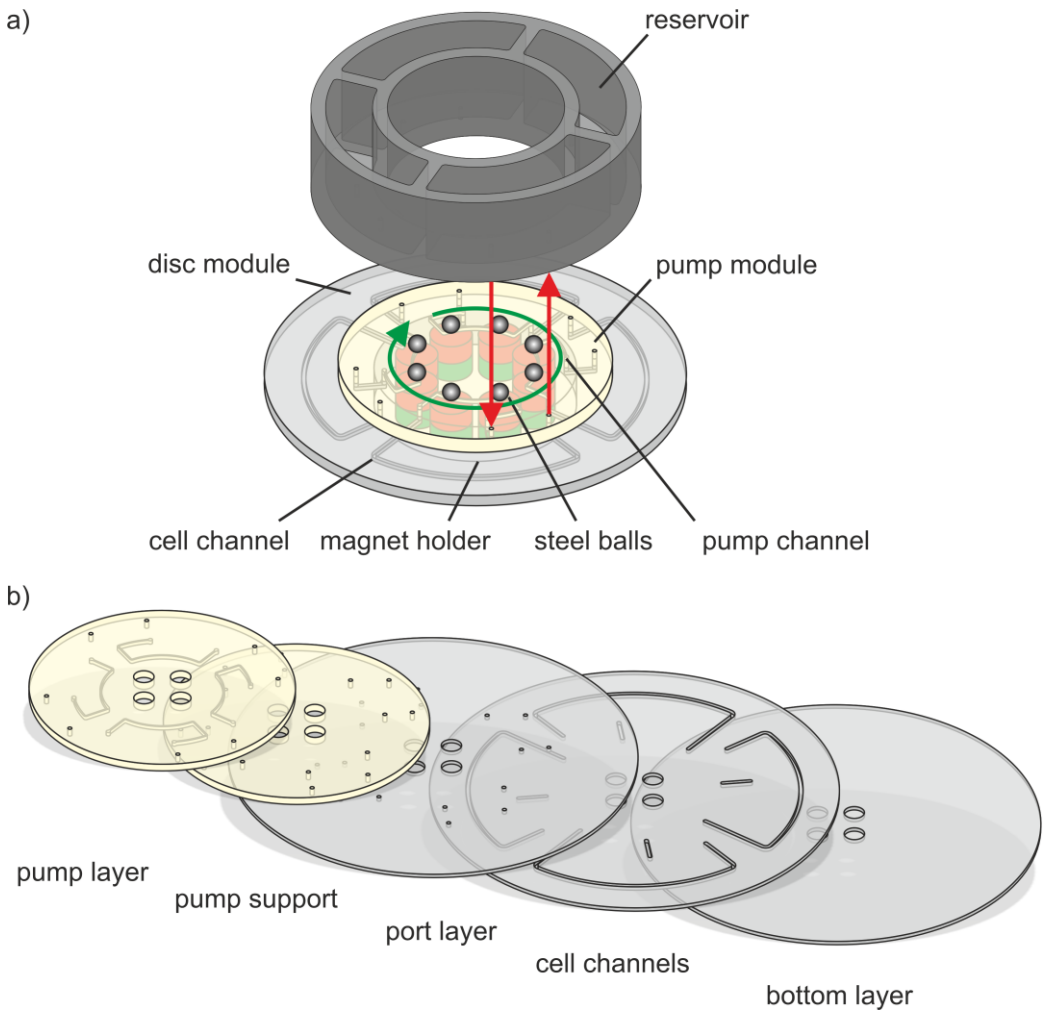

Figure 6.7 Implementation of peristaltic pumping in Organ-Discs: a) A flexible pump module with pump channels is added on top of the Organ-Disc for peristaltic, on-disc perfusion. The symmetric arrangement of multiple systems and rolling steel balls allows for the simultaneous perfusion of several systems on the disc. b) Flexible, pump and pump support layer form together the pump module and are added on top of the three thermoplastic layers forming cell channels. Figure adapted from Ref. [227] with permission from the Royal Society of Chemistry available under the CC BY-NC 3.0 license.

7 Building Blocks

The results presented in this chapter, as specified in each case, were published in Ref. [226–228].

7.1 Microfabrication Technology

The overall microfabrication of the Organ-Disc aims at a scalable and precise construction of microfluidic devices in industry-compatible materials. This included 2D structuring of thermoplastic foils and hot embossing of flexible TPE layers as well as fusing the individual microstructured layers by solvent or thermal bonding approaches.

7.1.1 Structuring

2D Structuring

The Organ-Disc is a multi-layered, microfluidic system with channels formed by stacking several layers on top of each other [226]. Thereby, the channel side walls are generated by cutting through the entire material thickness of the middle layer, whereas channel ceiling and bottom are generated by adding closed layers on top and below.

CO_2 laser cutting (Figure 7.1 a) as well as plotting (Figure 7.1 b) – also called xurography [67] – have been applied for the generation of channel side walls in thermoplastic films. Both structuring techniques allow for rapid prototyping as they enable the direct transfer of channel layouts generated with computer-aided design (CAD) tools into thermoplastic layers without intermediate steps.

In the case of 175 µm thick PMMA, CO_2 laser cutting achieved minimal lateral dimensions of 150-200 µm, as in the shaft region of the dogbone-shaped tissue chamber, which was adapted from previously presented heart-on-chip systems [147, 235]. Compared to structuring with a drag knife, laser cutting provided more freedom in structure design (*cf.* Table 7.1). In general for xurography, sharp, inner edges require modified cutting lines of the drag knife [67]. Therefore, laser cutting was chosen for Organ-Disc layers with sophisticated structures as the dogbone-shaped tissue chamber (Figure 7.1 c). An advantage of plotting, however, is the generation of smoother cuts through the material compared to the relatively rough edges generated with a CO_2 laser. Therefore, plotting was well-suited for structuring of the media channels in order to limit air bubble trapping on rough channel edges (Figure 7.1 d).

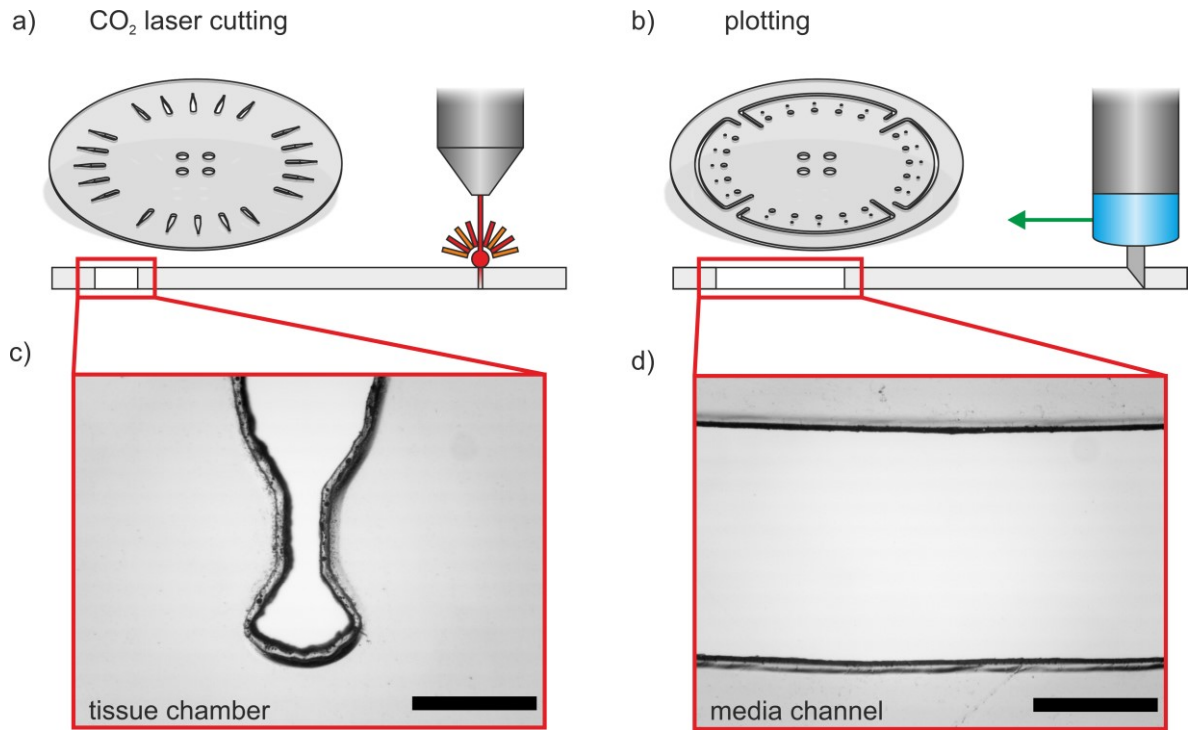

Figure 7.1 2D structuring techniques: Microstructuring of the individual Organ-Disc layers by either a) CO_2 laser cutting or b) plotting. c) Dogbone-shaped tissue chamber in 175 µm PMMA structured by CO_2 laser cutting. d) Media channel cut into 75 µm PMMA by a cutting plotter. Scale bars: c), d) 750 µm. a), b) adapted from Ref. [226] available under the CC BY 4.0 license.

Both 2D structuring processes allow for fast structuring in less than 5 min per Organ-Disc layer. The overall process time was mainly depending on the post processing such as removal of cutouts and cleaning of the surfaces for subsequent bonding steps. The two different structuring processes differed especially in the effort for cleaning of the surface. During CO_2 laser cutting, particles formed on the substrate that had to be removed, *e.g.* by manual whipping with clean room tissues. On the other hand, plotting is a pure mechanical structuring process and formed no residues on the surface of the thermoplastic foils.

Table 7.1 Comparison between CO_2 laser cutting and plotting for 2D structuring of Organ-Disc layers. Classification: "+" (good), "+/–" (medium), "–" (poor)

Process	Freedom of design	Quality of edges	Post-processing
CO_2 laser	+	–	–
Plotting	+/–	+	+/–

Hot Embossing

The integration of peristaltic pumps required the fabrication of pump channels in an elastic material [227]. Flexible TPE, more precisely SEBS, provides a promising alternative to frequently used elastomers, such as PDMS [228]. TPE is usually structured by injection molding or hot embossing [59, 60]. Due to the lower demand in equipment and machining, hot embossing with temperature stable epoxy stamps fabricated by replica molding was chosen for TPE structuring [227, 228].

The overall fabrication of epoxy-based hot embossing stamps is adapted from previous studies [83, 229] and targets the accurate transfer of precise but often fragile microstructures into a rigid and temperature stable material. The stamp fabrication starts with the fabrication of initial SU-8 microstructures by standard UV lithography (Figure 7.2 a). In the second step, the photoresist structures are replica molded with PDMS (Figure 7.2 b). This results in an intermediate, negative PDMS mold, which acts as a master for the second replica molding step with epoxy resin (Figure 7.2 c). After curing and tempering for improved temperature stability, the epoxy stamp features the initial SU-8 microstructure profile and provides a rigid hot embossing stamp for subsequent structuring of TPE (Figure 7.2 d).

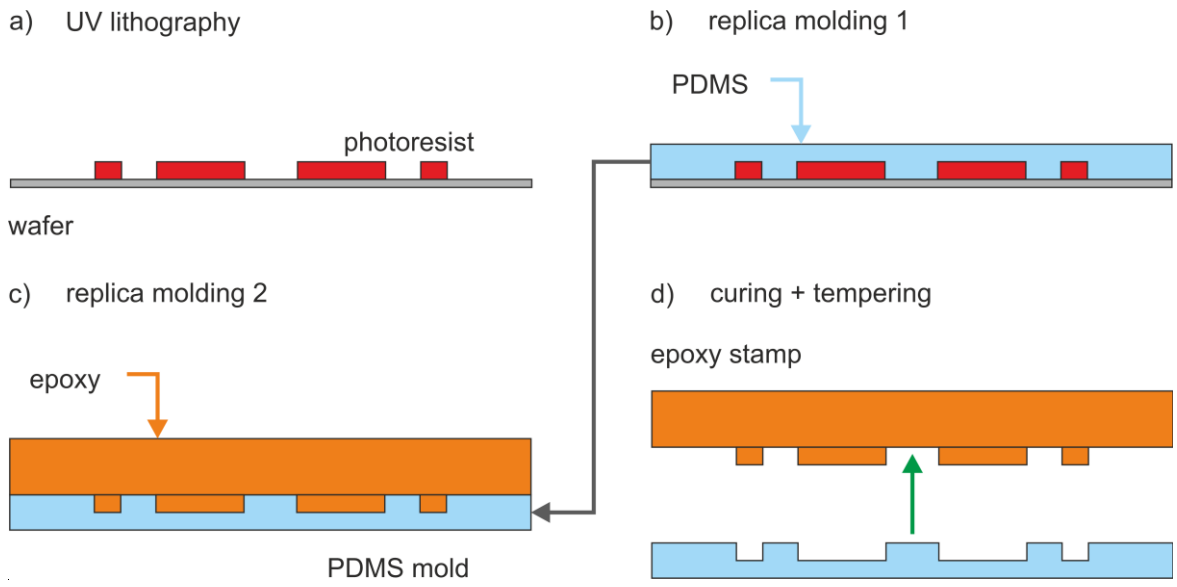

Figure 7.2 Epoxy stamp fabrication: a) Standard UV lithography is used to generate microstructures in photoresist. b) An intermediate mold is generated with PDMS. c) PDMS is replica molded with epoxy resin. d) After curing and tempering, a temperature stable epoxy stamp with the initial structure profile is obtained.

For improved handling of the epoxy resin and precise structure transfer, a molding tool was designed for epoxy replica molding of the intermediate PDMS master. A vacuum chuck builds the basis of the tool and allows for the fixture of the PDMS master as well as the removal of trapped air bubbles during epoxy injection (Figure 7.3 a, b). An 8 mm high aluminum ring with an inner diameter of 110 mm is added on top of the PDMS master and forms a cavity for the injection of epoxy resin. A planar back side of the epoxy stamp is achieved by adding a PMMA plate on top of the aluminum ring. The interface between PMMA and aluminum ring is sealed with an O-ring to prevent leakage. Two syringes are connected to the PMMA top plate for epoxy injection (Figure 7.3 c). The first syringe is filled with epoxy resin that flows into the cavity by generating a small vacuum with the other syringe. If air bubbles are trapped during epoxy injection, applying vacuum underneath the PDMS layer allows for gas diffusion through the gas permeable PDMS and complete filling of the channel structures with epoxy resin (Figure 7.3 d).

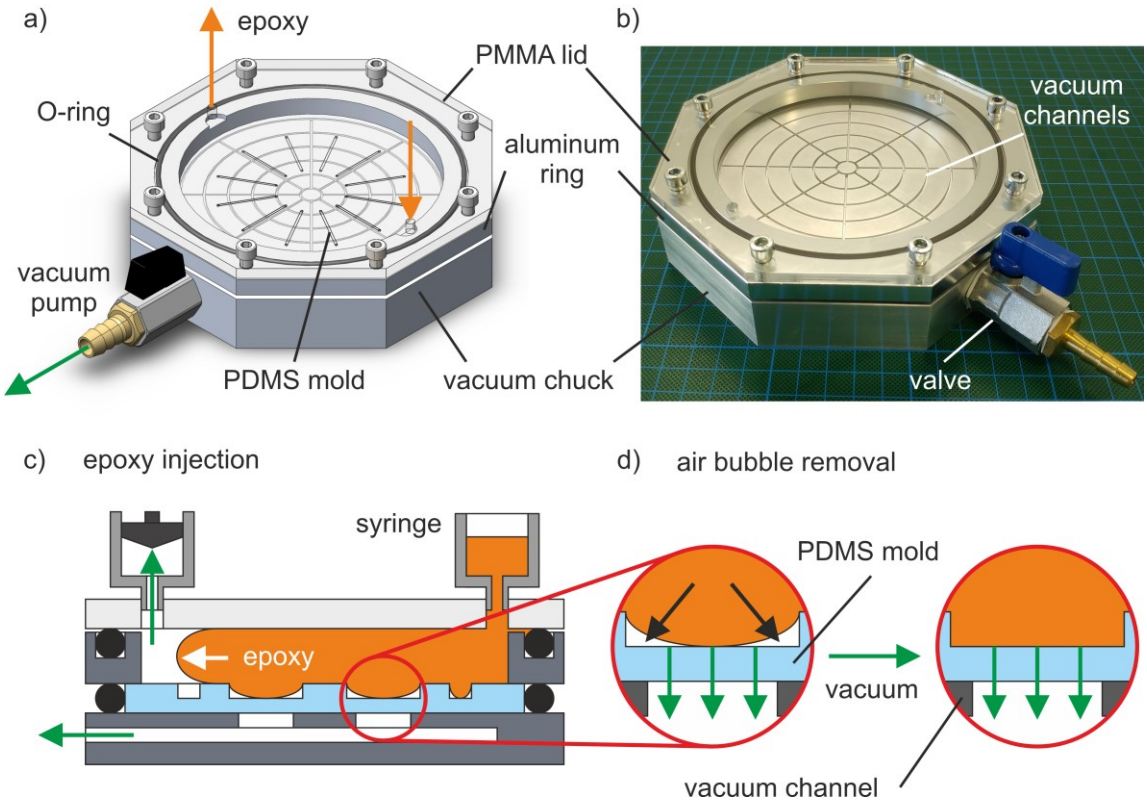

Figure 7.3 Epoxy molding tool: a) 3D view of the CAD model and b) photograph of the epoxy molding tool for replica molding of PDMS structures with epoxy resin. b) Epoxy resin injection into the molding tool and c) air bubble removal by applying vacuum underneath the PDMS mold. a, c, d) adapted from Ref. [227] with permission from the Royal Society of Chemistry available under the CC BY-NC 3.0 license and b) adapted from Ref. [228] available under the CC BY 4.0 license.

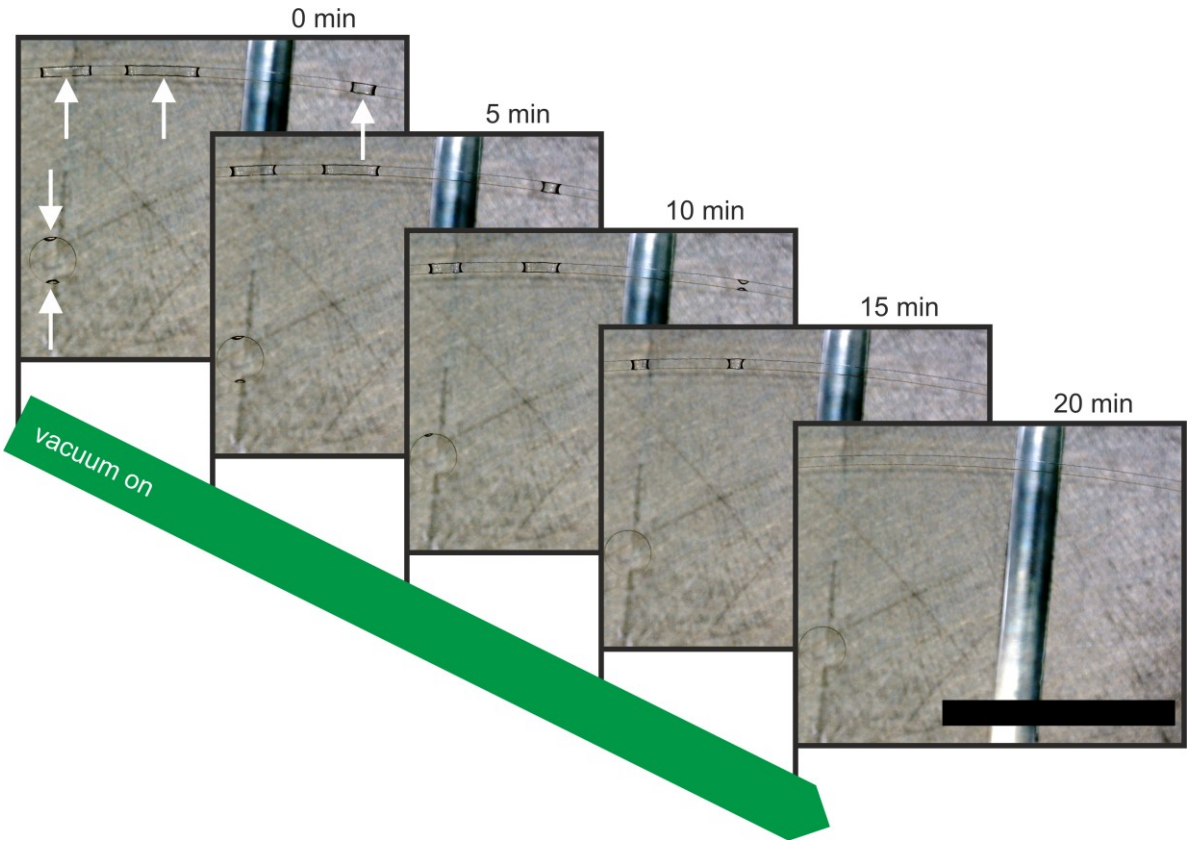

Figure 7.4 Visualization of air bubble removal: Time lapse images of vacuum-assisted removal of air bubbles trapped in PDMS cavities that are covered by water. Air bubbles (white arrows) shrink over time and are completely removed within 20 min. Scale bar: 5 mm. Figure shows time-laps images adapted from Ref. [227] with permission from the Royal Society of Chemistry available under the CC BY-NC 3.0 license.

The removal of air bubbles through a PDMS master in the epoxy molding tool was demonstrated using water and monitored over time (Figure 7.4). Air bubbles trapped in the PDMS cavities disappeared completely within 20 min of vacuum application (≥ 100 mbar, absolute pressure). After the curing and tempering of epoxy stamps, they were used for structuring of extruded TPE layers by hot embossing. Therefore, epoxy stamps were pressed (140 °C, 0.4 MPa, 10 min) into TPE, laminated on a PTFE foil, which provided a temporary carrier layer during hot embossing (Figure 7.5 a). TPE layers were easily removable from both the epoxy stamp and the PTFE foil after cool-down (< 40 °C) by applying a few drops of IPA (Figure 7.5 b). Thereby, the epoxy stamps allowed for multiple hot embossing and demolding cycles without any visible damage to the microstructures. At the same time, a precise transfer of microstructures all the way from photoresist structures to the final hot embossed TPE was achieved. This was demonstrated by comparing channel dimensions measured from side cuts of PDMS replica molds of the initial photoresist microstructures and the fabricated epoxy stamp as well as cross-sections from the resulting TPE channels after hot embossing (Figure 7.5 c).

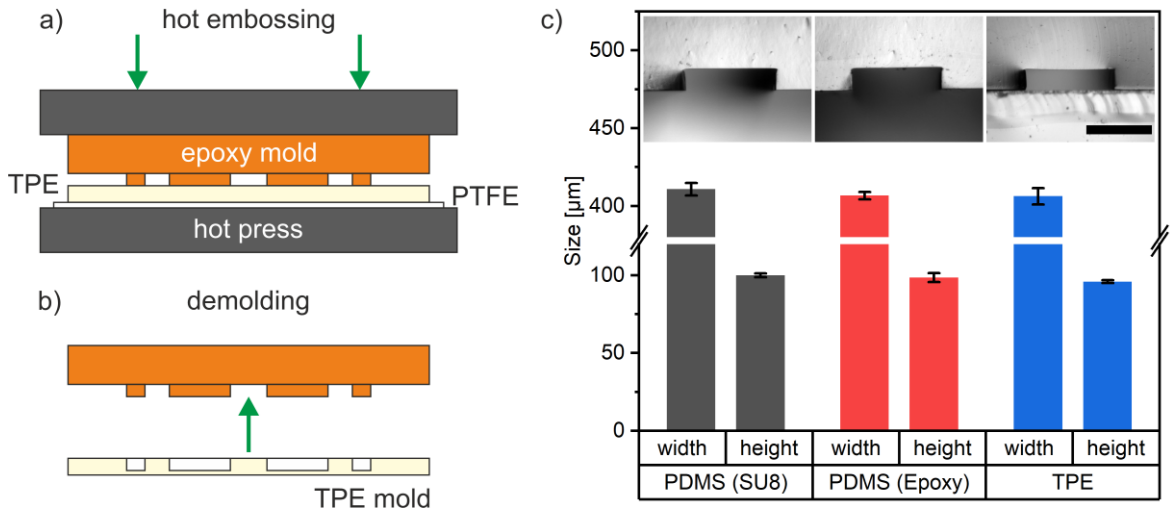

Figure 7.5 Structuring by hot embossing: a) Hot embossing of flexible TPE layers. Epoxy stamps are placed on top of TPE, laminated on a PTFE foil, and embossed using a hot press. b) After cool-down, TPE molds are removed from the epoxy and the PTFE foil. c) Images and dimensions of channel cross-sections of PDMS replica molds from initial SU-8 structures and the epoxy mold as well as the final, hot embossed TPE channel ($N = 4$ channels). Scale bar: 300 µm. a, c) adapted from Ref. [227] with permission from the Royal Society of Chemistry available under the CC BY-NC 3.0 license.

To provide more flexibility in terms of channel geometries, TPE hot embossing was combined with rapid-prototyping techniques for the stamp fabrication. Therefore, embossing stamps were fabricated by SLA 3D printing using a temperature stable printing resin (Figure 7.6 a, b).

Besides faster generation of the stamps compared to epoxy-based stamp fabrication, the 3D-printed stamps allowed for more flexibility of the 3D structure of the embossed channels. This was demonstrated by SLA printed stamps with semicircular structures for hot embossing of round channels into TPE. The resulting channel cross-sections were precisely adaptable to a predefined object. This enabled, for instance, the integration of cylindrical objects (Figure 7.6 c-e), such as a hollow fiber membrane provided by Dr. Thomas Schiestel (Fraunhofer Institute for Interfacial Engineering and Biotechnology IGB, Stuttgart, Germany).

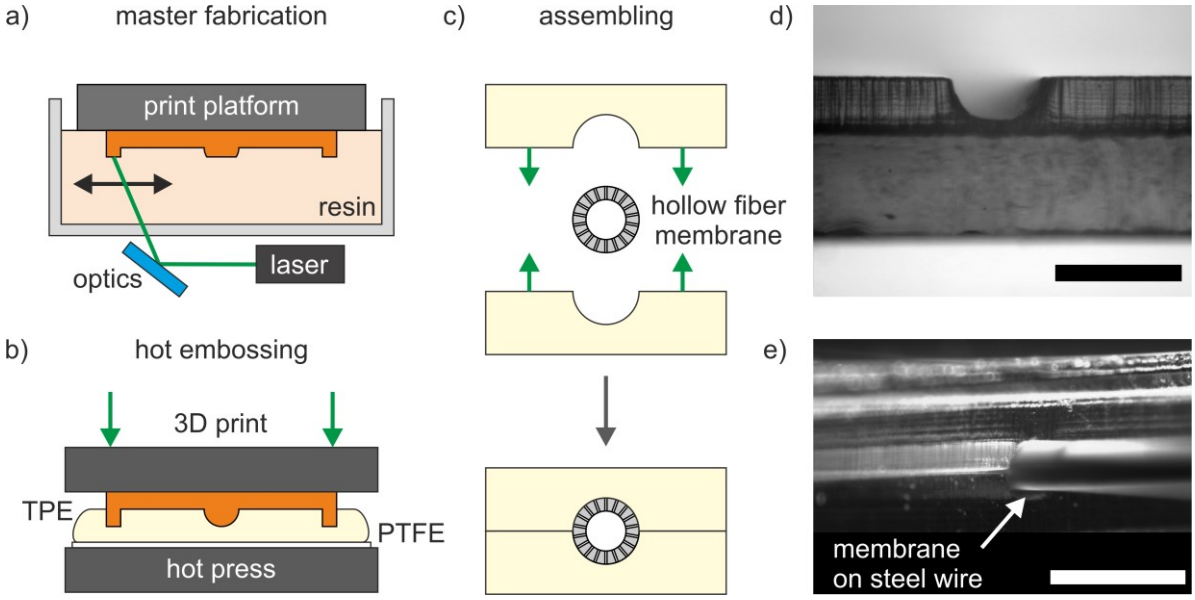

Figure 7.6 Hot embossing of round channels: a) Hot embossing stamp fabrication by SLA printing using laser-based structuring of a photo-sensitive and temperature-stable resin. b) Hot embossing with 3D-printed stamps and semicircular channel geometries. c) Round channels in TPE enable the integration of a cylindrical object, *e.g.* a hollow fiber membrane. d) Side view of TPE channel after hot embossing with 3D printed stamp. e) Hollow fiber membrane, provided by Dr. Thomas Schiestel, between two TPE layers with round channels. Scale bars: c) 500 µm, d) 1 mm.

Besides the fabrication of flexible layers, hot embossing was further optimized for the fabrication of a rigid composite material by combining TPE and thermoplastic PC [228]. Microstructured PC/TPE-hybrid layers are generated in a single hot embossing cycle that includes structuring of TPE and simultaneous fusing to PC (Figure 7.7 a, b).

As analyzed in collaboration with Eduardo J. S. Brás (NMI Natural and Medical Sciences Institute at the University of Tübingen, Reutlingen, Germany), the resulting composite material combines features of both materials [228]. TPE allowed for precise structuring and robust bonding to several materials (*cf.* section 7.1.2). The PC layer provided a rigid and polished support for the flexible TPE and resulted in a PC/TPE composite module with increased structural support (Figure 7.7 c). This is especially important for multi-layered systems that require the alignment of several layers to each other. This fabrication step is, however, difficult in the case of standard TPE layers that tend to bend and spontaneously adhere to other surfaces during the alignment process.

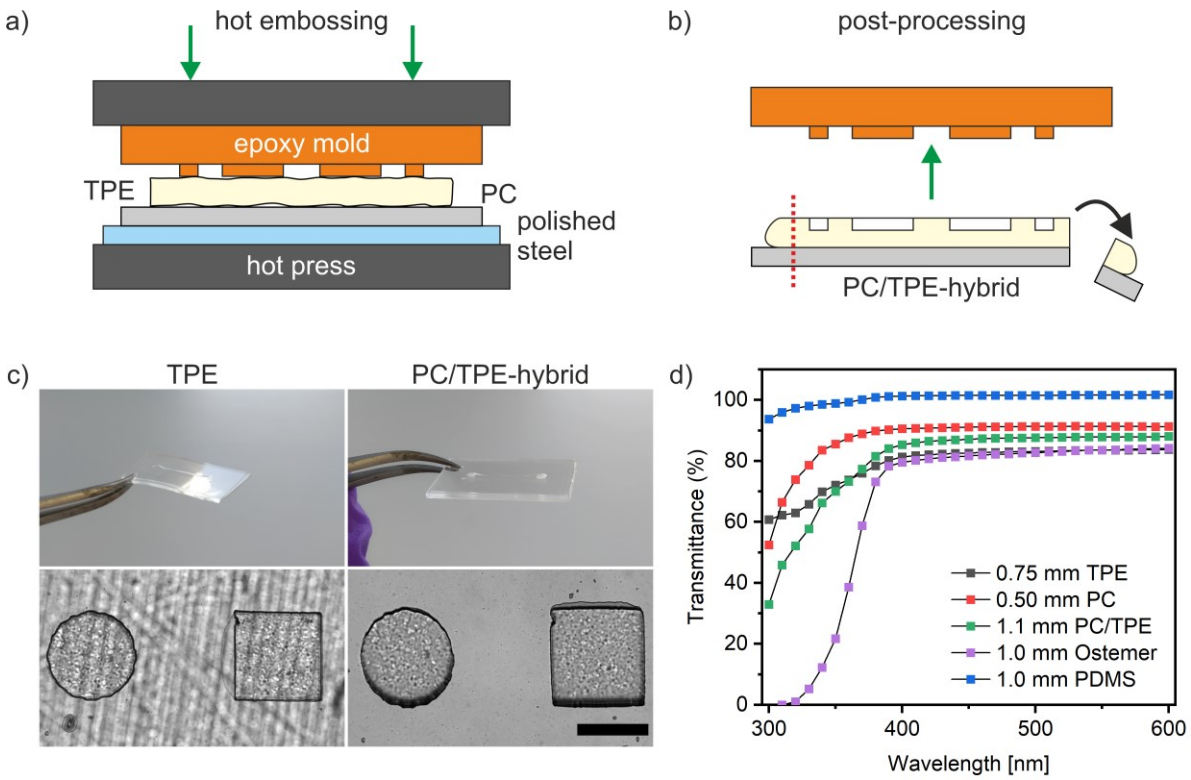

Figure 7.7 PC/TPE-hybrid devices: a) Simultaneous structuring of TPE and fusing to PC by a single hot embossing step. b) After post-processing, TPE and PC layers are combined to a microstructured composite material. c) PC/TPE-hybrid layers allow for better structural support and improved microscopy compared to standard TPE layers. Scale bar: 300 µm. d) Transmittance of the base materials, the 0.75 mm, unprocessed TPE and 0.50 mm PC, as well as the final, 1.1 mm thick PC/TPE-hybrid. 1.0 mm Ostemer and 1.0 mm PDMS layers are included for comparison to other standard materials used for microfluidic systems. Results shown in c) and d) were obtained in collaboration with Eduardo J. S. Brás. c, d) adapted from Ref. [228] available under the CC BY 4.0 license.

At the same time, the polished surface of the PC support improved the microcopy capabilities of the composite by reducing the overall roughness on the backside of the hybrid. Standard TPE layers featured a rougher backside due to the PTFE carrier layer. Furthermore, the transmittance of the 1.1 mm thick composite was in the same range as the individual base materials, 0.75 mm thick TPE and 0.50 mm thick PC (Figure 7.7 d). This demonstrates that the combination of both materials is not accompanied by loss of transparency. In comparison to common materials in microfluidic research, PC/TPE-hybrid layers were less transparent than PDMS but revealed better optical properties than Ostemer, another alternative material to PDMS [47, 48].

7.1.2 Bonding

Solvent Vapor Bonding

Solvent vapor bonding was used for the fabrication of multi-layer Organ-Discs that consisted of 2D structured thermoplastic layers [226]. The overall applied bonding approach is adapted from Ogilvie *et al.* demonstrating the solvent-based fabrication of microfluidic devices in PMMA and COC [230].

The individual layers of the Organ-Disc were stepwise joined by solvent vapor treatment (Figure 7.8 a) and subsequent bonding in a hydraulic press at ambient temperature (Figure 7.8 b). Solvent vapor treatment was achieved by attaching PMMA layers to the lid of a Petri dish that was filled with chloroform. Thereby, only one side of the individual PMMA layers came in direct contact to the chloroform vapor and developed a softer and swollen surface. A 4 min solvent vapor exposure at RT was sufficient for rendering the treated PMMA layer adhesive to another untreated PMMA substrate. This allowed for a stepwise bonding at RT with pressures in the range of 6-10 MPa of the individual Organ-Disc layers. The individual bonding steps took 10 min each, which enabled the complete fabrication of Organ-Discs with up to six layers within 2 h, followed by overnight incubation in a vacuum oven for removal of remaining solvent (Figure 7.8 c). At the same time, single sided solvent exposure avoided repeated solvent exposure of already bonded layers. This bonding approach also allowed for the integration of thin and fragile PET membranes by only treating the PMMA counterpart and pressing it on the untreated membrane surface.

In addition to fusion of thermoplastic layers, solvent vapor exposure is suitable for polishing of rough thermoplastic surfaces as shown by Ogilvie *et al.* [230]. This effect was beneficial for rough channel edges from 2D structuring and resulted in better channel wall quality after vapor exposure and bonding (Figure 7.8 d). However, longer solvent vapor exposure than 4 min resulted in severe loss of material stiffness. Especially for the thin media layer from 75 µm PMMA foils, this resulted in low yield for correct alignment and lamination to another substrate.

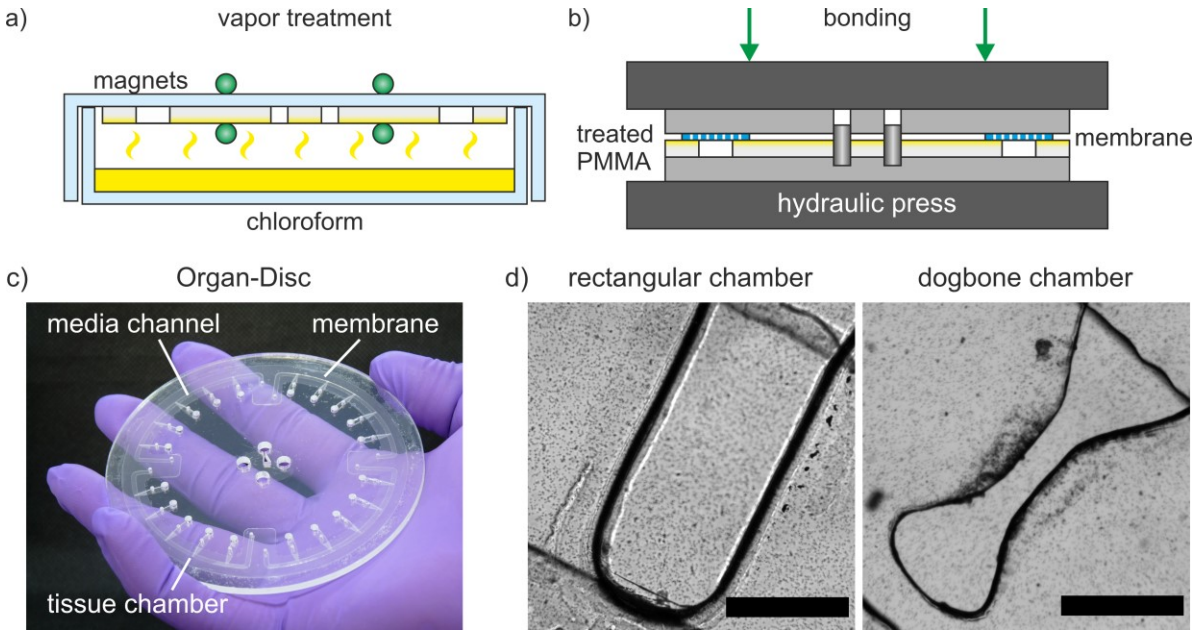

Figure 7.8 Solvent vapor bonding: a) Solvent vapor treatment of thermoplastic disc layers in a Petri dish filled with chloroform. b) After solvent exposure, layers were stepwise bonded in a hydraulic press. c) Organ-Disc after complete bonding and solvent removal using a vacuum oven. d) Bright field images of rectangular and dogbone-shaped tissue chambers have smooth channel edges after solvent vapor bonding. Scale bars: 500 µm. a), b) and c) adapted from Ref. [226] available under the CC BY 4.0 license.

A limitation of this bonding approach is the dependence of the bond quality on the respective material combination. Solvent vapor bonding for membrane integration resulted in a relatively low yield compared to bonding two identical PMMA layers, such as the 175 µm PMMA layers for tissue and bottom layer. The main reasons for this were the general challenge of solvent bonding dissimilar materials, such as PET and PMMA [237], and the difficult handling of the 15 µm thin membranes during alignment and lamination. Similarly, direct connections between media layers (75 µm thick PMMA) and port layers (2 mm thick PMMA), both from different manufactures, were often prone to delamination during subsequent disc operation. This was counteracted by adding an intermediate connector layer (175 µm thick PMMA) that showed sufficient bonding to both media and port layer material.

Thermal Fusion Bonding

Thermal fusion bonding is based on controlled application of heat and pressure to fuse thermoplastic layers and provides an alternative to solvent-based bonding [40]. The main goals of implementing thermal bonding were the avoidance of toxic solvents and further scale-up of the Organ-Disc fabrication.

A bonding tool for simultaneous bonding of up to seven discs was developed for robust and parallelizable thermal fusion bonding of the Organ-Disc [227]. The tool consists of two aluminum plates for base and cover, silicone layers as well as polished, stainless steel plates (Figure 7.9 a). The outer dimensions of the bonding tool are equal to the 320 × 320 mm^2 large plates of the hot press and provide space for up to seven Organ-Discs, each with a footprint of a 10 cm circle (Figure 7.9 b). Elastic silicone was used for soft layers between aluminum and steel plates in order to compensate irregularities in parallelism and planarity as well as to achieve conformal contact for unrestricted heat conduction. The laser-cut, mirror polished steel plates on both sides of the polymer layer stacks provide a smooth and easily replaceable contact surface (Figure 7.9 c). Four pins are inserted into the base plate and allow for the correct alignment of the individual disc layers at each bonding position in the tool.

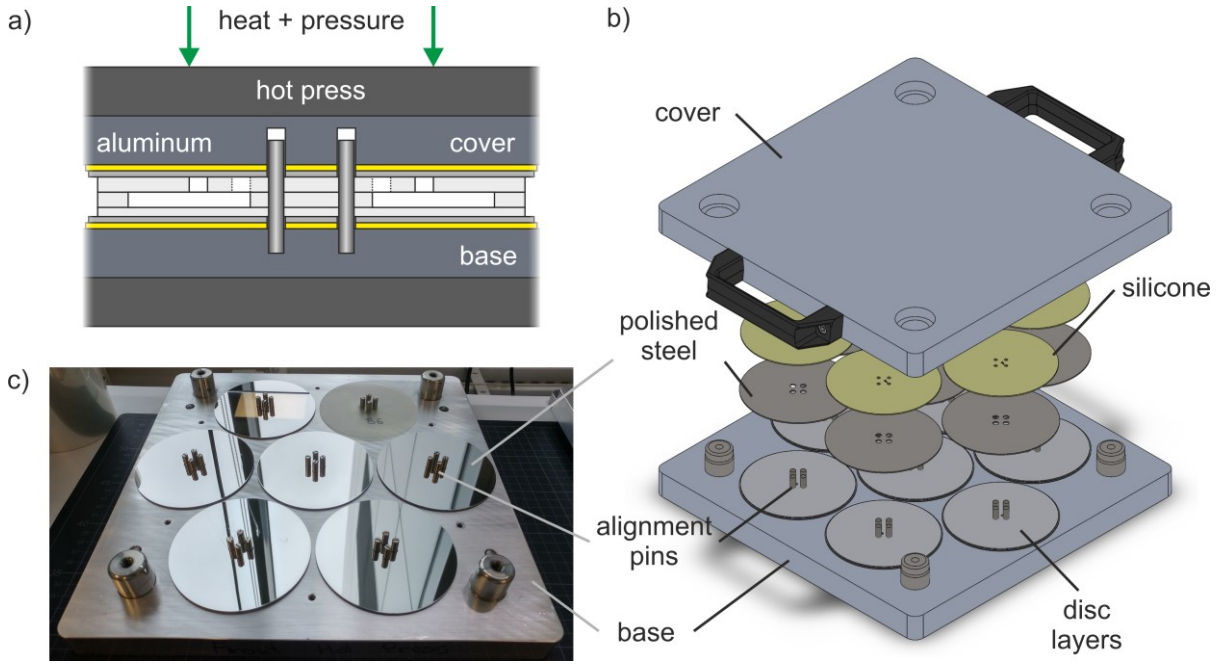

Figure 7.9 Thermal fusion bonding setup: a) Cross-section of a single position in the bonding tool for thermal fusion bonding. b) 3D view of the CAD model of the bonding tool for bonding up to seven polymer stacks with a footprint of a 10 cm circle. c) Photograph of the open bonding tool with base plate, silicone layers, mirror polished steel plates and alignment pins. a), b) adapted from Ref. [227] with permission from the Royal Society of Chemistry available under the CC BY-NC 3.0 license.

The overall bonding process can be separated in three consecutive steps: 1) heating the tool inside a hot press to the bonding temperature, 2) increasing the pressure for bonding of the thermoplastic layers and 3) cooling down to RT (Figure 7.10 a). The third step is achieved by removing the tool from the press and leaving it overnight at RT before opening it since the applied hot press lacked active cooling capabilities.

Temperature measurements at four different positions inside the tool confirmed the optimized temperature distribution inside the tool due to the symmetric arrangement of the bonding positions and the soft elastomer layers assuring that no air pockets limit the heat transfer (Figure 7.10 a). The bonding temperature was highly stable after the pre-heating step and fluctuations were bellow 1 °C from the desired temperature.

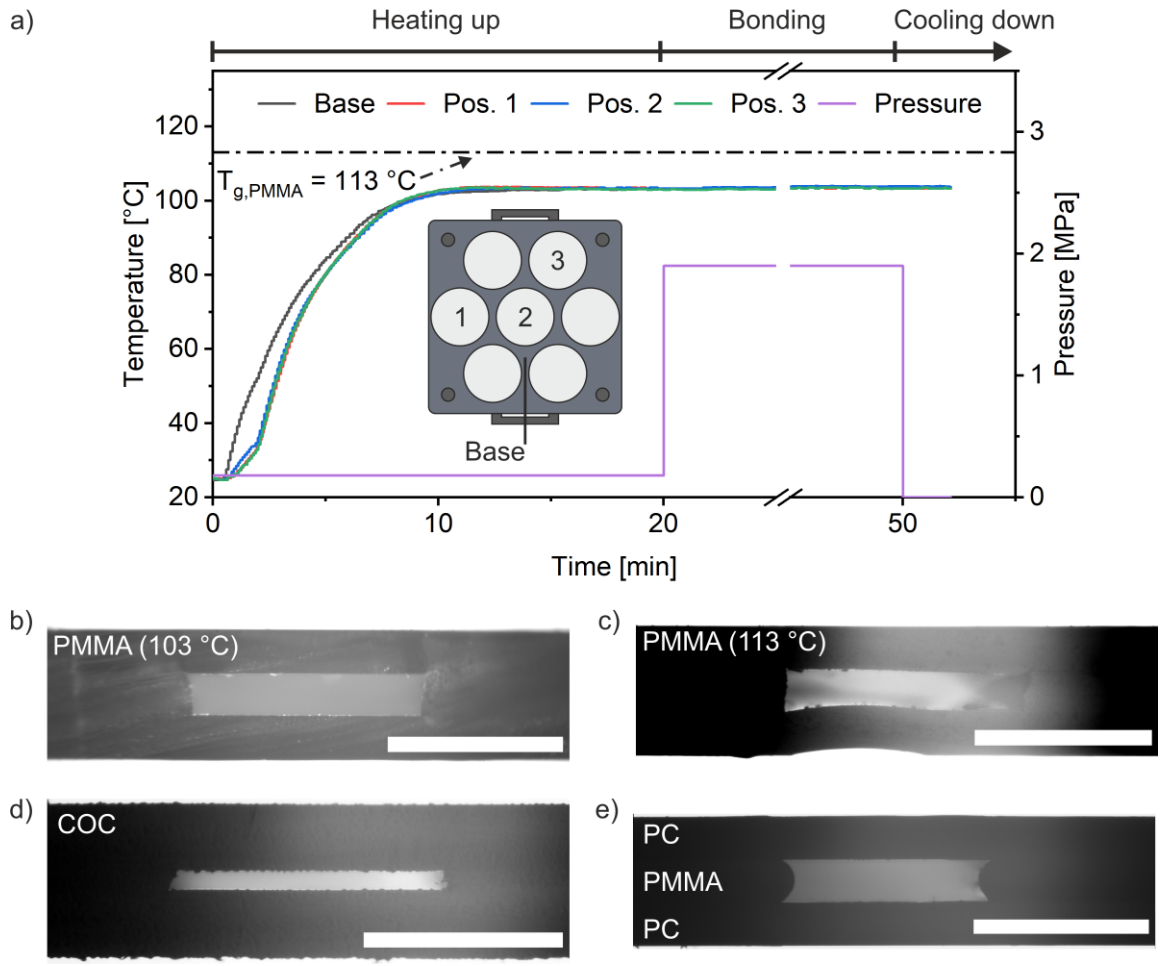

Figure 7.10 Thermal fusion bonding: a) PMMA bonding process. Temperature at four different positions in the tool as well as applied pressure over time. b-e) Channel cross-sections from discs fabricated in b, c) PMMA at different bonding temperatures as well as other thermoplastic materials, such as d) COC or e) a combination of PC and PMMA. Scale bars: b-e) 750 µm. b) adapted from Ref. [227] with permission from the Royal Society of Chemistry available under the CC BY-NC 3.0 license.

The developed bonding tool allowed for versatile and precise thermal fusion bonding of several thermoplastic materials, such as PMMA, PC and COC. Thereto, the respective bonding parameters – temperature, pressure and time – had to be adapted in each case (*cf.* Table 7.2). Suitable bonding results for PMMA were achieved by applying approx. 1.9 MPa for 30 min at 103 °C, 10 °C below the material's glass transition temperature (Figure 7.10 b). For instance, bonding at T_g = 113 °C resulted in increased collapse of bottom or top layer (Figure 7.10 c).

Additionally to PMMA as the mainly explored materials for Organ-Disc fabrication, the fabrication of COC-based Organ-Discs was implemented in order to provide a wider material selection and to demonstrate the adaptability of the thermal fusion bonding setup. Bonding 5 °C below the material's glass transition (T_g = 142 °C) allowed for the fabrication of approx. 72 µm high channels without channel collapse (Figure 7.10 d).

Besides reduced bonding temperatures, distortion and collapse during thermal fusion bonding can be counteracted by combining materials with different glass transition temperatures [80, 161, 238]. Thereto, PMMA, as low-T_g material, was used for channel side walls and PC, as a higher temperature stable polymer, for top and bottom layer. Bonding in between the glass transition temperatures of PMMA and PC at 133 °C prevented collapse of the top and bottom PC layer but led to slightly rounded channel side walls due to softening of the PMMA middle layer (Figure 7.10 d). However, the average deviation to the intended channel dimensions after bonding was below 10% for all materials (Table 7.2). Furthermore, the resulting bonds could stand a nitrogen pressure of 3.5 bar without failure. This was the highest possible pressure of the regulator used for the burst pressure test of the individual Organ-Discs. Thereby, thermal fusion bonding provides sufficient bond strength that exceeds the need of conventional OoC and microfluidic cell culture devices.

Table 7.2 Thermal fusion bonding parameters for different thermoplastic materials and resulting channel properties. $N \geq 4$ channel cross-sections and $N \geq 3$ burst pressure tests. Values of PMMA Organ-Discs are published in Ref. [227].

	PMMA, *cf.* Ref. [227]	COC	PC-PMMA-PC
Temperature [°C]	103	137	133
Pressure [MPa]	1.9	2.7	1.9
Time [min]	30	30	60
Channel height (foil thickness) [µm]	170 ± 15 (175)	72 ± 5 (80)	176 ± 9 (175)
Channel width (CAD) [µm]	963 ± 28 (1000)	941 ± 55 (1000)	909 ± 100 (1000)
Deviation H | W [%]	− 2.7% − 3.7%	− 9.7% − 5.9%	0.1% − 9.1%
Pressure test (max. 3.5 bar)	passed	passed	passed

TPE Bonding

Thermal fusion bonding of TPE was applied for the integration of flexible, hot embossed pump layers on top of a PMMA-based disc module [227]. TPE was plasma activated for improved adhesion [239], laminated on top of the Organ-Disc (Figure 7.11 a) and then thermal fusion bonded (95 °C, 6-15 kPa, 1 h) with a small weight added on top (Figure 7.11 b).

Due to the self-adhesive properties of the SEBS material, this simple bonding approach was sufficient for the integration of flexible pumping layers on top of the Organ-Disc (Figure 7.11 c) and allowed for distortion-free pump channels after bonding (Figure 7.11 d). Furthermore, the obtained bonds were stable up to a pressure of 3.1 ± 0.3 bar ($N = 3$, failure at TPE-TPE interface) and allowed for several days of peristaltic Organ-Disc perfusion at 95% humidity and 37 °C (*cf.* section 9.4).

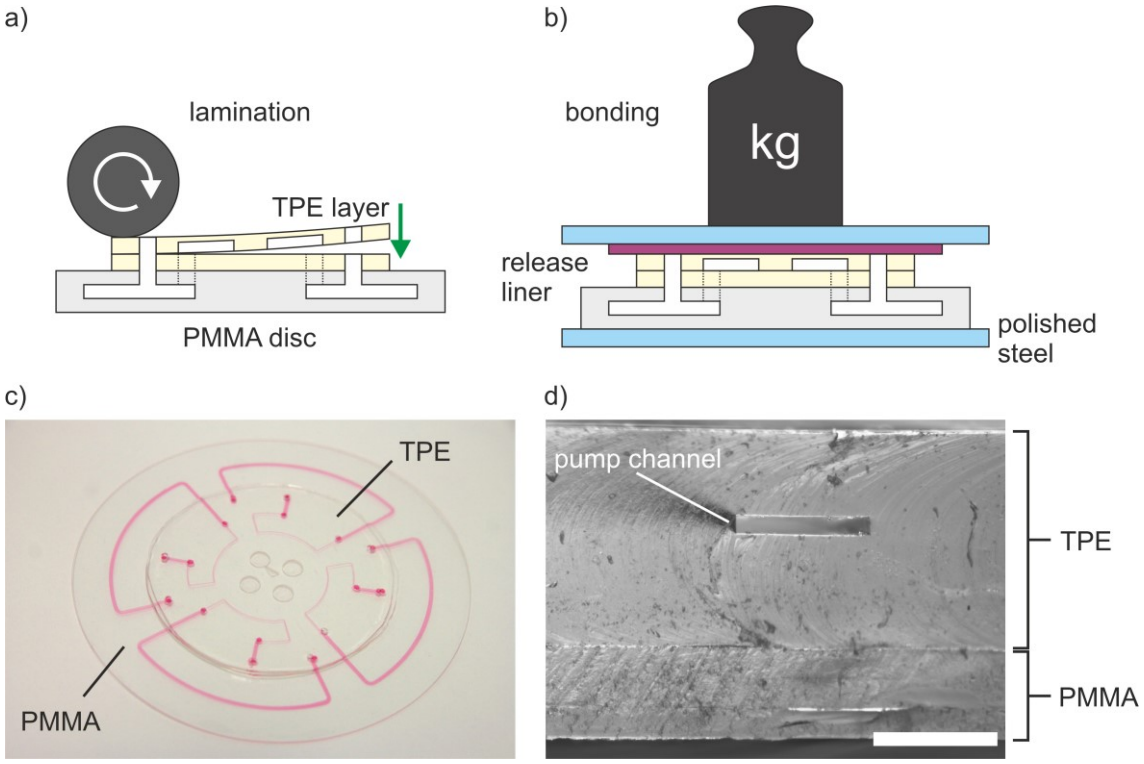

Figure 7.11 TPE bonding: a) Lamination of flexible TPE layers on top of PMMA-based Organ-Discs. b) Thermal fusion bonding of TPE using an oven and a small weight added on top. c) Organ-Disc with a TPE pump module on top. The disc is filled with colored water for visualization of the functional channel layout. d) Distortion-free pump channel in TPE after bonding to a PMMA disc. Scale bar: 750 µm. a), d) adapted from Ref. [227] with permission from the Royal Society of Chemistry available under the CC BY-NC 3.0 license.

For further characterization of TPE-based microfluidic devices, PC/TPE-hybrid layers were combined with multiple materials and analyzed in collaboration with Eduardo J. S. Brás (NMI Natural and Medical Sciences Institute at the University of Tübingen, Reutlingen, Germany) [228]. Thereto, the SEBS surfaces of PC/TPE hybrid layers were bonded to extruded TPE sheets and alternative thermoplastic substrates, such as COC, PS and PC. The respective combinations were thermal fusion bonded by an even simpler approach using overnight incubation in an oven at 60 °C without any additional applied bonding pressure.

All material combinations were stress tested right after bonding and after seven days submerged in PBS at 37 °C. Maximum working pressures were tested by applying nitrogen pressure, sealing the outlet and placing the chip under water for observation of leakage (Figure 7.12 a). Under both conditions, bonds between PC/TPE-hybrid layers and COC, PS, or PC substrates did not delaminate even at the highest possible output pressure of 7.5 bar of the nitrogen line (Figure 7.12 b). Solely bonds between PC/TPE-hybrid layers to TPE substrates could not stand pressures above 4.7 ± 0.2 bar or 3.2 ± 0.9 bar after chip submersion respectively. Further increased gas pressure led to clearly visible deformation of the flexible TPE substrate, however, not in bond failure or gas leakage.

Therefore, for all material combinations and under both exposure conditions, the achieved pressure stability is well-suited for OoC applications if, for instance, physiologic blood pressure is used as a reference [240]. Even after seven days under culture conditions, the obtained bond strength is still comparable or even higher than previously reported values [83, 84].

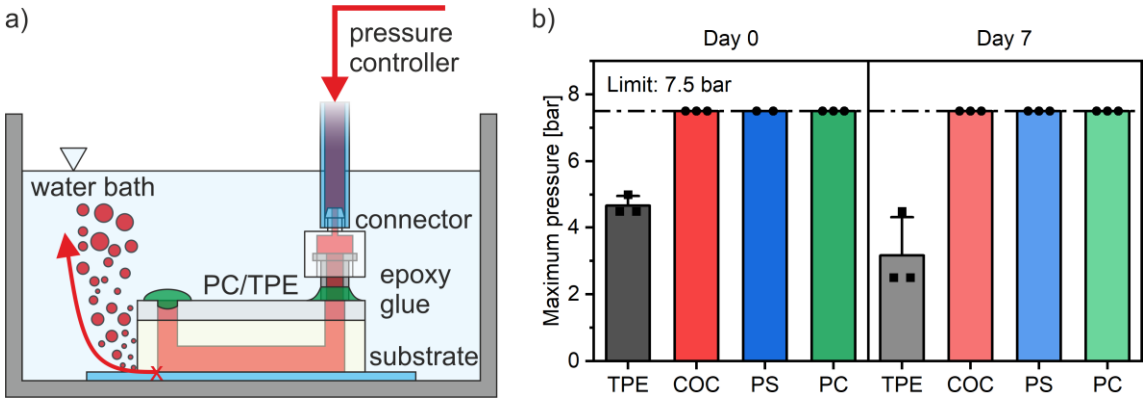

Figure 7.12 TPE bonding strength: a) Burst pressure setup used for bond strength assessment. A nitrogen pressure line is connected to a chip with sealed outlet. The chip is placed in a water bath for better observation of bond failure. b) Maximum working pressure of TPE-based microfluidic devices. Chips consisted of PC/TPE hybrid layers bonded to TPE and several thermoplastic substrates and were tested after bonding (Day 0) and after seven days submerged in PBS at 37 °C (Day 7). Results shown in b) were obtained in collaboration with Eduardo J. S. Brás. b) adapted from Ref. [228] available under the CC BY 4.0 license.

7.2 Organ-Disc Spinner

Different Organ-Disc spinners were developed for the individual rotation-based processes of the Organ-Disc. The setups used for centrifugal loading and centrifugal perfusion were developed in collaboration with Oliver Schneider (Fraunhofer Institute for Interfacial Engineering and Biotechnology IGB, Stuttgart, Germany) [226].

The spinner for centrifugal loading was designed in a compact format allowing for Organ-Disc cell loading inside a standard laminar flow bench under sterile conditions (Figure 7.13 a). A brushless DC motor, integrated into a PMMA housing, allowed for Organ-Disc rotation at 500-4,000 rpm and was used for channel wetting and cell loading.

For centrifugal perfusion, Organ-Discs were spun at up to 200 rpm by a stepper motor, which was attached to a PMMA base plate. This plate was connected to a standard incubator shelf to enable Organ-Disc rotation under culture conditions (Figure 7.13 b).

A similar perfusion setup, featuring a stepper motor for rotation of a magnetic holder for dragging steel balls on top of the Organ-Disc (Figure 7.13 c), was used for integrated, peristaltic pumping [227]. The main difference, however, was that Organ-Discs were fixed to a platform instead to the spinning motor shaft. Thereby, the magnetic holder connected to the motor could rotate freely underneath the stationary Organ-Discs, which was positioned slightly above the magnets.

In all perfusion setups, the remaining electronic components, such as display and rotary encoder providing a user-interface for setting rotation parameters, were left outside the incubator and connected to the motor by a thin cable (Figure 7.13 d). Thereby, all electronic components but the motor remained outside the hot and humid incubator environment while the Organ-Disc was spun under standard culture conditions.

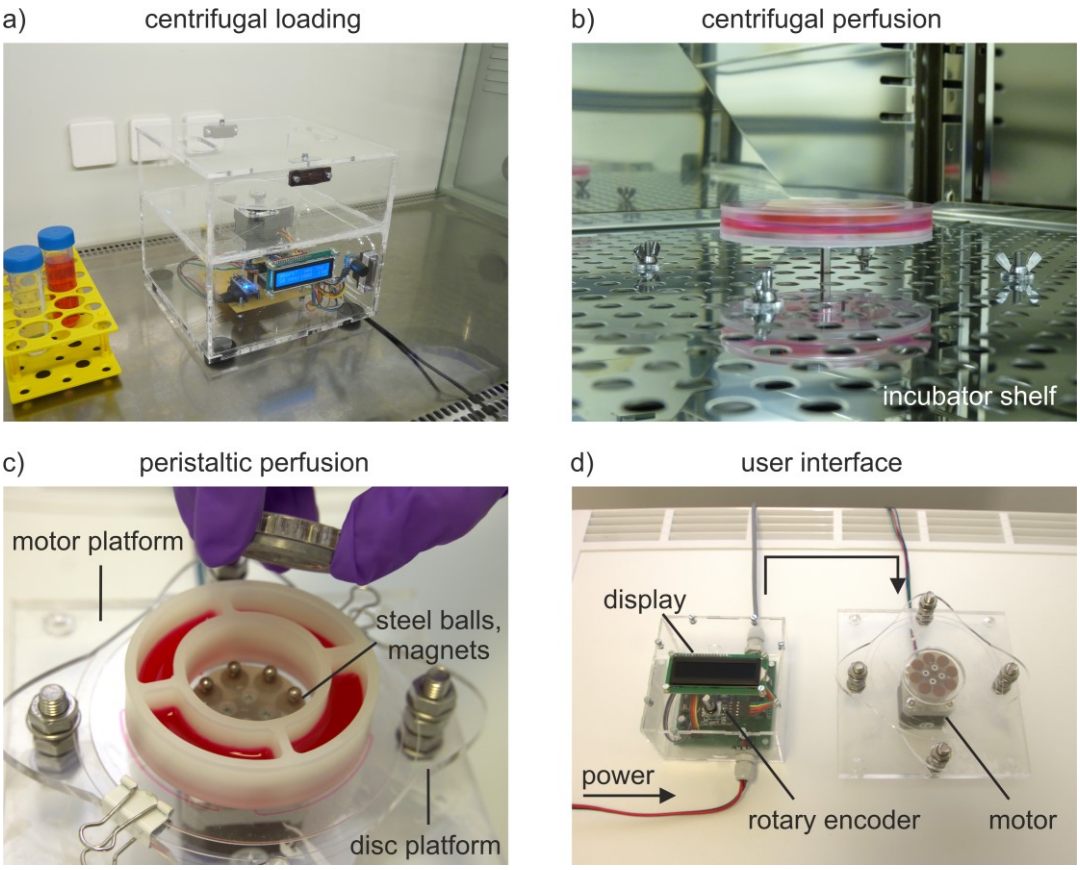

Figure 7.13 Organ-Disc spinner: a) Centrifugal loading setup for cell loading of the Organ-Disc under sterile conditions. b) Centrifugal perfusion setup for media supply by rotation of the Organ-Disc inside an incubator. c) Peristaltic perfusion setup for integrated, closed-loop pumping in the Organ-Disc. A magnetic holder spins underneath the disc and drags steel balls on top the pump module. d) Display and rotary encoder provide a user interface for setting rotation parameters and are connected by a cable to the motor, which is placed inside an incubator for Organ-Disc perfusion under culture conditions. a, b) adapted from Ref. [226] available under the CC BY 4.0 license. c) adapted from Ref. [227] with permission from the Royal Society of Chemistry available under the CC BY-NC 3.0 license.

8 Perfusion

The results presented in section 8.1 were published in Ref. [226], whereas results presented in section 8.2 are published in Ref. [227].

8.1 Centrifugal Pumping

Linear, centrifugal perfusion in the Organ-Disc is based on centrifugal pumping [27, 209], which is achieved by rotation of the disc and its reservoir [226]. For OoC and microfluidic cell culture in general, media supply by centrifugal pumping has to meet two main requirements: 1) The achieved flow rates in the Organ-Disc have to be controllable and in the range of usual values applied in OoC systems. 2) The centrifugal forces for pumping must not tremendously succeed conditions in stationary systems and moderate centrifugal accelerations are required in order to avoid hyper-gravity conditions.

Before starting centrifugal perfusion, the central reservoir compartment is filled up to its lid with fresh cell culture media, while the outer effluent compartments are empty. As soon as the Organ-Disc and its reservoir start to spin, both centrifugal and hydrostatic pressure gradients are present across the media channel (Figure 8.1 a). Therefore, both pressure gradients contribute to the resulting flow rate Q in the media channel with

$$\mathrm{Q} = \frac{\Delta p_\mathrm{c} + \Delta p_\mathrm{h}}{R_\mathrm{hyd}} \tag{8.1}$$

whereby Δp_c is the centrifugal and Δp_h the hydrostatic pressure gradient as well as $R_\mathrm{hyd} = 10.8\ 10^{11}$ Pa·s/m^3 the hydraulic resistance of the rectangular media channel using equation (2.18) with $W = 1400$ µm, $H = 75$ µm, $L = 74$ mm and $\eta_{\mathrm{water,\ 37\ °C}} \sim 0.693$ mPa·s (linear interpolation of values in Ref. [21]).

The centrifugal pressure gradient can be estimated from equation (2.24). Here, the different radii for inner and outer boundaries of the fluid are $r_1 = 21.7$ mm, the central radial position of the inner reservoir compartment and $r_2 = 35.7$ mm, the radial positon of the exit port (Figure 8.1 a). Here, r_1 provides a compromise for varying fluid levels in the compartment for fresh cell culture media. As the effluent is pushed past the exit port, r_2 remains fixed at the outlet position. This also leads to a constant hydrostatic pressure gradient between both reservoir compartments, which is determined from the reservoir height $h = 8$ mm.

Centrifugal perfusion experiments for flow rate measurements were conducted up to rotation speeds of 200 rpm or centrifugal accelerations of up to 1.86 × *g* at the tissue chamber positon respectively (Figure 8.1 b). On average, flow rates were between 3 µL/h and 445 µL/h at 0-200 rpm. Already at 100 rpm or 0.46 × *g*, a flow rate of about 97 µL/h was achieved, which allows for media supply that is comparable to OoC systems based on perfusion by *e.g.* syringe pumps [111, 116, 118, 147]. Under these conditions, both standard gravity on earth and centrifugal acceleration result in 1.1 × *g* and, hence, only minimal elevated gravity conditions.

According to equation (2.24) for centrifugal pressure gradients $\Delta p_c \sim \omega^2$. Also the measured flow rates revealed a super-linear relationship to the applied rotation speed (Figure 8.1 b). However, flow rates in the Organ-Disc were clearly below expected values when both centrifugal and hydrostatic pressure gradients are considered. Especially at very low rotation speed < 50 rpm, flow rates were almost zero. Capillary pinning at the exit port provides a plausible explanation for this observation (*cf.* section 2.1.4), besides other reasons potentially reducing the measured flow rate, *e.g.* motor speed fluctuations or elevated evaporation at 37 °C.

If capillary pinning occurs at the exit port in the reservoir, a capillary burst valve with a burst pressure Δp_v is created. Below the critical angular frequency ω_0, no liquid would leave the media channel. At $\omega > \omega_0$, liquid would leave the media channel and is pushed radially outwards. Therefore, as long as no liquid accumulates above the media channel outlet, the total pressure gradient between in- and outlet of the media channel would be reduced by Δp_v.

Testing this hypothesis, the measured flow rates were approximated using

$$Q = \begin{cases} 0 & \text{if } \omega < \omega_0 \\ \dfrac{\Delta p_c + \Delta p_h - \Delta p_v}{R_{\text{hyd, rect.}}} = B(\omega^2 - \omega_0^2) & \text{if } \omega \geq \omega_0 \end{cases} \tag{8.2}$$

with a variable burst pressure Δp_v. Thereby, Q can be approximated using

$$\omega_0^2 = \frac{\Delta p_v - \Delta p_h}{\frac{1}{2}\rho(r_2^2 - r_1^2)} \tag{8.3}$$

as critical angular frequency that only depends on Δp_v and the constant parameter

$$B = \frac{H^3 \cdot W}{12\eta \cdot L}\left[1 - 0.630\frac{H}{W}\right]\left[\frac{1}{2}\rho(r_2^2 - r_1^2)\right] \tag{8.4}$$

solely depending on geometry parameters and fluid properties. This approximation results in a burst pressure of Δp_v = 97 Pa as well as a coefficient of determination of R^2 = 0.7. Compared

to flow rate calculations considering centrifugal, hydrostatic or both centrifugal and hydrostatic pressure gradients, this approximated flow provides a better matching to the measured flow rates (Figure 8.1 b).

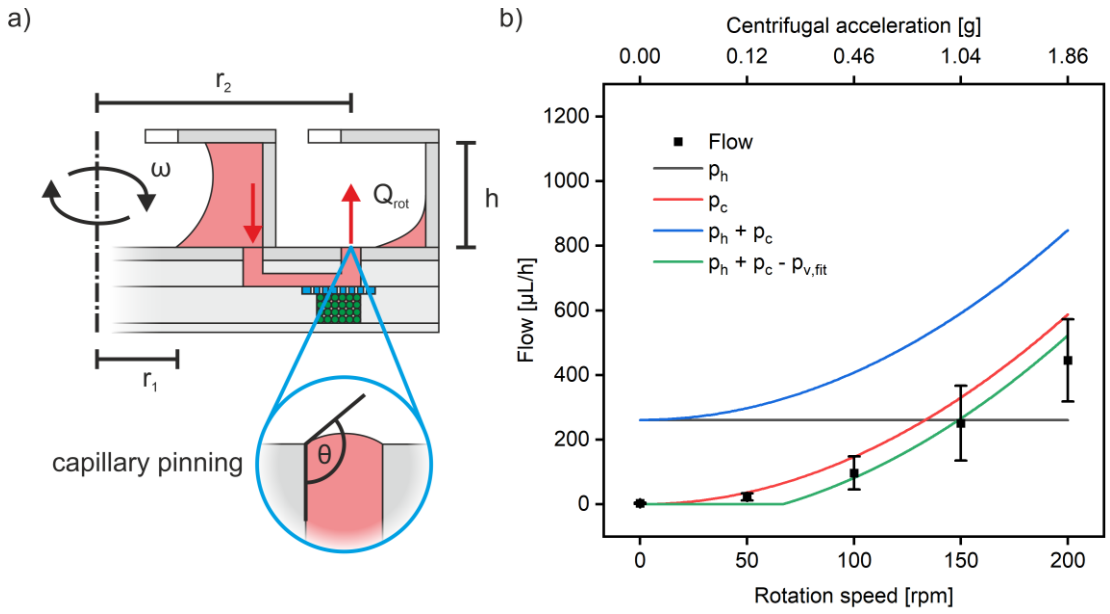

Figure 8.1 Centrifugal Organ-Disc perfusion: a) Pressure gradients during centrifugal pumping. Rotation of the Organ-Disc leads to a centrifugal pressure gradient, different fluid levels above in- and outlet result in a hydrostatic pressure gradient and capillary pining at the exit port creates a capillary burst valve. b) Flow rates by centrifugal pumping. Measured (squares, $N \geq 8$) and calculated flow rates considering hydrostatic ("p_h"), centrifugal ("p_c"), combined hydrostatic and centrifugal pressure as well as fitted flow using an approximated burst pressure ("$p_h + p_c - p_{v,fit}$"). Figure adapted from Ref. [226] available under the CC BY 4.0 license.

8.2 Peristaltic Pumping

Peristaltic pumping in the Organ-Disc provides an alternative to centrifugal pumping and does not require rotation of the disc [227]. Thereby, peristaltic Organ-Disc perfusion avoids centrifugal forces that could impact microtissues during culture and achieves a closed-loop media supply. By adding a flexible pump module on top of the Organ-Disc, peristaltic pumping is achieved in a stationary disc, while steel balls, dragged by a magnetic holder underneath the disc, roll over the pump channels. In total eight steel balls roll sequentially over the flexible pump module, compress the pump channel and push liquid through the disc.

Both the distance between the steel balls as well as the pump channel length are adjusted in a way that the pump channel is constantly sealed by at least one steel ball to prevent back flow (Figure 8.2 a). Due to the arrangement of pump channels and steel balls, a constant fluid volume is trapped between two neighboring steel balls and pumped through the system (Figure 8.2 b). For b = 8 steel balls, the trapped volume V_{trapped} can be estimated as

$$V_{\text{trapped}} = \frac{\pi \cdot d_t \cdot A_c}{b} - \alpha \tag{8.5}$$

with d_t = 30 mm the diameter of the steel balls' trajectory on the disc, A_c = 100 × 400 µm² the pump channel cross-section and α the displacement of the steel balls. Hence, at a certain number of motor revolutions per time U_{Motor}, the resulting flow rate Q is

$$Q = U_{\text{Motor}} \cdot b \cdot V_{\text{trapped}} \tag{8.6}$$

In the simplest case of α = 0, the limit of the pumped flow rate can be estimated. In the case of α = 0, the reduction of the trapped volume between two steel balls through their compression of the pump channel is ignored. Nevertheless, this simplified estimation is in good agreement to the measured flow rates. The actual measured flow rates indicate that V_{trapped} is approx. 15% lower. This relates to a volume of α = 0.071 µL, which is displaced by the compression of the steel balls (Figure 8.2 c). The calculated flow rates according to equation (8.6) with α = 0.071 µL closely follow the experimental flow rate measurement.

As expected for a peristaltic pump, the measured flow rates revealed a linear relation between flow rate and motor speed with a coefficient of determination close to one (R^2 = 0.99999). Motor speeds at 100-800 rph induced average flow rates of 0.32-2.6 mL/h and WSS of 0.19-1.5 dyn/cm² in the approx. 175 µm high channels using equation (2.20) for parallel-plate flow.

Feed and effluent were stored in syringes attached to channel inlet and outlet for flow rate measurements (Figure 8.2 d). Therefore, the experimental setup allowed for assessing the

influence of back pressure on the peristaltic pump. The difference in water level between both syringes and corresponding hydrostatic pressure difference increased up to approx. 450 Pa during flow measurements. No reduction of the measured flow rate was observed up to this maximum back pressure (Figure 8.2 e). Overall, this indicates a proper pump channel sealing by the steel balls and successful prevention of back flow during peristaltic pumping.

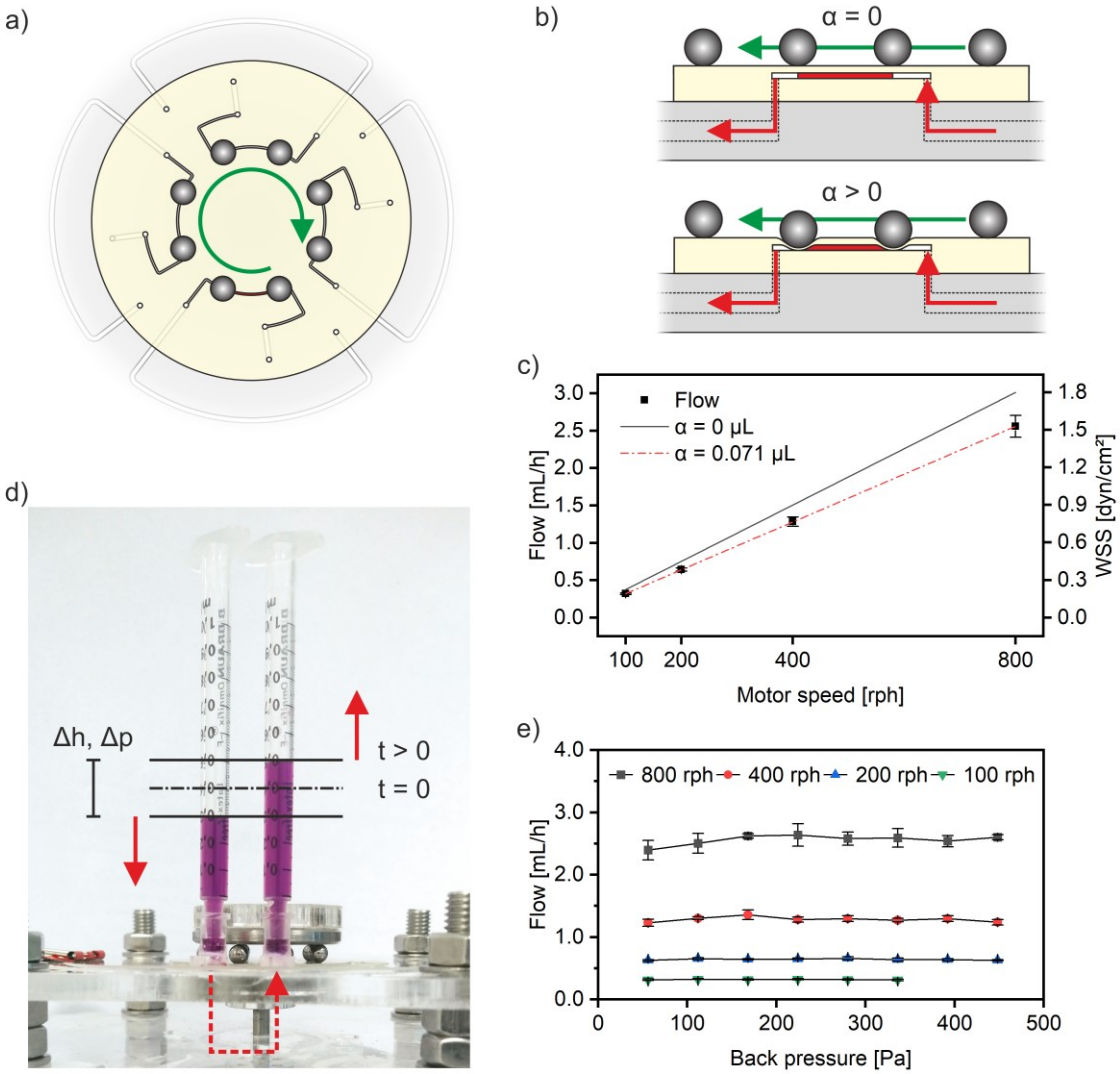

Figure 8.2 Peristaltic Organ-Disc perfusion: a) Top view of the peristaltic pump module with eight steel balls rolling over the four TPE pump channels. b) Schematic side view of a pump channel. Estimation of the volume (marked in red) between two steel balls without compression ($\alpha = 0$). Due to pump channel compression, the actual perfused volume is lower ($\alpha > 0$). Not drawn to scale. c) Flow rate and WSS at different motor speeds as well as calculated flow rates for no compression by the steel balls ($\alpha = 0$ µL) and steel ball compression from experimental data ($\alpha = 0.071$ µL). d) Photograph of the experimental flow measurement setup. The increasing difference in fluid level (Δh) during flow measurements allows for assessing the back pressure influence (Δp). e) Flow rates at different levels of back pressure for different rotation speeds. Measurements in c) and e) from two, independent systems, each measured three times. Figure adapted from Ref. [227] with permission from the Royal Society of Chemistry available under the CC BY-NC 3.0 license.

9 Tissue Generation and Culture

The results presented in sections 9.1 and 9.2 were published in Ref. [226], whereas results presented in sections 9.3 and 9.4 are published in Ref. [227].

9.1 3D Tissue Generation

Organ-Discs allow for the generation of dense 3D tissues using centrifugal forces for cell loading [226]. Thereto, 20,000-40,000 cells, depending on the cell type and tissue chamber size, were pipetted into each cell channel and loaded by centrifugal forces through rotation of the Organ-Disc into the individual tissue chambers.

Standard cell biology procedures, such as pellet generation after passaging adherent cells, were used as a guideline and upper limits for centrifugal cell loading parameters in the Organ-Disc. Spinning the Organ-Disc at 1,000 rpm, or 46 × *g* at the radial position of the tissue chambers, were sufficient for cell loading. Thereby, the centrifugal forces acting on the cells were even lower than during standard centrifugation of 5 min at 100 × *g* in conventional cell culture [241]. Furthermore, Organ-Disc cell loading results in cell pellets in all 20 tissue chambers generated with less than one million cells and simultaneously within a single loading step (Figure 9.1 a). Overall, this demonstrates that the cell loading process in the Organ-Disc is scalable, efficient and gentle at the same time. This enables subsequent tissue generation within 24 h using centrifugal perfusion at 100 rpm or 0.46 × *g*. Thereby, the cells inside a tissue chamber transform form a cell pellet with individual cells to a single, connected tissue (Figure 9.1 b). At this point, both FB and ASC tissues were stained with FDA and PI for evaluating cell viability. Live/Dead staining of both cell types revealed that the tissues were overall FDA-positive (live) with small amounts of PI-positive (dead) cells.

The structure of the tissues in the Organ-Disc can be defined by the geometry of the tissue chamber. This was visualized by a phalloidin and DAPI staining for fluorescent labeling of filamentous actin and cell nuclei respectively in a FB tissue after 24 h of on-disc culture. The FB tissue developed two anchor points on both sides of the tissue with high amounts of DAPI-positive cells. The labeled actin fibers of cells in the middle segment revealed a prominent cell alignment in direction to the anchor points. The resulting tissue thickness was measured by confocal microscopy and revealed a height of 150-170 µm, which is in relationship to the approx. 175 µm high tissue chamber. This shows that both the lateral structure and the thickness of the tissue are definable by the tissue chamber geometry and, hence, demonstrates the Organ-Disc's potential for the generation of tailored 3D tissues.

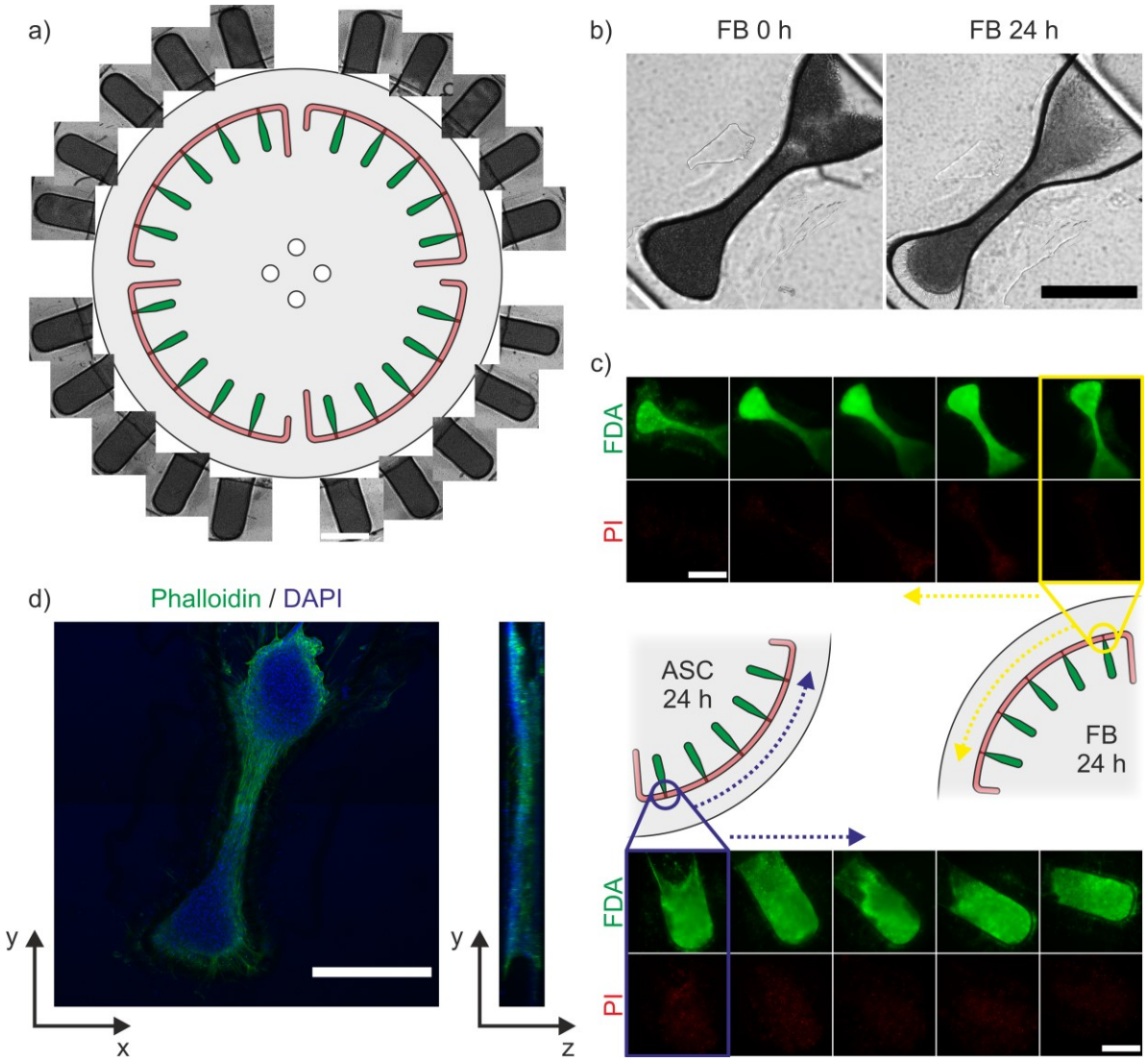

Figure 9.1 Centrifugal tissue generation: a) Bright field images of ASC cell pellets after cell loading in all of the 20 tissue chambers of a single Organ-Disc. b) Bright field images of FB cell pellet after cell loading and after 24 h of centrifugal perfusion. c) Live/Dead staining of FB and ASC tissues after 24 h of centrifugal perfusion. Schematic shows the relative position of the individual tissue chambers inside an in-line connected system. Shown are maximum intensity projections from z-stacks of the 3D tissues. d) Phalloidin/DAPI staining of a FB tissue after 24 h of centrifugal perfusion in a dogbone-shaped tissue chamber. Shown are maximum intensity projections in horizontal and vertical direction of the 3D tissue. Scale bars: b-d) 500 µm. Contrast adjusted for visualization. Figure adapted from Ref. [226] available under the CC BY 4.0 license.

9.2 Stratified Tissue Construction

In addition to tailoring the outer dimensions of 3D tissues with specific tissue chamber geometries, centrifugal cell loading allows for the construction of stratified tissues [226]. Adapting a previously presented approach [220], centrifugal cell loading was repeated sequentially with different cell types in each step (Figure 9.2 a).

Prior to loading, FB and ASC were labeled with different fluorescent dyes in order to distinguish between the different cell types. For each cell layer, approx. 5,000 cells were loaded into a rectangular tissue chamber. Cells were loaded with higher centrifugal acceleration of approx. 100 × *g* compared to standard cell loading for a higher compaction and clear separation of the individual cell layers. This process of stepwise injection resulted in dense and clearly separated cell layers of FB and ASC in rectangular tissue chambers (Figure 9.2 b). The stratified cell pellets compacted into dense tissues during following culture via centrifugal perfusion and maintained, even after 24 h, their intended layer structure of clearly separated FB and ASC.

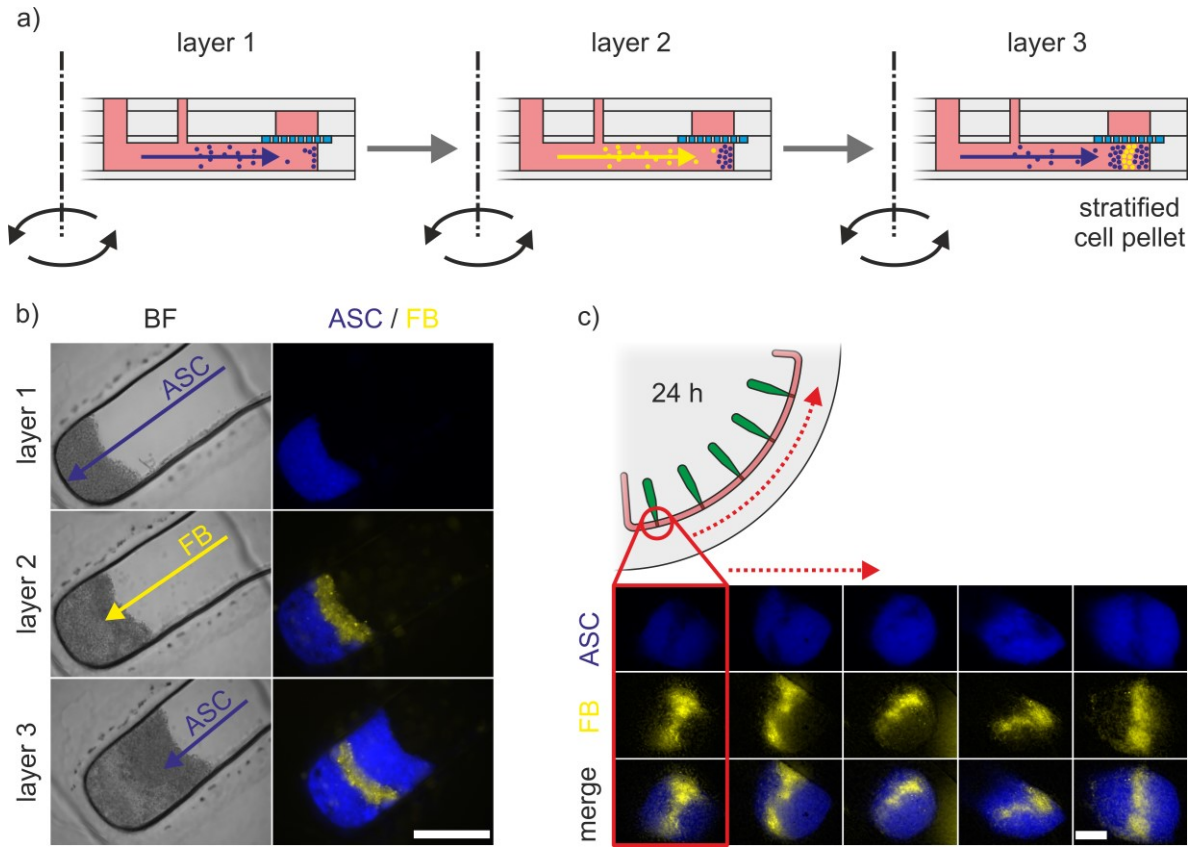

Figure 9.2 Stratified tissue generation: a) Stepwise, centrifugal loading for the generation of stratified cell pellets with multiple cell layers of different cell type. b) Bright flied and fluorescent microscopy images of each loading step. ASC and FB are labeled with different fluorescent dyes. c) Stratified tissues of an in-line connected system after 24 h of centrifugal perfusion. Scale bars b, c): 500 µm. Contrast adjusted for visualization. b, c) adapted from Ref. [226] available under the CC BY 4.0 license.

9.3 Generation of Endothelial-lined Channels

Besides leveraging the Organ-Disc for tailored 3D tissues, Organ-Disc channels were lined with endothelial cells in order to generate blood vessel-like structures [227]. Additionally demonstrating the capabilities of the Organ-Disc's tunable peristaltic pump for on-disc cell culture, cell channels were first lined with endothelial cells (HUVEC) and subsequently perfused under different shear stress conditions (Figure 9.3 a).

Thereto, HUVEC were injected into cell channels and pre-cultured for 72 h for complete cell channel lining under a gentle media circulation, which was achieved by pumping at 10 rph motor speed. The resulting flow rate and shear stress were estimated from extrapolation of experimental flow rates (*cf.* section 8.2). The estimated flow rates during pre-culture were approx. 30 µL/h and the corresponding WSS approx. 0.02 dyn/cm^2. During this period, the injected endothelial cells adhered and expanded to all inner cell channel surfaces. After completed cell channel lining with HUVEC, the endothelial cells were exposed to elevated shear stress levels, either 1.5 dyn/cm² or 0.19 dyn/cm², for another 24 h by integrated peristaltic pumping.

Subsequent fluorescence microscopy demonstrated complete cell-lining over the entire length of cell channels with adherent HUVEC on all inner channel surfaces (Figure 9.3 b). HUVEC were positive for CD31 (platelet endothelial cell adhesion molecule 1; PECAM-1) under both shear stress conditions (Figure 9.3 c). HUVEC cultured at higher shear stress of 1.5 dyn/cm² displayed more characteristic cell-cell contacts. Both flow conditions did not result in distinct endothelial cell alignment to the flow direction. This observation is in agreement with previous studies reporting HUVEC alignment at shear stress levels ≥ 7.2 dyn/cm² [242–244]. However, under both shear stress conditions, endothelial cells were overall viable as confirmed by live/dead staining using FDA and PI (Figure 9.3 d).

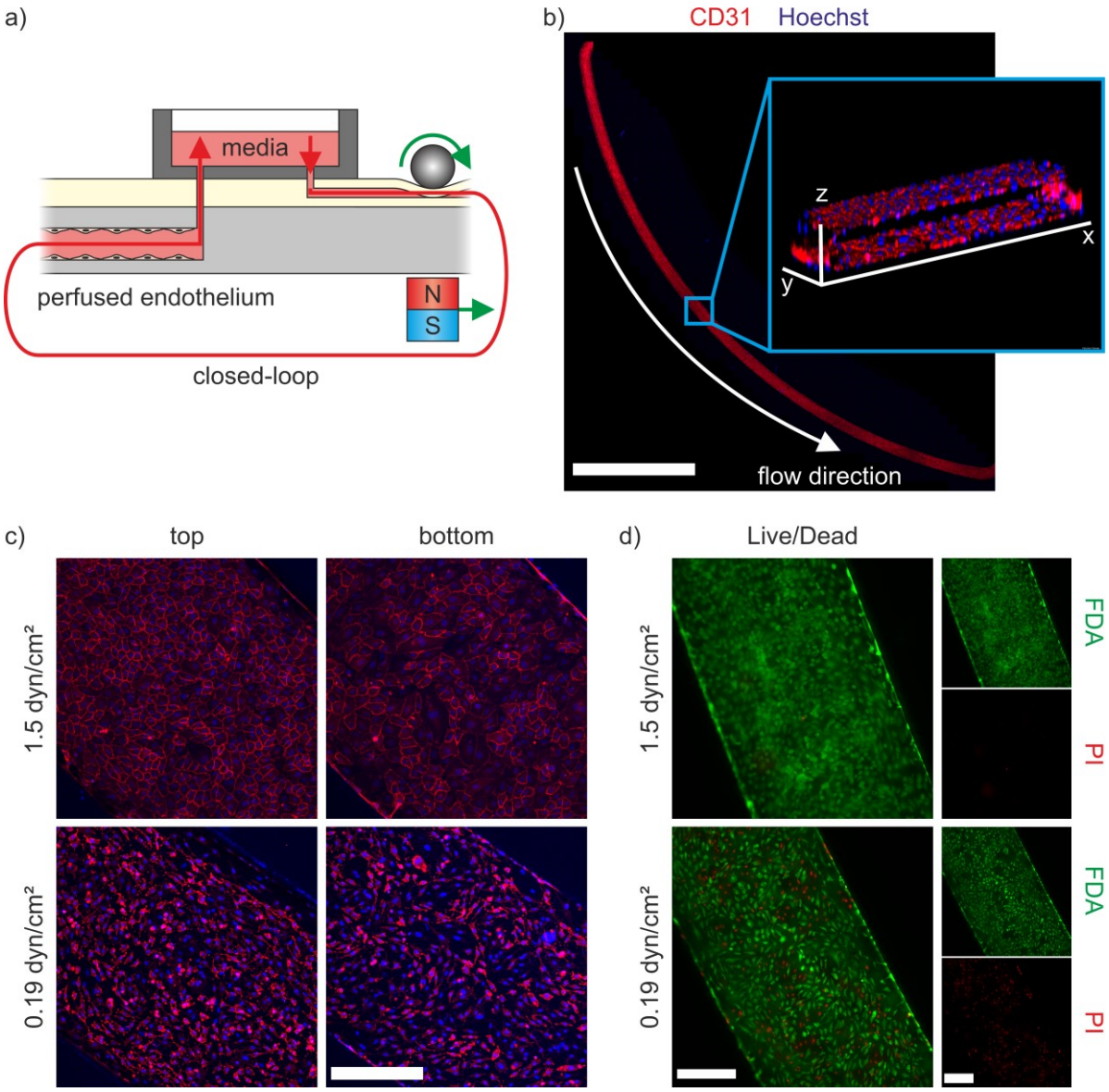

Figure 9.3 Perfused endothelium generation: a) Schematic setup for on-disc endothelium generation and perfusion under tunable, closed-loop perfusion. b) CD31 and Hoechst staining of a cell channel lined with HUVEC (1.5 dyn/cm^2 condition, maximum intensity projection). Inset shows a 3D rendered z-stack from channel center. c) CD31 and Hoechst staining of HUVEC under different shear stress conditions at top and bottom of cell channels (maximum intensity projection). d) Live/Dead staining of HUVEC cultured under different shear stress (left: composite, right: individual channels). Scale bars: b) 10 mm, c, d) 300 µm. Contrast adjusted for visualization. Figure adapted from Ref. [227] with permission from the Royal Society of Chemistry available under the CC BY-NC 3.0 license.

9.4 Perfusion of Endothelial-lined Channels

The concept of integrated perfusion with an open reservoir on top of the Organ-Disc provides continuous access to the perfused medium for user-friendly analysis and cell treatment.

9.4.1 Media Monitoring

The capability to continuously monitor the perfused media was demonstrated by assessing evaporation and cell metabolism over several days of on-disc endothelial cell culture [227]. Thereby, qualitative flow tests (*cf.* section 5.6.2) throughout the culture confirmed the functionality of the peristaltic pump and the presents of fluid flow.

Evaporation

Standard cell culture at 37 °C usually requires a humidified environment in order to limit evaporation and accompanied changes to the solute concentrations in the cell culture media. Especially in microwell plates or microfluidic devices with open reservoirs, limiting evaporation is a general concern due to the large surface-to-volume ratio and the open air-liquid interface [245].

In the Organ-Disc with closed-loop perfusion, a gas permeable tape is applied on top of the open reservoir in order to allow for sufficient gas exchange to the cell culture media and limiting evaporation at the same time. However, evaporation can still occur by water vapor diffusing through the breathable tape or the channel walls. Therefore, water loss was quantified during long-term culture by measuring ion concentrations in system without cells perfused with cell culture media at 100 rph or 0.32 mL/h. This so-called reference system was run in parallel under equal conditions to systems used for long-term endothelial cell culture in the Organ-Disc (*cf.* section “Cell Metabolism”).

The strategy for assessing evaporative water loss included the analysis of four different ions, potassium (K^+), sodium (Na^+), chloride (Cl^-) and calcium (Ca^{2+}), at each day of culture in the reference system. At each sampling time point t and for each ion, the total amount of substance n was balanced using

$$n_t = n_{t-1} + V_P[c_0 - c_{t-1}] \tag{9.1}$$

with the measured molar concentration c inside the sample volume $V_P = 110$ µL. After sampling, the withdrawn media volume was refilled with fresh cell culture media with the initial composition c_0.

In the case of media exchanges, the remaining supernatant in the reservoir was analyzed (c_t), subsequently completely aspirated and refilled with V_0 = 5 mL of fresh cell culture media. A small amount of old media remained in the microchannel V_S (approx. 24 µL) with a concentration of $c_S = c_t$. Hence, after refilling the reservoir with fresh media (t = exchanged), the total amount of each ion was

$$n_{t\,=\,\text{exchanged}} = V_0 c_0 + V_S c_t \tag{9.2}$$

Using equation (9.1) and (9.2) to calculate the total amount of ions n at each day t, allows for assessing the remaining liquid volume V in the system using

$$V_t = \frac{n_t}{c_t} \tag{9.3}$$

The calculated evaporation revealed an average liquid loss of 4.4 ± 2.5% inside the reference system. Evaporative loss accumulated to 13.2 ± 3.0% or approx. 0.66 mL within 72 h, which was set as the time period between media exchanges and corresponds to the interval used in conventional endothelial cell culture. Media exchanges after every three days maintained a stable sawtooth profile of the relative media volume, oscillating around a steady state (Figure 9.4 a).

The calculated water loss per day derived from the different ions varied slightly between the highest value of 6.3% (K^+) to the lowest rate of 2.7% (Ca^{2+}) as well as rates close to the mean with 4.2% (Na^+) and 4.3% (Cl^-). Therefore, evaporation was estimated from the average over all four ions. A similar divergence of evaporation estimated from different dissolved species was observed previously by measuring ion concentrations in the media during cell culture [246].

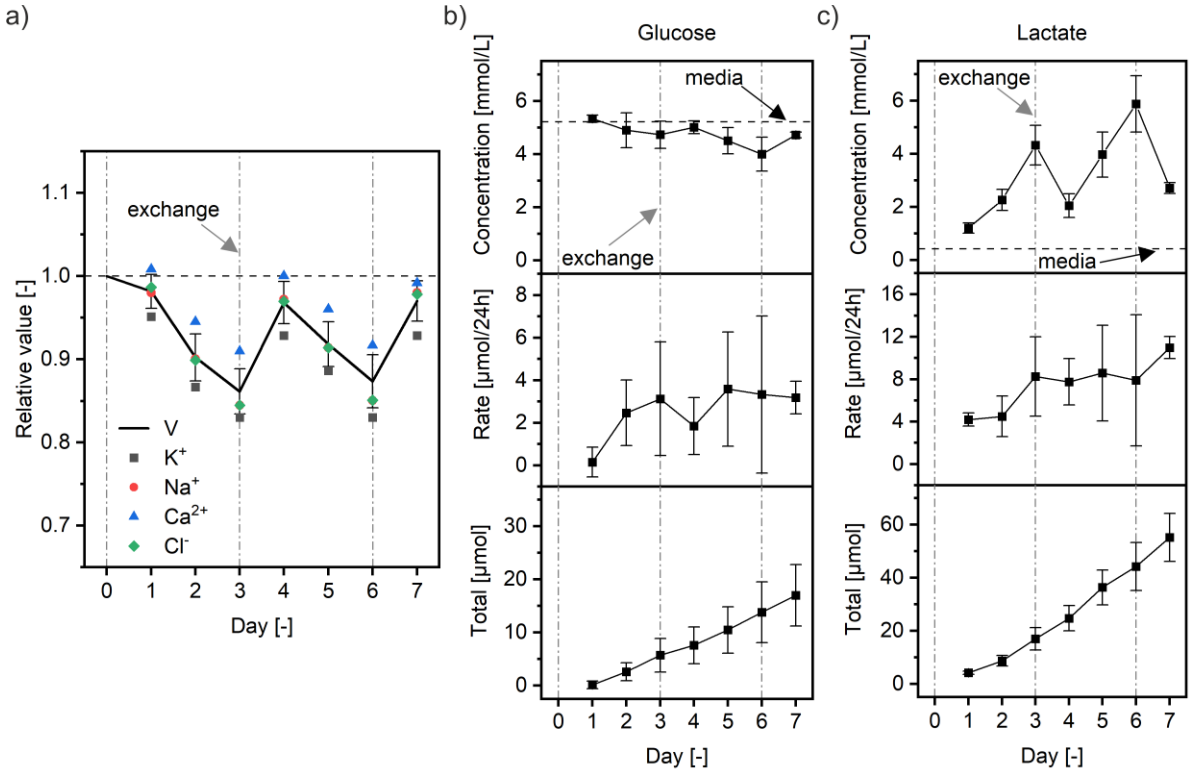

Figure 9.4 Cell culture media monitoring: a) Ion concentrations for calculating liquid loss in a perfused reference system without cells. Symbols refer to ion concentrations relative to the composition of fresh cell culture media. Black line marks the remaining, relative volume inside the reservoir calculated from the average of all ion concentration profiles. b) Glucose and c) lactate monitoring during long-term culture of HUVEC in the Organ-Disc. Measured, raw concentrations (upper panel) are corrected for evaporative loss and transferred into consumption and production rates per day (central panels) and absolute changes to nutrients and metabolites (lower panels). (Day 1 and 2: $N = 4$, all others: $N = 5$) a-c) Lines labeled with "media" refer to fresh cell culture media and lines labeled with "exchange" show media exchange time points. Figure adapted from Ref. [227] with permission from the Royal Society of Chemistry available under the CC BY-NC 3.0 license.

Cell Metabolism

Cells are able to utilize glucose as nutrient and to metabolize it into lactate by glycolysis [247]. Therefore, for evaluation of the metabolic activity of HUVEC, glucose and lactate concentrations were monitored in the perfused cell culture media during long-term culture in the Organ-Disc. The culture conditions, flow rate (0.32 mL/h at 100 rph) and intervals of media exchanges (every 72 h) were kept identically to the reference system running in parallel for assessing the evaporative water loss (*cf.* section "Evaporation").

With exception of the first 24 h (Day 1 measurement) of on-disc, long-term culture, a clear reduction of the glucose concentration in the perfused cell culture media was detected (Figure 9.4 b, upper panel). Every three days, the supernatant was exchanged and fresh cell culture

media with initial glucose concentration added in the reservoir. This resulted in a characteristic sawtooth profile of decreasing glucose concentration. According to the cell metabolism, an inverted sawtooth profile of increasing lactate concentration is detectable in the perfused cell culture media (Figure 9.4 c, upper panel).

Simultaneous monitoring of evaporation during long-term culture, allows for the detection of actual glucose consumption rates (Figure 9.4 b, central panel) as well as lactate production rates (Figure 9.4 c, central panel). Evaporative water loss, which results in an overlapping concentration increase, is corrected by calculation of the remaining media volume inside the reservoir compartment. Thereto, the total amount of species *n* for both glucose and lactate are determined for each day *t* from the respective concentration *c* using

$$n_t = V_t \cdot c_t \tag{9.4}$$

with V_t the remaining liquid volume calculated from salt concentrations in the reference system. Consumption and production rates, within Δt = 24 h, are

$$\frac{|n_t - n_{t-1}|}{\Delta t} \tag{9.5}$$

Accordingly, the absolute amounts of metabolized glucose (Figure 9.4 b, lower panel) or produced lactate (Figure 9.4 c, lower panel) are detectable. The total consumption or production over time is

$$\frac{|n_t - n_0|}{t} \tag{9.6}$$

The average glucose consumption over the whole culture was 2.5 ± 2.2 µmol/day, whereas lactate production was 7.5 ± 3.5 µmol/day.

9.4.2 Inflammatory Cell Stimulation

For the demonstration of the physiological function of on-disc cultured endothelial cells, the response of HUVEC to inflammatory stimulation with TNF-α was analyzed in collaboration with Julia Rogal (Fraunhofer Institute for Interfacial Engineering and Biotechnology IGB, Stuttgart, Germany) [227].

Cell channels were lined with HUVEC during 72 h of on-disc culture at approx. 30 µL/h of closed-loop media perfusion. Subsequently, HUVEC were activated by pumping cell culture media containing 20 ng/mL TNF-α for another 24 h under the same flow conditions through the endothelial cell lined channels. After cell stimulation, the expression of CD106 (vascular cell adhesion molecule 1; VCAM-1), was determined via fluorescent antibody staining of TNF-α treated and untreated HUVEC (Figure 9.5 a). HUVEC with comparable cell density for both conditions, as confirmed by phase contrast microscopy, showed an increased CD106 signal when treated with TNF-α. These results are in agreement with previous reports demonstrating an increased CD106 expression of TNF-α treated endothelial cells [248, 249].

Besides analyzing CD106 expression, the cytokine release of HUVEC into the perfused medium was analyzed. Thereto, a fluorescent bead-based multiplex assay was applied, which allowed for the simultaneous quantification of several types of cytokines by flow cytometry. Over a period of 24 h, TNF-α treated HUVEC released significantly more proinflammatory cytokines compared to untreated cells (Figure 9.5 b).

In detail, the concentrations of IL-6, IL-8 and Ang-2 were 12-fold, 38-fold and 2.5-fold increased respectively in the supernatant of TNF-α treated HUVEC compared to untreated cells. Demonstrating a stable baseline cytokine release, media from untreated HUVEC contained comparable amounts of the analyzed cytokines before and after the incubation period. Increased release of IL-6 and IL-8 from HUVEC in response to TNF-α stimulation [250, 251], as well as, upregulated Ang-2 expression in endothelial cells after TNF-α treatment has been reported frequently [252].

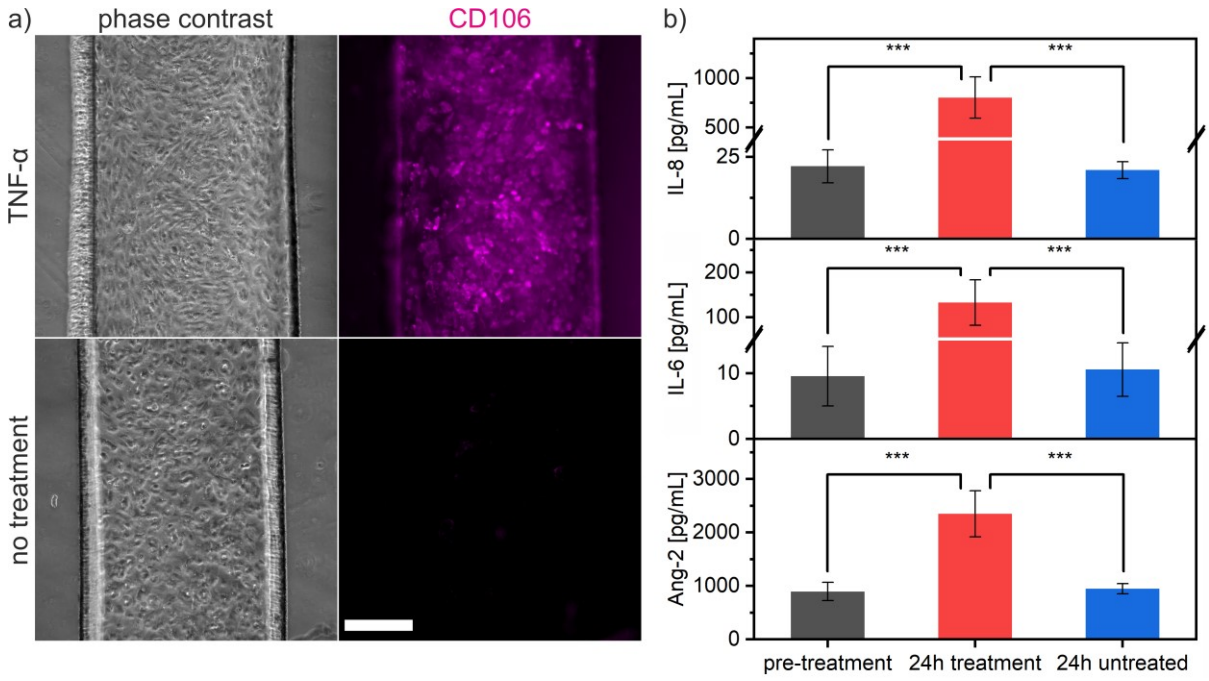

Figure 9.5 Inflammatory cell stimulation: a) Images from TNF-α treated and untreated HUVEC by phase contrast microscopy and CD106 antibody staining. Contrast adjusted for visualization. Scale bar: 300 µm. b) Cytokine concentrations measured by Julia Rogal via a fluorescent bead-based multiplex assay read by flow cytometry. Evaluation of cytokine content in the perfused medium from HUVEC before ("pre-treatment", $N = 8$), after ("24 h treatment, $N = 4$) and without TNF-α stimulation ("24 h untreated", $N = 4$). IL-8, IL-6 and Ang-2 concentrations in the media are significantly increased ($p < 0.001$) after activation of HUVEC with TNF-α. Figure adapted from Ref. [227] with permission from the Royal Society of Chemistry available under the CC BY-NC 3.0 license.

9.4.3 Whole Blood Perfusion

The capability of the Organ-Disc to generate a perfused, blood vessel like structure allows for minimized exposure of the channel walls to the perfused media. This enables even the perfusion of sensitive medium as demonstrated by on-disc perfusion of human whole blood with fluorescently labeled platelets [227].

Prior blood injection, HUVEC were cultured on-disc for 96 h with gentle media circulation at approx. 30 µL/h for complete cell channel lining. Freshly collected whole blood was supplemented with re-calcification buffer containing ions required for blood coagulation as well as CD41 antibody for platelet labeling [234]. Subsequently, blood was perfused by the integrated, peristaltic pump through the HUVEC-lined cell channels.

Different to closed-loop perfusion, blood was pumped through the system between pipette tips connected to the respective reservoir ports at channel in- and outlet (Figure 9.6 a). Blood

perfusion was achieved simultaneously in all four systems, and resulted in complete cell channel filling with blood and clearly visible changes of the blood level in the respective pipette tips. After whole blood pumping for 5 min at 800 rph, the pipette tips were removed and the remaining blood in the cell channels flushed out by media previously filled in the reservoir compartments. All channels remained intact as no clogging appeared and complete blood removal was achievable in all systems.

Platelet adhesion plays an important role during plug formation in injured blood vessels preventing blood loss but can also lead to thrombosis and stroke [253]. Adding CD41 antibody to the fresh whole blood for fluorescent labeling of platelets, enabled monitoring of platelet adhesion to the endothelium after blood perfusion (Figure 9.6 b). Fluorescent microscopy revealed both a strong CD31 signal from the intact endothelium after 96 h of on-disc culture and blood perfusion and clearly visible domains of CD41-poitive platelets adhering to HUVEC (Figure 9.6 c).

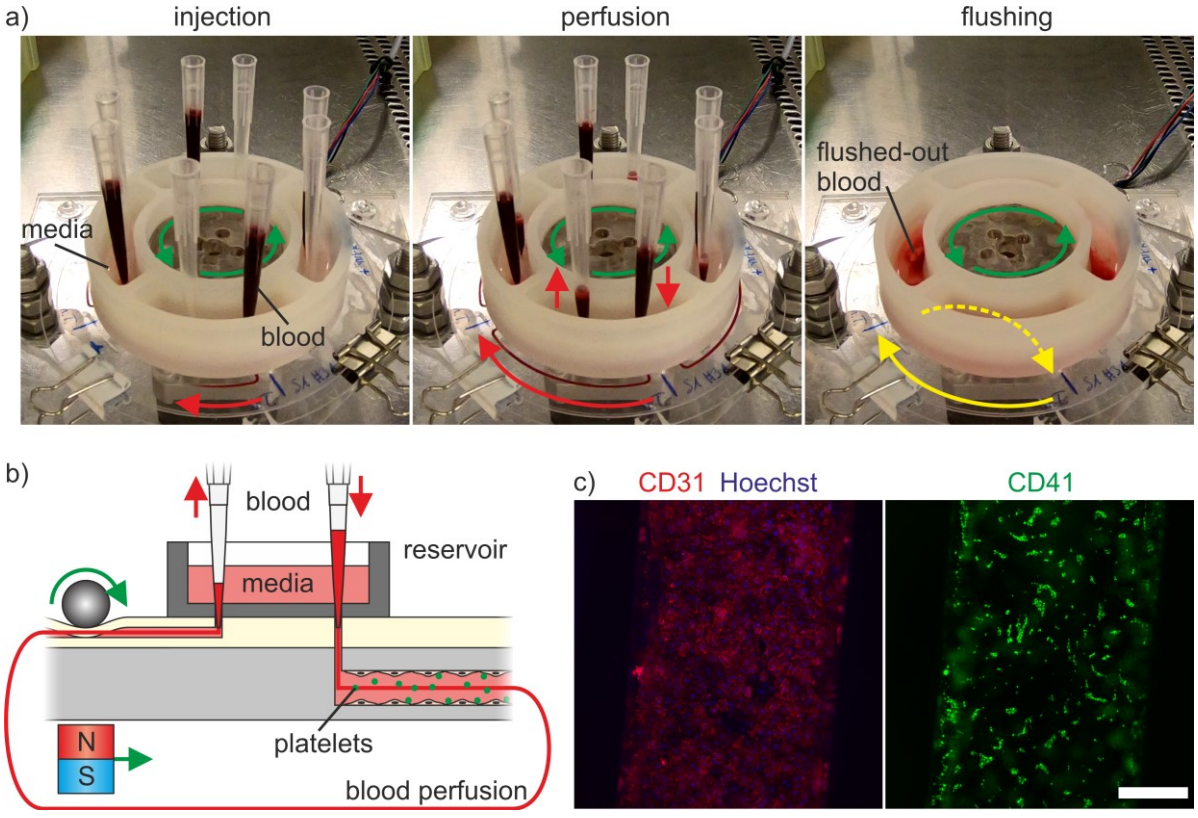

Figure 9.6 Whole blood perfusion: a) Photographs of peristaltic pumping of whole blood showing the injection and perfusion of blood from pipette tips attached to the reservoir ports. Media allows for subsequent channel flushing after the blood-filled pipette tips are removed. b) Blood containing fluorescently labeled platelets is pumped through cell channels lined with endothelial cells. c) Fluorescence microscopy images of endothelial cells (CD31, Hoechst) after blood perfusion with adherent, fluorescently labeled platelets (CD41). Contrast adjusted for visualization. Scale bar: 300 µm. Figure adapted from Ref. [227] with permission from the Royal Society of Chemistry available under the CC BY-NC 3.0 license.

10 Discussion

The following sections discuss the concepts and designs as well as the results of the different Organ-Disc versions, which are partially published in Ref. [226–228], in an overall context.

10.1 Organ-Disc Technology

The Organ-Disc combines existing concepts from different fields of microfluidic research and tissue engineering and, thereby, creates a novel platform technology for OoC research with higher throughput capabilities.

The Organ-Disc is a multi-layered, microfluidic module with a compact, rotational symmetric channel layout. The symmetric channel arrangement around the Organ-Disc achieves a parallelization "by design" and allows for a simple scale-up of the number of individual systems or tissues per disc. Thereby, the Organ-Disc follows a different approach for parallelization compared, for instance, to multiplexed fluidic circuits [186]. The multi-layer design enables a separation of perfused media channels and non-perfused cell channels by sandwiching a porous membrane in between the tissue chambers and the media channels. On the one hand, the porous membrane allows for the recapitulation of the *in vivo* endothelial barrier shielding tissues form shear forces and allowing for diffusive nutrient and metabolite transport [115, 116]. On the other hand, this arrangement achieves the supply of multiple, in-line connected microtissues by a shared media channel, which paves the way for tissue-tissue communication and multi-organ systems [192].

The fabrication of multi-layered OoC devices is well-established in PDMS-based systems but usually not straightforward with alternative materials [80]. The Organ-Disc uses thermoplastics for the disc base and TPE for components that required a flexible chip material. Besides the well-known limitations of PDMS as a chip material for microfluidic cell culture [32], the main reason was to achieve a mechanically rigid system for user-friendly handling and to prevent disc deformation during rotation. This required the development and optimization of the fabrication of robust Organ-Discs with precise features, however, resulted in a scalable process that paves the way for industry-scale production.

Inspired from the overall LoD concept [209], rotation of the disc or components drives the individual Organ-Disc processes, such as cell loading and pumping. Centrifugal cell loading by precisely controllable rotation of the Organ-Disc provides the basis for parallelized and simultaneous cell injection into multiple tissue chambers. The generated centrifugal forces act

homogenously in the symmetrically arranged cell channels, which are located on identical radial positions. The cell transport is based on sedimentation, which enables the formation of a dense cell pellet and subsequent generation of tailored 3D tissues with a definable outer and internal tissue structure.

While centrifugal cell loading enables the recapitulation of dense, parenchymal tissues, it is not ideally suited for the generation of *in vivo* 2D cell structures, such as blood-tissue barriers. Therefore, an optimized process for complete lining of channels with endothelial cells was implemented on the Organ-Disc as well. This endothelial cell lining achieves perfused, blood vessel-like structures on the Organ-Disc and paves the way for applications focusing on vasculature research [254].

The reliable on-disc culture of 3D tissues and blood vessel-like structures requires a precisely controllable fluid transport on the Organ-Disc. In most OoC systems, this is usually achieved by external pumps and tubing connections [111, 118]. At first glance, external pumps provide a straightforward solution for on-chip fluid transport but require time-consuming, error-prone handling and potentially limit the transfer to higher-throughput applications. The Organ-Disc achieves an integrated fluid transport by either centrifugal pumping through Organ-Disc rotation, or peristaltic pumping through fluid displacement. This provides an alternative to conventional approaches but requires the development of suitable Organ-Disc spinner hardware. However, as demonstrated for all Organ-Disc processes, a simple setup is sufficient that features an electric motor for rotation of the disc or for rotation of objects on the disc. Furthermore, the required manual handling for the individual Organ-Disc processes is limited to standard procedures such as pipetting. At the same time, equipment and procedures interfering with automation attempts, such as tubing or external pump connections, are completely avoided.

Overall, this combination of rotation-based concepts creates a novel platform technology for OoC research that enables the parallelized generation and culture of multiple microtissues using automatable processes with minimal handling and equipment requirements.

10.2 Scalable, Precise and Robust Organ-Disc Fabrication

Even though PDMS is probably still the most frequently used material for microfluidic chip fabrication, it is more and more becoming an undesired material for microfluidic cell culture applications and especially OoC systems [32, 138]. This is mainly due to the high absorption of hydrophobic, small molecules into the bulk of PDMS [37], high water transmission resulting in osmolality shifts [141] and leaching of uncrosslinked PDMS components into the microchannels [38]. While PDMS allows for precise and simple fabrication techniques by replica molding and plasma activated bonding [54], the overall fabrication throughput is limited. For instance, PDMS curing times are hardly reducible as shrinkage occurs at higher temperatures required for faster crosslinking [136, 137]. In contrast to that, Organ-Discs are fabricated using thermoplastics and TPE as alternative materials in order to overcome the limitations of PDMS-based devices and to create robust modules for user-friendly Organ-Disc operation.

10.2.1 Fabrication of Thermoplastic Organ-Discs

Thermoplastic Organ-Disc modules are fabricated by a two-step process: 1) the 2D structuring of several thermoplastic layers and 2) the fusion of the individual layers. In the first step, the 2D structuring techniques CO_2 laser cutting and plotting allow for the rapid prototyping of thermoplastic disc layers. Thereto, both structuring techniques enable the direct and fast transfer of CAD designs into the thermoplastic foil. In both cases, the actual structuring per Organ-Disc layer takes less than 5 min. This makes the manual post-processing, such as cleaning, the primary bottleneck, which is greatly reduced in the case of plotting compared to CO_2 laser cutting. Nevertheless, the overall structuring process of an entire Organ-Disc takes less than 1 h and hence results in a clearly higher throughput even compared to highly optimized PDMS processing applying curing steps of at least 4 h [135].

Following a fit for purpose approach, plotting was chosen for sharp and smooth media channels or cell channels in the peristaltic Organ-Disc, whereas laser cutting was applied for thicker materials and the smaller tissue chambers. However, the general approach of generating through-hole structures and stacking multiple microstructured layers is not limited to those techniques. For even smaller features, Organ-Disc layers could be structured by high-resolution laser cutting using, for instance, femtosecond pulsed lasers at 800 nm as previously used for 50 µm wide channels in polyester films [70]. Though those systems are usually more expansive than CO_2 laser systems or cutting plotter, ablation using ultrashort pulse laser systems benefits

from a reduced thermal impact on the material resulting in minimal heat-affected zones and precise structures [71].

The individual thermoplastic Organ-Disc layers were bonded after structuring by either solvent, or thermal bonding approaches. Solvent vapor bonding is ideally suited for rapid prototyping approaches and provides an alternative to, *e.g.*, adhesives. A suitable solvent results in the intertwining of polymer chains across the bonding interface and a highly robust connection after evaporation of the solvent [82]. In principle, overexposure and destruction of channel features is a general complication during solvent bonding, especially using liquid solvents. Thereto, protecting, sacrificial layers have been introduced into channels and removed after solvent exposure and bonding [255]. However, this approach requires the complete removal of the sacrificial material, which would be complicated for the dead-end cell channels in the Organ-Disc. Thereto, solvent vapor bonding provides an alternative to using liquid solvents and was adapted for the Organ-Disc fabrication from a previously published bonding protocol [230].

Solvent vapor bonding allowed for a rapid fabrication of Organ-Discs and achieved bonding of up to six disc layers within 2 h. The adapted process of solvent vapor bonding does not necessarily require heating during pressing the treated layers. For the Organ-Disc fabrication, the bonding was performed at RT different to the original protocol applying an increased temperature of 65 °C [230]. This allowed for overall faster bonding cycles as no additional heating or cooling steps were conducted. Solely the pressure had to be increased for successful bonding comparable to similar bonding protocols recently presented for bonding cyclic olefin polymer (COP) with a pressure of 13.79 MPa at RT [256].

One of the limitations of solvent-based bonding approaches are the necessity to match suitable polymer and solvent combinations [40]. Also solvent vapor bonding for Organ-Discs revealed a material influence on the individual layer connections in the Organ-Disc. This material dependency was even observable for PMMA-PMMA bonds, such as the bonding of the 75 µm thin PMMA foils (media layer) to layers from cast PMMA plates (port layer). This connection was usually error-prone and required an additional connector layer from another PMMA material in between media and port layer. It is also worth mentioning that the portfolio of commercially available PMMA foils with thicknesses below 100 µm is rather small, which makes PMMA material exchanges difficult. Similarly, the tight integration of PET membranes was challenging, and resulted in occasional delamination from the tissue chamber. In those cases, this resulted in cell transport during centrifugal cell loading in between membrane and tissue layer material in gaps around the tissue chamber. Here, an alternative material

combination might provide a better bonding between channel and membrane, such as PP or PC membranes in combination with PMMA [165, 166]. Another solution for tight membrane integration is presented by PC/TPE-hybrid devices allowing for simple and robust bonding of PET membranes and preventing cell transport out of the chamber (*cf.* appendix, section 13.1).

Another limitation of solvent vapor bonding is the high amount of manual handling required for the step-wise solvent exposure, alignment, lamination and pressing of the individual layers. Furthermore, the subsequent removal of the solvent had to be assured, which was conducted by overnight incubation in a vacuum oven and increased the overall fabrication time. Additionally, the necessity of working in a well ventilated environment such as a fume hood due to the toxicity of the applied solvent increased the risk of dust particle contamination on the Organ-Disc layers. In principle, the overall handling of solvent vapor bonding could be further improved. Giselbrecht *et al.* presented a combined vapor exposure and bonding setup for the simultaneous fabrication of in total four cell culture scaffolds [166]. Such a bonding system could reduce the risk of particle contamination due to a reduction of handling steps outside of an enclosed containment but would still result in several bonding cycles in the case of the multi-layer Organ-Disc.

While higher amounts of manual handling are suitable for rapid prototyping, it creates a bottleneck for scale-up. In contrast to solvent vapor bonding, thermal fusion bonding does not require toxic chemicals and no post-processing for solvent removal. Furthermore, stacking of the individual layers in to the bonding tool is safely performed in a laminar flow bench or inside a clean room without the need of working inside a fume hood. After closing the bonding tool, particle contamination is prevented and the following process steps can be proceeded in a standard lab environment.

At the same time, the thermal fusion bonding tool enables a parallelized, higher-throughput fabrication. No additional treatment or lamination is required besides stacking of the individual layers, while the correct alignment is assured by pins located at each bonding position. Leveraging the full plate size of the automated hot press, the tool allows for the parallel bonding of up to seven discs (*cf.* appendix, section Figure 13.3).

Thermal fusion bonding relies on fusion of polymer chains under heat and pressure, while care has to be taken to limit distortion due to the softening of the polymers at temperatures in the range of their glass transition [40]. This requires strict control over the applied pressure and the bonding temperature. Thereto, the bonding tool uses a symmetric arrangement of the individual

bonding positions and soft elastomer layers. This enables homogenous conditions inside the tool and temperature deviations between different bonding positons below 1 °C.

Several material combinations have been successfully bonded using the developed thermal fusion bonding setup. Besides PMMA, this enabled the fabrication of COC and PC-PMMA discs and provides more flexibility in the disc material for future applications. For instance, COC provides excellent transparency in the visible and near UV range [257].

Due to the different material specifications, bonding parameters had to be adapted in each case. Especially bending of channel top or bottom layers was a result of not optimized bonding conditions and impaired microscopy of cells inside the microchannels. A suitable measure against channel distortion is lowering the bonding temperature below their respective T_g [40]. For PMMA discs the temperature had to be reduced by 10 °C and for COC discs 5 °C below T_g respectively. Another strategy is combining materials with different glass transition temperatures [80, 161, 238]. In the case of PC-PMMA discs, bonding below the T_g of PC and above the T_g of PMMA prevents bending of top and bottom PC layers with only slightly rounded PMMA channel edges.

For all settings and materials the presented thermal fusion bonding achieves channel geometries that differ less than 10% from their desired dimensions and bonds withstanding physiologic blood pressure levels [240] and even the highest, expected fluid pressures during peristaltic pumping (*cf.* appendix, section 13.4) without difficulty. Overall, thermal fusion bonding achieves precise channel features and Organ-Disc stability more than enough for standard OoC applications.

10.2.2 Fabrication of TPE Modules

The peristaltic pump required pump channels in an elastic material. For this, flexible TPE based on SEBS was chosen as an alternative to the elastomer PDMS. The applied TPE material is based on medically approved raw materials according to the TPE manufacturer and was previously applied for microfluidic devices [167]. Furthermore, the chosen TPE is approx. five times cheaper than PDMS, provides a biocompatible cell culture substrate and leads to reduced absorption of small molecules in direct comparison to PDMS (*cf.* appendix, section 13.5) [228].

The commonly applied microstructuring techniques for TPE are injection molding [60] and hot embossing [59], which stem from conventional replication techniques for thermoplastic materials, but also replica molding using dissolved TPE [84]. Hot embossing of TPE was

chosen as structuring technique for the flexible pump channels, which does not require toxic solvents for dissolving TPE and is achievable even with low-cost hot presses [83]. Besides the hot press, the essential elements of TPE hot embossing are a TPE film and a suitable embossing stamp that is pressed into the bulk of the TPE film under heat and pressure.

Due to the small portfolio of commercially available TPE films [83], film extrusion of TPE pellets with customizable film thicknesses in the range of 30 µm to 3 mm is a frequently applied alternative [51, 52, 60]. Because of the increased flexibility in terms of base material and film properties, custom TPE film extrusion was chosen for the fabrication of flexible pump modules, as well as PC/TPE-hybrid devices.

Different to the TPE film fabrication, the range of fabrication methods for embossing stamps is rather wide. Hot embossing stamps have been fabricated, for instance, by replica molding using epoxy resin [61–63], by micromilling of metal [64] or by etching of silicon [65]. Additionally the direct embossing using photoresist structures [65] and PDMS molds has been presented [258]. Due to the high requirements in terms of specialized equipment and process complexity, both micromilling and silicon etching were not pursued further. PDMS masters are generally easy to fabricate but are relatively soft, which usually requires modified mixing ratios and tempering for precise hot embossing [258]. Even though direct embossing of SU-8 into TPE has been reported [51, 52, 59], initial attempts of hot embossing TPE pump modules for the Organ-Disc with SU-8 structures failed sometimes already after the first cycle due to photoresist delamination during TPE demolding.

Therefore, the focus was laid on epoxy-based stamps, which are frequently applied as an alternative to direct embossing of photoresist structures and obtained by epoxy-based replica molding of an intermediate PDMS master [83, 229]. This combined approach allows for the accurate transfer of precise but usually fragile structures from a photoresist into a rigid and temperature stable epoxy. Avoiding direct molding of the photoresist with epoxy resin, PDMS acts as an intermediate master with an excellent replication fidelity below the 0.1 µm range [33]. In the following step of replica molding the PDMS master with epoxy resin, it has to be assured that cavities in the PDMS are completely filled with resin and that the epoxy mold remains planar and parallel after curing.

For this purpose an epoxy tool was developed that enables the injection of epoxy resin in a cavity above the PDMS mold that is fixed to a vacuum chuck by applying a small vacuum. Different to a similar, commercial molding tool (Epoxym molding kit, Eden Tech), a planar and parallel back side of the epoxy is assured by adding a PMMA plate on top of the cavity

with ports for epoxy injection. Thereby, a planar backside and parallelism between front and backside of the mold are achieved in a simple way. The need for precisely leveled surfaces during curing or further post-processing steps, such as milling a planar backside [63], are thereby completely avoided.

In order to assure complete PDMS cavity filling, the vacuum underneath the PDMS mold is maintained during the first 24 h of curing. This vacuum aims at the removal of air bubbles in the cavities by gas diffusion through the gas permeable PDMS [34, 35]. As this process is not visible due the opaque epoxy resin inside the tool, a proof-of-concept is provided by demonstrating this process with water resulting in complete air bubble removal within 20 min. A small and inexpensive pump is suitable for air bubble removal with a maximum absolute pressure of 100 mbar. Overall, the epoxy stamp fabrication achieves a precise transfer from SU-8 structures into the final epoxy mold as demonstrated from channel cross-sections in PDMS molds from both SU-8 and epoxy structures.

Styrene block copolymers lose their elastic properties above the T_g of the rigid styrene block at approx. 90 °C and start to behave as a thermoplastic polymer [51]. This leads to lower hot embossing temperatures for TPE compared to standard thermoplastics. Therefore, the applied epoxy resin and its temperature stability up to 177 °C after tempering (manufacturer information) is sufficient for TPE hot embossing. In fact, an embossing temperature in the range of 130-140 °C was suitable for precise structuring of TPE. No damage to the epoxy stamp was observable even after more than 10-20 embossing cycles. Thereby, a precise hot embossing process with epoxy stamps was achievable. The deviation between a PDMS mold obtained from the epoxy stamp and the embossed TPE channel sizes were only 0.2% in width and 2% in height.

Furthermore, hot embossing of TPE is fast and scalable. The overall process time of one hot embossing cycle was approx. 45 min. However, only 10 min were spent on the actual embossing step. The manual lab press was the bottleneck of the process, which required 30 min for pre-heating and 5 min for cooling. Therefore, an even higher throughput is expected for a hot embossing process using industry-scale presses with faster heating and cooling cycles.

Finally demonstrating the versatility of TPE chip fabrication, hot embossing of TPE was combined with SLA printed stamps or the simultaneous fusion of TPE with a PC support layer during a single embossing cycle. The 3D printed stamps enable versatile channel geometries in TPE layers, such as round channels and an overall faster stamp fabrication within one day from CAD to stamp. However, the surface roughness and resolution of SLA printing remain a general

limitation [259]. While SLA-based stamp fabrication is ideal for rapid prototyping in TPE, the epoxy stamp fabrication is the process of choice for precise and smooth structures. Especially in combination with the developed PC/TPE-hybrid approach, limiting factors as the difficult handling of flexible and self-adhesive TPE layers are eliminated by providing more structural support. At the same time, the combination of TPE and PC results in comparable optical properties as the individual base materials and maintain the simple and robust bonding capabilities of standard TPE layers.

10.2.3 Integration of TPE Modules to Organ-Discs

The bonding of TPE to itself or thermoplastics was characterized for the stable bonding of pump channels to Organ-Discs for peristaltic perfusion, or for the fabrication of rigid PC/TPE-hybrid devices.

The on-disc peristaltic pump required a robust bonding of pump and pump support layer on top of the PMMA disc. TPE provides a very good adhesion to itself or other thermoplastics as previously demonstrated [83, 84]. Different to thermal fusion bonding of thermoplastics, no hot press was required for stable bonds. Instead, a simple setup of adding a small weight on top and putting the layers in an oven was sufficient. Nevertheless, this simple bonding setup allowed for collapse-free bonding with undistorted channel cross-sections and bonds that could stand over 3 bar of nitrogen pressure. Furthermore, peristaltic pumping was possible for over 180 h at 100 rph. Overall, this relates to more than 144,000 actuations of each pump channel with a steel ball in a humid and 37 °C warm environment without bond failure.

The robust bonding capabilities of the applied TPE material were analyzed in more detail by bonding TPE hybrid layers to multiple substrates. Thereby, it could be shown that the developed PC/TPE-hybrid bonding achieved bond strengths comparable or above other TPE bonding protocols. For instance, Lachaux *et al.* report TPE-TPE bonds withstanding pressures up to 2 bar after bonding for 1 h at 85 °C [83]. Similarly, Borysiak *et al.* report TPE-bonds to TPE, PS or glass after 30 min at 75 °C that are stable up to 60 psi (= 4.1 bar) without delamination [84]. Even after seven days of incubation in physiologic buffer and at 37 °C the individual bonds presented here withstand rather extreme pressures for conventional OoC applications. In the case of connections between TPE and thermoplastic substrates, the achieved bonding strength exceeds even a pressure of 7.5 bar without bursting of the chip.

Expanding the field of future applications, for instance the integration of thin-film sensors on glass [260], a robust connection of TPE and glass is achievable as demonstrated in collaboration with Eduardo J. S. Brás [228]. Robust bonding between TPE and glass requires solely a simple surface treatment of TPE. Thereby, TPE is functionalized and bonded to plasma activated glass with an adapted surface treatment using bis-[3-(trimethoxysilyl)-propyl]-amine [79]. This approach achieves TPE-glass bonds that stand a pressure of 7.5 bar without failure even after the incubation in buffer for seven days. This demonstrates even more that TPE provides a versatile alternative to PDMS-based fabrication protocols for monolithic or hybrid devices. TPE enables similar or higher bond strength than PDMS-based fabrication protocols (Table 10.1). Different to plasma activated PDMS bonding, all material combinations but TPE-glass bonds are achieved without activation steps by simple overnight bonding in an oven at 60 °C without any additional pressure [228].

Table 10.1 Bonding strength to different substrates of previously reported PDMS devices in comparison to PC/TPE-hybrid devices. Reported burst pressures from PDMS devices are converted in bar and rounded. TPE bonding strength from samples tested immediately after bonding and without incubation in buffer at 37 °C. Bonding strength values for TPE were obtained in collaboration with Eduardo J. S. Brás. Table adapted from Ref. [228] available under the CC BY 4.0 license.

Substrate material	TPE bonding [bar]	PDMS bonding [bar] from literature	
PDMS	N/A	2.9-6.7	[76]
TPE	4.7	N/A	
Glass	> 7.5	1.7-5.1	[77]
PC	> 7.5	3.8	[261]
		4.1	[262]
COC	> 7.5	> 8	[263]
PS	> 7.5	4.5	[261, 262]

10.3 Tunable, Pump- and Tubing-free Perfusion

The perfusion of microtissues on the Organ-Disc without external pumping equipment is a key element of the Organ-Disc technology. For this, two rotation-based pumping mechanisms, centrifugal and peristaltic pumping, were implemented on the Organ-Disc.

Centrifugal pumping was originally implemented for fluid transport in LoD devices and applied *e.g.* for parallelized, enzymatic assays [27, 209]. However, centrifugal pumping provides also a suitable fluid transport mechanism that can be applied for cell culture procedures. For instance, centrifugal pumping achieved the exchange of culture medium inside a chamber with adherent cell layers [222] or a compartment filled with a suspension of *Caenorhabditis elegans* [224].

The Organ-Disc applies centrifugal pumping for the continuous transport of cell culture media in the media channels during on-disc tissue generation. This enables the generation of microtissues from cell pellets inside the tissue chambers, which are separated by a porous membrane from the perfused media channels.

The primary goal of centrifugal pumping are sufficient flow rates, while limiting centrifugal forces on the microtissues. The flow rate characterization reveals flow rates of up to 445 µL/h with a centrifugal acceleration of 1.86 × *g* acting on the tissues. However, already centrifugal accelerations as low as 0.46 × *g* achieve flow rates in the range of common OoC systems [111, 116, 118, 147]. Under these conditions, the flow rates are 97 µL/h in average, whereas the tissues sense only a 10% higher gravitation of 1.1 × *g* in combination with gravity on earth.

Experimental flow rates were lower as predicted flow rates with hydrostatic and centrifugal pressure gradients in the Organ-Disc. Here, capillary pinning provides a plausible explanation that reduces the actual pressure gradient across the media channel. The proposed theory allows for a close fit of experimental values. Potentially, centrifugal pumping could be further improved by including an overflow structure inside the reservoir above the exit port (Figure 10.1). This would result in a constant fluid volume above the exit port, elimination of capillary pinning effects and render centrifugal pressure as the only gradient contributing to the pumped flow rate.

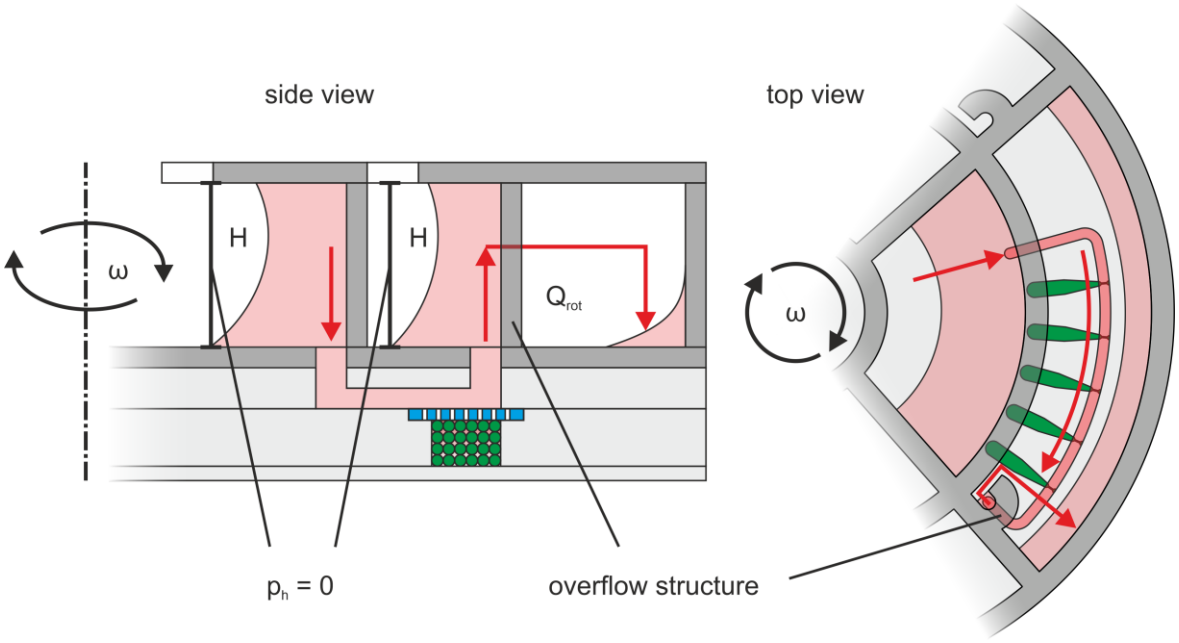

Figure 10.1 Concept of overflow structure in the in Organ-Disc reservoir that eliminates hydrostatic pressure differences and capillary pinning at the reservoir exit port. Media is held back above the exit port until it flows over the rim of the overflow and is collected in the outer reservoir compartment.

However, a general limitation of centrifugal pumping for OoC applications is the lack of continuous media circulation [187]. Several approaches for pumping liquid in radially inward direction have been implemented on LoD systems, however, do not achieve unidirectional, fluid recirculation [20]. Therefore, peristaltic pumping was implemented on the Organ-Disc footprint as mechanism allowing for unidirectional, closed-loop perfusion. This provides an important step towards a closer recapitulation of the *in vivo* human blood circulation.

The advantage of a peristaltic pumping mechanism is the linear relationship between flow rate and actuation frequency. This enables a better control over the resulting flow rate as centrifugal pumping and results in a highly linear flow rate depending on the motor speed. Furthermore, peristaltic pumping is achieved in a stationary Organ-Disc. This eliminates the potential impact of centrifugal forces on the tissues completely.

The peristaltic pump for the Organ-Disc uses magnetically dragged steel balls compressing a flexible channel. The overall setup shares similarities to previously presented micropumps for fluid supply to microfluidic devices [205, 206]. However, an important advantage of the Organ-Disc pump is the complete avoidance of PDMS as flexible channel material. The Organ-Disc uses TPE as an alternative elastic material to PDMS for the flexible pump channels with favorable properties such as a lower absorption of small molecules and lower water transmission [60, 228].

Another key aspect of the peristaltic pump on the Organ-Disc is the direct integration of the pump into the disc module. Thereby, reservoir, pump and cell channels are in direct contact to each other without interconnecting tubing, which allows for an overall improved and faster handling. Tubing involves time consuming preparation, for instance cleaning and sterilization, and connection steps between chip and external pump that goes along with the risk of introducing air bubbles into the system [192].

Furthermore, the tubing between chip and pump is a relevant but often overlooked factor in common microfluidic systems besides the applied chip material itself [193]. The inner tubing surface is usually high compared to the inner surface of the microchannels, which makes the tubing material a dominant and critical component in the overall system. It has been shown that several types of commercial tubing lead to drug sorption (ad- and/or absorption) and that sorption increases with the dwell time inside the tubing [194]. It is plausible that especially in systems with a high dwell time, such as closed-loop perfused systems, sorption might influence the media composition. During long-term endothelial culture, media circulates for up to 72 h inside the disc until the next media exchange. Therefore, this emphasizes the relevance of the tubing-free Organ-Disc configuration with a low-absorbing pump channel material.

Peristaltic pumping extends the range of achievable flow rates in the Organ-Disc and achieves flow rates of up to 2.6 mL/h at 800 rph motor speed. In principle, even higher flow rates are achievable by either more actuations per time or increased volume displacement per actuation. Further increased motor speed for faster actuation resulted in either bonding failure between pump and pump support layer or rupture of the flexible channel lid. This relates to the high mechanical stress during peristaltic pumping, which is also a common case of failure in commercial peristaltic pump tubing [264]. Thereto, current advances regarding the tuning of mechanical properties of SEBS materials, such as higher creep resistance, provide the opportunity to further improve the long-term stability of future pump modules [265].

Besides a higher actuation frequency, the peristaltic pump rate is depending linearly on the trapped volume between two, neighboring steel balls in the pump channel (*cf.* section 8.2). Therefore, the pumping rate could be increased through adaptions to the pump channel. Possible measures are a bigger cross-section in combination with bigger steel balls for sealing the channel. Alternatively, an increased diameter of the steel balls' trajectory on the disc could as well increase the pumped flow rate. This would be plausible by placing the pump channel at the periphery of the Organ-Disc. In principle, both adaptions lead to a higher displaced volume per actuation and provide a promising alternative for applications requiring further increased

flow rates without increasing the motor speed. Overall, this should limit the mechanical stress on the TPE and its degradation.

At lower pumping frequency, the peristaltic pump enabled the long-term perfused culture of endothelial cells for over seven days in total with qualitative flow tests showing the pump functionality at each day of culture. Furthermore, quantitative measurements on three consecutive days revealed highly comparable pumped fluid volumes per motor revolution and conclude the high stability of the peristaltic pump (*cf.* appendix, section 13.6).

Overall, both centrifugal and peristaltic pumping allow for the tunable perfusion in Organ-Discs without the need for expensive and bulky external pumps or error-prone and interfering tubing connections. Both approaches are based on rotation-based processes and require primarily a simple electric motor. In direct comparison of centrifugal and peristaltic pumping, it becomes clear that centrifugal pumping allows for a linear perfusion with less requirements to the disc materials and the spinner setup. On the other hand, peristaltic pumping enables circulatory perfusion without centrifugal forces and provides better control of the flow rate in a wider range.

10.4 On-Disc Tissue Culture

10.4.1 3D Tissues

OoC systems focus frequently on the generation of 2D cell layers on both sides of a porous membrane [117]. Such a system is predestined for the recapitulation of endothelial-epithelial barriers, for instance, in the lung [118, 121], kidney [266], and placenta [267], or other *in vivo* barriers, *e.g.* the blood brain barrier [268]. However, this approach lacks the capability to generate replicates of parenchymal tissue beyond the blood-tissue barrier, which is built up from dense and organized 3D cell constructs [7].

3D tissues in OoC devices are frequently formed by injection of cell-laden hydrogels [98–100], bioprinting of hydrogel-cell mixtures [103–105], retention of cells from a suspension by filtration [106–108], self-assembly in hanging drops [113], or generated by standard cell culture techniques and transferred into OoC devices [109–112].

In order to allow for the recapitulation of tissues with a complex 3D structure, the Organ-Disc technology provides a tool for the generation of tailorable and dense tissues. Thereto, the Organ-Disc uses previously presented approaches based on centrifugation for cell loading and spheroid

formation into microchambers [147, 220]. Going even one step further, the Organ-Disc technology simplifies the subsequent culture after the tissue generation by adding an active on-disc perfusion. This is different to the previous systems using centrifugal cell loading that either lack active perfusion at all [220], or rely on external syringe pumps for media supply during culture [147].

In general, cell centrifugation into dense pellets is a standard technique in cell culture. Therefore, well-defined centrifugation parameters are available and provide a basis for the implementation in the Organ-Disc [241]. The Organ-Disc achieves dense cell pellets already at gentle centrifugal accelerations of 46 × *g* and well below the usually applied 100 × *g* during cell passaging. For both explored cell types for 3D tissue generation, FB and ASC, these centrifugal accelerations achieved closely packed cell pellets that compacted into dense and viable tissues within 24 h. However, centrifugal cell loading can achieve even denser tissues without exceeding standard cell culture centrifugation parameters. This is demonstrated by stratified pellets and tissues loaded at approx. 100 × *g* with denser and clearly separated cell layers of different cell type.

The capability of the Organ-Disc technology to manipulate tissue densities marks an important difference, for instance, to systems applying cell-laden hydrogels or filtration-based systems. In the case of cell-laden hydrogels, a general concern is the low cell densities achievable by embedding single cells loosely into a hydrogel scaffold. This has led to scaffold-free printing advances with pre-formed, dense cell spheroids that fuse into a connected, macroscopic tissue [269]. At first glance, filtering cells from a cell suspension is suitable for higher cell densities in the generated cell pellet. The overall concept relies on the cell transport into the filter chamber by fluid flow. As the cells are retained by the porous barrier and accumulate in front of the pores, the hydraulic resistance of the porous barrier is increasing with advancing cell accumulation (Figure 10.2 a).

The pore clogging mechanism in microfluidic systems depends on multiple parameters besides the ratio between particle and pore size. Pore clogging can occur with both cells that are larger and cells that are smaller than a single pore [270]. Even though small rim structures or channels surrounding the porous barrier can achieve that single cells do not reach and completely close individual pores [107], the accumulating cell layer in front of the porous wall creates an additional hydraulic resistance across the permeable barrier. In this case, higher pressure gradients for fluid transport across the barrier will be necessary in order to prevent declining flow rates of cell suspension and declining cell transport into the chamber.

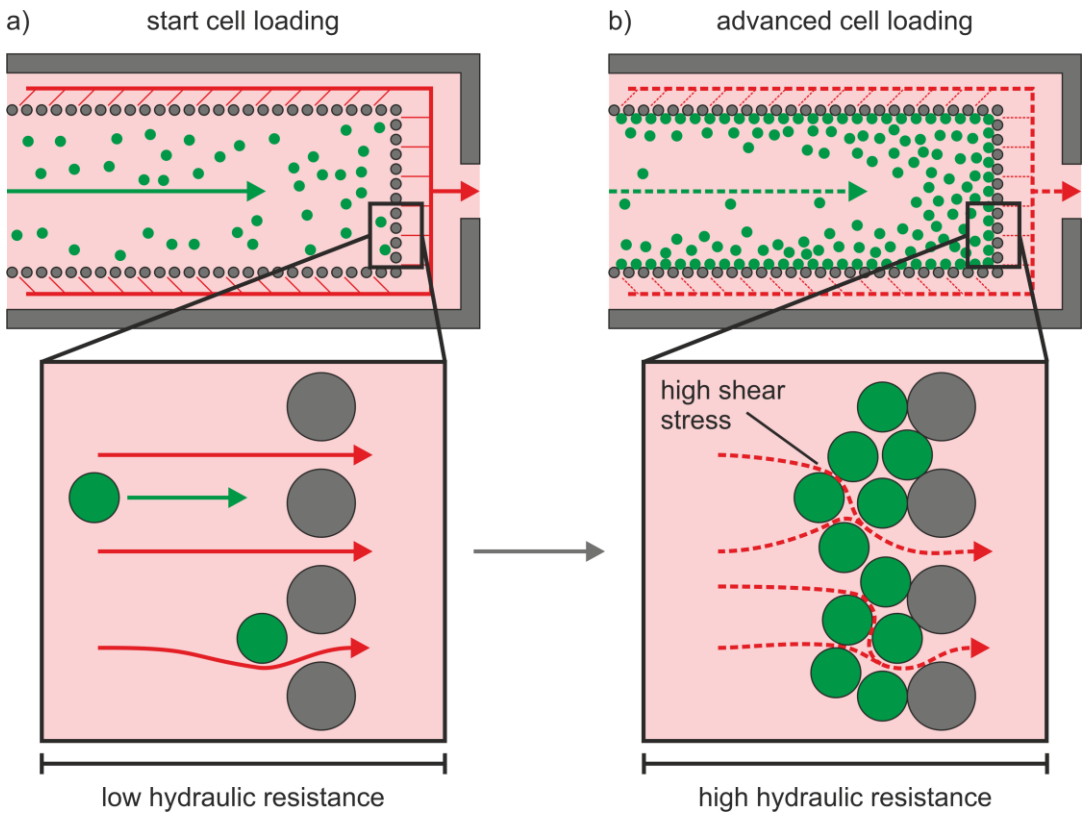

Figure 10.2 Cell loading by filtration. a) During early cell loading, the required pressure for fluid transport is low. b) Advancing cell accumulation in front of the porous barrier around the tissue chamber leads to an increase of the hydraulic resistance. Higher pressure gradients are necessary for fluid transport. This can lead to high shear stress on the cell.

Pressure pumps allow for limiting the loading pressure of the cell suspension [107], but cells accumulating in front of the porous barrier can still be exposed to very high shear rates generated by the excess media flowing around the cells and leaving the filter chamber (Figure 10.2 b). Therefore, filtration-based cell loading bears the risk of flow-induced damage to the accumulating cells in front of the porous barrier [271]. This has been observed in the case of too high flow rates using a syringe pump for cell loading and resulted in reduced cell viability [108].

Different to filtration-based cell loading, the Organ-Disc uses cell sedimentation, which does not require fluid flow. Hence, whether the membrane between cell and media layer, nor the accumulating cells inside the chamber, create a bottleneck for dense cell packing. At the same time, centrifugal cell loading is highly efficient and achieves 20 dense cell pellets with less than one million cells.

In order to put this cell number into perspective, one could compare the injected cell number to a previously reported heart-on-chip system [106]. The presented tissue chamber has an approx. 15-24 times smaller volume than the tissue chambers on the Organ-Disc (estimate from UV

lithography protocol and microscopy images in Ref. [106]). The authors added pipette tips with up to one million cells in suspension for loading a single tissue chamber with cardiomyocytes by filtration [106]. A fair comparison between tissue densities is difficult due to the different cell sizes and the not exactly known captured cell number inside the tissue chambers of both systems. Nevertheless, the clearly different requirements in cell amount serve as a demonstration of the cell efficient and parallelized centrifugal tissue generation in the Organ-Disc.

At the same time, centrifugal tissue generation on the Organ-Disc allows for precisely tailorable tissues. This is demonstrated with single cell type tissues with customizable geometries, for instance rectangular ASC and elongated FB tissues, as well as stratified tissues with separated layers of different cell type. This demonstrates that both the outer as well as the internal tissue structure are designable on the Organ-Disc. This allows for several, potential applications, for instance, the generation of fiber-like heart tissues [147, 235], or the recapitulation of *in vivo* stratified tissues such as liver [272], retina [273], or bone tissue [274]. Alternative approaches for stratified tissue generation are usually not scaffold-free, such as multi-layer bioprinting of hydrogels with different embedded cell types [275], hence often limited in tissue density. The scaffold-free bioprinting alternative with pre-formed spheroids allows for high complexity but creates tissue constructs in the mm to low cm range [269], which limits the adaptability for OoC systems with channels in the µm to low mm range.

Centrifugal cell loading might provide even more flexibility in tissue generation. In principle, this process is not limited to cell suspensions and loading single cells into a chamber. It is plausible that centrifugal cell loading is transferable to loading spheroids form single or multiple cell types into the tissue chambers. This would allow to load spheroids, or even organoids, that are usually generated in advanced, time-consuming cell culture protocols and integrate them into the Organ-Disc. Thereby, the Organ-Disc could take on the role of a parallelized culture platform with integrated perfusion similar to hanging drop systems. In general, hanging drop networks can be perfused by external or integrated pumps for a perfused spheroid culture [113, 276]. However, hanging drops can drip-off due to handling errors of the chip and evaporation in those systems requires a compensation strategy in order to limit liquid loss [113]. Therefore, the Organ-Disc might provide a more robust platform as the tissues are enclosed inside a rigid channel. Finally, the Organ-Disc platform allows for a simple scale-up with even more tissues per disc in future versions. This could be achieved by simply arranging more tissue channels on the disc footprint or using cell channel designs achieving a cell compartmentalization into chambers lying next to each other [147].

10.4.2 Blood Vessel-like Structures

Vasculature-like perfusion is a key element in OoC research for a physiologic tissue or organ model. In recent years, the combination of more physiologic vascular networks and OoC systems has come into focus and has led to several integration approaches [277]. Thereby, endothelial cells are an essential component of vascular networks as they line the inner surface of all blood vessels in the human body [278].

Endothelial-lining of the inner channel surfaces has been achieved in channel networks with rectangular and round cross-section [279, 280]. Thereto, fabrication protocols have been presented for the generation of tubular PDMS [279], or hydrogel structures inside a rectangular channel [281]. However, the individual seeding protocols for complete endothelial-lining of the inner channel surfaces vary. After a coating with ECM proteins, rectangular PDMS channels have been perfused with a HUVEC suspension over two days using a syringe pump for the endothelial lining [280]. Round channels have been lined with endothelial cells by four consecutive seeding steps and turning the chip 90° in each step for cell attachment on the respective surface [279]. An automated version of this approach was used in a hydrogel lumen by attaching the chip to a slowly rotating motor for a homogenous cell distribution and attachment over the inner channel perimeter [282].

Blood vessel-like structures on the Organ-Disc are achieved by first lining the top of the channel with endothelial cells and the remaining inner surfaces over three days under gentle, closed-loop media flow in order to allow for sufficient nutrient supply and metabolite removal. Thereby, an advantage of the peristaltic pump setup using a stepper motor is that the flow can be ramped up very slowly in order to avoid abrupt increases in flow rate and cell detachment. In conventional OoC systems, this would usually require an external peristaltic pump allowing for a programmable flow speed pattern.

Furthermore, the on-disc pump allowed for the perfusion of blood vessel-like structures for more than seven days, which demonstrates the suitability of the setup for long-term, on-disc culture. Additionally, HUVEC were exposed to increased shear stress levels leveraging the capability of the on-disc pump to generate high flow rates. Pumping at the maximum applied rate achieves an estimated WSS of up to 1.5 dyn/cm². HUVEC that were cultured under these conditions revealed a high viability and an intact endothelial structure, however, no cell alignment in flow direction. This was expected and in agreement with previous studies [242–244], as this WSS level is at the lower range of physiological levels and comparable to WSS in large veins [283].

As already discussed, pumping with even higher fluid flows for increased WSS is plausible but will require an adjustment of the pump channel design in order to achieve a higher displaced volume per actuation. Alternatively, thinner cell channel designs provide another strategy next to higher flow rates as WSS increases geometrically with decreasing channel height in rectangular channels. HUVEC alignment is reported for WSS at 7.2 dyn/cm² and higher [242–244]. In principle, those WSS levels would be achieved in an 80 µm high channel if the peristaltic pump transports the same volume per time. However, this will also result in an over ten times higher hydraulic resistance that might require stronger magnets for compression and sealing and a more powerful motor for actuation. Therefore, a combination of pump channels with higher displaced volume per actuation and slightly thinner cell channels might provide a suitable compromise for applications focusing on the effects of shear stress on endothelial cells without overall changes to the Organ-Disc layout and spinner hardware.

Finally, the generation of perfused blood-vessel like structures on the Organ-Disc platform creates the basis for future applications aiming for an even closer recapitulation of vasculature-like perfused 3D tissues. In principle, the channel design of endothelial lined channels in peristaltic Organ-Discs is compatible with the media channel in disc versions used for 3D tissue generation. Thereto, a closed-loop perfused and endothelial-lined media channel could be added above the porous membrane and tissue chamber incorporating a 3D tissue. Approaches demonstrating the plausibility of this combination have been presented previously and generated media channels with an inner endothelial lining neighboring a channel with an intestinal epithelium [284].

10.4.3 Tissue Characterization and Treatment

The primary characterization methods in OoC research are optical readouts, such as microscopy for the analysis of cell morphology and fluorescent antibody staining. Ideally, the materials separating a tissue inside a microfluidic system from the optical sensor or microscope lenses should be as transparent and as thin as possible in order to limit light absorbance and to enable the use of high-magnification lenses, which are usually limited in working distance.

For this purpose, the Organ-Disc features a thin bottom layer from highly transparent thermoplastic foils for unrestricted microscopy using an inverted microscope. The main material for Organ-Discs was PMMA, which was suitable for high-resolution images using bright field and fluorescence microscopy. COC is an alternative material for applications requiring even better optical properties, for instance, in the near UV spectra for further enhanced

fluorescence readouts [257]. Thereto, the fabrication of Organ-Discs in COC by thermal fusion bonding is achievable and has been demonstrated using the developed thermal fusion bonding tool.

In comparison to conventional OoC systems relying on external pump perfusion, the Organ-Disc allows for a user-friendly imaging as the risk of failing tubing connections during handling on a microscope stage is eliminated. In both Organ-Disc version, using either centrifugal or peristaltic perfusion, the reservoir can maintain attached to the disc during image acquisition. As the reservoirs are reversibly attached to Organ-Disc by mechanical clamping or double sided tapes, reservoir removal is possible and simple to perform. This enables improved handling during endpoint analysis, such as fluorescent microscopy of antibody stained tissues after fixation.

Microscopy of tissues during on-disc culture required the short interruption of the perfusion for removal of the Organ-Disc form the respective spinner and transfer to a microscope. However, future versions of Organ-Disc spinner can include integrated imaging equipment.

The peristaltic Organ-Disc remains stationary during culture, which allows for imaging setups inside the spinner that are adapted from conventional microscopy setups, for instance, using a microscope lens on a motorized stage [285]. Even during on-disc culture with centrifugal perfusion, such a system would be sufficient if short perfusion interruptions are accepted during image acquisition. Nevertheless, several optical readout setups have been developed in the field of LoD that are capable of imaging during fast disc rotation [286]. Grumann *et al.* presented a setup that achieves a spatial imaging resolution below 5 µm from structures on a disc at a radial position of 5 cm spinning at 150 Hz (approx. 47 m/s) [287]. Also setups for fluorescence microscopy of 20 µm objects moving at approx. 17 m/s were previously presented [288]. All processes on the Organ-Disc happen at a rotation speed ≤ 1500 rpm (approx. 8 m/s). Therefore, it is plausible that all processes on the Organ-Disc, even centrifugal cell loading, can be monitored during rotation by implementing spinner hardware from LoD systems into future Organ-Disc spinners.

Besides the characterization of tissues by microscopy, the perfused media was collected for subsequent analysis or supplemented with compounds for cell treatments. Thereto, the Organ-Disc reservoir guarantees continuous, user-friendly access to the perfused media throughout on-disc culture. The individual pipetting steps are simple, fast and comparable to standard cell culture procedures, hence completely automatable with appropriate liquid handling equipment

[289]. In the case of the peristaltic Organ-Disc, sampling or adding stimuli to the media is even possible without stopping the perfusion.

However, a limitation of open reservoir setups are high evaporation rates under cell culture conditions [245]. At the same time, essential gas diffusion of oxygen and carbon dioxide to the media needs to be assured, which excludes gas tight sealing of reservoirs as a measure against evaporation. Oxygen and carbon dioxide transport was assured by using breathable tapes on top of the reservoirs. However, those tapes are not completely impermeable for water vapor. In order to provide an estimate of the degree of evaporative liquid loss, four different ion concentrations were monitored in a cell-free reference system comparable to a previously presented assessment of evaporation in a micro-bioreactor platform [246].

The calculated liquid loss of 4% per day and 13% within the 72 h media exchange interval demonstrate the relevance to determine evaporation during on-disc culture. Otherwise, this liquid loss would influence other solute concentrations in an uncontrolled manner. The evaporation estimates allow for normalizing nutrients and metabolites to the remaining liquid inside the reservoir compartments. Thereby, the cell metabolism can be assessed without overlapping water loss.

Additionally, the evaporation assessment highlights the importance of taking measures against excessive liquid loss, such as periodic media exchanges, in closed-loop perfused systems in order to maintain suitable culture conditions. For instance, evaporative liquid loss and accompanied osmolality shifts can impact cells [141]. In the Organ-Disc, the periodic media exchanges, which replicate standard cell culture procedures, achieve a stable sawtooth profile of ion concentrations without net increase over time. In principle, the evaporative loss could be alternatively compensated by adding according amounts of water to the reservoir at each sampling day or by an optimized feeding strategy of fresh media and buffer [246]. Additionally, replacing the breathable tape with fluorinated ethylene–propylene (FEP) might provide a reduced water transmission rate, while providing relatively high oxygen and carbon dioxide permeability [290].

Identically to ion concentrations, nutrient and metabolite concentrations were monitored in the perfused media. The concentration profiles of the nutrient glucose and the metabolite lactate demonstrate the metabolic activity of on-disc cultured HUVEC. Both profiles are inverted and origin from the conversion of glucose to lactate by glycolysis. In general, cells are able to perform glycolysis under anaerobic as well as aerobic conditions [247]. Anaerobic conditions are not expected due to the breathable sealing tape on top of the reservoir, which is frequently

applied as gas permeable cover in cell culture [291–294]. However, glycolysis is also possible under aerobic conditions through the so-called Warburg effect, which is reported for tumor cells and proliferating cells [295]. Especially endothelial cells have been identified to favor glycolysis compared to alternative metabolic processes, such as oxidative phosphorylation [296].

Though the exact oxygen levels are not known in proximity to the cells, oxygen depletion of cell culture media inside the cell channel can be estimated in order to bring it into context to the observed metabolic activity. The basal mitochondrial respiration of 30,000 HUVEC is approx. 80×10^{-12} mol/min [297]. This relates to an oxygen consumption per cell *OC* of 2.7×10^{-15} mol/min/cell. The cell number inside a cell channel of the peristaltic Organ-Disc *CN* is approx. 180,000 cells. This cell number can be estimated from nuclei counts from a confluent channel section (1080 cells/mm^2), which is extrapolated to the inner surface of a cell channel (approx. 167 mm^2). Assuming steady state conditions and oxygen saturated media inside the reservoir with a concentration c_{in} of 192×10^{-6} mol/L [298], the oxygen content in the media leaving the channel at a flow rate *Q* is

$$c_{out} = c_{in} - \frac{OC \cdot CN}{Q} \tag{10.1}$$

The lowest expected oxygen content is 0.10 mmol/L at a flow rate of 0.32 mL/h (100 rph), which was applied for perfusion during monitoring the metabolic activity of HUVEC. This oxygen content relates to an oxygen saturation of 53% of the cell culture media under atmospheric conditions (21% partial pressure of oxygen). Physiologic oxygen levels depend on the specific region in the human body but are usually below 10% partial oxygen pressure [299], which would relate to approx. 50% oxygen saturation [300]. Therefore, it is plausible that neither anaerobic nor hypoxic conditions are present inside the disc. Overall, this indicates that the observed metabolic activity is aerobic glycolysis and not anaerobic glycolysis due to the absence of oxygen.

Nutrient and metabolite concentrations corrected for evaporative loss revealed an average glucose consumption and lactate production of 2.5 ± 2.2 µmol/day and 7.5 ± 3.5 µmol/day respectively. Kim *et al.* report that HUVEC convert nearly 90% of glucose to lactate, with 1.74 produced lactate molecules per glucose molecule [301]. Considering the standard deviation of both rates, the measured glucose consumption and lactate production are in reasonable agreement, however, slightly too high compared to the study of Kim *et al.* It is expected that this deviation stems from the different sensitivity of glucose and lactate measurements. The

high basal glucose content in the cell culture media results in relatively small reduction of the glucose content due to cell metabolism. The overall changes in glucose concentration between two measurements are close to the standard deviation of the mean. In contrast to that, the lactate concentration in the basal media is almost zero. Therefore, already small amounts of secreted lactate result in a distinct increase of lactate concentrations.

Besides off-disc media analysis, future Organ-Disc versions can leverage the portfolio of integrated sensor technology for cell culture and OoC applications [302, 303]. Weltin *et al.* presented an electro (bio)chemical sensor system for online oxygen, pH, glucose and lactate measurements fabricated on a glass substrate [260]. The integration of glass-based sensors into thermoplastic systems is usually complex but plausible for TPE-based Organ-Discs using the robust and simple bonding of TPE to glass substrates [228]. Alternatively, several optical chemical sensors have been developed in recent years [304]. Optical sensors, for instance in the form of sensor spots or particles [122, 305], primarily require a transparent chip material, hence are well suited for sensing applications in the Organ-Disc.

Furthermore, the Organ-Disc technology provides a user-friendly platform for cell treatments and readout of the respective cell responses. Thereto, compounds or stimuli can be simply added into the reservoir and perfused, for instance, by peristaltic pumping over a defined period, whereas the perfused media is accessible throughout the exposure for analysis.

As a proof-of-concept for on-disc treatments and additional readout, the functionality of the on-disc cultured endothelial cells is demonstrated in response to inflammatory cell stimulation with TNF-α. Thereby, the increased CD106 expression of HUVEC after the TNF-α exposure is in well agreement with previous studies and an expected inflammatory response of functional endothelial cells [248, 249]. Additionally, the significantly higher release of the proinflammatory cytokines IL-6 and IL-8 of TNF-α treated HUVEC compared to untreated HUVEC provides another plausible demonstration of functional endothelial cells. Both IL-6 and IL-8 are secreted to a higher extend after TNF-α treatment from endothelial cells [250, 251]. Similarly, the increased expression of Ang-2 in TNF-α treated endothelial cells is well known [252]. As demonstrated by Fiedler *et al.*, Ang-2 is stored and released from Weibel-Palade bodies in endothelial cells after exposure to certain stimuli [306]. However, it is worth mentioning that Fiedler *et al.* did not observe an Ang-2 release after short-term stimulation with TNF-α [306]. In contrast to that the TNF-α stimulation in the Organ-Disc resulted in a significantly higher Ang-2 concentration in the media. In the Organ-Disc, however, HUVEC were treated for 24 h with TNF-α and the released Ang-2 accumulated over this period in the

perfused media, which might trigger different cell reactions. Nevertheless, this demonstrates that the Organ-Disc with closed-loop perfusion provides a tool for long-term stimulation experiments with both circulating compounds and accumulating cell products, hence, enables the observation of time-dependent reactions.

10.5 On-Disc Blood Perfusion

As demonstrated in previous studies, endothelial cell-lining is the basis for the emulation of *in vitro* capillaries that are amenable for blood perfusion [307, 308]. In the human body, endothelial cells line all blood capillaries and are in direct contact to the perfused blood [278]. If blood comes in contact with other surfaces, such as bare polymer surfaces, a blood clotting cascade can be triggered resulting in blood coagulation and the formation of a thrombus [309].

Therefore, the lining of Organ-Disc channels with functional endothelial cells achieves an important step towards artificial, perfused blood vessels. In order to limit the exposure of blood to the cell channel, the complete endothelial lining in the Organ-Disc is achieved using the optimized cell seeding process. Starting with an initial, sub-confluent cell seeding on the ceiling of the cell channel, endothelial cells proliferate and spread on the inner surfaces up to a confluent lining under a continuous, peristaltic perfusion.

As a proof-of-concept, perfusion experiments with fresh, human whole blood were conducted after the complete lining. Thereto, human whole blood were injected and actively pumped through the cell channels using the integrated peristaltic pump. The absence of channel clogging during blood perfusion and the complete, subsequent flush-out of blood in all of the four channels demonstrates the successful on-disc blood perfusion.

At the same time, on-disc blood perfusion is combinable with platelet adhesion monitoring. Platelet adhesion is an important process in injured blood vessels in order to prevent blood loss but is also involved during thrombosis and stroke [253]. Platelet adhesion can be observed in the Organ-Disc by fluorescently labeling of platelets in the perfused whole blood. After the blood perfusion, adherent platelets on an endothelial cell structure with a physiologic morphology are clearly observable.

These findings demonstrate that the Organ-Disc combines an integrated perfusion system that is capable of pumping blood through a cell channel with a functional endothelial lining. This provides the basis for future applications in the field of vascular research. For instance, an automated readout of platelet adhesion to the endothelial cells using optimized readout

protocols for the analysis of microscopy images [234]. Alternatively, future Organ-Disc applications could study the effect of different shear rates during blood perfusion using the tunable on-disc pump [310, 311]. Different compounds, such as vitamin E (α-tocopherol) [312], influence platelet adhesion. As demonstrated, the Organ-Disc enables user-friendly cell treatments and readouts through the open reservoir setup. This could be further used for combinations of blood perfusion with drug exposures, which overall opens up a broad spectrum of future application in vasculature research but also other fields of OoC relying on a close emulation of *in vivo* blood flow.

11 Summary and Conclusion

OoC systems culture human tissues in a precisely controllable microfluidic environment and recapitulate tissue and organ-level functionality [114, 117]. Current advances in the field of OoC demonstrate the potential of this technology as new microphysiologic tool with benefits over traditional, non-physiological cell assays and ethically problematic animal tests for drug development and precision medicine [7, 133]. However, unmet challenges, such as low fabrication scalability, chip material related constrains, low parallelization and elaborate perfusion setups, remain limitations of this technology [7, 13].

The focus of this thesis was the development of a novel platform technology paving the way towards higher-throughput OoC systems. This platform is called the Organ-Disc and combines concepts from centrifugal microfluidics, tissue engineering and OoC research. This combination enables a disruptive approach towards parallelization and automation of OoC systems using rotation-based processes for the generation and perfusion of microtissues. On the one hand, this eliminates the need for external pumps and error-prone tubing connections that interfere with automation approaches. On the other hand, parallelization solely requires a symmetric arrangement of multiple system on a single disc.

The Organ-Disc itself is a multi-layer, microfluidic system and made of industry-compatible materials, such as thermoplastics and TPE, which eliminates the need for PDMS and its related limitations for OoC systems [32, 138]. The thermoplastic disc modules can be fabricated from a wide portfolio of thin and highly transparent materials as demonstrated using commercially available PMMA, PC and COC foils in combination with rapid and precise microstructuring techniques such as, plotting or laser cutting. Subsequent fusing of the individual thermoplastic layers into rigid disc modules is achieved by solvent vapor bonding or thermal fusion bonding. Whereas, solvent vapor bonding is ideally suited for the rapid prototyping of Organ-Discs, thermal fusion bonding provides great potential for the fabrication scale-up. The presented thermal fusion bonding tool enables precise control over the bonding process and is suitable for the simultaneous fabrication of up to seven, highly stable discs. Functional elements that require a flexible and sturdy material were fabricated using the TPE SEBS as promising alternative to the elastomer PDMS. Hot embossing with rigid and temperature-stable epoxy stamps, which recapitulate precise SU-8 structures utilizing the presented epoxy molding tool, was implemented as structuring technique for TPE. The integration of TPE modules to the Organ-Disc is achieved by a simple thermal bonding that withstands even extreme pressures, beyond the usual OoC system requirements.

The Organ-Disc technology enables the generation and culture of multiple tissue types with tailorable structure under controllable perfusion actuated by rotation. Centrifugal cell loading provides the basis for the parallelized generation of dense, 3D tissues and relies on the transport of cells into tissue chambers by centrifugal forces. This process results in the rapid, cell-efficient and simultaneous formation of up to 20 cell pellets in one spinning step taking only 5 min and requiring less than one million cells. Subsequently, the individual cells inside the pellet fuse together into a dense, precisely tailorable and viable 3D microtissue. This has been demonstrated for both FB and ASC tissues adapting to different tissue chamber designs or even developing a stratification with adjacent cell layers of different cell type using a stepwise repeated loading. In addition to 3D tissues, blood vessel-like structures were generated in the Organ-Disc by completely lining inner channel surfaces with endothelial cells. The generated endothelial tissues display a high viability as well as a physiologic morphology and protein expression and are even perfusable with human whole blood. The on-disc generation of tailored 3D tissues and functional endothelial tissues paves the way for future studies on both parenchymal tissue and *in vivo* barriers and demonstrates the versatility of the Organ-Disc platform.

Physiological perfusion is a necessity in OoC systems but a major technical challenge if one aims at reduction of tubing and external pumping equipment. Thereto, the Organ-Disc applies either centrifugal pumping or integrated, peristaltic pumping for the continuous perfusion during tissue generation and culture. Centrifugal pumping achieves a linear, open-loop fluid flow and solely requires rotation of the Organ-Disc below $1 \times g$ for sufficient pumping rates. Closed-loop perfusion is achieved by adding a peristaltic pumping mechanism on-disc using magnetically dragged steel balls for fluid displacement on top of the stationary disc. This enables programmable flow patterns, an extended range of flow rates and the complete avoidance of hyper-gravity conditions. The on-disc pump allows for tunable shear stress acting on cells lining the microchannels, long-term culture for over seven days and even the pumping of whole blood.

Several tissue characterization techniques are compatible with the Organ-Disc platform. The Organ-Disc features a thin bottom layer allowing for high-resolution microscopy. This has been utilized for fluorescent antibody staining and the detection of platelet adhesion on endothelial cells. The open Organ-Disc reservoirs provide continuous access to the perfused media for cell treatments and analysis. Supernatant analysis included the assessment of evaporative liquid loss, a highly relevant aspect of microfluidics in general, and nutrient and metabolite content for the monitoring of cell metabolism. As proof-of-concept for on-disc cell treatments,

endothelial cells are stimulated with TNF-α and the corresponding, inflammatory response is monitored. Thereby, the cytokines released from the cells into the perfused media and fluorescent staining of the endothelial cells revealed an expected cell response to TNF-α and demonstrate the functionality of on-disc cultured endothelial cells.

Building on the presented achievements, the Organ-Disc platform paves the way for various applications. The generation of stratified tissues with tunable centrifugal forces paves the way for the recapitulation of *in vivo* tissues and organs built up of layers with different properties, such as cell type or packing density. Future Organ-Discs can combine peristaltic pumping and centrifugal, 3D tissue generation. This will go one step further in the direction of blood flow-like tissue perfusion by adding a perfused endothelial barrier and the possibility of programmable flow patterns. Thereby, the combination of TPE and thermoplastics will facilitate future Organ-Disc fabrication even more. The presented PC/TPE-hybrid layers combine the simple and precise structuring capabilities of TPE with the mechanical support of rigid thermoplastics. They are generated and structured by a single hot embossing step. The resulting modules are highly transparent, biocompatible, display a low absorption of small, hydrophobic molecules and can be bonded to glass, which will facilitate future sensor integration. As demonstrated, minimal equipment, such as simple electric motors, are sufficient for driving the individual processes on the Organ-Disc. By leveraging the achievements in the field of LoD and associated developments of CD player-like hardware for spinning, imaging and screening, the Organ-Disc technology has the potential to be transferred into benchtop settings and high-throughput workflows.

Overall, the presented work demonstrates that the Organ-Disc technology achieves parallelization and automation with minimal requirements for manual handling and equipment, therefore creates a novel enabling technology for the next generation of OoC systems.

12 References

[1] Scannell, J. W., Blanckley, A., Boldon, H. and Warrington, B. Diagnosing the decline in pharmaceutical R&D efficiency. *Nature Reviews Drug Discovery*. 2012. Vol. 11, no. 3, p. 191–200. DOI 10.1038/nrd3681.

[2] DiMasi, J. A., Grabowski, H. G. and Hansen, R. W. Innovation in the pharmaceutical industry: New estimates of R&D costs. *Journal of Health Economics*. 2016. Vol. 47, p. 20–33. DOI 10.1016/j.jhealeco.2016.01.012.

[3] Munos, B. Lessons from 60 years of pharmaceutical innovation. *Nature Reviews Drug Discovery*. 2009. Vol. 8, no. 12, p. 959–968. DOI 10.1038/nrd2961.

[4] Paul, S. M., Mytelka, D. S., Dunwiddie, C. T., Persinger, C. C., Munos, B. H., Lindborg, S. R. and Schacht, A. L. How to improve R&D productivity: the pharmaceutical industry's grand challenge. *Nature Reviews Drug Discovery*. 2010. Vol. 9, no. 3, p. 203–214. DOI 10.1038/nrd3078.

[5] Harrison, R. K. Phase II and phase III failures: 2013–2015. *Nature Reviews Drug Discovery*. 2016. Vol. 15, no. 12, p. 817–818. DOI 10.1038/nrd.2016.184.

[6] Marx, U., Akabane, T., Andersson, T. B., Baker, E., Beilmann, M., Beken, S., Brendler-Schwaab, S., Cirit, M., David, R., Dehne, E.-M., Durieux, I., Ewart, L., Fitzpatrick, S. C., Frey, O., Fuchs, F., Griffith, L. G., Hamilton, G. A., Hartung, T., Hoeng, J., Hogberg, H., Hughes, D. J., Ingber, D. E., Iskandar, A., Kanamori, T., Kojima, H., Kuehnl, J., Leist, M., Li, B., Loskill, P., Mendrick, D. L., Neumann, T., Pallocca, G., Rusyn, I., Smirnova, L., Steger-Hartmann, T., Tagle, D. A., Tonevitsky, A., Tsyb, S., Trapecar, M., Van de Water, B., Van den Eijnden-van Raaij, J., Vulto, P., Watanabe, K., Wolf, A., Zhou, X. and Roth, A. Biology-inspired microphysiological systems to advance patient benefit and animal welfare in drug development. *ALTEX*. 2020. Vol. 37, no. 3, p. 365–394. DOI 10.14573/altex.2001241.

[7] Zhang, B., Korolj, A., Lai, B. F. L. and Radisic, M. Advances in organ-on-a-chip engineering. *Nature Reviews Materials*. 2018. Vol. 3, no. 8, p. 257–278. DOI 10.1038/s41578-018-0034-7.

[8] Esch, E. W., Bahinski, A. and Huh, D. Organs-on-chips at the frontiers of drug discovery. *Nature reviews. Drug discovery*. 2015. Vol. 14, no. 4, p. 248–260. DOI 10.1038/nrd4539.

[9] Franzen, N., Van Harten, W. H., Retèl, V. P., Loskill, P., Van den Eijnden-van Raaij, J. and IJzerman, M. Impact of organ-on-a-chip technology on pharmaceutical R&D costs. *Drug Discovery Today*. 2019. Vol. 24, no. 9, p. 1720–1724. DOI 10.1016/j.drudis.2019.06.003.

[10] Zhang, B. and Radisic, M. Organ-on-a-chip devices advance to market. *Lab on a Chip*. 2017. Vol. 17, no. 14, p. 2395–2420. DOI 10.1039/C6LC01554A.

[11] Ewart, L. and Roth, A. Opportunities and challenges with microphysiological systems: a pharma end-user perspective. *Nature Reviews Drug Discovery*. 2021. Vol. 20, no. 5, p. 327–328. DOI 10.1038/d41573-020-00030-2.

[12] An, W. F. and Tolliday, N. Cell-Based Assays for High-Throughput Screening. *Molecular Biotechnology*. 2010. Vol. 45, no. 2, p. 180–186. DOI 10.1007/s12033-010-9251-z.

[13] Probst, C., Schneider, S. and Loskill, P. High-throughput organ-on-a-chip systems: Current status and remaining challenges. *Current Opinion in Biomedical Engineering*. 2018. Vol. 6, p. 33–41. DOI 10.1016/j.cobme.2018.02.004.

[14] Strohmeier, O., Keller, M., Schwemmer, F., Zehnle, S., Mark, D., Von Stetten, F., Zengerle, R. and Paust, N. Centrifugal microfluidic platforms: advanced unit operations and

applications. *Chemical Society Reviews*. 2015. Vol. 44, no. 17, p. 6187–6229. DOI 10.1039/C4CS00371C.

[15] Thorsen, T., Maerkl, S. J. and Quake, S. R. Microfluidic Large-Scale Integration. *Science*. 2002. Vol. 298, no. 5593, p. 580–584. DOI 10.1126/science.1076996.

[16] Melin, J. and Quake, S. R. Microfluidic Large-Scale Integration: The Evolution of Design Rules for Biological Automation. *Annual Review of Biophysics and Biomolecular Structure*. 2007. Vol. 36, no. 1, p. 213–231. DOI 10.1146/annurev.biophys.36.040306.132646.

[17] Gorkin, R., Park, J., Siegrist, J., Amasia, M., Lee, B. S., Park, J.-M., Kim, J., Kim, H., Madou, M. and Cho, Y.-K. Centrifugal microfluidics for biomedical applications. *Lab on a Chip*. 2010. Vol. 10, no. 14, p. 1758–1773. DOI 10.1039/b924109d.

[18] Ducrée, J., Haeberle, S., Lutz, S., Pausch, S., Stetten, F. von and Zengerle, R. The centrifugal microfluidic Bio-Disk platform. *Journal of Micromechanics and Microengineering*. 2007. Vol. 17, no. 7, p. S103–S115. DOI 10.1088/0960-1317/17/7/s07.

[19] Burger, R., Kirby, D., Glynn, M., Nwankire, C., O'Sullivan, M., Siegrist, J., Kinahan, D., Aguirre, G., Kijanka, G., Gorkin, R. A. and Ducrée, J. Centrifugal microfluidics for cell analysis. *Current Opinion in Chemical Biology*. 2012. Vol. 16, no. 3–4, p. 409–414. DOI 10.1016/j.cbpa.2012.06.002.

[20] Clime, L., Daoud, J., Brassard, D., Malic, L., Geissler, M. and Veres, T. Active pumping and control of flows in centrifugal microfluidics. *Microfluidics and Nanofluidics*. 2019. Vol. 23, no. 3, p. 29. DOI 10.1007/s10404-019-2198-x.

[21] Bruus, H. *Theoretical microfluidics*. Oxford ; New York : Oxford University Press, 2008. Oxford master series in physics, 18. ISBN 978-0-19-923509-4. TJ853 .B78 2008

[22] Eckhardt, B. Turbulence transition in pipe flow: some open questions. *Nonlinearity*. 2007. Vol. 21, no. 1, p. T1–T11. DOI 10.1088/0951-7715/21/1/t01.

[23] Avila, K., Moxey, D., De Lozar, A., Avila, M., Barkley, D. and Hof, B. The Onset of Turbulence in Pipe Flow. *Science*. 2011. Vol. 333, no. 6039, p. 192–196. DOI 10.1126/science.1203223.

[24] Chung, B. J., Robertson, A. M. and Peters, D. G. The numerical design of a parallel plate flow chamber for investigation of endothelial cell response to shear stress. *Computers & Structures*. 2003. Vol. 81, no. 8–11, p. 535–546. DOI 10.1016/S0045-7949(02)00416-9.

[25] Madadelahi, M., Acosta-Soto, L. F., Hosseini, S., Martinez-Chapa, S. O. and Madou, M. J. Mathematical modeling and computational analysis of centrifugal microfluidic platforms: a review. *Lab Chip*. 2020. Vol. 20, no. 8, p. 1318–1357. DOI 10.1039/C9LC00775J.

[26] Cho, H., Kim, H.-Y., Kang, J. Y. and Kim, T. S. How the capillary burst microvalve works. *Journal of Colloid and Interface Science*. 2007. Vol. 306, no. 2, p. 379–385. DOI 10.1016/j.jcis.2006.10.077.

[27] Duffy, D. C., Gillis, H. L., Lin, J., Sheppard, N. F. and Kellogg, G. J. Microfabricated Centrifugal Microfluidic Systems: Characterization and Multiple Enzymatic Assays. *Analytical Chemistry*. 1999. Vol. 71, no. 20, p. 4669–4678. DOI 10.1021/ac990682c.

[28] Bauer, M., Ataei, M., Caicedo, M., Jackson, K., Madou, M. and Bousse, L. Burst valves for commercial microfluidics: a critical analysis. *Microfluidics and Nanofluidics*. 2019. Vol. 23, no. 7, p. 86. DOI 10.1007/s10404-019-2252-8.

[29] Whitesides, G. M. The origins and the future of microfluidics. *Nature*. 2006. Vol. 442, no. 7101, p. 368–373. DOI 10.1038/nature05058.

[30] Young, R. J. and Lovell, P. A. Concepts and Nomenclature. In : *Introduction to Polymers*. 3rd Edition. Boca Raton : CRC Press, 2011. p. 3–14. ISBN 978-0-429-10948-5.

[31] Biron, M. 2 - Thermoplastic Specific Properties. In : Biron, M. (ed.), *Material Selection for Thermoplastic Parts*. Oxford : William Andrew Publishing, 2016. p. 39–75. ISBN 978-0-7020-6284-1.

[32] Berthier, E., Young, E. W. K. and Beebe, D. Engineers are from PDMS-land, Biologists are from Polystyrenia. *Lab on a Chip*. 2012. Vol. 12, no. 7, p. 1224–1237. DOI 10.1039/c2lc20982a.

[33] McDonald, J. C. and Whitesides, G. M. Poly(dimethylsiloxane) as a Material for Fabricating Microfluidic Devices. *Accounts of Chemical Research*. 2002. Vol. 35, no. 7, p. 491–499. DOI 10.1021/ar010110q.

[34] Stern, S. A., Shah, V. M. and Hardy, B. J. Structure-permeability relationships in silicone polymers. *Journal of Polymer Science Part B: Polymer Physics*. 1987. Vol. 25, no. 6, p. 1263–1298. DOI 10.1002/polb.1987.090250607.

[35] Merkel, T. C., Bondar, V. I., Nagai, K., Freeman, B. D. and Pinnau, I. Gas sorption, diffusion, and permeation in poly(dimethylsiloxane). *Journal of Polymer Science Part B: Polymer Physics*. 2000. Vol. 38, no. 3, p. 415–434. DOI 10.1002/(SICI)1099-0488(20000201)38:3<415::AID-POLB8>3.0.CO;2-Z.

[36] Zhang, Y., Ishida, M., Kazoe, Y., Sato, Y. and Miki, N. Water-vapor permeability control of PDMS by the dispersion of collagen powder. *IEEJ Transactions on Electrical and Electronic Engineering*. 2009. Vol. 4, no. 3, p. 442–449. DOI 10.1002/tee.20429.

[37] Toepke, M. W. and Beebe, D. J. PDMS absorption of small molecules and consequences in microfluidic applications. *Lab on a Chip*. 2006. Vol. 6, no. 12, p. 1484–1486. DOI 10.1039/b612140c.

[38] Regehr, K. J., Domenech, M., Koepsel, J. T., Carver, K. C., Ellison-Zelski, S. J., Murphy, W. L., Schuler, L. A., Alarid, E. T. and Beebe, D. J. Biological implications of polydimethylsiloxane-based microfluidic cell culture. *Lab on a Chip*. 2009. Vol. 9, no. 15, p. 2132–2139. DOI 10.1039/b903043c.

[39] Becker, H. and Gärtner, C. Polymer microfabrication technologies for microfluidic systems. *Analytical and Bioanalytical Chemistry*. 2008. Vol. 390, no. 1, p. 89–111. DOI 10.1007/s00216-007-1692-2.

[40] Tsao, C.-W. and DeVoe, D. L. Bonding of thermoplastic polymer microfluidics. *Microfluidics and Nanofluidics*. 2009. Vol. 6, no. 1, p. 1–16. DOI 10.1007/s10404-008-0361-x.

[41] Tsao, C.-W. Polymer Microfluidics: Simple, Low-Cost Fabrication Process Bridging Academic Lab Research to Commercialized Production. *Micromachines*. 2016. Vol. 7, no. 12, p. 225. DOI 10.3390/mi7120225.

[42] Metz, S., Holzer, R. and Renaud, P. Polyimide-based microfluidic devices. *Lab on a Chip*. 2001. Vol. 1, no. 1, p. 29–34. DOI 10.1039/b103896f.

[43] Sollier, E., Murray, C., Maoddi, P. and Di Carlo, D. Rapid prototyping polymers for microfluidic devices and high pressure injections. *Lab Chip*. 2011. Vol. 11, no. 22, p. 3752–3765. DOI 10.1039/C1LC20514E.

[44] Metz, S., Jiguet, S., Bertsch, A. and Renaud, Ph. Polyimide and SU-8 microfluidic devices manufactured by heat-depolymerizable sacrificial material technique. *Lab Chip*. 2004. Vol. 4, no. 2, p. 114–120. DOI 10.1039/B310866J.

[45] Fiorini, G. S., Yim, M., Jeffries, G. D. M., Schiro, P. G., Mutch, S. A., Lorenz, R. M. and Chiu, D. T. Fabrication improvements for thermoset polyester (TPE) microfluidic devices. *Lab Chip*. 2007. Vol. 7, no. 7, p. 923–926. DOI 10.1039/B702548C.

[46] Kim, S. H., Yang, Y., Kim, M., Nam, S.-W., Lee, K.-M., Lee, N. Y., Kim, Y. S. and Park, S. Simple Route to Hydrophilic Microfluidic Chip Fabrication Using an Ultraviolet (UV)-Cured Polymer. *Advanced Functional Materials*. 2007. Vol. 17, no. 17, p. 3493–3498. DOI 10.1002/adfm.200601203.

[47] Saharil, F., Forsberg, F., Liu, Y., Bettotti, P., Kumar, N., Niklaus, F., Haraldsson, T., Van der Wijngaart, W. and Gylfason, K. B. Dry adhesive bonding of nanoporous inorganic membranes to microfluidic devices using the OSTE(+) dual-cure polymer. *Journal of Micromechanics and Microengineering*. 2013. Vol. 23, no. 2, p. 025021. DOI 10.1088/0960-1317/23/2/025021.

[48] Sticker, D., Rothbauer, M., Lechner, S., Hehenberger, M.-T. and Ertl, P. Multi-layered, membrane-integrated microfluidics based on replica molding of a thiol–ene epoxy thermoset for organ-on-a-chip applications. *Lab on a Chip*. 2015. Vol. 15, no. 24, p. 4542–4554. DOI 10.1039/C5LC01028D.

[49] Yoda, R. Elastomers for biomedical applications. *Journal of Biomaterials Science, Polymer Edition*. 1998. Vol. 9, no. 6, p. 561–626. DOI 10.1163/156856298X00046.

[50] Sudarsan, A. P., Wang, J. and Ugaz, V. M. Thermoplastic Elastomer Gels: An Advanced Substrate for Microfluidic Chemical Analysis Systems. *Analytical Chemistry*. 2005. Vol. 77, no. 16, p. 5167–5173. DOI 10.1021/ac050448o.

[51] Roy, E., Galas, J.-C. and Veres, T. Thermoplastic elastomers for microfluidics: Towards a high-throughput fabrication method of multilayered microfluidic devices. *Lab on a Chip*. 2011. Vol. 11, no. 18, p. 3193–3196. DOI 10.1039/c1lc20251k.

[52] Geissler, M., Roy, E., Diaz-Quijada, G. A., Galas, J.-C. and Veres, T. Microfluidic Patterning of Miniaturized DNA Arrays on Plastic Substrates. *ACS Applied Materials & Interfaces*. 2009. Vol. 1, no. 7, p. 1387–1395. DOI 10.1021/am900285g.

[53] Drobny, J. G. 5 - Styrenic Block Copolymers. In : Drobny, J. G. (ed.), *Handbook of Thermoplastic Elastomers (Second Edition)*. Second Edition. Oxford : William Andrew Publishing, 2014. p. 175–194. Plastics Design Library. ISBN 978-0-323-22136-8.

[54] Duffy, D. C., McDonald, J. C., Schueller, O. J. A. and Whitesides, G. M. Rapid Prototyping of Microfluidic Systems in Poly(dimethylsiloxane). *Analytical Chemistry*. 1998. Vol. 70, no. 23, p. 4974–4984. DOI 10.1021/ac980656z.

[55] Martinez-Duarte, R. and Madou, M. J. SU-8 Photolithography and Its Impact on Microfluidics. In : Mitra, S. K. and Chakraborty, S. (eds.), *Microfluidics and Nanofluidics Handbook: Fabrication, Implementation, and Applications*. 1. Boca Raton : CRC Press, 2012. p. 231–268. ISBN 978-0-429-09337-1.

[56] Peng, L., Deng, Y., Yi, P. and Lai, X. Micro hot embossing of thermoplastic polymers: a review. *Journal of Micromechanics and Microengineering*. 2014. Vol. 24, no. 1, p. 013001. DOI 10.1088/0960-1317/24/1/013001.

[57] Attia, U. M., Marson, S. and Alcock, J. R. Micro-injection moulding of polymer microfluidic devices. *Microfluidics and Nanofluidics*. 2009. Vol. 7, no. 1, p. 1–28. DOI 10.1007/s10404-009-0421-x.

[58] Truckenmüller, R., Giselbrecht, S., Rivron, N., Gottwald, E., Saile, V., Van den Berg, A., Wessling, M. and Van Blitterswijk, C. Thermoforming of Film-Based Biomedical

Microdevices. *Advanced Materials*. 2011. Vol. 23, no. 11, p. 1311–1329. DOI 10.1002/adma.201003538.

[59] Brassard, D., Clime, L., Li, K., Geissler, M., Miville-Godin, C., Roy, E. and Veres, T. 3D thermoplastic elastomer microfluidic devices for biological probe immobilization. *Lab on a Chip*. 2011. Vol. 11, no. 23, p. 4099–4107. DOI 10.1039/c1lc20714h.

[60] Domansky, K., Sliz, J. D., Wen, N., Hinojosa, C., Thompson, G., Fraser, J. P., Hamkins-Indik, T., Hamilton, G. A., Levner, D. and Ingber, D. E. SEBS elastomers for fabrication of microfluidic devices with reduced drug absorption by injection molding and extrusion. *Microfluidics and Nanofluidics*. 2017. Vol. 21, no. 6, p. 107. DOI 10.1007/s10404-017-1941-4.

[61] Jeon, J. S., Chung, S., Kamm, R. D. and Charest, J. L. Hot embossing for fabrication of a microfluidic 3D cell culture platform. *Biomedical Microdevices*. 2011. Vol. 13, no. 2, p. 325–333. DOI 10.1007/s10544-010-9496-0.

[62] Young, E. W. K., Berthier, E., Guckenberger, D. J., Sackmann, E., Lamers, C., Meyvantsson, I., Huttenlocher, A. and Beebe, D. J. Rapid Prototyping of Arrayed Microfluidic Systems in Polystyrene for Cell-Based Assays. *Analytical Chemistry*. 2011. Vol. 83, no. 4, p. 1408–1417. DOI 10.1021/ac102897h.

[63] Konstantinou, D., Shirazi, A., Sadri, A. and Young, E. W. K. Combined hot embossing and milling for medium volume production of thermoplastic microfluidic devices. *Sensors and Actuators B: Chemical*. 2016. Vol. 234, p. 209–221. DOI 10.1016/j.snb.2016.04.147.

[64] Hupert, M. L., Guy, W. J., Llopis, S. D., Shadpour, H., Rani, S., Nikitopoulos, D. E. and Soper, S. A. Evaluation of micromilled metal mold masters for the replication of microchip electrophoresis devices. *Microfluidics and Nanofluidics*. 2006. Vol. 3, no. 1, p. 1–11. DOI 10.1007/s10404-006-0091-x.

[65] Esch, M. B., Kapur, S., Irizarry, G. and Genova, V. Influence of master fabrication techniques on the characteristics of embossed microfluidic channels. *Lab on a Chip*. 2003. Vol. 3, no. 2, p. 121–127. DOI 10.1039/b300730h.

[66] Guckenberger, D. J., De Groot, T. E., Wan, A. M. D., Beebe, D. J. and Young, E. W. K. Micromilling: a method for ultra-rapid prototyping of plastic microfluidic devices. *Lab Chip*. 2015. Vol. 15, no. 11, p. 2364–2378. DOI 10.1039/C5LC00234F.

[67] Bartholomeusz, D. A., Boutte, R. W. and Andrade, J. D. Xurography: rapid prototyping of microstructures using a cutting plotter. *Journal of Microelectromechanical Systems*. 2005. Vol. 14, no. 6, p. 1364–1374. DOI 10.1109/JMEMS.2005.859087.

[68] Shaegh, S. A. M., Pourmand, A., Nabavinia, M., Avci, H., Tamayol, A., Mostafalu, P., Ghavifekr, H. B., Aghdam, E. N., Dokmeci, M. R., Khademhosseini, A. and Zhang, Y. S. Rapid prototyping of whole-thermoplastic microfluidics with built-in microvalves using laser ablation and thermal fusion bonding. *Sensors and Actuators B: Chemical*. 2018. Vol. 255, p. 100–109. DOI 10.1016/j.snb.2017.07.138.

[69] Liu, Y., Rauch, C. B., Stevens, R. L., Lenigk, R., Yang, J., Rhine, D. B. and Grodzinski, P. DNA Amplification and Hybridization Assays in Integrated Plastic Monolithic Devices. *Analytical Chemistry*. 2002. Vol. 74, no. 13, p. 3063–3070. DOI 10.1021/ac020094q.

[70] Khan Malek, C., Robert, L. and Salut, R. Femtosecond laser machining and lamination for large-area flexible organic microfluidic chips. *The European Physical Journal Applied Physics*. 2009. Vol. 46, no. 1, p. 12503. DOI 10.1051/epjap/2009027.

[71] Lippert, T. Interaction of Photons with Polymers: From Surface Modification to Ablation. *Plasma Processes and Polymers*. 2005. Vol. 2, no. 7, p. 525–546. DOI 10.1002/ppap.200500036.

[72] Au, A. K., Lee, W. and Folch, A. Mail-order microfluidics: evaluation of stereolithography for the production of microfluidic devices. *Lab Chip*. 2014. Vol. 14, no. 7, p. 1294–1301. DOI 10.1039/C3LC51360B.

[73] Bhattacharjee, N., Urrios, A., Kang, S. and Folch, A. The upcoming 3D-printing revolution in microfluidics. *Lab Chip*. 2016. Vol. 16, no. 10, p. 1720–1742. DOI 10.1039/C6LC00163G.

[74] Hillborg, H., Ankner, J. F., Gedde, U. W., Smith, G. D., Yasuda, H. K. and Wikström, K. Crosslinked polydimethylsiloxane exposed to oxygen plasma studied by neutron reflectometry and other surface specific techniques. *Polymer*. 2000. Vol. 41, no. 18, p. 6851–6863. DOI 10.1016/S0032-3861(00)00039-2.

[75] Morra, M., Occhiello, E., Marola, R., Garbassi, F., Humphrey, P. and Johnson, D. On the aging of oxygen plasma-treated polydimethylsiloxane surfaces. *Journal of Colloid and Interface Science*. 1990. Vol. 137, no. 1, p. 11–24. DOI 10.1016/0021-9797(90)90038-P.

[76] Eddings, M. A., Johnson, M. A. and Gale, B. K. Determining the optimal PDMS–PDMS bonding technique for microfluidic devices. *Journal of Micromechanics and Microengineering*. 2008. Vol. 18, no. 6, p. 067001. DOI 10.1088/0960-1317/18/6/067001.

[77] Bhattacharya, S., Datta, A., Berg, J. M. and Gangopadhyay, S. Studies on surface wettability of poly(dimethyl) siloxane (PDMS) and glass under oxygen-plasma treatment and correlation with bond strength. *Journal of Microelectromechanical Systems*. 2005. Vol. 14, no. 3, p. 590–597. DOI 10.1109/JMEMS.2005.844746.

[78] Aran, K., Sasso, L. A., Kamdar, N. and Zahn, J. D. Irreversible, direct bonding of nanoporous polymer membranes to PDMS or glass microdevices. *Lab on a Chip*. 2010. Vol. 10, no. 5, p. 548–552. DOI 10.1039/b924816a.

[79] Sip, C. G. and Folch, A. Stable chemical bonding of porous membranes and poly(dimethylsiloxane) devices for long-term cell culture. *Biomicrofluidics*. 2014. Vol. 8, no. 3, p. 036504. DOI 10.1063/1.4883075.

[80] Schneider, S., Gruner, D., Richter, A. and Loskill, P. Membrane integration into PDMS-free microfluidic platforms for organ-on-chip and analytical chemistry applications. *Lab Chip*. 2021. Vol. 21, no. 10, p. 1866–1885. DOI 10.1039/D1LC00188D.

[81] Butler, C. A., Mccullough, R. L., Pitchumani, R. and Gillespie, J. W. An Analysis of Mechanisms Governing Fusion Bonding of Thermoplastic Composites. *Journal of Thermoplastic Composite Materials*. 1998. Vol. 11, no. 4, p. 338–363. DOI 10.1177/089270579801100404.

[82] Troughton, M. J. (ed.). Chapter 16 - Solvent Welding. In : Troughton, M. J. (ed.), *Handbook of Plastics Joining (Second Edition)*. Second Edition. Boston : William Andrew Publishing, 2009. p. 139–143. ISBN 978-0-8155-1581-4.

[83] Lachaux, J., Alcaine, C., Gómez-Escoda, B., Perrault, C. M., Duplan, D. O., Wu, P.-Y. J., Ochoa, I., Fernandez, L., Mercier, O., Coudreuse, D. and Roy, E. Thermoplastic elastomer with advanced hydrophilization and bonding performances for rapid (30 s) and easy molding of microfluidic devices. *Lab on a Chip*. 2017. Vol. 17, no. 15, p. 2581–2594. DOI 10.1039/C7LC00488E.

[84] Borysiak, M. D., Bielawski, K. S., Sniadecki, N. J., Jenkel, C. F., Vogt, B. D. and Posner, J. D. Simple replica micromolding of biocompatible styrenic elastomers. *Lab on a Chip*. 2013. Vol. 13, no. 14, p. 2773–2784. DOI 10.1039/c3lc50426c.

[85] Harrison, R. G. On the Stereotropism of Embryonic Cells. *Science*. 1911. Vol. 34, no. 870, p. 279–281. JSTOR

[86] Gallo–Ramírez, L. E., Nikolay, A., Genzel, Y. and Reichl, U. Bioreactor concepts for cell culture-based viral vaccine production. *Expert Review of Vaccines*. 2015. Vol. 14, no. 9, p. 1181–1195. DOI 10.1586/14760584.2015.1067144.

[87] Li, F., Vijayasankaran, N., Shen, A. (Yijuan), Kiss, R. and Amanullah, A. Cell culture processes for monoclonal antibody production. *mAbs*. 2010. Vol. 2, no. 5, p. 466–479. DOI 10.4161/mabs.2.5.12720.

[88] Kapałczyńska, M., Kolenda, T., Przybyła, W., Zajączkowska, M., Teresiak, A., Filas, V., Ibbs, M., Bliźniak, R., Łuczewski, Ł. and Lamperska, K. 2D and 3D cell cultures – a comparison of different types of cancer cell cultures. *Arch Med Sci*. 2018. Vol. 14, no. 4, p. 910–919. DOI 10.5114/aoms.2016.63743.

[89] Pampaloni, F., Reynaud, E. G. and Stelzer, E. H. K. The third dimension bridges the gap between cell culture and live tissue. *Nature Reviews Molecular Cell Biology*. 2007. Vol. 8, no. 10, p. 839–845. DOI 10.1038/nrm2236.

[90] Thomas, R. J., Chandra, A., Liu, Y., Hourd, P. C., Conway, P. P. and Williams, D. J. Manufacture of a human mesenchymal stem cell population using an automated cell culture platform. *Cytotechnology*. 2007. Vol. 55, no. 1, p. 31–39. DOI 10.1007/s10616-007-9091-2.

[91] Konagaya, S., Ando, T., Yamauchi, T., Suemori, H. and Iwata, H. Long-term maintenance of human induced pluripotent stem cells by automated cell culture system. *Scientific Reports*. 2015. Vol. 5, no. 1, p. 16647. DOI 10.1038/srep16647.

[92] Wu, M.-H., Huang, S.-B. and Lee, G.-B. Microfluidic cell culture systems for drug research. *Lab Chip*. 2010. Vol. 10, no. 8, p. 939–956. DOI 10.1039/B921695B.

[93] El-Ali, J., Sorger, P. K. and Jensen, K. F. Cells on chips. *Nature*. 2006. Vol. 442, no. 7101, p. 403–411. DOI 10.1038/nature05063.

[94] Young, E. W. K. and Simmons, C. A. Macro- and microscale fluid flow systems for endothelial cell biology. *Lab Chip*. 2010. Vol. 10, no. 2, p. 143–160. DOI 10.1039/B913390A.

[95] Hansmann, J., Groeber, F., Kahlig, A., Kleinhans, C. and Walles, H. Bioreactors in tissue engineering—principles, applications and commercial constraints. *Biotechnology Journal*. 2013. Vol. 8, no. 3, p. 298–307. DOI 10.1002/biot.201200162.

[96] Pörtner, R., Nagel-Heyer, S., Goepfert, C., Adamietz, P. and Meenen, N. M. Bioreactor design for tissue engineering. *Journal of Bioscience and Bioengineering*. 2005. Vol. 100, no. 3, p. 235–245. DOI 10.1263/jbb.100.235.

[97] Godara, P., McFarland, C. D. and Nordon, R. E. Design of bioreactors for mesenchymal stem cell tissue engineering. *Journal of Chemical Technology & Biotechnology*. 2008. Vol. 83, no. 4, p. 408–420. DOI 10.1002/jctb.1918.

[98] Sidorov, V. Y., Samson, P. C., Sidorova, T. N., Davidson, J. M., Lim, C. C. and Wikswo, J. P. I-Wire Heart-on-a-Chip I: Three-dimensional cardiac tissue constructs for physiology and pharmacology. *Acta Biomaterialia*. 2017. Vol. 48, p. 68–78. DOI 10.1016/j.actbio.2016.11.009.

[99] Rogal, J., Binder, C., Kromidas, E., Roosz, J., Probst, C., Schneider, S., Schenke-Layland, K. and Loskill, P. WAT-on-a-chip integrating human mature white adipocytes for

mechanistic research and pharmaceutical applications. *Scientific Reports*. 2020. Vol. 10, no. 1, p. 6666. DOI 10.1038/s41598-020-63710-4.

[100] Lai, B. F. L., Huyer, L. D., Lu, R. X. Z., Drecun, S., Radisic, M. and Zhang, B. InVADE: Integrated Vasculature for Assessing Dynamic Events. *Advanced Functional Materials*. 2017. Vol. 27, no. 46, p. 1703524. DOI 10.1002/adfm.201703524.

[101] Unagolla, J. M. and Jayasuriya, A. C. Hydrogel-based 3D bioprinting: A comprehensive review on cell-laden hydrogels, bioink formulations, and future perspectives. *Applied materials today*. 2020. Vol. 18, p. 100479. DOI 10.1016/j.apmt.2019.100479. PubMed: 32775607

[102] Chen, E. P., Toksoy, Z., Davis, B. A. and Geibel, J. P. 3D Bioprinting of Vascularized Tissues for in vitro and in vivo Applications. *Frontiers in Bioengineering and Biotechnology*. 2021. Vol. 9, p. 664188. DOI 10.3389/fbioe.2021.664188.

[103] Park, J. Y., Ryu, H., Lee, B., Ha, D.-H., Ahn, M., Kim, S., Kim, J. Y., Jeon, N. L. and Cho, D.-W. Development of a functional airway-on-a-chip by 3D cell printing. *Biofabrication*. 2018. Vol. 11, no. 1, p. 015002. DOI 10.1088/1758-5090/aae545.

[104] Zhang, Y. S., Arneri, A., Bersini, S., Shin, S.-R., Zhu, K., Goli-Malekabadi, Z., Aleman, J., Colosi, C., Busignani, F., Dell'Erba, V., Bishop, C., Shupe, T., Demarchi, D., Moretti, M., Rasponi, M., Dokmeci, M. R., Atala, A. and Khademhosseini, A. Bioprinting 3D microfibrous scaffolds for engineering endothelialized myocardium and heart-on-a-chip. *Biomaterials*. 2016. Vol. 110, p. 45–59. DOI 10.1016/j.biomaterials.2016.09.003.

[105] Kolesky, D. B., Homan, K. A., Skylar-Scott, M. A. and Lewis, J. A. Three-dimensional bioprinting of thick vascularized tissues. *Proceedings of the National Academy of Sciences*. 2016. Vol. 113, no. 12, p. 3179–3184. DOI 10.1073/pnas.1521342113.

[106] Mathur, A., Loskill, P., Shao, K., Huebsch, N., Hong, S., Marcus, S. G., Marks, N., Mandegar, M., Conklin, B. R., Lee, L. P. and Healy, K. E. Human iPSC-based Cardiac Microphysiological System For Drug Screening Applications. *Scientific Reports*. 2015. Vol. 5, no. 1, p. 8883. DOI 10.1038/srep08883.

[107] Lee, P. J., Hung, P. J. and Lee, L. P. An artificial liver sinusoid with a microfluidic endothelial-like barrier for primary hepatocyte culture. *Biotechnology and Bioengineering*. 2007. Vol. 97, no. 5, p. 1340–1346. DOI 10.1002/bit.21360.

[108] Toh, Y.-C., Zhang, C., Zhang, J., Khong, Y. M., Chang, S., Samper, V. D., Van Noort, D., Hutmacher, D. W. and Yu, H. A novel 3D mammalian cell perfusion-culture system in microfluidic channels. *Lab Chip*. 2007. Vol. 7, no. 3, p. 302–309. DOI 10.1039/B614872G.

[109] Kim, J.-Y., Fluri, D. A., Marchan, R., Boonen, K., Mohanty, S., Singh, P., Hammad, S., Landuyt, B., Hengstler, J. G., Kelm, J. M., Hierlemann, A. and Frey, O. 3D spherical microtissues and microfluidic technology for multi-tissue experiments and analysis. *Journal of Biotechnology*. 2015. Vol. 205, p. 24–35. DOI 10.1016/j.jbiotec.2015.01.003.

[110] Lohasz, C., Rousset, N., Renggli, K., Hierlemann, A. and Frey, O. Scalable Microfluidic Platform for Flexible Configuration of and Experiments with Microtissue Multiorgan Models. *SLAS TECHNOLOGY: Translating Life Sciences Innovation*. 2019. Vol. 24, no. 1, p. 79–95. DOI 10.1177/2472630318802582.

[111] Achberger, K., Probst, C., Haderspeck, J., Bolz, S., Rogal, J., Chuchuy, J., Nikolova, M., Cora, V., Antkowiak, L., Haq, W., Shen, N., Schenke-Layland, K., Ueffing, M., Liebau, S. and Loskill, P. Merging organoid and organ-on-a-chip technology to generate complex multi-layer tissue models in a human retina-on-a-chip platform. *eLife*. 2019. Vol. 8, p. e46188. DOI 10.7554/eLife.46188.

[112] Zbinden, A., Marzi, J., Schlünder, K., Probst, C., Urbanczyk, M., Black, S., Brauchle, E. M., Layland, S. L., Kraushaar, U., Duffy, G., Schenke-Layland, K. and Loskill, P. Non-invasive marker-independent high content analysis of a microphysiological human pancreas-on-a-chip model. *Matrix Biology*. 2020. Vol. 85–86, p. 205–220. DOI 10.1016/j.matbio.2019.06.008.

[113] Frey, O., Misun, P. M., Fluri, D. A., Hengstler, J. G. and Hierlemann, A. Reconfigurable microfluidic hanging drop network for multi-tissue interaction and analysis. *Nature Communications*. 2014. Vol. 5, no. 1, p. 4250. DOI 10.1038/ncomms5250.

[114] Mastrangeli, M., Millet, S., The ORCHID partners and Van den Eijnden-van Raaij, J. Organ-on-chip in development: Towards a roadmap for organs-on-chip. *ALTEX*. 2019. Vol. 36, no. 4, p. 650–668. DOI 10.14573/altex.1908271.

[115] Carraro, A., Hsu, W.-M., Kulig, K. M., Cheung, W. S., Miller, M. L., Weinberg, E. J., Swart, E. F., Kaazempur-Mofrad, M., Borenstein, J. T., Vacanti, J. P. and Neville, C. In vitro analysis of a hepatic device with intrinsic microvascular-based channels. *Biomedical Microdevices*. 2008. Vol. 10, no. 6, p. 795–805. DOI 10.1007/s10544-008-9194-3.

[116] Loskill, P., Sezhian, T., Tharp, K. M., Lee-Montiel, F. T., Jeeawoody, S., Reese, W. M., Zushin, P.-J. H., Stahl, A. and Healy, K. E. WAT-on-a-chip: a physiologically relevant microfluidic system incorporating white adipose tissue. *Lab on a Chip*. 2017. Vol. 17, no. 9, p. 1645–1654. DOI 10.1039/C6LC01590E.

[117] Bhatia, S. N. and Ingber, D. E. Microfluidic organs-on-chips. *Nature Biotechnology*. 2014. Vol. 32, no. 8, p. 760–772. DOI 10.1038/nbt.2989.

[118] Huh, D., Matthews, B. D., Mammoto, A., Montoya-Zavala, M., Hsin, H. Y. and Ingber, D. E. Reconstituting Organ-Level Lung Functions on a Chip. *Science*. 2010. Vol. 328, no. 5986, p. 1662–1668. DOI 10.1126/science.1188302.

[119] Van Dijk, C. G. M., Brandt, M. M., Poulis, N., Anten, J., Van der Moolen, M., Kramer, L., Homburg, E. F. G. A., Louzao-Martinez, L., Pei, J., Krebber, M. M., Van Balkom, B. W. M., De Graaf, P., Duncker, D. J., Verhaar, M. C., Luttge, R. and Cheng, C. A new microfluidic model that allows monitoring of complex vascular structures and cell interactions in a 3D biological matrix. *Lab Chip*. 2020. Vol. 20, no. 10, p. 1827–1844. DOI 10.1039/D0LC00059K.

[120] Kim, H. J., Huh, D., Hamilton, G. and Ingber, D. E. Human gut-on-a-chip inhabited by microbial flora that experiences intestinal peristalsis-like motions and flow. *Lab on a Chip*. 2012. Vol. 12, no. 12, p. 2165–2174. DOI 10.1039/c2lc40074j.

[121] Stucki, A. O., Stucki, J. D., Hall, S. R. R., Felder, M., Mermoud, Y., Schmid, R. A., Geiser, T. and Guenat, O. T. A lung-on-a-chip array with an integrated bio-inspired respiration mechanism. *Lab on a Chip*. 2015. Vol. 15, no. 5, p. 1302–1310. DOI 10.1039/C4LC01252F.

[122] Müller, B., Sulzer, P., Walch, M., Zirath, H., Buryška, T., Rothbauer, M., Ertl, P. and Mayr, T. Measurement of Respiration and Acidification Rates of Mammalian Cells in Thermoplastic Microfluidic Devices. *Sensors and Actuators B: Chemical*. 2021. Vol. 334, p. 129664. DOI 10.1016/j.snb.2021.129664.

[123] Huh, D., Fujioka, H., Tung, Y.-C., Futai, N., Paine, R., Grotberg, J. B. and Takayama, S. Acoustically detectable cellular-level lung injury induced by fluid mechanical stresses in microfluidic airway systems. *Proceedings of the National Academy of Sciences*. 2007. Vol. 104, no. 48, p. 18886–18891. DOI 10.1073/pnas.0610868104.

[124] Rohr, S., Schölly, D. M. and Kléber, A. G. Patterned growth of neonatal rat heart cells in culture. Morphological and electrophysiological characterization. *Circulation Research*. 1991. Vol. 68, no. 1, p. 114–130. DOI 10.1161/01.RES.68.1.114.

[125] Viravaidya, K., Sin, A. and Shuler, M. L. Development of a Microscale Cell Culture Analog To Probe Naphthalene Toxicity. *Biotechnology Progress*. 2004. Vol. 20, no. 1, p. 316–323. DOI 10.1021/bp0341996.

[126] Sin, A., Chin, K. C., Jamil, M. F., Kostov, Y., Rao, G. and Shuler, M. L. The Design and Fabrication of Three-Chamber Microscale Cell Culture Analog Devices with Integrated Dissolved Oxygen Sensors. *Biotechnology Progress*. 2004. Vol. 20, no. 1, p. 338–345. DOI 10.1021/bp034077d.

[127] Takahashi, K. and Yamanaka, S. Induction of Pluripotent Stem Cells from Mouse Embryonic and Adult Fibroblast Cultures by Defined Factors. *Cell*. 2006. Vol. 126, no. 4, p. 663–676. DOI 10.1016/j.cell.2006.07.024.

[128] Takahashi, K., Tanabe, K., Ohnuki, M., Narita, M., Ichisaka, T., Tomoda, K. and Yamanaka, S. Induction of Pluripotent Stem Cells from Adult Human Fibroblasts by Defined Factors. *Cell*. 2007. Vol. 131, no. 5, p. 861–872. DOI 10.1016/j.cell.2007.11.019.

[129] Park, I.-H., Arora, N., Huo, H., Maherali, N., Ahfeldt, T., Shimamura, A., Lensch, M. W., Cowan, C., Hochedlinger, K. and Daley, G. Q. Disease-Specific Induced Pluripotent Stem Cells. *Cell*. 2008. Vol. 134, no. 5, p. 877–886. DOI 10.1016/j.cell.2008.07.041.

[130] Passier, R., Orlova, V. and Mummery, C. Complex Tissue and Disease Modeling using hiPSCs. *Cell Stem Cell*. 2016. Vol. 18, no. 3, p. 309–321. DOI 10.1016/j.stem.2016.02.011.

[131] Clevers, H. Modeling Development and Disease with Organoids. *Cell*. 2016. Vol. 165, no. 7, p. 1586–1597. DOI 10.1016/j.cell.2016.05.082.

[132] Benam, K. H., Villenave, R., Lucchesi, C., Varone, A., Hubeau, C., Lee, H.-H., Alves, S. E., Salmon, M., Ferrante, T. C., Weaver, J. C., Bahinski, A., Hamilton, G. A. and Ingber, D. E. Small airway-on-a-chip enables analysis of human lung inflammation and drug responses in vitro. *Nature Methods*. 2016. Vol. 13, no. 2, p. 151–157. DOI 10.1038/nmeth.3697.

[133] Van den Berg, A., Mummery, C. L., Passier, R. and Van der Meer, A. D. Personalised organs-on-chips: functional testing for precision medicine. *Lab on a Chip*. 2019. Vol. 19, no. 2, p. 198–205. DOI 10.1039/C8LC00827B.

[134] Sia, S. K. and Whitesides, G. M. Microfluidic devices fabricated in Poly(dimethylsiloxane) for biological studies. *ELECTROPHORESIS*. 2003. Vol. 24, no. 21, p. 3563–3576. DOI 10.1002/elps.200305584.

[135] Novak, R., Didier, M., Calamari, E., Ng, C. F., Choe, Y., Clauson, S. L., Nestor, B. A., Puerta, J., Fleming, R., Firoozinezhad, S. J. and Ingber, D. E. Scalable Fabrication of Stretchable, Dual Channel, Microfluidic Organ Chips. *Journal of Visualized Experiments*. 2018. No. 140, p. 58151. DOI 10.3791/58151.

[136] Madsen, M. H., Feidenhans'l, N. A., Hansen, P.-E., Garnæs, J. and Dirscherl, K. Accounting for PDMS shrinkage when replicating structures. *Journal of Micromechanics and Microengineering*. 2014. Vol. 24, no. 12, p. 127002. DOI 10.1088/0960-1317/24/12/127002.

[137] Lee, S. W. and Lee, S. S. Shrinkage ratio of PDMS and its alignment method for the wafer level process. *Microsystem Technologies*. 2007. Vol. 14, no. 2, p. 205–208. DOI 10.1007/s00542-007-0417-y.

[138] Campbell, S. B., Wu, Q., Yazbeck, J., Liu, C., Okhovatian, S. and Radisic, M. Beyond Polydimethylsiloxane: Alternative Materials for Fabrication of Organ-on-a-Chip Devices and Microphysiological Systems. *ACS Biomaterials Science & Engineering*. 2021. Vol. 7, no. 7, p. 2880–2899. DOI 10.1021/acsbiomaterials.0c00640.

[139] Van Meer, B. J., De Vries, H., Firth, K. S. A., Van Weerd, J., Tertoolen, L. G. J., Karperien, H. B. J., Jonkheijm, P., Denning, C., IJzerman, A. P. and Mummery, C. L. Small molecule absorption by PDMS in the context of drug response bioassays. *Biochemical and Biophysical Research Communications*. 2017. Vol. 482, no. 2, p. 323–328. DOI 10.1016/j.bbrc.2016.11.062.

[140] Carter, S.-S. D., Atif, A.-R., Kadekar, S., Lanekoff, I., Engqvist, H., Varghese, O. P., Tenje, M. and Mestres, G. PDMS leaching and its implications for on-chip studies focusing on bone regeneration applications. *Organs-on-a-Chip*. 2020. Vol. 2, p. 100004. DOI 10.1016/j.ooc.2020.100004.

[141] Heo, Y. S., Cabrera, L. M., Song, J. W., Futai, N., Tung, Y.-C., Smith, G. D. and Takayama, S. Characterization and Resolution of Evaporation-Mediated Osmolality Shifts That Constrain Microfluidic Cell Culture in Poly(dimethylsiloxane) Devices. *Analytical Chemistry*. 2007. Vol. 79, no. 3, p. 1126–1134. DOI 10.1021/ac061990v.

[142] Aghvami, S. A., Opathalage, A., Zhang, Z. K., Ludwig, M., Heymann, M., Norton, M., Wilkins, N. and Fraden, S. Rapid prototyping of cyclic olefin copolymer (COC) microfluidic devices. *Sensors and Actuators B: Chemical*. 2017. Vol. 247, p. 940–949. DOI 10.1016/j.snb.2017.03.023.

[143] Lee, U. N., Su, X., Guckenberger, D. J., Dostie, A. M., Zhang, T., Berthier, E. and Theberge, A. B. Fundamentals of rapid injection molding for microfluidic cell-based assays. *Lab Chip*. 2018. Vol. 18, no. 3, p. 496–504. DOI 10.1039/C7LC01052D.

[144] Occhetta, P., Mainardi, A., Votta, E., Vallmajo-Martin, Q., Ehrbar, M., Martin, I., Barbero, A. and Rasponi, M. Hyperphysiological compression of articular cartilage induces an osteoarthritic phenotype in a cartilage-on-a-chip model. *Nature Biomedical Engineering*. 2019. Vol. 3, no. 7, p. 545–557. DOI 10.1038/s41551-019-0406-3.

[145] Park, S.-H., Sim, W. Y., Min, B.-H., Yang, S. S., Khademhosseini, A. and Kaplan, D. L. Chip-Based Comparison of the Osteogenesis of Human Bone Marrow- and Adipose Tissue-Derived Mesenchymal Stem Cells under Mechanical Stimulation. Kerkis, I. (ed.), *PLoS ONE*. 2012. Vol. 7, no. 9, p. e46689. DOI 10.1371/journal.pone.0046689.

[146] Marsano, A., Conficconi, C., Lemme, M., Occhetta, P., Gaudiello, E., Votta, E., Cerino, G., Redaelli, A. and Rasponi, M. Beating heart on a chip: a novel microfluidic platform to generate functional 3D cardiac microtissues. *Lab on a Chip*. 2016. Vol. 16, no. 3, p. 599–610. DOI 10.1039/C5LC01356A.

[147] Schneider, O., Zeifang, L., Fuchs, S., Sailer, C. and Loskill, P. User-Friendly and Parallelized Generation of Human Induced Pluripotent Stem Cell-Derived Microtissues in a Centrifugal Heart-on-a-Chip. *Tissue Engineering Part A*. 2019. Vol. 25, no. 9–10, p. 786–798. DOI 10.1089/ten.tea.2019.0002.

[148] Busek, M., Nøvik, S., Aizenshtadt, A., Amirola-Martinez, M., Combriat, T., Grünzner, S. and Krauss, S. Thermoplastic Elastomer (TPE)–Poly(Methyl Methacrylate) (PMMA) Hybrid Devices for Active Pumping PDMS-Free Organ-on-a-Chip Systems. *Biosensors*. 2021. Vol. 11, no. 5, p. 162. DOI 10.3390/bios11050162.

[149] Wei, H., Chueh, B., Wu, H., Hall, E. W., Li, C., Schirhagl, R., Lin, J.-M. and Zare, R. N. Particle sorting using a porous membrane in a microfluidic device. *Lab Chip*. 2011. Vol. 11, no. 2, p. 238–245. DOI 10.1039/C0LC00121J.

[150] Gao, J., Xu, J., Locascio, L. E. and Lee, C. S. Integrated Microfluidic System Enabling Protein Digestion, Peptide Separation, and Protein Identification. *Analytical Chemistry*. 2001. Vol. 73, no. 11, p. 2648–2655. DOI 10.1021/ac001126h.

[151] Ismagilov, R. F., Ng, J. M. K., Kenis, P. J. A. and Whitesides, G. M. Microfluidic Arrays of Fluid−Fluid Diffusional Contacts as Detection Elements and Combinatorial Tools. *Analytical Chemistry*. 2001. Vol. 73, no. 21, p. 5207–5213. DOI 10.1021/ac010502a.

[152] Kuo, T.-C., Cannon, D. M., Shannon, M. A., Bohn, P. W. and Sweedler, J. V. Hybrid three-dimensional nanofluidic/microfluidic devices using molecular gates. *Sensors and Actuators A: Physical*. 2003. Vol. 102, no. 3, p. 223–233. DOI 10.1016/S0924-4247(02)00394-1.

[153] Illa, X., Vila, S., Yeste, J., Peralta, C., Gracia-Sancho, J. and Villa, R. A Novel Modular Bioreactor to In Vitro Study the Hepatic Sinusoid. Avila, M. A. (ed.), *PLoS ONE*. 2014. Vol. 9, no. 11, p. e111864. DOI 10.1371/journal.pone.0111864.

[154] Moya, A., Ortega-Ribera, M., Guimerà, X., Sowade, E., Zea, M., Illa, X., Ramon, E., Villa, R., Gracia-Sancho, J. and Gabriel, G. Online oxygen monitoring using integrated inkjet-printed sensors in a liver-on-a-chip system. *Lab on a Chip*. 2018. Vol. 18, no. 14, p. 2023–2035. DOI 10.1039/C8LC00456K.

[155] Flachsbart, B. R., Wong, K., Iannacone, J. M., Abante, E. N., Vlach, R. L., Rauchfuss, P. A., Bohn, P. W., Sweedler, J. V. and Shannon, M. A. Design and fabrication of a multilayered polymer microfluidic chip with nanofluidic interconnects via adhesive contact printing. *Lab on a Chip*. 2006. Vol. 6, no. 5, p. 667–674. DOI 10.1039/b514300d.

[156] Ogilvie, I. R. G., Sieben, V. J., Cortese, B., Mowlem, M. C. and Morgan, H. Chemically resistant microfluidic valves from Viton® membranes bonded to COC and PMMA. *Lab on a Chip*. 2011. Vol. 11, no. 14, p. 2455–2459. DOI 10.1039/c1lc20069k.

[157] Nguyen, T., Jung, S. H., Lee, M. S., Park, T.-E., Ahn, S. and Kang, J. H. Robust chemical bonding of PMMA microfluidic devices to porous PETE membranes for reliable cytotoxicity testing of drugs. *Lab on a Chip*. 2019. Vol. 19, no. 21, p. 3706–3713. DOI 10.1039/C9LC00338J.

[158] Metz, S., Trautmann, C., Bertsch, A. and Renaud, P. Polyimide microfluidic devices with integrated nanoporous filtration areas manufactured by micromachining and ion track technology. *Journal of Micromechanics and Microengineering*. 2004. Vol. 14, no. 3, p. 324–331. DOI 10.1088/0960-1317/14/3/002.

[159] De Jong, J., Ankoné, B., Lammertink, R. G. H. and Wessling, M. New replication technique for the fabrication of thin polymeric microfluidic devices with tunable porosity. *Lab on a Chip*. 2005. Vol. 5, no. 11, p. 1240–1247. DOI 10.1039/b509280a.

[160] Kappings, V., Grün, C., Ivannikov, D., Hebeiss, I., Kattge, S., Wendland, I., Rapp, B. E., Hettel, M., Deutschmann, O. and Schepers, U. vasQchip: A Novel Microfluidic, Artificial Blood Vessel Scaffold for Vascularized 3D Tissues. *Advanced Materials Technologies*. 2018. Vol. 3, no. 4, p. 1700246. DOI 10.1002/admt.201700246.

[161] Wang, Z. F., Seah, Y. P. and Wang, Z. P. Seamless joining of porous membrane with thermoplastic microfluidic devices. *Microelectronic Engineering*. 2013. Vol. 110, p. 386–391. DOI 10.1016/j.mee.2013.02.074.

[162] Runge, T., Sackmann, J., Schomburg, W. K. and Blank, L. M. Ultrasonically manufactured microfluidic device for yeast analysis. *Microsystem Technologies*. 2017. Vol. 23, no. 6, p. 2139–2144. DOI 10.1007/s00542-016-3007-z.

[163] Rundel, J. T., Paul, B. K. and Remcho, V. T. Organic solvent nanofiltration for microfluidic purification of poly(amidoamine) dendrimers. *Journal of Chromatography A*. 2007. Vol. 1162, no. 2, p. 167–174. DOI 10.1016/j.chroma.2007.06.042.

[164] Shah, P., Vedarethinam, I., Kwasny, D., Andresen, L., Dimaki, M., Skov, S. and Svendsen, W. E. Microfluidic bioreactors for culture of non-adherent cells. *Sensors and Actuators B: Chemical*. 2011. Vol. 156, no. 2, p. 1002–1008. DOI 10.1016/j.snb.2011.02.021.

[165] Petersen, N. J., Jensen, H., Hansen, S. H., Foss, S. T., Snakenborg, D. and Pedersen-Bjergaard, S. On-chip electro membrane extraction. *Microfluidics and Nanofluidics*. 2010. Vol. 9, no. 4–5, p. 881–888. DOI 10.1007/s10404-010-0603-6.

[166] Giselbrecht, S., Gottwald, E., Truckenmueller, R., Trautmann, C., Welle, A., Guber, A., Saile, V., Gietzelt, T. and Weibezahn, K.-F. Microfabrication of chip-sized scaffolds for three-dimensional cell cultivation. *Journal of visualized experiments : JoVE*. 2008. No. 15, p. 699. DOI 10.3791/699. PubMed: 19066590

[167] Didar, T. F., Li, K., Tabrizian, M. and Veres, T. High throughput multilayer microfluidic particle separation platform using embedded thermoplastic-based micropumping. *Lab on a Chip*. 2013. Vol. 13, no. 13, p. 2615–2622. DOI 10.1039/c3lc50181g.

[168] Phan, D. T. T., Wang, X., Craver, B. M., Sobrino, A., Zhao, D., Chen, J. C., Lee, L. Y. N., George, S. C., Lee, A. P. and Hughes, C. C. W. A vascularized and perfused organ-on-a-chip platform for large-scale drug screening applications. *Lab on a Chip*. 2017. Vol. 17, no. 3, p. 511–520. DOI 10.1039/C6LC01422D.

[169] Sobrino, A., Phan, D. T. T., Datta, R., Wang, X., Hachey, S. J., Romero-López, M., Gratton, E., Lee, A. P., George, S. C. and Hughes, C. C. W. 3D microtumors in vitro supported by perfused vascular networks. *Scientific Reports*. 2016. Vol. 6, no. 1, p. 31589. DOI 10.1038/srep31589.

[170] Trietsch, S. J., Israëls, G. D., Joore, J., Hankemeier, T. and Vulto, P. Microfluidic titer plate for stratified 3D cell culture. *Lab on a Chip*. 2013. Vol. 13, no. 18, p. 3548–3554. DOI 10.1039/c3lc50210d.

[171] Trietsch, S. J., Naumovska, E., Kurek, D., Setyawati, M. C., Vormann, M. K., Wilschut, K. J., Lanz, H. L., Nicolas, A., Ng, C. P., Joore, J., Kustermann, S., Roth, A., Hankemeier, T., Moisan, A. and Vulto, P. Membrane-free culture and real-time barrier integrity assessment of perfused intestinal epithelium tubes. *Nature Communications*. 2017. Vol. 8, no. 1, p. 262. DOI 10.1038/s41467-017-00259-3.

[172] Van Duinen, V., Stam, W., Mulder, E., Famili, F., Reijerkerk, A., Vulto, P., Hankemeier, T. and Van Zonneveld, A. J. Robust and Scalable Angiogenesis Assay of Perfused 3D Human iPSC-Derived Endothelium for Anti-Angiogenic Drug Screening. *International Journal of Molecular Sciences*. 2020. Vol. 21, no. 13, p. 4804. DOI 10.3390/ijms21134804.

[173] Vulto, P., Podszun, S., Meyer, P., Hermann, C., Manz, A. and Urban, G. A. Phaseguides: a paradigm shift in microfluidic priming and emptying. *Lab on a Chip*. 2011. Vol. 11, no. 9, p. 1596–1602. DOI 10.1039/c0lc00643b.

[174] Tan, K., Keegan, P., Rogers, M., Lu, M., Gosset, J. R., Charest, J. and Bale, S. S. A high-throughput microfluidic microphysiological system (PREDICT-96) to recapitulate hepatocyte function in dynamic, re-circulating flow conditions. *Lab on a Chip*. 2019. Vol. 19, no. 9, p. 1556–1566. DOI 10.1039/C8LC01262H.

[175] Tan, K., Coppeta, J., Azizgolshani, H., Isenberg, B. C., Keegan, P. M., Cain, B. P., Patterson, A. J., Kim, E. S., Kratchman, L. B., Rogers, M., Haroutunian, N., Newlin, V., Golmon, S., Tandon, V., Lu, M., Gosset, J. R., Vedula, E. M., Charest, J. L. and Bale, S. S. Correction: A high-throughput microfluidic microphysiological system (PREDICT-96) to recapitulate hepatocyte function in dynamic, re-circulating flow conditions. *Lab Chip*. 2020. Vol. 20, no. 19, p. 3653–3653. DOI 10.1039/D0LC90069A.

[176] Azizgolshani, H., Coppeta, J. R., Vedula, E. M., Marr, E. E., Cain, B. P., Luu, R. J., Lech, M. P., Kann, S. H., Mulhern, T. J., Tandon, V., Tan, K., Haroutunian, N. J., Keegan, P., Rogers, M., Gard, A. L., Baldwin, K. B., De Souza, J. C., Hoefler, B. C., Bale, S. S., Kratchman, L. B., Zorn, A., Patterson, A., Kim, E. S., Petrie, T. A., Wiellette, E. L., Williams, C., Isenberg, B. C. and Charest, J. L. High-throughput organ-on-chip platform with integrated programmable fluid flow and real-time sensing for complex tissue models in drug development workflows. *Lab Chip*. 2021. Vol. 21, no. 8, p. 1454–1474. DOI 10.1039/D1LC00067E.

[177] Nicolas, A., Schavemaker, F., Kosim, K., Kurek, D., Haarmans, M., Bulst, M., Lee, K., Wegner, S., Hankemeier, T., Joore, J., Domansky, K., Lanz, H. L., Vulto, P. and Trietsch, S. J. High throughput transepithelial electrical resistance (TEER) measurements on perfused membrane-free epithelia. *Lab Chip*. 2021. Vol. 21, no. 9, p. 1676–1685. DOI 10.1039/D0LC00770F.

[178] Domansky, K., Inman, W., Serdy, J., Dash, A., Lim, M. H. M. and Griffith, L. G. Perfused multiwell plate for 3D liver tissue engineering. *Lab Chip*. 2010. Vol. 10, no. 1, p. 51–58. DOI 10.1039/B913221J.

[179] Edington, C. D., Chen, W. L. K., Geishecker, E., Kassis, T., Soenksen, L. R., Bhushan, B. M., Freake, D., Kirschner, J., Maass, C., Tsamandouras, N., Valdez, J., Cook, C. D., Parent, T., Snyder, S., Yu, J., Suter, E., Shockley, M., Velazquez, J., Velazquez, J. J., Stockdale, L., Papps, J. P., Lee, I., Vann, N., Gamboa, M., LaBarge, M. E., Zhong, Z., Wang, X., Boyer, L. A., Lauffenburger, D. A., Carrier, R. L., Communal, C., Tannenbaum, S. R., Stokes, C. L., Hughes, D. J., Rohatgi, G., Trumper, D. L., Cirit, M. and Griffith, L. G. Interconnected Microphysiological Systems for Quantitative Biology and Pharmacology Studies. *Scientific Reports*. 2018. Vol. 8, no. 1, p. 4530. DOI 10.1038/s41598-018-22749-0.

[180] Trapecar, M., Wogram, E., Svoboda, D., Communal, C., Omer, A., Lungjangwa, T., Sphabmixay, P., Velazquez, J., Schneider, K., Wright, C. W., Mildrum, S., Hendricks, A., Levine, S., Muffat, J., Lee, M. J., Lauffenburger, D. A., Trumper, D., Jaenisch, R. and Griffith, L. G. Human physiomimetic model integrating microphysiological systems of the gut, liver, and brain for studies of neurodegenerative diseases. *Science Advances*. 2021. Vol. 7, no. 5, p. eabd1707. DOI 10.1126/sciadv.abd1707.

[181] Coppeta, J. R., Mescher, M. J., Isenberg, B. C., Spencer, A. J., Kim, E. S., Lever, A. R., Mulhern, T. J., Prantil-Baun, R., Comolli, J. C. and Borenstein, J. T. A portable and reconfigurable multi-organ platform for drug development with onboard microfluidic flow control. *Lab on a Chip*. 2017. Vol. 17, no. 1, p. 134–144. DOI 10.1039/C6LC01236A.

[182] Gumuscu, B., Albers, H. J., Van den Berg, A., Eijkel, J. C. T. and Van der Meer, A. D. Compartmentalized 3D Tissue Culture Arrays under Controlled Microfluidic Delivery. *Scientific Reports*. 2017. Vol. 7, no. 1, p. 3381. DOI 10.1038/s41598-017-01944-5.

[183] Unger, M. A., Chou, H.-P., Thorsen, T., Scherer, A. and Quake, S. R. Monolithic Microfabricated Valves and Pumps by Multilayer Soft Lithography. *Science*. 2000. Vol. 288, no. 5463, p. 113–116. DOI 10.1126/science.288.5463.113.

[184] Gómez-Sjöberg, R., Leyrat, A. A., Pirone, D. M., Chen, C. S. and Quake, S. R. Versatile, Fully Automated, Microfluidic Cell Culture System. *Analytical Chemistry*. 2007. Vol. 79, no. 22, p. 8557–8563. DOI 10.1021/ac071311w.

[185] Zhang, C., Tu, H.-L., Jia, G., Mukhtar, T., Taylor, V., Rzhetsky, A. and Tay, S. Ultra-multiplexed analysis of single-cell dynamics reveals logic rules in differentiation. *Science Advances*. 2019. Vol. 5, no. 4, p. eaav7959. DOI 10.1126/sciadv.aav7959.

[186] Vollertsen, A. R., De Boer, D., Dekker, S., Wesselink, B. A. M., Haverkate, R., Rho, H. S., Boom, R. J., Skolimowski, M., Blom, M., Passier, R., Van den Berg, A., Van der Meer, A.

D. and Odijk, M. Modular operation of microfluidic chips for highly parallelized cell culture and liquid dosing via a fluidic circuit board. *Microsystems & Nanoengineering*. 2020. Vol. 6, no. 1, p. 107. DOI 10.1038/s41378-020-00216-z.

[187] Byun, C. K., Abi-Samra, K., Cho, Y.-K. and Takayama, S. Pumps for microfluidic cell culture: Microfluidics and Miniaturization. *ELECTROPHORESIS*. 2014. Vol. 35, no. 2–3, p. 245–257. DOI 10.1002/elps.201300205.

[188] Wang, Y. I., Carmona, C., Hickman, J. J. and Shuler, M. L. Multiorgan Microphysiological Systems for Drug Development: Strategies, Advances, and Challenges. *Advanced Healthcare Materials*. 2018. Vol. 7, no. 2, p. 1701000. DOI 10.1002/adhm.201701000.

[189] De Graaf, M. N. S., Cochrane, A., Van den Hil, F. E., Buijsman, W., Van der Meer, A. D., Van den Berg, A., Mummery, C. L. and Orlova, V. V. Scalable microphysiological system to model three-dimensional blood vessels. *APL Bioengineering*. 2019. Vol. 3, no. 2, p. 026105. DOI 10.1063/1.5090986.

[190] Deinhardt-Emmer, S., Rennert, K., Schicke, E., Cseresnyés, Z., Windolph, M., Nietzsche, S., Heller, R., Siwczak, F., Haupt, K. F., Carlstedt, S., Schacke, M., Figge, M. T., Ehrhardt, C., Löffler, B. and Mosig, A. S. Co-infection with *Staphylococcus aureus* after primary influenza virus infection leads to damage of the endothelium in a human alveolus-on-a-chip model. *Biofabrication*. 2020. Vol. 12, no. 2, p. 025012. DOI 10.1088/1758-5090/ab7073.

[191] Qian, T., Gil, D. A., Contreras Guzman, E., Gastfriend, B. D., Tweed, K. E., Palecek, S. P. and Skala, M. C. Adaptable pulsatile flow generated from stem cell-derived cardiomyocytes using quantitative imaging-based signal transduction. *Lab Chip*. 2020. Vol. 20, no. 20, p. 3744–3756. DOI 10.1039/D0LC00546K.

[192] Renggli, K. and Frey, O. Chapter 12 - Design and engineering of multiorgan systems. In : Hoeng, J., Bovard, D. and Peitsch, M. C. (eds.), *Organ-on-a-chip: engineered microenvironments for safety and efficacy testing*. London : Elsevier, Academic Press, 2020. p. 393–427. ISBN 978-0-12-817202-5.

[193] Winkler, T. E. and Herland, A. Sorption of neuropsychopharmaca in microfluidic materials for in-vitro studies. *bioRxiv* [online]. 2021. [Accessed 19 July 2021]. DOI 10.1101/2021.05.26.445264. Available from: https://www.biorxiv.org/content/early/2021/05/27/2021.05.26.445264

[194] Tokhadze, N., Chennell, P., Bernard, L., Lambert, C., Pereira, B., Mailhot-Jensen, B. and Sautou, V. Impact of alternative materials to plasticized PVC infusion tubings on drug sorption and plasticizer release. *Scientific Reports*. 2019. Vol. 9, no. 1, p. 18917. DOI 10.1038/s41598-019-55113-x.

[195] Goral, V. N., Zhou, C., Lai, F. and Ki Yuen, P. A continuous perfusion microplate for cell culture. *Lab Chip*. 2013. Vol. 13, no. 6, p. 1039–1043. DOI 10.1039/C2LC41102D.

[196] Zhu, X., Yi Chu, L., Chueh, B., Shen, M., Hazarika, B., Phadke, N. and Takayama, S. Arrays of horizontally-oriented mini-reservoirs generate steady microfluidic flows for continuous perfusion cell culture and gradient generation. *Analyst*. 2004. Vol. 129, no. 11, p. 1026–1031. DOI 10.1039/B407623K.

[197] Wang, C., Baker, B. M., Chen, C. S. and Schwartz, M. A. Endothelial Cell Sensing of Flow Direction. *Arteriosclerosis, Thrombosis, and Vascular Biology*. 2013. Vol. 33, no. 9, p. 2130–2136. DOI 10.1161/ATVBAHA.113.301826.

[198] Esch, M. B., Ueno, H., Applegate, D. R. and Shuler, M. L. Modular, pumpless body-on-a-chip platform for the co-culture of GI tract epithelium and 3D primary liver tissue. *Lab Chip*. 2016. Vol. 16, no. 14, p. 2719–2729. DOI 10.1039/C6LC00461J.

[199] Wang, Y. I. and Shuler, M. L. UniChip enables long-term recirculating unidirectional perfusion with gravity-driven flow for microphysiological systems. *Lab Chip*. 2018. Vol. 18, no. 17, p. 2563–2574. DOI 10.1039/C8LC00394G.

[200] Maschmeyer, I., Lorenz, A. K., Schimek, K., Hasenberg, T., Ramme, A. P., Hübner, J., Lindner, M., Drewell, C., Bauer, S., Thomas, A., Sambo, N. S., Sonntag, F., Lauster, R. and Marx, U. A four-organ-chip for interconnected long-term co-culture of human intestine, liver, skin and kidney equivalents. *Lab on a Chip*. 2015. Vol. 15, no. 12, p. 2688–2699. DOI 10.1039/C5LC00392J.

[201] Inman, W., Domansky, K., Serdy, J., Owens, B., Trumper, D. and Griffith, L. G. Design, modeling and fabrication of a constant flow pneumatic micropump. *Journal of Micromechanics and Microengineering*. 2007. Vol. 17, no. 5, p. 891–899. DOI 10.1088/0960-1317/17/5/007.

[202] Gu, W., Zhu, X., Futai, N., Cho, B. S. and Takayama, S. Computerized microfluidic cell culture using elastomeric channels and Braille displays. *Proceedings of the National Academy of Sciences*. 2004. Vol. 101, no. 45, p. 15861–15866. DOI 10.1073/pnas.0404353101.

[203] Husband, B., Bu, M., Evans, A. G. R. and Melvin, T. Investigation for the operation of an integrated peristaltic micropump. *Journal of Micromechanics and Microengineering*. 2004. Vol. 14, no. 9, p. S64–S69. DOI 10.1088/0960-1317/14/9/011.

[204] Pan, T., McDonald, S. J., Kai, E. M. and Ziaie, B. A magnetically driven PDMS micropump with ball check-valves. *Journal of Micromechanics and Microengineering*. 2005. Vol. 15, no. 5, p. 1021–1026. DOI 10.1088/0960-1317/15/5/018.

[205] Yobas, L., Tang, K.-C., Yong, S.-E. and Kye-Zheng Ong, E. A disposable planar peristaltic pump for lab-on-a-chip. *Lab on a Chip*. 2008. Vol. 8, no. 5, p. 660–662. DOI 10.1039/b720024b.

[206] Du, M., Ye, X., Wu, K. and Zhou, Z. A Peristaltic Micro Pump Driven by a Rotating Motor with Magnetically Attracted Steel Balls. *Sensors*. 2009. Vol. 9, no. 4, p. 2611–2620. DOI 10.3390/s90402611.

[207] Anderson, N. G. Analytical techniques for cell fractions: XII. A multiple-cuvet rotor for a new microanalytical system. *Analytical Biochemistry*. 1969. Vol. 28, p. 545–562. DOI 10.1016/0003-2697(69)90209-7.

[208] Burtis, C. A., Mailen, J. C., Johnson, W. F., Scott, C. D., Tiffany, T. O. and Anderson, N. G. Development of a Miniature Fast Analyzer. *Clinical Chemistry*. 1972. Vol. 18, no. 8, p. 753–761. DOI 10.1093/clinchem/18.8.753.

[209] Madou, M. J. and Kellogg, G. J. LabCD: a centrifuge-based microfluidic platform for diagnostics. In : Cohn, G. E. and Owicki, J. C. (eds.), *Systems and Technologies for Clinical Diagnostics and Drug Discovery*. San Jose, CA, United States : Proc. SPIE, 1998. p. 80 – 93.

[210] Woo, H.-K., Sunkara, V., Park, J., Kim, T.-H., Han, J.-R., Kim, C.-J., Choi, H.-I., Kim, Y.-K. and Cho, Y.-K. Exodisc for Rapid, Size-Selective, and Efficient Isolation and Analysis of Nanoscale Extracellular Vesicles from Biological Samples. *ACS Nano*. 2017. Vol. 11, no. 2, p. 1360–1370. DOI 10.1021/acsnano.6b06131.

[211] Kim, C.-J., Ki, D. Y., Park, J., Sunkara, V., Kim, T.-H., Min, Y. and Cho, Y.-K. Fully automated platelet isolation on a centrifugal microfluidic device for molecular diagnostics. *Lab Chip*. 2020. Vol. 20, no. 5, p. 949–957. DOI 10.1039/C9LC01140D.

[212] Kim, H., Lim, M., Kim, J. Y., Shin, S.-J., Cho, Y.-K. and Cho, C. H. Circulating Tumor Cells Enumerated by a Centrifugal Microfluidic Device as a Predictive Marker for Monitoring Ovarian Cancer Treatment: A Pilot Study. *Diagnostics*. 2020. Vol. 10, no. 4, p. 249. DOI 10.3390/diagnostics10040249.

[213] Rombach, M., Hin, S., Specht, M., Johannsen, B., Lüddecke, J., Paust, N., Zengerle, R., Roux, L., Sutcliffe, T., Peham, J. R., Herz, C., Panning, M., Donoso Mantke, O. and Mitsakakis, K. RespiDisk: a point-of-care platform for fully automated detection of respiratory tract infection pathogens in clinical samples. *Analyst*. 2020. Vol. 145, no. 21, p. 7040–7047. DOI 10.1039/D0AN01226B.

[214] Hin, S., Baumgartner, D., Specht, M., Lüddecke, J., Mahmodi Arjmand, E., Johannsen, B., Schiedel, L., Rombach, M., Paust, N., Von Stetten, F., Zengerle, R., Wipf, N., Müller, P., Mavridis, K., Vontas, J. and Mitsakakis, K. VectorDisk: A Microfluidic Platform Integrating Diagnostic Markers for Evidence-Based Mosquito Control. *Processes*. 2020. Vol. 8, no. 12, p. 1677. DOI 10.3390/pr8121677.

[215] Perebikovsky, A., Liu, Y., Hwu, A., Kido, H., Shamloo, E., Song, D., Monti, G., Shoval, O., Gussin, D. and Madou, M. Rapid sample preparation for detection of antibiotic resistance on a microfluidic disc platform. *Lab Chip*. 2021. Vol. 21, no. 3, p. 534–545. DOI 10.1039/D0LC00838A.

[216] Lee, S.-W., Kang, J. Y., Lee, I.-H., Ryu, S.-S., Kwak, S.-M., Shin, K.-S., Kim, C., Jung, H.-I. and Kim, T.-S. Single-cell assay on CD-like lab chip using centrifugal massive single-cell trap. *Sensors and Actuators A: Physical*. 2008. Vol. 143, no. 1, p. 64–69. DOI 10.1016/j.sna.2007.06.043.

[217] Kubo, I., Furutani, S. and Matoba, K. Use of a novel microfluidic disk in the analysis of single-cell viability and the application to Jurkat cells. *Journal of Bioscience and Bioengineering*. 2011. Vol. 112, no. 1, p. 98–101. DOI 10.1016/j.jbiosc.2011.03.016.

[218] Burger, R., Kurzbuch, D., Gorkin, R., Kijanka, G., Glynn, M., McDonagh, C. and Ducrée, J. An integrated centrifugo-opto-microfluidic platform for arraying, analysis, identification and manipulation of individual cells. *Lab Chip*. 2015. Vol. 15, no. 2, p. 378–381. DOI 10.1039/C4LC01002G.

[219] King, D., Glynn, M., Cindric, S., Kernan, D., O'Connell, T., Hakimjavadi, R., Kearney, S., Ackermann, T., Berbel, X. M., Llobera, A., Simonsen, U., Laursen, B. E., Redmond, E. M., Cahill, P. A. and Ducrée, J. Label-Free Multi Parameter Optical Interrogation of Endothelial Activation in Single Cells using a Lab on a Disc Platform. *Scientific Reports*. 2019. Vol. 9, no. 1, p. 4157. DOI 10.1038/s41598-019-40612-8.

[220] Park, J., Lee, G.-H., Yull Park, J., Lee, J. C. and Kim, H. C. Hypergravity-induced multicellular spheroid generation with different morphological patterns precisely controlled on a centrifugal microfluidic platform. *Biofabrication*. 2017. Vol. 9, no. 4, p. 045006. DOI 10.1088/1758-5090/aa9472.

[221] Ungrin, M. D., Joshi, C., Nica, A., Bauwens, C. and Zandstra, P. W. Reproducible, Ultra High-Throughput Formation of Multicellular Organization from Single Cell Suspension-Derived Human Embryonic Stem Cell Aggregates. *PLOS ONE*. 2008. Vol. 3, no. 2, p. e1565. DOI 10.1371/journal.pone.0001565.

[222] Thomas, N., Ocklind, A., Blikstad, I., Griffiths, S., Kenrick, M., Derand, H., Ekstrand, G., Ellström, C., Larsson, A. and Andersson, P. Integrated Cell Based Assays in Microfabricated Disposable CD Devices. In : Van den Berg, A., Olthuis, W. and Bergveld, P. (eds.), *Micro Total Analysis Systems 2000*. Dordrecht : Springer Netherlands, 2000. p. 249–252. ISBN 978-94-017-2264-3.

[223] Ren, Y., Chow, L. M.-C. and Leung, W. W.-F. Cell culture using centrifugal microfluidic platform with demonstration on Pichia pastoris. *Biomedical Microdevices*. 2013. Vol. 15, no. 2, p. 321–337. DOI 10.1007/s10544-012-9735-7.

[224] Kim, N., Dempsey, C. M., Zoval, J. V., Sze, J.-Y. and Madou, M. J. Automated microfluidic compact disc (CD) cultivation system of Caenorhabditis elegans. *Sensors and Actuators B: Chemical*. 2007. Vol. 122, no. 2, p. 511–518. DOI 10.1016/j.snb.2006.06.026.

[225] Kim, J., Lee, C., Kim, I., Ro, J., Kim, J., Min, Y., Park, J., Sunkara, V., Park, Y.-S., Michael, I., Kim, Y.-A., Lee, H. J. and Cho, Y.-K. Three-Dimensional Human Liver-Chip Emulating Premetastatic Niche Formation by Breast Cancer-Derived Extracellular Vesicles. *ACS Nano*. 2020. Vol. 14, no. 11, p. 14971–14988. DOI 10.1021/acsnano.0c04778.

[226] Schneider, S., Erdemann, F., Schneider, O., Hutschalik, T. and Loskill, P. Organ-on-a-disc: A platform technology for the centrifugal generation and culture of microphysiological 3D cell constructs amenable for automation and parallelization. *APL Bioengineering*. 2020. Vol. 4, no. 4, p. 046101. DOI 10.1063/5.0019766.

[227] Schneider, S., Bubeck, M., Rogal, J., Weener, H. J., Rojas, C., Weiss, M., Heymann, M., Van der Meer, A. D. and Loskill, P. Peristaltic on-chip pump for tunable media circulation and whole blood perfusion in PDMS-free organ-on-chip and Organ-Disc systems. *Lab Chip*. 2021. Vol. 21, no. 20, p. 3963–3978. DOI 10.1039/D1LC00494H.

[228] Schneider, S., Brás, E. J. S., Schneider, O., Schlünder, K. and Loskill, P. Facile Patterning of Thermoplastic Elastomers and Robust Bonding to Glass and Thermoplastics for Microfluidic Cell Culture and Organ-on-Chip. *Micromachines*. 2021. Vol. 12, no. 5, p. 575. DOI 10.3390/mi12050575.

[229] Roy, E., Stewart, G., Mounier, M., Malic, L., Peytavi, R., Clime, L., Madou, M., Bossinot, M., Bergeron, M. G. and Veres, T. From cellular lysis to microarray detection, an integrated thermoplastic elastomer (TPE) point of care Lab on a Disc. *Lab on a Chip*. 2015. Vol. 15, no. 2, p. 406–416. DOI 10.1039/C4LC00947A.

[230] Ogilvie, I. R. G., Sieben, V. J., Floquet, C. F. A., Zmijan, R., Mowlem, M. C. and Morgan, H. Reduction of surface roughness for optical quality microfluidic devices in PMMA and COC. *Journal of Micromechanics and Microengineering*. 2010. Vol. 20, no. 6, p. 065016. DOI 10.1088/0960-1317/20/6/065016.

[231] Schindelin, J., Arganda-Carreras, I., Frise, E., Kaynig, V., Longair, M., Pietzsch, T., Preibisch, S., Rueden, C., Saalfeld, S., Schmid, B., Tinevez, J.-Y., White, D. J., Hartenstein, V., Eliceiri, K., Tomancak, P. and Cardona, A. Fiji: an open-source platform for biological-image analysis. *Nature Methods*. 2012. Vol. 9, no. 7, p. 676–682. DOI 10.1038/nmeth.2019.

[232] Pudlas, M., Koch, S., Bolwien, C., Thude, S., Jenne, N., Hirth, T., Walles, H. and Schenke-Layland, K. Raman Spectroscopy: A Noninvasive Analysis Tool for the Discrimination of Human Skin Cells. *Tissue Engineering Part C: Methods*. 2011. Vol. 17, no. 10, p. 1027–1040. DOI 10.1089/ten.tec.2011.0082.

[233] Volz, A.-C., Huber, B., Schwandt, A. M. and Kluger, P. J. EGF and hydrocortisone as critical factors for the co-culture of adipogenic differentiated ASCs and endothelial cells. *Differentiation*. 2017. Vol. 95, p. 21–30. DOI 10.1016/j.diff.2017.01.002.

[234] Albers, H. J., Passier, R., Van den Berg, A. and Van der Meer, A. D. Automated Analysis of Platelet Aggregation on Cultured Endothelium in a Microfluidic Chip Perfused with Human Whole Blood. *Micromachines*. 2019. Vol. 10, no. 11, p. 781. DOI 10.3390/mi10110781.

[235] Huebsch, N., Loskill, P., Deveshwar, N., Spencer, C. I., Judge, L. M., Mandegar, M. A., B. Fox, C., Mohamed, T. M. A., Ma, Z., Mathur, A., Sheehan, A. M., Truong, A., Saxton, M., Yoo, J., Srivastava, D., Desai, T. A., So, P.-L., Healy, K. E. and Conklin, B. R. Miniaturized iPS-Cell-Derived Cardiac Muscles for Physiologically Relevant Drug Response Analyses. *Scientific Reports*. 2016. Vol. 6, no. 1, p. 24726. DOI 10.1038/srep24726.

[236] Lin, R.-Z. and Chang, H.-Y. Recent advances in three-dimensional multicellular spheroid culture for biomedical research. *Biotechnology Journal*. 2008. Vol. 3, no. 9–10, p. 1172–1184. DOI 10.1002/biot.200700228.

[237] Chen, P.-C. and Duong, L. H. Novel solvent bonding method for thermoplastic microfluidic chips. *Sensors and Actuators B: Chemical*. 2016. Vol. 237, p. 556–562. DOI 10.1016/j.snb.2016.06.135.

[238] Steigert, J., Haeberle, S., Brenner, T., Müller, C., Steinert, C. P., Koltay, P., Gottschlich, N., Reinecke, H., Rühe, J., Zengerle, R. and Ducrée, J. Rapid prototyping of microfluidic chips in COC. *Journal of Micromechanics and Microengineering*. 2007. Vol. 17, no. 2, p. 333–341. DOI 10.1088/0960-1317/17/2/020.

[239] Yu, S., Ng, S. P., Wang, Z., Tham, C. L. and Soh, Y. C. Thermal bonding of thermoplastic elastomer film to PMMA for microfluidic applications. *Surface and Coatings Technology*. 2017. Vol. 320, p. 437–440. DOI 10.1016/j.surfcoat.2016.11.102.

[240] Lifton, R. P., Gharavi, A. G. and Geller, D. S. Molecular Mechanisms of Human Hypertension. *Cell*. 2001. Vol. 104, no. 4, p. 545–556. DOI 10.1016/S0092-8674(01)00241-0.

[241] Masters, J. R. and Stacey, G. N. Changing medium and passaging cell lines. *Nature Protocols*. 2007. Vol. 2, no. 9, p. 2276–2284. DOI 10.1038/nprot.2007.319.

[242] Tkachenko, E., Gutierrez, E., Ginsberg, M. H. and Groisman, A. An easy to assemble microfluidic perfusion device with a magnetic clamp. *Lab on a Chip*. 2009. Vol. 9, no. 8, p. 1085–1095. DOI 10.1039/b812184b.

[243] Tkachenko, E., Gutierrez, E., Saikin, S. K., Fogelstrand, P., Kim, C., Groisman, A. and Ginsberg, M. H. The nucleus of endothelial cell as a sensor of blood flow direction. *Biology Open*. 2013. Vol. 2, no. 10, p. 1007–1012. DOI 10.1242/bio.20134622.

[244] Sonmez, U. M., Cheng, Y.-W., Watkins, S. C., Roman, B. L. and Davidson, L. A. Endothelial cell polarization and orientation to flow in a novel microfluidic multimodal shear stress generator. *Lab on a Chip*. 2020. Vol. 20, no. 23, p. 4373–4390. DOI 10.1039/D0LC00738B.

[245] Scott Lynn, N., Henry, C. S. and Dandy, D. S. Evaporation from microreservoirs. *Lab Chip*. 2009. Vol. 9, no. 12, p. 1780–1788. DOI 10.1039/B900556K.

[246] Wiegmann, V., Martinez, C. B. and Baganz, F. A simple method to determine evaporation and compensate for liquid losses in small-scale cell culture systems. *Biotechnology Letters*. 2018. Vol. 40, no. 7, p. 1029–1036. DOI 10.1007/s10529-018-2556-x.

[247] Rogatzki, M. J., Ferguson, B. S., Goodwin, M. L. and Gladden, L. B. Lactate is always the end product of glycolysis. *Frontiers in Neuroscience*. 2015. Vol. 9, p. 22. DOI 10.3389/fnins.2015.00022.

[248] Osborn, L., Hession, C., Tizard, R., Vassallo, C., Luhowskyj, S., Chi-Rosso, G. and Lobb, R. Direct expression cloning of vascular cell adhesion molecule 1, a cytokine-induced endothelial protein that binds to lymphocytes. *Cell*. 1989. Vol. 59, no. 6, p. 1203–1211. DOI 10.1016/0092-8674(89)90775-7.

[249] Lechleitner, S., Gille, J., Johnson, D. R. and Petzelbauer, P. Interferon Enhances Tumor Necrosis Factor–induced Vascular Cell Adhesion Molecule 1 (CD106) Expression in Human Endothelial Cells by an Interferon-related Factor 1–dependent Pathway. *Journal of Experimental Medicine*. 1998. Vol. 187, no. 12, p. 2023–2030. DOI 10.1084/jem.187.12.2023.

[250] Yamagishi, S., Inagaki, Y., Nakamura, K. and Imaizumi, T. Azelnidipine, A Newly Developed Long-Acting Calcium Antagonist, Inhibits Tumor Necrosis Factor-α-Induced Interleukin-8 Expression in Endothelial Cells through its Anti-Oxidative Properties. *Journal of Cardiovascular Pharmacology*. 2004. Vol. 43, no. 5, p. 724–730.

[251] Yamagishi, S.-I., Inagaki, Y., Nakamura, K., Abe, R., Shimizu, T., Yoshimura, A. and Imaizumi, T. Pigment epithelium-derived factor inhibits TNF-α-induced interleukin-6 expression in endothelial cells by suppressing NADPH oxidase-mediated reactive oxygen species generation. *Journal of Molecular and Cellular Cardiology*. 2004. Vol. 37, no. 2, p. 497–506. DOI 10.1016/j.yjmcc.2004.04.007.

[252] Kim, I., Kim, J.-H., Ryu, Y. S., Liu, M. and Koh, G. Y. Tumor Necrosis Factor-α Upregulates Angiopoietin-2 in Human Umbilical Vein Endothelial Cells. *Biochemical and Biophysical Research Communications*. 2000. Vol. 269, no. 2, p. 361–365. DOI 10.1006/bbrc.2000.2296.

[253] Nieswandt, B., Pleines, I. and Bender, M. Platelet adhesion and activation mechanisms in arterial thrombosis and ischaemic stroke: Platelet adhesion and activation mechanisms. *Journal of Thrombosis and Haemostasis*. 2011. Vol. 9, p. 92–104. DOI 10.1111/j.1538-7836.2011.04361.x.

[254] Van der Meer, A. D., Poot, A. A., Duits, M. H. G., Feijen, J. and Vermes, I. Microfluidic Technology in Vascular Research. Martins-Green, M. (ed.), *Journal of Biomedicine and Biotechnology*. 2009. Vol. 2009, p. 823148. DOI 10.1155/2009/823148.

[255] Kelly, R. T., Pan, T. and Woolley, A. T. Phase-Changing Sacrificial Materials for Solvent Bonding of High-Performance Polymeric Capillary Electrophoresis Microchips. *Analytical Chemistry*. 2005. Vol. 77, no. 11, p. 3536–3541. DOI 10.1021/ac0501083.

[256] Chen, C.-F., Liu, J., Chang, C.-C. and DeVoe, D. L. High-pressure on-chip mechanical valves for thermoplastic microfluidic devices. *Lab on a Chip*. 2009. Vol. 9, no. 24, p. 3511–3516. DOI 10.1039/b912014a.

[257] Khanarian, G. Optical properties of cyclic olefin copolymers. *Optical Engineering*. 2001. Vol. 40, no. 6, p. 1024–1029. DOI 10.1117/1.1369411.

[258] Kim, M., Moon, B.-U. and Hidrovo, C. H. Enhancement of the thermo-mechanical properties of PDMS molds for the hot embossing of PMMA microfluidic devices. *Journal of Micromechanics and Microengineering*. 2013. Vol. 23, no. 9, p. 095024. DOI 10.1088/0960-1317/23/9/095024.

[259] Piironen, K., Haapala, M., Talman, V., Järvinen, P. and Sikanen, T. Cell adhesion and proliferation on common 3D printing materials used in stereolithography of microfluidic devices. *Lab Chip*. 2020. Vol. 20, no. 13, p. 2372–2382. DOI 10.1039/D0LC00114G.

[260] Weltin, A., Slotwinski, K., Kieninger, J., Moser, I., Jobst, G., Wego, M., Ehret, R. and Urban, G. A. Cell culture monitoring for drug screening and cancer research: a transparent, microfluidic, multi-sensor microsystem. *Lab Chip*. 2014. Vol. 14, no. 1, p. 138–146. DOI 10.1039/C3LC50759A.

[261] Sivakumar, R., Trinh, K. T. L. and Lee, N. Y. Heat and pressure-resistant room temperature irreversible sealing of hybrid PDMS–thermoplastic microfluidic devices via

carbon–nitrogen covalent bonding and its application in a continuous-flow polymerase chain reaction. *RSC Adv.* 2020. Vol. 10, no. 28, p. 16502–16509. DOI 10.1039/D0RA02332A.

[262] Sivakumar, R. and Lee, N. Y. Chemically robust succinimide-group-assisted irreversible bonding of poly(dimethylsiloxane)–thermoplastic microfluidic devices at room temperature. *Analyst*. 2020. Vol. 145, no. 21, p. 6887–6894. DOI 10.1039/D0AN01268H.

[263] Cortese, B., Mowlem, M. C. and Morgan, H. Characterisation of an irreversible bonding process for COC–COC and COC–PDMS–COC sandwich structures and application to microvalves. *Sensors and Actuators B: Chemical*. 2011. Vol. 160, no. 1, p. 1473–1480. DOI 10.1016/j.snb.2011.07.040.

[264] Bahal, S. M. and Romansky, J. M. Spalling and Sorption of Tubing for Peristaltic Pumps. *Pharmaceutical Development and Technology*. 2002. Vol. 7, no. 3, p. 317–323. DOI 10.1081/PDT-120005728.

[265] Blackwell, R. I. and Mauritz, K. A. Mechanical creep and recovery of poly(styrene-b-ethylene/butylene-b-styrene) (SEBS), sulfonated SEBS (sSEBS), and sSEBS/silicate nanostructured materials. *Polymers for Advanced Technologies*. 2005. Vol. 16, no. 2–3, p. 212–220. DOI 10.1002/pat.574.

[266] Musah, S., Mammoto, A., Ferrante, T. C., Jeanty, S. S. F., Hirano-Kobayashi, M., Mammoto, T., Roberts, K., Chung, S., Novak, R., Ingram, M., Fatanat-Didar, T., Koshy, S., Weaver, J. C., Church, G. M. and Ingber, D. E. Mature induced-pluripotent-stem-cell-derived human podocytes reconstitute kidney glomerular-capillary-wall function on a chip. *Nature Biomedical Engineering*. 2017. Vol. 1, no. 5, p. 0069. DOI 10.1038/s41551-017-0069.

[267] Blundell, C., Tess, E. R., Schanzer, A. S. R., Coutifaris, C., Su, E. J., Parry, S. and Huh, D. A microphysiological model of the human placental barrier. *Lab Chip*. 2016. Vol. 16, no. 16, p. 3065–3073. DOI 10.1039/C6LC00259E.

[268] Zakharova, M., Palma do Carmo, M. A., Van der Helm, M. W., Le-The, H., De Graaf, M. N. S., Orlova, V., Van den Berg, A., Van der Meer, A. D., Broersen, K. and Segerink, L. I. Multiplexed blood–brain barrier organ-on-chip. *Lab Chip*. 2020. Vol. 20, no. 17, p. 3132–3143. DOI 10.1039/D0LC00399A.

[269] Norotte, C., Marga, F. S., Niklason, L. E. and Forgacs, G. Scaffold-free vascular tissue engineering using bioprinting. *Biomaterials*. 2009. Vol. 30, no. 30, p. 5910–5917. DOI 10.1016/j.biomaterials.2009.06.034.

[270] Dressaire, E. and Sauret, A. Clogging of microfluidic systems. *Soft Matter*. 2017. Vol. 13, no. 1, p. 37–48. DOI 10.1039/C6SM01879C.

[271] Shen, F., Li, X. and Li, P. C. H. Study of flow behaviors on single-cell manipulation and shear stress reduction in microfluidic chips using computational fluid dynamics simulations. *Biomicrofluidics*. 2014. Vol. 8, no. 1, p. 014109. DOI 10.1063/1.4866358.

[272] Godoy, P., Hewitt, N. J., Albrecht, U., Andersen, M. E., Ansari, N., Bhattacharya, S., Bode, J. G., Bolleyn, J., Borner, C., Böttger, J., Braeuning, A., Budinsky, R. A., Burkhardt, B., Cameron, N. R., Camussi, G., Cho, C.-S., Choi, Y.-J., Craig Rowlands, J., Dahmen, U., Damm, G., Dirsch, O., Donato, M. T., Dong, J., Dooley, S., Drasdo, D., Eakins, R., Ferreira, K. S., Fonsato, V., Fraczek, J., Gebhardt, R., Gibson, A., Glanemann, M., Goldring, C. E. P., Gómez-Lechón, M. J., Groothuis, G. M. M., Gustavsson, L., Guyot, C., Hallifax, D., Hammad, S., Hayward, A., Häussinger, D., Hellerbrand, C., Hewitt, P., Hoehme, S., Holzhütter, H.-G., Houston, J. B., Hrach, J., Ito, K., Jaeschke, H., Keitel, V., Kelm, J. M., Kevin Park, B., Kordes, C., Kullak-Ublick, G. A., LeCluyse, E. L., Lu, P., Luebke-Wheeler, J., Lutz, A., Maltman, D. J., Matz-Soja, M., McMullen, P., Merfort, I., Messner, S., Meyer, C., Mwinyi, J., Naisbitt, D.

J., Nussler, A. K., Olinga, P., Pampaloni, F., Pi, J., Pluta, L., Przyborski, S. A., Ramachandran, A., Rogiers, V., Rowe, C., Schelcher, C., Schmich, K., Schwarz, M., Singh, B., Stelzer, E. H. K., Stieger, B., Stöber, R., Sugiyama, Y., Tetta, C., Thasler, W. E., Vanhaecke, T., Vinken, M., Weiss, T. S., Widera, A., Woods, C. G., Xu, J. J., Yarborough, K. M. and Hengstler, J. G. Recent advances in 2D and 3D in vitro systems using primary hepatocytes, alternative hepatocyte sources and non-parenchymal liver cells and their use in investigating mechanisms of hepatotoxicity, cell signaling and ADME. *Archives of Toxicology*. 2013. Vol. 87, no. 8, p. 1315–1530. DOI 10.1007/s00204-013-1078-5.

[273] Milam, A. H., Li, Z.-Y. and Fariss, R. N. Histopathology of the human retina in retinitis pigmentosa. *Progress in retinal and eye research*. 1998. Vol. 17, no. 2, p. 175—205. DOI 10.1016/s1350-9462(97)00012-8.

[274] Florencio-Silva, R., Sasso, G. R. da S., Sasso-Cerri, E., Simões, M. J. and Cerri, P. S. Biology of Bone Tissue: Structure, Function, and Factors That Influence Bone Cells. Lattanzi, W. (ed.), *BioMed Research International*. 2015. Vol. 2015, p. 421746. DOI 10.1155/2015/421746.

[275] Kolesky, D. B., Truby, R. L., Gladman, A. S., Busbee, T. A., Homan, K. A. and Lewis, J. A. 3D Bioprinting of Vascularized, Heterogeneous Cell-Laden Tissue Constructs. *Advanced Materials*. 2014. Vol. 26, no. 19, p. 3124–3130. DOI 10.1002/adma.201305506.

[276] Rismani Yazdi, S., Shadmani, A., Bürgel, S. C., Misun, P. M., Hierlemann, A. and Frey, O. Adding the 'heart' to hanging drop networks for microphysiological multi-tissue experiments. *Lab on a Chip*. 2015. Vol. 15, no. 21, p. 4138–4147. DOI 10.1039/C5LC01000D.

[277] Lin, D. S. Y., Guo, F. and Zhang, B. Modeling organ-specific vasculature with organ-on-a-chip devices. *Nanotechnology*. 2018. Vol. 30, no. 2, p. 024002. DOI 10.1088/1361-6528/aae7de.

[278] Alberts, B., Johnson, A., Lewis, J., Raff, M., Roberts, K. and Walter, P. Blood vessels and endothelial cells. In : *Molecular Biology of the Cell.* [online]. 4th edition. New York : Garland Science, 2002. [Accessed 23 July 2021]. Available from: https://www.ncbi.nlm.nih.gov/books/NBK26848/

[279] Fiddes, L. K., Raz, N., Srigunapalan, S., Tumarkan, E., Simmons, C. A., Wheeler, A. R. and Kumacheva, E. A circular cross-section PDMS microfluidics system for replication of cardiovascular flow conditions. *Biomaterials*. 2010. Vol. 31, no. 13, p. 3459–3464. DOI 10.1016/j.biomaterials.2010.01.082.

[280] Tsvirkun, D., Grichine, A., Duperray, A., Misbah, C. and Bureau, L. Microvasculature on a chip: study of the Endothelial Surface Layer and the flow structure of Red Blood Cells. *Scientific Reports*. 2017. Vol. 7, no. 1, p. 45036. DOI 10.1038/srep45036.

[281] Bischel, L. L., Lee, S.-H. and Beebe, D. J. A Practical Method for Patterning Lumens through ECM Hydrogels via Viscous Finger Patterning. *Journal of Laboratory Automation*. 2012. Vol. 17, no. 2, p. 96–103. DOI 10.1177/2211068211426694.

[282] Bischel, L. L., Young, E. W. K., Mader, B. R. and Beebe, D. J. Tubeless microfluidic angiogenesis assay with three-dimensional endothelial-lined microvessels. *Biomaterials*. 2013. Vol. 34, no. 5, p. 1471–1477. DOI 10.1016/j.biomaterials.2012.11.005.

[283] Ballermann, B. J., Dardik, A., Eng, E. and Liu, A. Shear stress and the endothelium. *Kidney International*. 1998. Vol. 54, p. S100–S108. DOI 10.1046/j.1523-1755.1998.06720.x.

[284] Jalili-Firoozinezhad, S., Prantil-Baun, R., Jiang, A., Potla, R., Mammoto, T., Weaver, J. C., Ferrante, T. C., Kim, H. J., Cabral, J. M. S., Levy, O. and Ingber, D. E. Modeling radiation

injury-induced cell death and countermeasure drug responses in a human Gut-on-a-Chip. *Cell Death & Disease*. 2018. Vol. 9, no. 2, p. 223. DOI 10.1038/s41419-018-0304-8.

[285] Merces, G. O. T., Kennedy, C., Lenoci, B., Reynaud, E. G., Burke, N. and Pickering, M. The incubot: A 3D printer-based microscope for long-term live cell imaging within a tissue culture incubator. *HardwareX*. 2021. Vol. 9, p. e00189. DOI 10.1016/j.ohx.2021.e00189.

[286] King, D., O'Sullivan, M. and Ducrée, J. Optical detection strategies for centrifugal microfluidic platforms. *Journal of Modern Optics*. 2014. Vol. 61, no. 2, p. 85–101. DOI 10.1080/09500340.2013.873496.

[287] Grumann, M., Brenner, T., Beer, C., Zengerle, R. and Ducrée, J. Visualization of flow patterning in high-speed centrifugal microfluidics. *Review of Scientific Instruments*. 2005. Vol. 76, no. 2, p. 025101. DOI 10.1063/1.1834703.

[288] Ukita, Y. and Takamura, Y. A new stroboscopic technique for the observation of microscale fluorescent objects on a spinning platform in centrifugal microfluidics. *Microfluidics and Nanofluidics*. 2015. Vol. 18, no. 2, p. 245–252. DOI 10.1007/s10404-014-1426-7.

[289] Novak, R., Ingram, M., Marquez, S., Das, D., Delahanty, A., Herland, A., Maoz, B. M., Jeanty, S. S. F., Somayaji, M. R., Burt, M., Calamari, E., Chalkiadaki, A., Cho, A., Choe, Y., Chou, D. B., Cronce, M., Dauth, S., Divic, T., Fernandez-Alcon, J., Ferrante, T., Ferrier, J., FitzGerald, E. A., Fleming, R., Jalili-Firoozinezhad, S., Grevesse, T., Goss, J. A., Hamkins-Indik, T., Henry, O., Hinojosa, C., Huffstater, T., Jang, K.-J., Kujala, V., Leng, L., Mannix, R., Milton, Y., Nawroth, J., Nestor, B. A., Ng, C. F., O'Connor, B., Park, T.-E., Sanchez, H., Sliz, J., Sontheimer-Phelps, A., Swenor, B., Thompson, G., Touloumes, G. J., Tranchemontagne, Z., Wen, N., Yadid, M., Bahinski, A., Hamilton, G. A., Levner, D., Levy, O., Przekwas, A., Prantil-Baun, R., Parker, K. K. and Ingber, D. E. Robotic fluidic coupling and interrogation of multiple vascularized organ chips. *Nature Biomedical Engineering*. 2020. Vol. 4, no. 4, p. 407–420. DOI 10.1038/s41551-019-0497-x.

[290] Potter, S. M. and DeMarse, T. B. A new approach to neural cell culture for long-term studies. *Journal of Neuroscience Methods*. 2001. Vol. 110, no. 1–2, p. 17–24. DOI 10.1016/S0165-0270(01)00412-5.

[291] Börner, J., Buchinger, S. and Schomburg, D. A high-throughput method for microbial metabolome analysis using gas chromatography/mass spectrometry. *Analytical Biochemistry*. 2007. Vol. 367, no. 2, p. 143–151. DOI 10.1016/j.ab.2007.04.036.

[292] Hsiao, V., De los Santos, E. L. C., Whitaker, W. R., Dueber, J. E. and Murray, R. M. Design and Implementation of a Biomolecular Concentration Tracker. *ACS Synthetic Biology*. 2015. Vol. 4, no. 2, p. 150–161. DOI 10.1021/sb500024b.

[293] Pinto, F., Thornton, E. L. and Wang, B. An expanded library of orthogonal split inteins enables modular multi-peptide assemblies. *Nature Communications*. 2020. Vol. 11, no. 1, p. 1529. DOI 10.1038/s41467-020-15272-2.

[294] Seyfarth, F., Schliemann, S., Elsner, P. and Hipler, U.-C. Antifungal effect of high- and low-molecular-weight chitosan hydrochloride, carboxymethyl chitosan, chitosan oligosaccharide and N-acetyl-d-glucosamine against Candida albicans, Candida krusei and Candida glabrata. *International Journal of Pharmaceutics*. 2008. Vol. 353, no. 1–2, p. 139–148. DOI 10.1016/j.ijpharm.2007.11.029.

[295] Vander Heiden, M. G., Cantley, L. C. and Thompson, C. B. Understanding the Warburg Effect: The Metabolic Requirements of Cell Proliferation. *Science*. 2009. Vol. 324, no. 5930, p. 1029–1033. DOI 10.1126/science.1160809.

[296] De Bock, K., Georgiadou, M., Schoors, S., Kuchnio, A., Wong, B. W., Cantelmo, A. R., Quaegebeur, A., Ghesquière, B., Cauwenberghs, S., Eelen, G., Phng, L.-K., Betz, I., Tembuyser, B., Brepoels, K., Welti, J., Geudens, I., Segura, I., Cruys, B., Bifari, F., Decimo, I., Blanco, R., Wyns, S., Vangindertael, J., Rocha, S., Collins, R. T., Munck, S., Daelemans, D., Imamura, H., Devlieger, R., Rider, M., Van Veldhoven, P. P., Schuit, F., Bartrons, R., Hofkens, J., Fraisl, P., Telang, S., DeBerardinis, R. J., Schoonjans, L., Vinckier, S., Chesney, J., Gerhardt, H., Dewerchin, M. and Carmeliet, P. Role of PFKFB3-Driven Glycolysis in Vessel Sprouting. *Cell*. 2013. Vol. 154, no. 3, p. 651–663. DOI 10.1016/j.cell.2013.06.037.

[297] Balogh, E., Veale, D. J., McGarry, T., Orr, C., Szekanecz, Z., Ng, C.-T., Fearon, U. and Biniecka, M. Oxidative stress impairs energy metabolism in primary cells and synovial tissue of patients with rheumatoid arthritis. *Arthritis Research & Therapy*. 2018. Vol. 20, no. 1, p. 95. DOI 10.1186/s13075-018-1592-1.

[298] Wagner, B. A., Venkataraman, S. and Buettner, G. R. The rate of oxygen utilization by cells. *Free Radical Biology and Medicine*. 2011. Vol. 51, no. 3, p. 700–712. DOI 10.1016/j.freeradbiomed.2011.05.024.

[299] Jagannathan, L., Cuddapah, S. and Costa, M. Oxidative Stress Under Ambient and Physiological Oxygen Tension in Tissue Culture. *Current Pharmacology Reports*. 2016. Vol. 2, no. 2, p. 64–72. DOI 10.1007/s40495-016-0050-5.

[300] Wenger, R. H., Kurtcuoglu, V., Scholz, C. C., Marti, H. H. and Hoogewijs, D. Frequently asked questions in hypoxia research. *Hypoxia*. 2015. Vol. 3, p. 35–43. DOI 10.2147/HP.S92198.

[301] Kim, B., Li, J., Jang, C. and Arany, Z. Glutamine fuels proliferation but not migration of endothelial cells. *The EMBO Journal*. 2017. Vol. 36, no. 16, p. 2321–2333. DOI 10.15252/embj.201796436.

[302] Soucy, J. R., Bindas, A. J., Koppes, A. N. and Koppes, R. A. Instrumented Microphysiological Systems for Real-Time Measurement and Manipulation of Cellular Electrochemical Processes. *iScience*. 2019. Vol. 21, p. 521–548. DOI 10.1016/j.isci.2019.10.052.

[303] Kieninger, J., Weltin, A., Flamm, H. and Urban, G. A. Microsensor systems for cell metabolism – from 2D culture to organ-on-chip. *Lab Chip*. 2018. Vol. 18, no. 9, p. 1274–1291. DOI 10.1039/C7LC00942A.

[304] Gruber, P., Marques, M. P. C., Szita, N. and Mayr, T. Integration and application of optical chemical sensors in microbioreactors. *Lab Chip*. 2017. Vol. 17, no. 16, p. 2693–2712. DOI 10.1039/C7LC00538E.

[305] Ungerböck, B., Fellinger, S., Sulzer, P., Abel, T. and Mayr, T. Magnetic optical sensor particles: a flexible analytical tool for microfluidic devices. *Analyst*. 2014. Vol. 139, no. 10, p. 2551–2559. DOI 10.1039/C4AN00169A.

[306] Fiedler, U., Scharpfenecker, M., Koidl, S., Hegen, A., Grunow, V., Schmidt, J. M., Kriz, W., Thurston, G. and Augustin, H. G. The Tie-2 ligand Angiopoietin-2 is stored in and rapidly released upon stimulation from endothelial cell Weibel-Palade bodies. *Blood*. 2004. Vol. 103, no. 11, p. 4150–4156. DOI 10.1182/blood-2003-10-3685.

[307] Costa, P. F., Albers, H. J., Linssen, J. E. A., Middelkamp, H. H. T., Van der Hout, L., Passier, R., Van den Berg, A., Malda, J. and Van der Meer, A. D. Mimicking arterial thrombosis in a 3D-printed microfluidic in vitro vascular model based on computed tomography angiography data. *Lab on a Chip*. 2017. Vol. 17, no. 16, p. 2785–2792. DOI 10.1039/C7LC00202E.

[308] Zheng, Y., Chen, J., Craven, M., Choi, N. W., Totorica, S., Diaz-Santana, A., Kermani, P., Hempstead, B., Fischbach-Teschl, C., López, J. A. and Stroock, A. D. In vitro microvessels for the study of angiogenesis and thrombosis. *Proceedings of the National Academy of Sciences*. 2012. Vol. 109, no. 24, p. 9342–9347. DOI 10.1073/pnas.1201240109.

[309] Bantjes, A. Clotting Phenomena at the Blood-Polymer Interface and Development of Blood Compatible Polymeric Surfaces. *British Polymer Journal*. 1978. Vol. 10, no. 4, p. 267–274. DOI 10.1002/pi.4980100410.

[310] Westein, E., Van der Meer, A. D., Kuijpers, M. J. E., Frimat, J.-P., Van den Berg, A. and Heemskerk, J. W. M. Atherosclerotic geometries exacerbate pathological thrombus formation poststenosis in a von Willebrand factor-dependent manner. *Proceedings of the National Academy of Sciences*. 2013. Vol. 110, no. 4, p. 1357–1362. DOI 10.1073/pnas.1209905110.

[311] Meza, D., Shanmugavelayudam, S. K., Mendoza, A., Sanchez, C., Rubenstein, D. A. and Yin, W. Platelets modulate endothelial cell response to dynamic shear stress through PECAM-1. *Thrombosis Research*. 2017. Vol. 150, p. 44–50. DOI 10.1016/j.thromres.2016.12.003.

[312] Szuwart, T., Brzoska, T., Luger, T. A., Filler, T., Peuker, E. and Dierichs, R. Vitamin E reduces platelet adhesion to human endothelial cells in vitro. *American Journal of Hematology*. 2000. Vol. 65, no. 1, p. 1–4. DOI 10.1002/1096-8652(200009)65:1<1::AID-AJH1>3.0.CO;2-8.

[313] Reese, W. M., Burch, P., Korpusik, A. B., Liu, S. E., Loskill, P., Messersmith, P. B. and Healy, K. E. Facile Macrocyclic Polyphenol Barrier Coatings for PDMS Microfluidic Devices. *Advanced Functional Materials*. 2020. Vol. 30, no. 48, p. 2001274. DOI 10.1002/adfm.202001274.

13 Appendix

13.1 Organ-Disc Layouts

The 2D layouts of the individual Organ-Disc versions are shown as top views, which were utilized for centrifugal cell loading and centrifugal perfusion (Figure 13.1 a) [226], or for peristaltic perfusion of a blood vessel-like structure (Figure 13.1 b) [227].

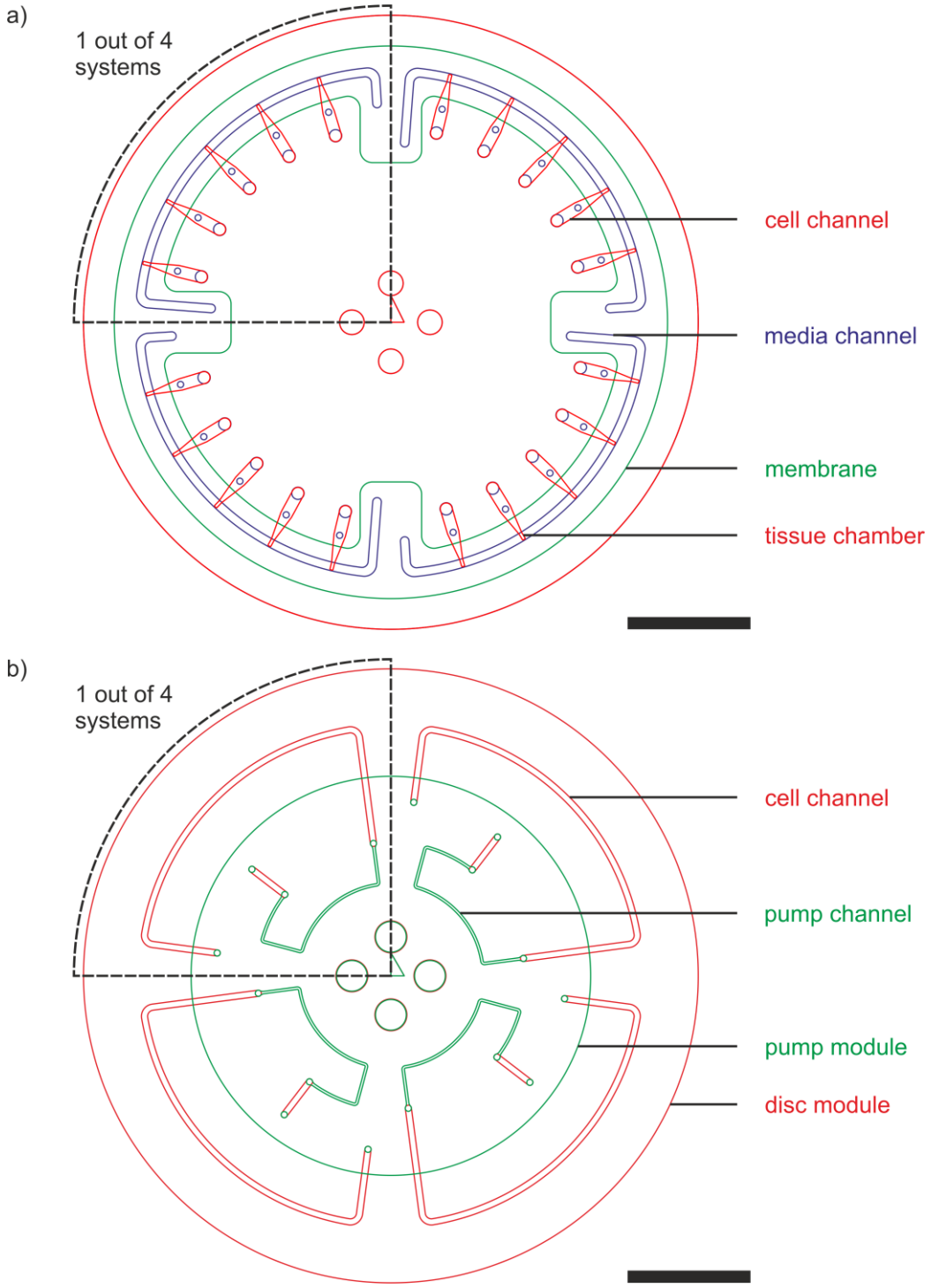

Figure 13.1 Organ-Disc layouts. a) Layout of the Organ-Disc used for centrifugal cell loading and centrifugal perfusion, here, shown with rectangular tissue chambers. b) Layout of the Organ-Disc with an integrated peristaltic pump. Scale bars: a, b) 20 mm. b) adapted from Ref. [227] with permission from the Royal Society of Chemistry available under the CC BY-NC 3.0 license.

13.2 PC/TPE-hybrid Organ-Disc

The overall Organ-Disc layout featuring a media and tissue layer separated by a porous membrane is transferable into PC/TPE-hybrid layers (Figure 13.2 a). The self-adhesive surface of TPE is ideally suited for the integration of fragile membranes. After placing the individual PET membranes into designated cavities in the tissue layer and adding a media layer on top, the final Organ-Disc bonding is achieved by overnight incubation at 60 °C in an oven without additional pressure. This process achieves precise channel structures as well as flat and tightly integrated membranes (Figure 13.2 b). The bonding between TPE layers and the PET membrane is sufficient for the centrifugal cell loading process and prevents cells from leaving the tissue chamber (Figure 13.2 c).

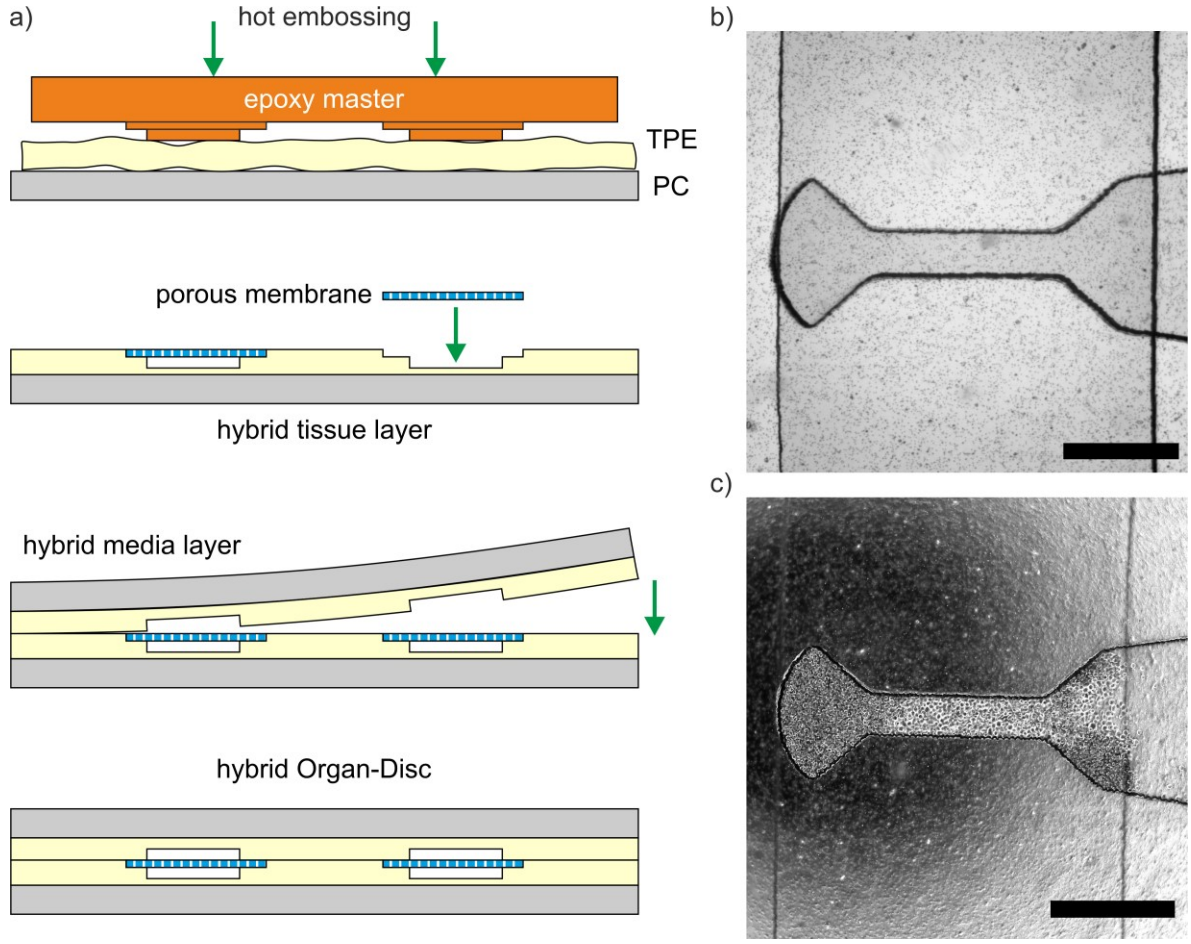

Figure 13.2 Hybrid Organ-Disc. a) The fabrication process of hybrid Organ-Discs includes the simultaneous structuring and bonding of TPE and PC layers by hot embossing, the membrane integration into the tissue layer and final assembly by adding a hybrid media layer and overnight incubation at 60 °C. b) Tissue chamber of a hybrid Organ-Disc. c) Tissue chamber of a hybrid Organ-Disc after centrifugal cell loading. Scale bars: b-c) 500 µm.

13.3 Parallelized Thermal Fusion Bonding

The presented thermal fusion bonding tool allows for the parallelized bonding of up to seven discs, each 10 cm in diameter, in one step. An exemplary bonding result of COC-based Organ-Discs with highlighted, non-bonded areas demonstrates the homogenous fusion of the individual Organ-Discs (Figure 13.3). Non-bonded areas are located outside of channel regions hence do not affect the Organ-Disc functionality.

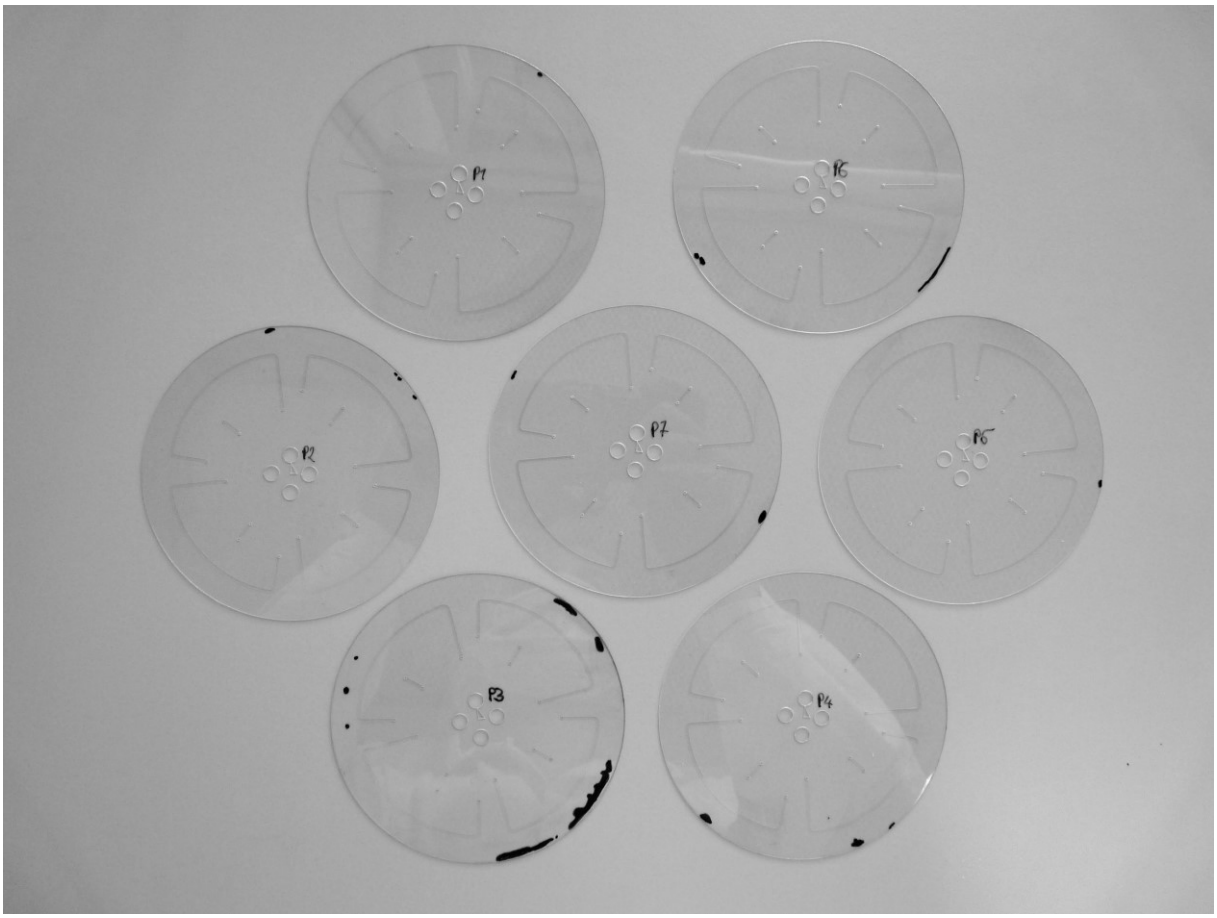

Figure 13.3 Individual Organ-Discs after thermal fusion bonding with non-bonded areas highlighted in black. Shown Organ-Discs are based on COC. Non-bonded areas were localized by eye and highlighted with a permanent marker. Each disc is 10 cm in diameter.

13.4 Pressure Drop

The theoretical calculation of the pressure drop during peristaltic pumping is described in more detail in Ref. [227]. Briefly, the maximum pressure drop is achieved at the highest flow rate Q = 2.6 mL/h at a motor setting of 800 rph of the integrated peristaltic pump. The sum of the individual hydraulic resistances of the in-line connected channel sections in the Organ-Disc result in a total, hydraulic resistance $R_{hyd} = 1.8 \times 10^{12}$ Pa·s/m^3. The resulting pressure drop at the highest pump rate is Δp = 1252 Pa.

13.5 Small Molecule Absorption into TPE vs. PDMS

The absorption of different rhodamine molecules were analyzed in collaboration with Oliver Schneider (Fraunhofer Institute for Interfacial Engineering and Biotechnology IGB, Stuttgart, Germany) and Eduardo J. S. Brás (NMI Natural and Medical Sciences Institute at the University of Tübingen, Reutlingen, Germany) and published in Ref. [228]. Briefly, PBS containing either 100 µM rhodamine B, rhodamine 6G or rhodamine 101 was injected into PC/TPE-hybrid or PDMS channels bonded to glass substrates and remained in the channels for three days. The individual rhodamine compounds have comparable molar weights (479-491 g/mol) and differ in hydrophobicity ($2.13 \leq \text{Log P} \leq 7.8$) [313]. Micrographs and fluorescent intensity profiles were acquired and analyzed by Oliver Schneider every 24 h and after the final washout of the rhodamine solutions on day 3 (Figure 13.4).

In direct comparison to PDMS, TPE devices showed a lower spreading of the fluorescent intensity profile and almost no visible, remaining fluorescent signal after washout of the rhodamine solutions. This serves as a qualitative demonstration that TPE shows lower absorption of small, hydrophobic molecules than PDMS. This observation is in agreement with previous studies on small molecule and drug absorption in SEBS chips [60].

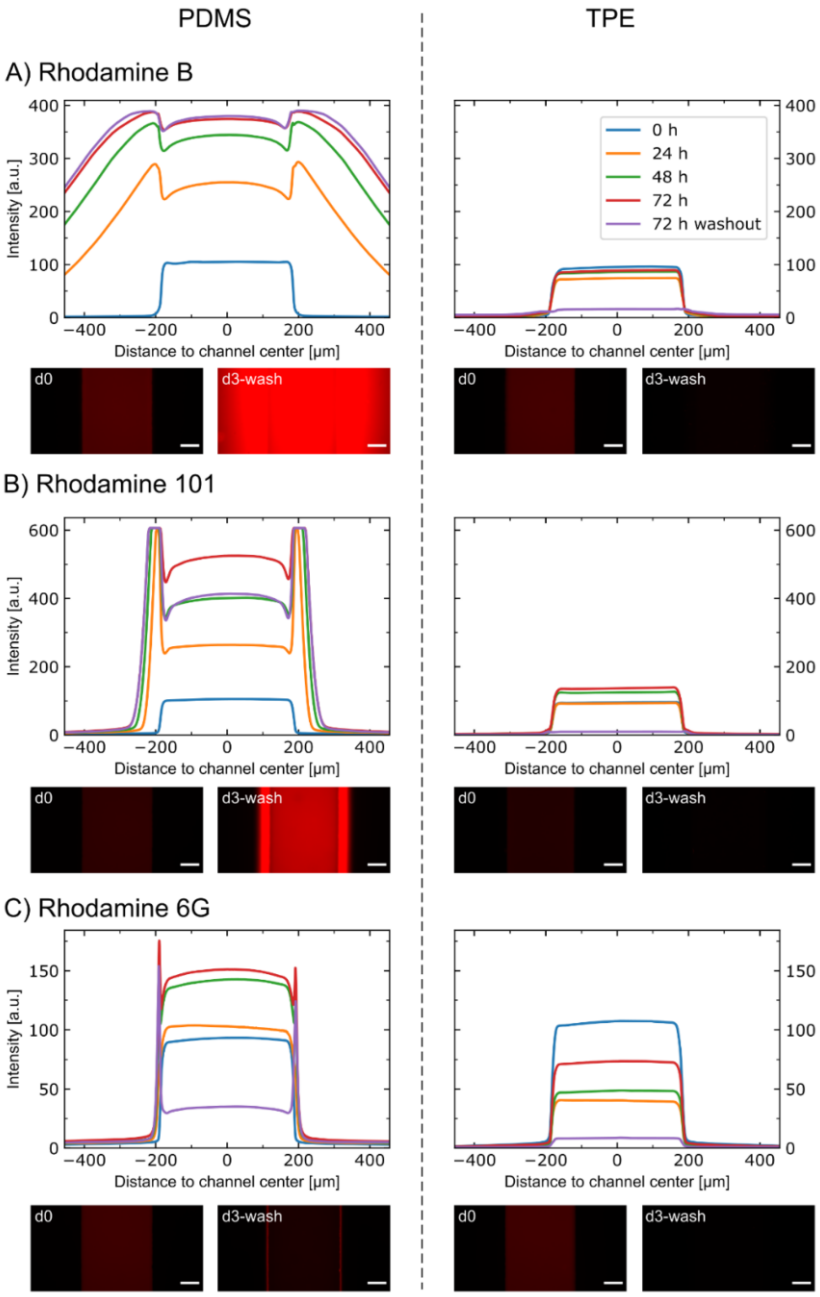

Figure 13.4 Absorption of a) rhodamine B, b) rhodamine 101 and c) rhodamine 6G into TPE and PDMS. Micrographs and averaged intensity profiles for different time points and after washout of the rhodamine solutions. Scale bars: 100 µm. Micrographs and fluorescent intensity profiles were obtained and analyzed by Oliver Schneider. Figure reprinted from Ref. [228] available under the CC BY 4.0 license.

13.6 Peristaltic Pump Stability

The results presented in this section were published in Ref. [227]. The peristaltic pump stability over longer periods is demonstrated by flow rate measurements, which were conducted on three consecutive days. The pumped volume per motor revolution was calculated for each measurement in order to allow for a comparison between different pump settings. Thereby, the pumped volumes were highly similar and close to the average (Figure 13.5).

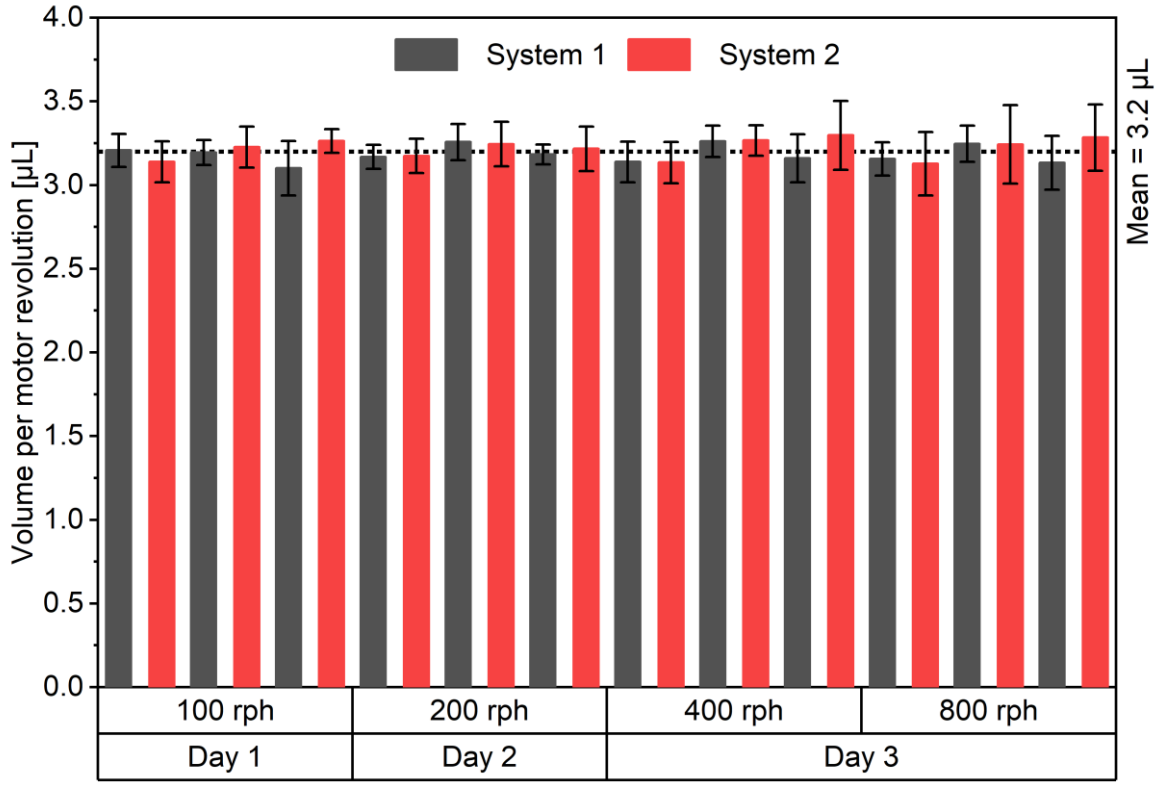

Figure 13.5 Peristaltic pump stability. Pumped volume of the integrated peristaltic pump per motor revolution. Flow rate measurements from three consecutive days with different pump settings and averaged, pumped volume per revolution over all measurements. Figure adapted from Ref. [227] with permission from the Royal Society of Chemistry available under the CC BY-NC 3.0 license.

Publications

First-Author Publications

- SCHNEIDER, Stefan, BUBECK, Marvin, ROGAL, Julia, WEENER, Huub J., ROJAS, Cristhian, WEISS, Martin, HEYMANN, Michael, VAN DER MEER, Andries D. and LOSKILL, Peter. Peristaltic on-chip pump for tunable media circulation and whole blood perfusion in PDMS-free organ-on-chip and Organ-Disc systems. *Lab Chip*. 2021. Vol. 21, no. 20, p. 3963–3978. DOI 10.1039/D1LC00494H.

- SCHNEIDER, Stefan #, BRÁS, Eduardo J. S. #, SCHNEIDER, Oliver, SCHLÜNDER, Katharina and LOSKILL, Peter. Facile Patterning of Thermoplastic Elastomers and Robust Bonding to Glass and Thermoplastics for Microfluidic Cell Culture and Organ-on-Chip. *Micromachines*. 2021. Vol. 12, no. 5, p. 575. DOI 10.3390/mi12050575.
  # These authors contributed equally to this manuscript.

- SCHNEIDER, Stefan, GRUNER, Denise, RICHTER, Andreas and LOSKILL, Peter. Membrane integration into PDMS-free microfluidic platforms for organ-on-chip and analytical chemistry applications. *Lab Chip*. 2021. Vol. 21, no. 10, p. 1866–1885. DOI 10.1039/D1LC00188D.

- SCHNEIDER, Stefan, ERDEMANN, Florian, SCHNEIDER, Oliver, HUTSCHALIK, Thomas and LOSKILL, Peter. Organ-on-a-disc: A platform technology for the centrifugal generation and culture of microphysiological 3D cell constructs amenable for automation and parallelization. *APL Bioengineering*. 2020. Vol. 4, no. 4, p. 046101. DOI 10.1063/5.0019766.

  → This paper was selected as “Featured”.

  → This paper was selected as “Scilight”, accessible at:
  GASPARINI, Allison. Organ-on-a-disc puts a spin on Organ-on-a-chip with centrifugal microfluidics. *Scilight*. 2020. Vol. 2020, no. 40, p. 401105. DOI 10.1063/10.0002249.

Co-Author Publications

- ROGAL, Julia, BINDER, Carina, KROMIDAS, Elena, ROOSZ, Julia, PROBST, Christopher, SCHNEIDER, Stefan, SCHENKE-LAYLAND, Katja and LOSKILL, Peter. WAT-on-a-chip integrating human mature white adipocytes for mechanistic research and pharmaceutical applications. *Scientific Reports*. 2020. Vol. 10, no. 1, p. 6666. DOI 10.1038/s41598-020-63710-4.
- PROBST, Christopher, SCHNEIDER, Stefan and LOSKILL, Peter. High-throughput organ-on-a-chip systems: Current status and remaining challenges. *Current Opinion in Biomedical Engineering*. 2018. Vol. 6, p. 33–41. DOI 10.1016/j.cobme.2018.02.004.

Conference Contributions

Oral Presentations

- Organ-on-a-disc technology for automated and parallelized microphysiological systems. EUROoCS Conference, July 2021, online
- Organ-on-a-Disc: a Platform Technology for the Automated and Parallelized Generation and Culture of Microphysiological 3D Tissues based on Centrifugal Forces. SLAS, January 2021, online
    - → Tony B. Academic Travel Award awarded from the Society for Laboratory Automation and Screening SLAS, 2021
    - → 1 out of 10 finalists of the SLAS Innovation Award from the Society for Laboratory Automation and Screening SLAS, 2021
- Organ-on-a-Disc – Enabling technology for the parallelization and automation of microphysiological systems. EUROoCS Conference, July 2019, Graz, Austria

Poster Presentations

- Organ-Disc – Enabling technology for 3D tissue generation and culture. EUROoCS Conference, July 2020, online
- Development and Characterization of the Organ-on-a-Disc Technology for the Parallelization and Automation of Microphysiological Systems. 3R Tierversuchsersatz in der personalisierten Medizin, December 2019, Tübingen, Germany
- Organ-on-a-Disc – Enabling Technology for the Parallelization and Automation of Microphysiological Systems. 22nd International Conference on Miniaturized Systems for Chemistry and Life Sciences, November, 2018, Kaohsiung, Taiwan
- Organ-on-a-Disc – Enabling technology for the parallelization and automation of microphysiological systems. 3D Cell Culture, June 2018, Freiburg, Deutschland

Patents

- Title: Device and method for cultivating cells
  International publication number: WO 2018/229157
  Publication data of the PCT international application: 20.12.2018
  Priority: DE 102017209942; 13.06.2017
  European patent number: EP3638768
  Publication date European patent: 07.04.2021
  Status European patent: The patent has been granted.
  Applicant: Fraunhofer-Gesellschaft zur Förderung der angewandten Forschung e.V.
  Inventors: LOSKILL, Peter, SCHNEIDER, Oliver, SCHNEIDER, Stefan